UNIVERSITAT POLITÈCNICA DE VALÈNCIA

Universitat Politècnica de València

Doctoral Thesis

Doctoral Programme in Biotechnology

DEVELOPMENT OF A 3D *IN VITRO* DISEASE MODEL FOR MULTIPLE MYELOMA

Sandra Clara Trujillo

July 2022

Supervised by:

Prof. José Luis Gómez Ribelles

Prof. Gloria Gallego Ferrer

Eso que tú me das

No creo lo tenga

merecido.

Todo lo que me das

Te estaré siempre agradecido.

…

Por todo lo que recibí

Estar aquí vale la pena.

Gracias a ti seguí

Remando contra la marea.

Eso Que Tú Me Das, Jarabe de Palo

Acknowledgements

En primer lugar, me gustaría agradecer a mis directores: Gloria y José Luis. Estos años he crecido gracias a las oportunidades que ellos me han dado y a su lado.

A José Luis que imaginó por primera vez el microgel y lo ha convertido en una oportunidad para todos los que trabajamos en él y, ojalá algún día, en una herramienta para los hematólogos y en esperanza para los pacientes de Mieloma múltiple. Gracias por las conversaciones inacabables sobre las posibilidades de las microesferas y por demostrarme en primera persona el valor de la inquietud y el amor por la ciencia como motor de la investigación. A Gloria, que fue la primera en introducirme en el mundo de la ingeniería tisular. Gracias por introducirme también en la familia del CBIT. Gracias por reorientar las conversaciones inacabables y focalizar los objetivos de esta Tesis; no sé cuándo habríamos acabado sin ti…Gracias por demostrarme la importancia de la dedicación día a día, por forzarme a razonar y cuestionar cada paso propuesto. A ambos, gracias por ofrecerme siempre nuevos retos y contar conmigo en vuestros diferentes proyectos. Por confiar en mí y darme la oportunidad de proponer, explorar mis ideas y equivocarme.

En especial, por mostrarme el valor añadido de trabajar para generar y cuidar un buen grupo de trabajo en todos los sentidos, pero especialmente en el factor humano. Entre los dos, castillos en el aire se han convertido en resultados tangibles y seguirán convirtiéndose.

Thanks to all the people from the CeMi for letting me in in your fantastic group. Especially to Catherine, for allowing me to enjoy new experiences in the last months of my PhD. Thank you for the opportunity to work on something different, in a new lab and learn every day. Especially, thank you for your closeness and for the time you've dedicated to guiding me.

A Lourdes y Amparo, por estar siempre disponibles para mejorar el trabajo y aportar su experiencia clínica a este proyecto. En especial a Lourdes por las horas de citómetro intentando adaptar todo a la presencia de microesferas.

A Laia, ha sido una suerte contar contigo y aprender de ti. Gracias por escuchar siempre nuestros problemas "bio" y contribuir con tu experiencia y tus recursos a avanzar en ellos. Seguiremos informándote de las aventuras de Pin y Pon.

A Laura Teruel, por solucionar todos los problemas del día a día y siempre con paciencia y una sonrisa. Gracias Laura por tu ayuda, y por la compañía en el turno de comida de las 15 h.

A todas las personas que en estos años han formado parte del CBIT, sobre todo a aquellas que han compartido conmigo la mayor parte del camino. Cada momento de trabajo o descanso me ha aportado algo gracias a vosotros. En especial a Hayk, Guillermo, Ximo, Luis, Annachiara, Rubén, Maria H., Pachi, Juan Jairo, Annj, Úrsula, Rafa, Darío, Esther, Estela, Raquel, Inma, Julio, Jose, Ana, Irene y Sandra. A Juan Carlos por compartir conmigo el inicio de este proyecto e infinitas tardes en La Fe; todavía se me hace raro estar en el laboratorio y no escucharte cantar cerca. En especial a Laura R., María y Sílvia, con quien he pasado más tiempo, dentro y fuera del CBIT.

A Laura, que siempre ha sido una guía en cultivos, muchas gracias por tu predisposición a ayudar y compartir. Ha sido para mí un reto y una suerte

trabajar contigo y esforzarme por estar a la altura (especialmente en cuanto a lo que a organización se refiere). Para siempre quedan las horas que hemos invertido juntas en el “Laboratorio Integrado” y lo que disfrutamos juntas en esas clases.

A María, que sé que leerá atentamente estas palabras: espero que no te decepcionen. Sin duda, compartir esta experiencia contigo ha sido el mayor reto y también el más sencillo. El mayor, porque hemos hecho dos tesis… Y el más sencillo porque las hemos hecho juntas, hasta el final y pasando por Glasgow. No sé si en nuestras diferencias está la clave para encajar tan bien en todos los sentidos, pero desde luego sé que sin ti el camino hasta aquí habría sido diferente. Tu compañía ha sido uno de los factores que más me han hecho crecer a nivel personal y profesional estos años. Probablemente no en la mesa de al lado, pero estoy segura que nos queda mucho camino juntas, incluidos papeleos interminables, episodios de veo veo, patas de cerdo, ramen gratis, comidas/cenas/chocolate para días duros, biodraminas traicioneras, salmón a la plancha (yo lo hago), pints of Guinness, abejas inoportunas, U.T.Is (no más, por favor), Highlands (ah no, esto no)… La lista podría ser interminable y curiosa. Muchas gracias, y ya sabes: “Roma no se construyó en un día”, así que seguiremos trabajando siempre.

A Sílvia, gracias por tu apoyo y ayuda constantes. Especialmente en los momentos más duros de esta tesis en los que has sabido hacerme recuperar el entusiasmo y las ganas. Tu compañía hace que cualquier rato sea un buen rato. Me llevo de estos años una lista de canciones increíble y alguna que otra cosa más…

A Mariam y Laura, que empezaron conmigo esta aventura muchos años antes y siguen conmigo en ella, por demostrar que las mesas de tres patas son las mejores. Y a Celia, la cuarta pata, que ha sabido hacer cortas las distancias y estar presente. A las tres, admiro mucho vuestro trabajo y espero que sigamos disfrutando juntas de la aventura.

A mi familia, que ha aguantado cada día bueno y malo de este camino y lo ha disfrutado conmigo. A mis padres, Satur y Paco, por darme siempre todas

las oportunidades y apoyarme en todas mis decisiones. Y por sacar la paella tarde los domingos para que yo llegará a tiempo del laboratorio. A mis hermanos, Iván y Belén, por ser tan diferentes y aportar su alegría enriqueciendo esta casa. Y en especial a mis abuelos, Agustín y Virginia, que han estado conmigo siempre y no han dejado de preguntarme por mi trabajo, aún sin entender bien lo que hago. Entre todos me habéis enseñado el valor del trabajo y el esfuerzo que me ha traído hasta aquí.

Me gustaría agradecer al Servicio de Microscopía de la UPV y a sus técnicos por su valiosa ayuda con las técnicas de microscopía electrónica. Y, por último, a la Agencia Estatal de Investigación (proyecto PID2019-106099RB-C41 / AEI / 10.13039/501100011033) y al Ministerio de Ciencia, Innovación y Universidades (ayuda predoctoral FPU17/05810) que han financiado esta Tesis.

Index

Figure list

Table list

Equation list

Abstract

In past decades tissue engineering has evolved from the development biological substitutes that restore the function of a tissue, towards modeling of human physiology *in vitro*, with the focus on precision medicine, drug testing and disease modeling. In the bone marrow (BM) the hematopoietic stem cells, through hematopoiesis produce all blood and immune populations. Different BM resident cells, soluble mediators and non-cellular elements such as the extracellular matrix (ECM) regulate this process. The complex BM microenvironment is likewise the home of some malignant processes, and the intricate interactions that maintain HSCs physiology also support hematological malignancies. Multiple myeloma (MM) is a hematological neoplasia characterized by aberrant proliferation and BM accumulation of monoclonal plasma cells. In last decades, treatments have improved, however MM remains incurable, as most patients relapse and become refractory to therapies. Different causes are involved in drug resistance (DR) generation, one of the most relevant is the tumor microenvironment. ECM molecules such as fibronectin (FN) or hyaluronic acid

(HA) have a recognized role in DR generation in MM. The inadequacy of two-dimensional preclinical models in reproducing MM microenvironment is one cause of the DR clinical problem, because of that, different approaches have attempted to reconstruct the MM microenvironment *in vitro*. However, all these studies are based on hydrogels and scaffolds designed for adherent cells while MM cells are suspension growing cells. It would be of great relevance to develop 3D models capable of respecting its dynamic and non-adherent nature. Microspheres as biomaterials offer extensive versatility for assembling a microenvironment of semi-solid nature, formed by suspended microspheres and cells. In addition, they can be functionalized with ECM molecules to increase biomimicry. The main objective of this Doctoral Thesis is to develop, optimize and validate a 3D culture platform, termed as microgel, based on microspheres suspended in a liquid media and coexisting with MM cells growing dynamically in suspension.

In the first experimental chapter, different microspheres with different functionalities were developed and characterized for their later implementation in the MM 3D cell culture platform. We optimized a suspension polymerization protocol for the obtention of acrylates-based microspheres with two different compositions: with presence (10%) or absence (0%) of acrylic acid (AA). Topography and size were characterized by field emission scanning electron microscope (FESEM). We obtained two different size distributions (< 60 and > 70 mm diameter). The presence of AA on 10% AA microsphere' surface was thoroughly characterized by X-ray photoelectron spectroscopy (XPS), thermogravimetric analysis (TGA) and toluidine blue O staining. FN was physically adsorbed on microsphere surface, while HA, collagen I and different peptide sequences were covalently grafted. All functionalizations were confirmed by XPS and colorimetric technics. As an alternative to acrylates microspheres, commercial Cytodex 1 microspheres were modified to adapt their characteristics

to the microgel platform. Layer-by-layer (LbL) technics were used to introduce HA and chondroitin sulfate (CS) on Cytodex 1 surface. The presence of the LbL coatings was confirmed by cryoFESEM and quantified by TGA. The LbL pair chitosan/CS generated thicker multilayers than the chitosan/HA. Two different crosslinking agents were used, glutaraldehyde and carbodiimide. Therefore, a wide repertoire of microspheres with different characteristics has been generated to develop microgels.

In the second experimental chapter, the culture conditions for the microgel platform were optimized and validated with 3 different MM cell lines. Microgels based on acrylates microspheres have been extensively used for this purpose. We determined that microsphere size has a relevant role on cell proliferation: cell-sized microspheres (< 60 μm diameter) showed higher proliferation of the MM lines RPMI8226, U226 and MM1.S. Agitation is needed to keep microspheres and cells in suspension, increasing agitation speed had negative effect on RPM8226 proliferation in conventional suspension culture. However, microgels reduced this negative effect. Optimal culture conditions were 150 rpm of stirring speed using orbital shaker and < 60 μm diameter microspheres. With the optimal culture conditions, microgels with different compositions (0% AA, 10% AA) and functionalizations (none, HA, FN, collagen 1 and peptide sequences) allowed good proliferation of RPMI8226, U226 and MM1.S cells under 3D conditions. All the 3D systems respected the suspension growth pattern which appears as key factor for their good performance in 3D culture. FN coated microgels were the only ones in which the formation of cell-cell, microsphere-microsphere, and cell-microsphere aggregates took place. In the initial DR studies using the microgel platform we found that MM cell line RPMI8226 cultured in microgels containing AA showed significantly higher resistance to dexamethasone than their conventional suspension cultures. And that MM cell lines RPMI8226, U226 and MM1.S cultured in microgels containing AA showed significantly higher resistance to borte-

zomib than their conventional suspension cultures. Thus, AA in the polymeric microsphere matrix showed a positive effect on the generation of DR *in vitro* and will require further studies. The scale-down of the system to work with smaller volumes of microspheres and reduced cell numbers has been validated, this is of great relevance for their future clinical application. Finally, preliminary cultures with the cell line RPMI8226 have been performed with the Cytodex 1-based microgels. Cytodex 1 microspheres without modification had a negative effect on MM cells viability. LbL modification with the pairs chitosan/CS and chitosan/HA increased MM cells viability and proliferation. However, these systems did not respect the non-adherent character of MM cells. From the two crosslinking methods tested, the glutaraldehyde resulted in MM decreased viability while the carbodiimide maintained the good viability of the non-crosslinked microgels.

We have developed and validated a novel cell culture system based on a semi-solid 3D media defined by microspheres and MM cells which is specially designed for cells in suspension. It represents a versatile tool that should be further explored for the 3D culture of hematological malignancies and drug resistance studies *in vitro*.

Resumen

En las últimas décadas, la ingeniería tisular ha evolucionado desde el desarrollo de sustitutos biológicos que restauran la función de un tejido, hacia el modelado de la fisiología humana *in vitro*, con especial atención a la medicina de precisión, el cribado de fármacos y el modelado de enfermedades. En la médula ósea (BM) las células madre hematopoyéticas, a través de la hematopoyesis, originan las células de la sangre y el sistema inmune. Diferentes células residentes en la BM, mediadores solubles y elementos no celulares como la matriz extracelular (ECM) regulan este proceso. El complejo microambiente de la BM es también el hogar de algunos procesos malignos, y las intrincadas interacciones que mantienen la fisiología de las HSC también respaldan las neoplasias hematológicas. El mieloma múltiple (MM) es una neoplasia hematológica caracterizada por una proliferación aberrante y acumulación en la BM de células plasmáticas monoclonales. En las últimas décadas, los tratamientos han mejorado, sin embargo, el MM sigue siendo incurable, ya que la mayoría de los pacientes recaen y se vuelven refractarios a las terapias. Diferentes causas están involucradas en la generación de resistencia a fármacos (DR), una de las más relevantes es el microambiente tumoral. Moléculas de ECM como la fibronectina (FN) o el ácido hialurónico (HA) tienen un papel reconocido en la generación de DR en MM. La inadecuación de los modelos preclínicos bidimensionales en la reproducción del

microambiente tumoral es una de las bases del problema clínico de DR, por lo que se han intentado diferentes enfoques para reconstruir el microambiente MM *in vitro*. Sin embargo, todos estos estudios se basan en hidrogeles y andamios celulares diseñados para células adherentes, mientras que las células de MM presentan crecimiento en suspensión. Sería de gran relevancia desarrollar modelos 3D capaces de respetar su naturaleza dinámica y no adherente. Las microesferas como biomateriales ofrecen una gran versatilidad para ensamblar un microambiente de naturaleza semisólida, formado por microesferas y células en suspensión. Además, pueden funcionalizarse con moléculas de la ECM para aumentar su biomimetismo. El objetivo principal de esta Tesis Doctoral es desarrollar, optimizar y validar una plataforma de cultivo 3D, denominada microgel, basada en microesferas en un medio líquido y que coexisten con células de MM creciendo dinámicamente en suspensión.

En el primer capítulo experimental se desarrollaron y caracterizaron diferentes microesferas con diferentes funcionalizaciones para su posterior implementación en la plataforma de cultivo 3D. Optimizamos un protocolo de polimerización en suspensión para la obtención de microesferas a base de acrilatos con dos composiciones diferentes: con presencia (10%) o ausencia (0%) de ácido acrílico (AA). La topografía y el tamaño se caracterizaron mediante microscopio electrónico de barrido de emisión de campo (FESEM). Se obtuvieron dos distribuciones de tamaño diferentes (< 60 y > 70 μm de diámetro). La presencia de AA en la superficie de microesferas de AA al 10 % se caracterizó minuciosamente mediante espectroscopía de fotoelectrones de rayos X (XPS), análisis termogravimétrico (TGA) y tinción con azul de toluidina O. La FN se adsorbió físicamente en la superficie de la microesfera, mientras que el HA, colágeno I y diferentes secuencias peptídicas se injertaron covalentemente. Todas las funcionalizaciones fueron confirmadas por XPS y técnicas colorimétricas. Como alternativa a las microesferas de acrilatos, se modificaron las microesferas comerciales Cytodex 1 para adaptar sus características a la plataforma del microgel. Se utilizaron técnicas capa

por capa (LbL) para introducir HA y sulfato de condroitina (CS) en la superficie de las Cytodex 1. La presencia de los recubrimientos de LbL fue confirmada por cryoFESEM y cuantificada por TGA. El par de LbL quitosano/CS generó multicapas más gruesas que el quitosano/HA. Se utilizaron dos agentes de reticulación diferentes, glutaraldehído y carbodiimida. Por tanto, se ha generado un amplio repertorio de microesferas con diferentes características para desarrollar microgeles.

En el segundo capítulo experimental, se optimizaron y validaron las condiciones de cultivo para la plataforma de microgel con 3 líneas celulares de MM diferentes. Los microgeles basados en microesferas de acrilatos se han utilizado ampliamente para este propósito. Determinamos que el tamaño de las microesferas tiene un papel relevante en la proliferación celular: las microesferas de tamaño celular (< 60 μm de diámetro) mostraron una mayor proliferación de las líneas RPMI8226, U226 y MM1.S. Se necesita agitación para mantener las microesferas y las células en suspensión; el aumento de la velocidad de agitación tuvo un efecto negativo en la proliferación de RPMI8226 en cultivos en suspensión convencionales. Sin embargo, los microgeles redujeron este efecto negativo. Las condiciones óptimas de cultivo se establecieron como 150 rpm de velocidad de agitación utilizando un agitador orbital y microesferas de < 60 μm de diámetro. Con estas condiciones, los microgeles con diferentes composiciones (0% AA, 10% AA) y funcionalizaciones (ninguna, HA, FN, colágeno 1 y secuencias peptídicas) permitieron una buena proliferación de las líneas RPMI8226, U226 y MM1.S en condiciones 3D. Todos los sistemas respetaron el patrón de crecimiento en suspensión, factor que ha demostrado ser clave para su buen desempeño en cultivo 3D. Los microgeles recubiertos con FN fueron los únicos en los que la formación de agregados célula-célula, microesfera-microesfera y célula-microesfera tuvo lugar. En estudios iniciales de DR en la plataforma de microgel, encontramos que la línea celular RPMI8226 cultivada en microgeles que contenían AA mostró una resistencia significativamente mayor a la dexametasona que sus cultivos en suspensión convencionales. Y que las líneas celulares RPMI8226, U226 y MM1.S cultivadas en microgeles que contenían

AA mostraron una resistencia significativamente mayor a bortezomib que sus cultivos en suspensión convencionales. Por lo tanto, la presencia de AA en la matriz polimérica de las microesferas mostró un efecto positivo en la generación de DR *in vitro* y requerirá más estudios. Se ha validado la reducción de escala del sistema para trabajar con volúmenes más pequeños de microesferas y números reducidos de células, lo que es de gran relevancia para su futura traslación clínica. Finalmente, se han realizado cultivos preliminares con la línea celular RPMI8226 en los microgeles basados en Cytodex 1. Las microesferas de Cytodex 1 sin modificación tuvieron un efecto negativo sobre la viabilidad de las células de MM. La modificación mediante LbL con los pares quitosano/CS y quitosano/HA aumentó la viabilidad y proliferación de células de MM. Sin embargo, estos sistemas no respetaron el carácter no adherente de las células MM. De los dos métodos de entrecruzamiento probados, el glutaraldehído dio como resultado una menor viabilidad celular mientras que la carbodiimida mantuvo la buena viabilidad celular de los microgeles no entrecruzados.

Hemos desarrollado y validado un novedoso sistema de cultivo basado en un medio 3D semisólido definido por microesferas y células de MM especialmente diseñado para células en suspensión. Este sistema constituye una herramienta versátil que debe explorarse más a fondo para el cultivo 3D de neoplasias hematológicas y para estudios de resistencia a fármacos *in vitro.*

Resum

En les últimes dècades, l'enginyeria tissular ha evolucionat des de la producció de substituts biològics que restauren la funció d'un teixit, cap al modelat de la fisiologia humana *in vitro*, amb especial atenció a la medicina de precisió, el rastreig de fàrmacs i el modelat de malalties. En la medul·la òssia (BM) les cèl·lules mare hematopoètiques, a través de la hematopoiesis, originen les cèl·lules de la sang i el sistema immune. Diferents cèl·lules residents a la BM, mediadors solubles i elements no cel·lulars com la matriu extracel·lular (ECM) regulen aquest procés. El complex microambient de la BM és també la llar d'alguns processos malignes, i les interaccions intrínseques que mantenen la fisiologia de les HSC també contribueixen a les neoplàsies hematològiques. El mieloma múltiple (MM) és una neoplàsia hematològica caracteritzada per una proliferació aberrant i acumulació a la BM de cèl·lules plasmàtiques monoclonals. A les últimes dècades, els tractaments han millorat, no obstant, el MM segueix sent incurable, donat que la majoria dels pacients recauen i es tornen refractaris a les teràpies. Diferents causes estan involucrades en la generació de resistència a fàrmacs (DR), una de les més

rellevants és el microambient tumoral. Molècules de la ECM com la fibronectina (FN) o l'àcid hialurònic (HA) tenen un paper reconegut en la generació de DR en MM. La inadequació dels models preclínics bidimensionals en la reproducció del microambient tumoral és una de les bases del problema clínic de DR. Per això, s'han intentat diferents aproximacions per reconstruir el microambient del MM *in vitro*. Tots aquests estudis es basen en hidrogels i andamis cel·lulars dissenyats per a cèl·lules adherents, mentre que les cèl·lules de MM presenten creixement en suspensió. Seria de gran rellevància desenvolupar models 3D capaços de respectar la naturalesa dinàmica i no adherent d'aquestes cèl·lules. Les microesferes com a biomaterials ofereixen una gran versatilitat per a generar microambients de natura semi-sòlida, formats per microesferes i cèl·lules en suspensió. A més, poden funcionalitzar-se amb molècules de l'ECM per augmentar el biomimetisme. L'objectiu principal d'aquesta Tesi Doctoral és desenvolupar, optimitzar i validar una plataforma de cultiu 3D, denominada microgel, basada en microesferes en un medi líquid i que coexisteixen amb cèl·lules de MM que creixen dinàmicament en suspensió.

En el primer capítol experimental s'han produït i caracteritzat diferents microesferes amb diferents funcionalitzacions per a la seua posterior implementació a la plataforma de cultiu 3D. S'ha optimitzat un protocol de polimerització en suspensió per a l'obtenció de microesferes d'acrilats amb dues composicions diferents: amb presència (10%) o absència (0%) d'àcid acrílic (AA). La topografia i el tamany s'han caracteritzat mitjançant microscòpia electrònica de rastreig d'emissió de camp (FESEM). Es varen obtenir dos distribucions de diàmetres diferents (< 60 i > 70 μm de diàmetre). La presencia d'AA a la superfície de les microesferes amb 10% d'AA es va analitzar amb espectroscòpia de fotoelectrons de rajos X (XPS), anàlisis per termogravimetria (TGA) i tinció amb blau de toluïdina O. La FN es va adsorbir físicament, mentre que el HA, el col·lagen 1 i diferents seqüències peptídiques es van unir covalentment mitjançant la química de la carbodiimida. La presència de totes les funcionalitzacions ha estat confirmades per XPS i tècniques colorimètriques.

Com a alternativa a les microesferes d'acrilats, s'han modificat les microesferes comercials Cytodex 1 per tal d'adaptar les seves característiques a la plataforma del microgel. Mitjançant tècniques capa a capa (LbL) s'han introduït HA i sulfat de condroïtina (CS) a la superfície de les Cytodex 1. La presencia dels recobriments es va confirmar mitjançant cryoFESEM i es va quantificar amb TGA. El parell de LbL quitosà/CS va generar multicapes de major grossor que el quitosà/HA. S'utilitzaren dos agents diferents per entrecreuar els recobriments, glutaraldehid i carbodiimida. Per tant, s'ha generat un ampli repertori de microesferes amb diferents característiques per desenvolupar microgels.

En el segon capítol experimental, es van optimitzar i validar les condicions de cultiu per a la plataforma de microgel amb 3 línies cel·lulars de MM diferents. Els microgels basats en microesferes d'acrilats s'han emprat àmpliament per amb aquesta finalitat. S'ha establert que el tamany de les microesferes té un paper rellevant en la proliferació cel·lular: les microesferas de tamany proper al cel·lular (< 60 μm de diàmetre) mostraren una major proliferació cel·lular de les línies RPMI8226, U226 i MM1.S. Es necessita agitació per mantenir les microesferes i les cèl·lules en suspensió; l'augment de la velocitat d'agitació va tenir un efecte negatiu en la proliferació de cèl·lules RPMI8226 en suspensió convencional. Tanmateix, els microgels van reduir aquest efecte negatiu. Les condicions òptimes de cultiu es varen establir com a 150 rpm de velocitat d'agitació utilitzant un agitador orbital i microesferes de < 60 μm de diàmetre. Amb aquestes condicions, els microgels amb diferents composicions (0% AA, 10% AA) i funcionalitzacions (cap, HA, FN, col·lagen 1 i seqüències peptídiques) van permetre una bona proliferació de les línies RPMI8226, U226 i MM1.S en condicions 3D . Tots els sistemes van respectar el patró de creixement en suspensió, factor que ha demostrat ser clau per al seu bon rendiment en cultius 3D. Els microgels recoberts amb FN van ser els únics en els quals la formació d'agregats cèl·lula-cél·lula, microesfera-microesfera i cèl·lula-microesfera van ocórrer. En estudis inicials de DR emprant la plataforma de microgel, trobem que la línia cel·lular RPMI8226

cultivada en microgels que contenien AA va mostrar una resistència significativament major a la dexametasona que els seus cultius en suspensió convencionals. I que línies RPMI8226, U226 i MM1.S cultivades en microgels que contenien AA mostraren una resistència significativament major a bortezomib que els seus cultius en suspensió convencionals. Per tant, la presencia d'AA a la matriu polimèrica de les microesferes va mostrar un efecte positiu en termes de generació de DR *in vitro*, cosa que requerirà estudis futurs. S'ha validat la reducció de l'escala del sistema per treballar amb volums més petits de microesferes i menys cèl·lules, el que és de gran rellevància per a la seva futura translació clínica. Finalment, s'han realitzat cultius preliminars amb la línia cel·lular RPMI8226 en els microgels basats en les Cytodex 1. Les microesferes de Cytodex 1 sense modificar van mostrar efecte negatiu sobre la viabilitat de les cèl·lules de MM. La modificació mitjançant LbL amb els parells quitosà/CS i quitosà/HA va augmentar la viabilitat i proliferació de cèl·lules MM. No obstant, aquests sistemes no respectaren el caràcter no adherent de les cèl·lules de MM. Dels dos mètodes d'entrecreuament testats, el glutaraldehid resultà en una menor viabilitat cel·lular mentre que la carbodiimida va mantindré la bona viabilitat cel·lular dels microgels no entrecreuats.

S'ha desenvolupat i validat un nou sistema de cultiu cel·lular basat en un medi 3D semisòlid definit per microesferes i cèl·lules de MM, especialment dissenyat per a cèl·lules no adherents. Aquest sistema constitueix una eina versàtil que ha de ser explorada per al cultiu 3D de neoplàsies hematològiques i per a estudis de resistència a fàrmacs *in vitro*.

Glossary

AA	Acrylic acid
aBMN	Arteriolar bone marrow niche
aEC	Arteriolar endothelial cell
AFM	Atomic force microscopy
Akt	Protein kinase B
ALL	Acute lymphoblastic leukemia
AML	Acute myeloid leukemia
ANG-1	Angiopoietin 1
ANOVA	Analysis of variance
ANXA2	Annexin A2
AP-1	Activator protein 1
APRIL	A proliferation-inducing ligand

ASCT	Autologous stem cell transplantation
B-ALL	B-cell acute lymphoblastic leukemia
b-FGF	Basic fibroblast growth factor
BAFF	B-cell activating factor
BAFFR	B-cell activating factor receptor
BCA	Bicinchoninic acid assay
Bcl-2	B-cell lymphoma 2
BCP	B-cell progenitor
BM	Bone marrow
BMN	Bone marrow niche
BMSC	Bone marrow stromal cell
BPO	Benzoyl peroxyde
BSA	Bovine Serum Albumina
BTZ	Bortezomib
CAF	Cancer asociated fibroblast
CAM-DR	Cell adhesion mediated drug resistance
CAR	CXCL-12 abundant reticular cells
CBMN	Central bone marrow niche
CCL-3	Chemokine ligand 3
CHI	Chitosan
CK1	Casein kinase 1
CLL	Chronic lymphoblastic leukemia
CLP	Common lymphoid progenitor

CML	Chronic myeloid leukemia
CMP	Common myeloid progenitor
COL	Collagen
COL 1	Collagen 1
cryoFESEM	Cryogenic field emission scanning electron microscope
CS	Chondroitin sulphate
CTC	Circulating tumor cell
CXCL-12	CXC motif chemokine ligand 12
CXCR-4	CXC chemokine receptor type 4
DEAE	N,N-diethylaminoethyl
DEX	Dexamethasone
DKK-1	Dickkopf-1
DMSO	Dimethyl sulfoxyde
DNA	Desoxiriblonucleic acid
DPBS	Dulbecco's phosphate buffer saline
DR	Drug resistance
DSC	Diferential scanning calorimetry
EA	Ethyl acrylate
EBMN	Endosteal bone marrow niche
EC	Endothelial cell
ECM	Extracellular matrix
EDC	1-Ethyl-3-(3-dimethylaminopropyl) carbodiimide
EGDMA	Ethylene glycol dimethacrylate

EMA	Ethyl methacrylate
Erk	Extracellular signal regulated kinase
EV	Extracellular vesicle
EWC	Equilibrium water content
FDA	Food and drug administration
FESEM	Field emission scanning electron microscope
FITC	Fluorescein-5-isothiocyanate
FN	Fibronectin
FoxO1	Forkhead box protein O1
FTIR	Fourier transformed infrared spectroscopy
G-CSF	Granulocyte-colony stimulating factor
GA	Glutaraldehyde
GC	Glucocorticoid
GDP	Guanosine-5'-diphosphate
GMP	Granulocyte-macrophage progenitor
Grb2	Growth factor receptor-bound protein 2
GSK3b	Glycogen synthase kinase 3b
GTP	Guanosine-5'-triphosphate
HA	Hyaluronic acid
HCl	Hydrochloric acid
HIF-1a	Hypoxia inducible factor 1a
HSC	Hematopoitic stem cell
ICAM-1	Intercellular adhesion molecule 1

IGF-1	Insulin growth factor 1
iHDAC	histone deacetylase inhibitor
IkB	Inhibitory kB
IkK	IkB kinase
IL-18	Interleukin 18
IL-1b	Interleukin-1β
IL-6	Interleukin 6
IL-6R	Interleukin 6 receptor
IL-7	Interleukin 7
IL6R	Interleukin 6 receptor
IMID	Immuno-modulatory drug
IP	Propidium iodide
JAK	Janus kinase
LbL	Layer-by-layer
LepR	Leptin receptor
LFA-1	Lymphocyte function associated antigen 1
LRP5/6	Lipoprotein receptor-related protein 5/6
LSCM	Laser scanning confocal microscopy
LT-HSC	Long-term hematopoietic stem cell
LTβ	Lymphotoxin β
mAb	Monoclonal antibody
MBD	Myeloma bone disease
MDR	Multi-drug resistance

MDS	Myelodisplasic syndrome
MEP	Megakaryocyte-erythroid progenitor
MGUS	Monoclonal gammopathy of undetermined clinical significance
MM	Multiple myeloma
MPN	Myeloproliferative neoplasms
MSC	Mesenchymal stem cell
mTOR	Mammalian target of rapamycin
mTORC	Mammalian target of rapamycin complex
MUC-1	Mucin-1 antigen
MWCO	Molecular weight cut off
NaCl	Sodium Chloride
NaOH	Sodium hydroxide
NEMO	NF-κB essential modulator
Nest	Nestin
NF-kB	Nuclear factor kB
NG-2	Neural glial antigen 2
NHS	N-hydroxy succinimide
NIK	NFkB inducing kinase
NK	Natural killer
nmSC	Non-myelinating Schwann cell
NOXA	Horbol-12-myristate-13-acetate-induced protein 1
OB	Osteoblast
OC	Osteoclast

ON	Overnight
OPN	Osteopontin
PBS	Phosphate buffer saline
PC	Plasma cell
PDK1	Inositide-dependent protein kinase 1
PDK2	Inositide-dependent protein kinase 2
PEG-$_{di}NH_2$	Polyethylene glycol bis amino terminated
PF-4/ CXCL-4	Platelet factor 4 /Chemokine CXCL-4
PI	Proteasome inhibitor
PI3K	Phosphatidyl-inositol-3-kinase
PIP_3	Phosphatidylinositol (3,4,5)-trisphosphate
PKB	Protein kinase B
PLGA	Poly lactic co-glycolic acid
Prx-1	Paired related homebox 1
PVA	Poly (vynil) alcohol
QCM	Quartz crystal microbalance
qPCR	Quantitative polymerase chain reaction
RANKL	Receptor activator of NFkB ligand
Rarg	Retinoic acid receptor g
Rb	Retinoblastoma
RCCS	Rotatory cell culture system
RHD	Rel homology domain
RNA	Ribonucleic acid

ROS	Reactive oxygen species
RT	Room temperature
RT-PCR	Reverse transciption polymerase chain reaction
sBMN	Sinusoidal bone marrow niche
SCF	Stem cell factor
SDF-1	Stromal cell derived factor 1
sEC	Sinusoidal endothelial cell
SF-DR	Soluble factor-mediated drug resistance
SGK	Serum-and glucocorticoid-induced protein kinase
SMM	smoldering myeloma
SNS	Sympathetic nervous system
Sos	Son of sevenless homolog
ST-HSC	Short-term hematopoietic stem cell
STAT	Signal transducer and activator of transcription
sulfo-NHS	Sulfo N-hydroxy succinimide
T	Temperature
TBO	Toloudine blue O
TERM	Tissue engineering and regenerative medicine
Tg	Glass transition temperature
TGA	Thermogravimetric analysis
TGF-b	Transforming growth factor beta
TNFR	Tumour necrosis factor receptor
TNFα	Tumour necrosis factor α

TNKP	T-natural killer cell progenitor
TPO	Thrombopoietin
TSP-1 /THBS-1	Trombospondin 1
TWEAK	NF-related weak inducer of apoptosis
VCAM-1	Vascular adhesion molecule 1
VEGF-A	Vascular endothelial growth factor A
WHO	World Health Organization
XPS	X-ray photoelectron spectroscopy

SECTION I.

GENERAL INTRODUCTION

Chapter 1. General introduction

1.1. Disease modeling and tissue engineering

Historically the objective of tissue engineering and regenerative medicine (TERM) has been to apply the principles of engineering and life sciences toward the development of biological substitutes that restore, maintain, or improve the function of a tissue or whole organ (Langer and Vacanti 1993). While this objective remains intact, the focus of the field has been extended in past decades to the implementation of engineered tissues that will never be implanted into patients, but will transform the way we study human physiology *in vitro* (Gomes et al. 2017; Khetani and Bhatia 2006; Kelm et al. 2019; Pradhan et al. 2016). These engineered tissues have been conceived with the focus on precision medicine, drug testing and disease modeling (Wobma and Vunjak-Novakovic 2016).

Each tissue and organ is unique and has well defined functions, anatomy, and cellular, molecular, and soluble components. *In vivo*, individual cells are

harbored in specific niches where they integrate many external cues; including those that arise from extracellular matrix (ECM), mechanical stimulation and soluble signals from adjacent and distant cells to generate a basal phenotype and respond to perturbations in their environment. The development of 3D platforms with well-defined architectures resembling these native cellular microenvironments has contributed to significant advances in liver or heart modelling among other tissues (Van Grunsven 2017; Tsukamoto, Akagi, and Akashi 2020; Z. Wang et al. 2018). The multidisciplinary of these works allowed the integration of tridimensionality, multi-cellular interactions, patient specific polymorphisms, fine control of chemical parameters (pH, oxygen level, biochemical gradients) and ECM composition as the main assets of these engineered tissues (Griffith and Swartz 2006; Khetani and Bhatia 2006; Schenke-Layland and Nerem 2011). This new approach of the field is leading to engineered tissue and organ mimics that can be employed for studies on the underlying mechanisms of embryology and adult physiology, as well as for the investigation of disease initiation and progression.

Different factors have driven the development of this field. The main factor is the need for *in vitro* models based on human cells. Conventional 2D *in vitro* culture is based on the use of human immortalized cell lines. Cell lines are highly selected populations that do not reflect the heterogeneous genetic and functional variability of complex pathologies such as cancer. Patient-derived primary cells would overcome this disadvantage, although their use is hindered by issues of patient sample acquisition, variability and the difficulties associated with their culture (Clara-Trujillo, Gallego Ferrer, and Gómez Ribelles 2020). However, the lack of the microenvironment that conditions cell behavior remains in these conventional 2D *in vitro* models. Animal models provide complex 3D models and can recapitulate several aspects of human physiology. Despite this, there are species specific pathogens or clinical problems, such as liver toxicity, that cannot be predicted by animal or *in vitro* conventional models. In this sense, there has been an extensive and fruitful work done in the field of *humanized* mice (Schenke-Layland and Nerem 2011). Humanized mouse models are mice engrafted with functional human

cells or tissues (Fujiwara 2018). This approach allows studying the development and function of human cells or tissues, or the function of certain gene products, *in vivo*. However, humanized mouse models present limitations. The technical complexity of these models makes challenging and expensive to adopt them for routine use in the clinical practice (Griffith and Swartz 2006). Moreover, the existence of fundamental differences in the microenvironment in which the human component is engrafted (such as lacking or insufficient immune systems or interspecies differences in receptors, growth factors or cytokines among others) or in the physiology of the animal (for example, in cancer models fundamental differences in the regulation of telomerase enzyme exist between humans and rodents) has generated doubts about tumor models based on humanized rodent systems (Abarrategi et al. 2018).

The appearance of new bioengineered constructs marks a new era of tissue engineering and *in vitro* models. Its development is making possible to work with human cells and tissues in more biologically relevant conditions that conventional *in vitro* models, as well as reducing the number of animals used in experimentation. The latter is of great importance, as it contributes towards the achievement of sustainable development goals. Nevertheless, it is important to consider what level of complexity is necessary (and possible) to incorporate into these systems (e.g., vasculature, extracellular matrix, immune system, diversity of cell types). Indeed, it is not possible (or even is not necessary) to reach a level of complete mimicry. The current difficulty lies in the fact of finding the balance and determining the point that allows *in vitro* conclusions to be extrapolated to the human body while incorporating the least possible complexity in the 3D model (Clara-Trujillo, Gallego Ferrer, and Gómez Ribelles 2020). One day, the development of this complex models could even lead to the replacement for animal models in drug testing or toxicity assessment. This is still far from happening, but meanwhile it is irrefutable the amount of information and possibilities they generate for basic and applied research.

Engineering and materials science contribution to this field has been, is and will be invaluable. The use of polymeric matrices has been essential for 3D

models refinement. It has allowed the design of the desired architectures and compartmentalization but also the incorporation of some functionalities (by directly using natural materials such as chitosan, collagen, or hyaluronic acid (Poveda-Reyes et al. 2015) or by decorating synthetic matrices with bioactive peptides or factors (Salmerón-Sánchez et al. 2011)). 3D substrates can be modified with the desired properties in terms of cell fate and function control. Moreover, time-dependent, or stimuli-respondent behaviors such as piezoelectricity can be incorporated to generate "smart" materials (Guillot-Ferriols et al. 2020). Also, incorporation of electronics, microfluidics devices and sensors can allow fine control of relevant biological parameters like oxygen levels, media renewal or shear flow (Håkanson, Cukierman, and Charnley 2013). All these parameters can be coordinated with the cellular component rising a 3D *in vitro* construct with higher complexity level than conventional *in vitro* models that would not have been possible without the development of tissue engineering.

1.2. The bone marrow microenvironment

The bone marrow (BM) can be found within the central cavity of long and axial bones (Figure 1, a). It comprises hematopoietic tissue islands "red marrow" and adipose tissue "yellow marrow" surrounded by vasculature and dispersed within a meshwork of trabecular bone (Figure 1, b). It accounts about 5% of the body weight in an adult human. Is the major hematopoietic organ and the primary lymphoid tissue (Travlos 2006).

In the 1990s, structural analysis of the BM revealed that it has a highly ordered structure which has a functional significance for hematopoiesis (Lord 1990). The "red marrow" has a predominant hematopoietic character and a highly vascularized anatomy. Arterial blood flow enters BM by nutrient vessels that penetrate cortical bone. These vessels merge and form the central artery. Arterioles branch and spread through the intramedullary cavity from the central artery toward cortical bone and anastomose with the sinusoid in

the medullary canal. Transition zone vessels connect arterioles and sinusoidal vessels in the proximities of bone surface. Sinusoidal vessels then connect with the central vein, and blood flows from bone marrow through the nutrient vein (Morikawa and Takubo 2017) (Figure 1, c). This vasculature structure defines different areas, termed as microenvironments or niches in which different cells or different functionalities of the same cell type can be predominantly found in one area or another.

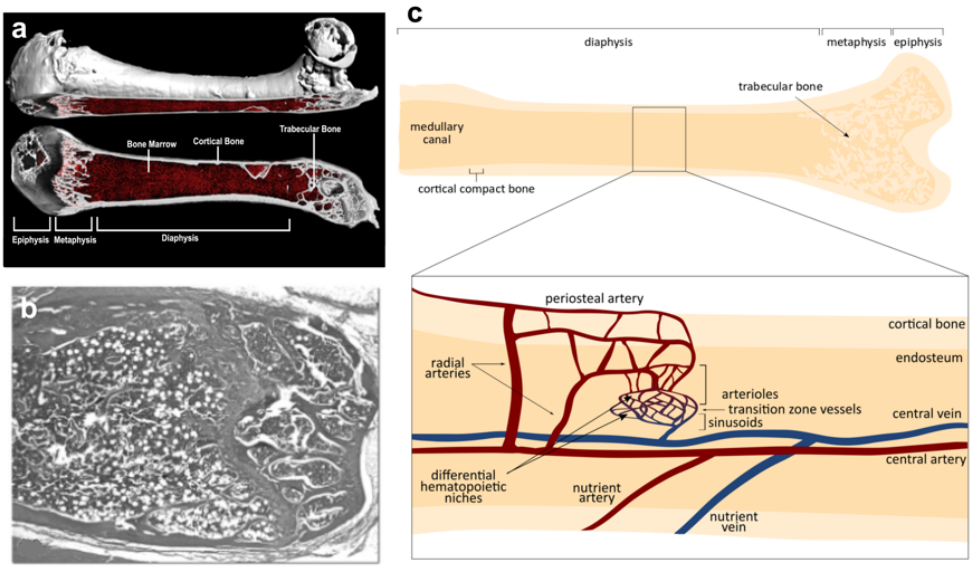

Figure 1. Bone marrow anatomy. a) A bisected mouse femur. Adapted from (Comazzetto, Shen and Morrison 2021)**. b) Example of the bone marrow cellularity in a normal adult mouse distal femur, the marrow spaces contain islands and clusters of hematopoietic cells admixed with adipocytes. Adapted from** (Travlos 2006)**. c) Diagram of bone marrow vasculature.**

1.2.1. Hematopoietic stem cells (HSC) and Hematopoiesis

The hematopoietic system is an extremely dynamic and complex cell network that accomplishes several functions in organisms: erythrocytes production for oxygen transportation, differentiation of immune cells from innate and adaptive systems or generation of thrombocytes that stop haemorrhages and con-

tribute to tissue repair. All these functions are critical throughout life of organisms and the hematopoietic system has developed complex regulatory and protective mechanisms to maintain its functional integrity during the whole lifespan (Olson, Kang, and Passegué 2020).

The hematopoietic system is defined by a hierarchical organization. The hematopoietic stem cells (HSCs) are the pluripotent stem cells that arise at the top of the hematopoietic hierarchy (Figure 2). They are characterized by its capability of differentiation and self-renewal. Through the process termed as hematopoiesis, HSCs arise into a progeny transiting through multiple differentiation states; progressing from lineage-biased but still multipotent progenitors to lineage-specific committed progenitors and precursors that will ultimately produce all blood and immune mature populations (Galán-Díez, Cuesta-Domínguez, and Kousteni 2018).

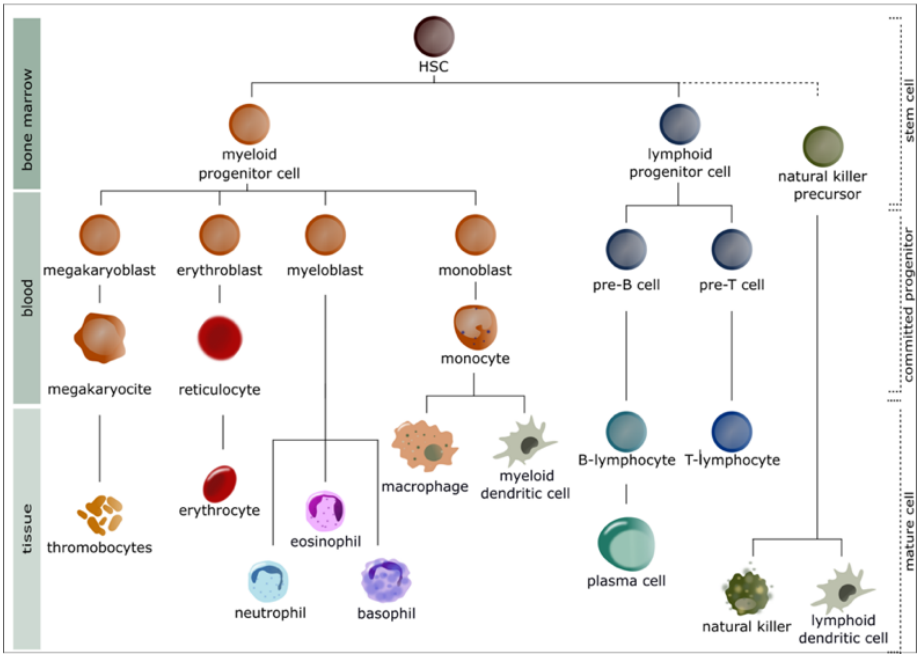

Figure 2. Hematopoiesis. Representation of the hematopoiesis process and the different immune and blood cell types differentiated from hematopoietic stem cells (HSCs) by this process.

As HSCs advance through this differentiation scale, their potency (ability of stem cells for differentiating into specialized cell types) decreases, until they become terminally differentiated cells.

By this process HSCs fulfil their function of active differentiation originating mature and functional blood and immune cells. However, HSCs undergo a second role related with the maintenance of the HSCs pool during whole lifespan of an individual, which is equally important. As the number of pluripotent stem cells is limited, it's crucial that the equilibrium between these active differentiation processes and the HSCs maintenance stays balanced to maintain the integrity of the entire hematopoietic tissue, preventing exhaustion of the stem cell pool or development of hematopoietic malignancies. HSCs self-renewal is experimentally defined as the capacity for long term reconstitution of all blood lineages upon transplantation into a recipient. However, the accumulation of damage in such cells can reduce their self-renewal capability and result in dysfunctional hematopoiesis including BM failure or malignant transformations. Quiescence is a fundamental characteristic of HSCs, as it contributes to HSCs longevity and function by protecting cells against genomic instability, replicative stress, metabolic stress, and functional decline.

Cellular quiescence is a dormant but reversible cellular state in which cell cycle entry and proliferation are prevented. Like somatic cells, HSCs progress through the four phases of the cell cycle (Figure 3): G1 phase, S phase, G2 phase and M phase. Cells that pass the restriction point in the G1 phase will proceed through cell cycle and divide. Oppositely, non-dividing cells can enter the G0 phase and become quiescent, losing the ability to cycle. Quiescent cells are non-dividing cells that exist in the G0 stage of the cell cycle in a temporary and reversible manner, in contrast with senescent cells, whereby irreversibly arrested in G0, and that will ultimately be leading to degeneration and death (Nakamura-Ishizu *et al.*, 2014).

HSCs are a functionally heterogeneous population regarding self-renewal capacity, lifespan and differentiation biases. The current model of hematopoiesis relies on the idea that the HSCs pool has at least two functionally different

HSC populations: the long-term HSCs (LT-HSCs), and the short-term HSCs (ST-HSCs) (Nakamura-Ishizu *et al.*, 2014).

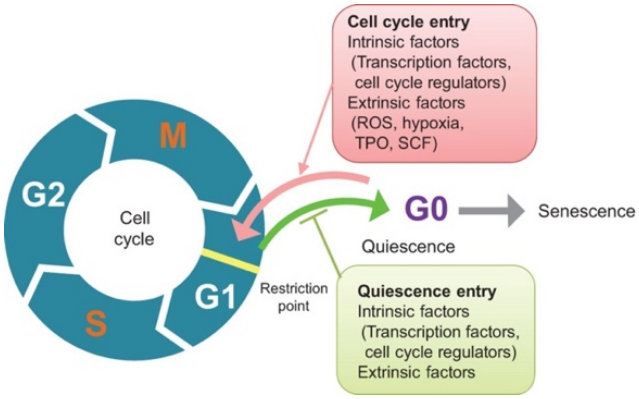

Figure 3. Cell cycle phases and its regulation in HSCs. Source: (Nakamura-Ishizu *et al.*, 2014)**. ROS, reactive oxygen species; TPO, thrombopoietin; SCF, stem cell factor.**

From LT-HSCs to ST-HSCs populations, a decrease in repopulation potential is shown. LT-HSCs have lifelong self-renewing potential, whereas the ST-HSCs (that present restricted self-renewing capacity) produce common myeloid progenitors (CMPs) and common lymphoid progenitors (CLPs). CLPs are the source of committed precursors of B and T lymphocytes, whereas CMPs give rise to megakaryocyte-erythroid progenitors (MEPs) and granulocyte-macrophage progenitors (GMPs) (Galán-Díez, Cuesta-Domínguez, and Kousteni 2018). In adult organism, HSCs remain quiescent, self-renew and differentiate mainly in BM niches, however other hematopoietic cells find their niches in secondary lymphoid organs, such as the spleen or the lymph nodes (Méndez-Ferrer et al. 2020).

This complex cellular system has developed adaptative response capacity; as it has to maintain homeostatic replacement of blood and immune cells (which is called steady state hematopoiesis), but also to rapidly increase this cellular output in a context of severe blood loss, infection and metabolic or toxic stress (which is known as emergency hematopoiesis). Under homeostatic conditions, LT-HSCs differentiate scarcely and remain largely in a qui-

escent state. In response to inflammatory signals that coordinate regeneration such as under infection or chemotherapy exposure, LT-HSCs become activated (Olson *et al.*, 2020). When regenerative signalling becomes hyperactivated, differentiation can be prioritized over self-renewal, leading to the loss of the LT-HSCs compartment. Opposite, in conditions in which differentiation is inhibited and self-renewal prioritized, because of somatic mutation or environmental cues, the HSCs compartment becomes hyperplastic at the expense of effective maintenance of blood production. In both cases, the hematopoietic system becomes exhausted, leading ultimately to BM failure.

1.2.2. HSCs location in healthy bone marrow microenvironment

The BM is therefore the natural location of HSCs during adulthood. The specialized microenvironments in which these cells rely on are broadly referred to as niches. BM niches supply essential and dynamic autocrine, endocrine, and paracrine soluble signals as well as direct cell-to-cell interactions and physico-chemical stimuli that influence the production of different blood cells and regulate HSCs fate (Galán-Díez, Cuesta-Domínguez, and Kousteni 2018). During the past decades, the understanding of the HSCs niches and BM microenvironment has enlarged, mainly due to research done in mouse samples, since the study of human BM samples with preserved anatomy (BM biopsies entail complications for the patient and have been almost completely replaced by BM aspirates in clinical procedures) is still challenging. However, some aspects remain controversial. In the BM niche, different HSCs with diverse differentiation biases (myeloid versus lymphoid) or different fates (quiescent versus activated) have been located in different anatomical sites, so, it is considered that spatially different niches exist for each of them (Méndez-Ferrer et al. 2020).

The main differentiated niches in the BM are distinguished based on anatomical criteria. Therefore, and despite controversies, it seems clear that at least two main different HSCs niches exist. The endosteal BM niche (EBMN) in the

endosteum and with low vascularity (few arteries and arterioles) and the central BM niche (CBMN) with higher vasculature, arterioles, and sinusoids, and enriched in HSCs in the distinct perivascular areas. In both niches endothelial cells, different stromal cells of mesenchymal origin, neurons or Schwann cells and mature blood or immune cells critically maintain and regulate HSCs location, number and fate. Other factors as oxygen tension, shear flow or reactive oxygen species (ROS) abundance also govern HSCs fate.

The CBMN comprises >90% of the BM volume and shelters 85% of the HSCs. Genotoxic stress or myeloablation damages the CBMN. It contains most sinusoids and arterioles. Specific and differentiated functions are linked to arteriolar (aBMN) or sinusoidal (sBMN) BM niches. However, these differences remain still controversial, as different results have been published by different laboratories. Sinusoidal areas are related with myelopoiesis, they lodge early myeloid progenitors (CMPs), and steady state hematopoiesis. More active HSCs and its transmigration and egression to blood has been localized in this sBMN, however quiescent HSCs can also be found. Differences in cellularity and physicochemical properties between sinusoidal an arteriolar niche determine their different functionality.

The EBMN seems to be a much smaller niche (less than 10% of total BM volume) with 15% of the total HSCs population. Several signals in this niche are related with the promotion of HSCs quiescence, which is essential to preserve their self-renewal and to guarantee the steady state hematopoiesis normalcy through lifespan. The endosteal niche has shown to be resistant to genotoxic stress and myeloablation. It is related with lymphopoiesis and harbours early lymphoid progenitors (CLPs). HSCs isolated from this region show higher proliferative potential as well as better long-term hematopoietic reconstitution potential (Méndez-Ferrer et al. 2020).

1.2.3. Bone marrow resident cells

The BM harbours several key cell types that contribute to hematopoiesis by direct or indirect interaction with HSCs. Figure 4 summarizers BMN interactions discussed in this section.

1.2.3.1. Mesenchymal stem cells

Mesenchymal stem cells (also known as mesenchymal stem and progenitor cells (MSCs)) are a multipotent population of cells able to produce mesenchymal lineage cells such as bone-forming cells (osteoblasts), fat cells (adipocytes) and cartilage cells (chondrocytes). These cells are important in healing and regeneration processes of the mentioned tissues, present immunomodulatory properties, and have a relevant role as niche-forming cells that critically maintain and regulate HSCs. MSCs can be found in many organs of the body, including the BM where they are defined by a set of different markers such as nestin (Nest), neural glial antigen 2 (NG-2), leptin receptor (LepR) or paired related homebox 1 (Prx-1).

Many subsets of BM-resident cells with MSC-like properties have been implicated in hematopoietic function. They present heterogeneous differentiation degree and surface markers pattern. Some works suggest that the different subpopulations are in differentiated anatomical locations and secrete determined HSCs supporting factors, such as CXC motif chemokine ligand 12 ((CXCL-12) also referred as stromal cell-derived factor 1 (SDF-1)), angiopoietin 1 (ANG-1) or stem cell factor (SCF). In adult human BM, MSCs can be enriched for the $lin^{-}/CD45^{-}/CD271^{+}/CD140a^{-/low}$ population where CD146 expression appears to discriminate perisinusoidal ($CD146^{+}$) from endosteal or periarteriolar ($CD146^{-/low}$) MSCs. Although it is difficult to enlighten the MSCs heterogeneous population into clearly delimitated subpopulations, it seems to be agreement about two main differentiated populations: LepR expressing (LepR+) cells, associated with perisinusoidal locations and the Nest expressing (Nest+) cells, located in proximity of arterioles and transition zone vessels.

LepR+ cells (Nest-GFP^{lo} LepR^{+}) express the LepR, which is a well-established marker for MSCs. Both LepR+ and CXCL-12 abundant reticular (CAR) cells (discussed below) are located mainly overlapping around the sinusoids and are a major source of growth factors crucial for the maintenance of HSCs. CAR cells are a subset of MSCs named for its high expression of CXCL-12. Most of the CAR cells that are in perivascular areas, are also LepR+ cells. This fact has led to the CAR cells often being termed in conjunction with the LepR+ cells (Nest-GFP^{lo} LepR^{+} CAR MSCs) in the context of the HSCs niche (Méndez-Ferrer et al. 2020; R. Kumar, Godavarthy, and Krause 2018; Galán-Díez, Cuesta-Domínguez, and Kousteni 2018).

1.2.3.2. Bone cells

Osteoblasts (OBs) are bone-forming cells that constitute the interface between calcified bone and the EBMN. They secrete vesicles containing concentrated calcium and phosphate for matrix mineralisation and are responsible for bone synthesis. OBs arise from MSCs because of Wnt/β-catenin signalling, during their differentiation process, they experience a morphological shift from spindle shaped to large cuboidal cells with large nuclei, extensive endoplasmic reticulum, and enlarged Golgi apparatus. Active OBs also secrete collagen I (COL I) and other matrix proteins. Following bone formation activity, OBs either apoptose, become osteocytes (90% of mature bone cells), or become flattened bone lining cells that form the endosteum, which are thought to be quiescent OBs (Clarke 2008).

OBs can also regulate HSCs number and function. Recent studies suggest that OBs regulation of hematopoiesis may depend on their differentiation state (Galán-Díez, Cuesta-Domínguez, and Kousteni 2018), thereafter in the past decade contributions of the osteoblastic niche to HSCs maintenance has been viewed critically, as a result of the heterogeneity amongst the OBs population and their varying degree of differentiation state. Recently this problem has been overcome using proximity-based single cell approaches that uncover the molecular heterogeneity among osteolineage cells. Thereby, the

RNase angiogenin, interleukin 18 (IL-18) and embigin were identified as regulators of HSCs quiescence produced by OBs (R. Kumar, Godavarthy, and Krause 2018). Furthermore, several other mechanisms participate in OBs and HSCs crosstalk. OBs produce cytokines and growth factors that regulate HSC fate. For example, ANG-1 interacts with ANG-1 receptor ((TIE-2) also known as CD202B) on HSCs to promote quiescence and adhesion. Expression of thrombopoietin (TPO) by OBs has been involved in the regulation of LT-HSCs quiescence (Galán-Díez, Cuesta-Domínguez, and Kousteni 2018). OBs also appear to regulate HSCs homing and engraftment in the EBMN after HSCs transplantation. In the case of osteocytes, as they are entrapped in the calcified bone matrix, their effect on the HSCs pool may not be direct but rather through the endosteal OBs. Osteocytes have been involved in the control of HSCs through the secretion of granulocyte-colony stimulating factor (G-CSF). Furthermore osteoclasts (OCs), bone degrading cells of monocytic origin, also affect hematopoiesis (Galán-Díez, Cuesta-Domínguez, and Kousteni 2018).

1.2.3.3. Endothelial cells

Endothelial cells (ECs) form the lining of all blood vessels, in a sheet termed the endothelium. In capillaries and sinusoids, which are abundant in the BM vascular system, the vessels consist entirely of endothelial cells, basal lamina, and pericytes. As such, they are a major constituent of the BM microenvironment. Sinusoids are highly fenestrated venous vessels, and are hence the main conduit for HSC egress from the BM. Also present are arterioles, small vessels that link arteries with capillary networks. In the BM microenvironment, ECs define a physical barrier that mediates the extramedullary exchanges of oxygen, nutrients and soluble factors, but also prevents BM entry of mature erythrocytes and thrombocytes from circulation and regulates cellular trafficking, hematopoiesis and osteogenesis (Itkin et al. 2016). BM ECs are phenotypically distinct from those found in the microvasculature of other organs, as they constitutively express cytokines and adhesion molecules.

They also exhibit specific binding affinity for CD34+ progenitors and megakaryocytes, indicating a role in regulating hematopoiesis. In the specialized perivascular microenvironments ECs regulate HSCs fate and maintenance by direct cell contact as well as by the secreted factors; additionally, different permeability properties of the blood vessels from different niches contribute to this regulation (R. Kumar, Godavarthy, and Krause 2018).

In agreement with the MSCs division between arteriolar or sinusoidal located cells, arteriolar (aECs) and sinusoidal ECs (sECs) present phenotypical and anatomical differences that determine its differentiated functionalities (Itkin et al. 2016). Therefore, arterioles arise in less permeable blood vessels than sinusoids. A functional consequence of high permeability is that exposure to blood plasma increases ROS intracellular levels in HSCs, augmenting their migration capacity (by the activation of cellular motility machinery) while compromising their self-renewal and survival potential, namely hampering quiescence, and accelerating their differentiation and exhaustion. Consequently, sinusoids promote HSCs activation and lodge immature and mature leukocyte trafficking to and from the BM, while lower frequencies of ROS^{high} HSCs have been found adjacent to arterioles.

1.2.3.4. Neurons and non-myelinating Schwann cells

The sympathetic nervous system (SNS) consists of various types of nerve fibres. It has emerged as a regulator of the BM niche as it is involved in BM structure and function. The SNS controls HSCs egress from the BM and bone remodelling among other functions. Signal transduction is non-synaptic and involves intercellular junctions. Non-myelinating Schwann cells (nmSCs) in sBMN regulate migration of HSCs through sinusoids by direct contact (Méndez-Ferrer et al. 2020). While Nest expressing non-myelinating Schwann cells (Nest+nmSCs) maintain hibernating HSCs in aBMN, contributing to metabolically “low” microenvironments (Itkin et al. 2016). Additionally, nmSCs associated with sympathetic nerve fibres can promote HSCs quiescence by activating latent transforming growth factor β (TFG-β) in endosteal or central BM niches (Galán-Díez, Cuesta-Domínguez, and Kousteni 2018).

But also, sympathetic nerves release soluble mediators as catecholamines from terminals. Noradrenaline, for example reduces CXCL-12 production by different niche-forming cells (Morikawa and Takubo 2017) inducing HSCs activation.

1.2.3.5. Relevant mediators of intercellular communication

Several of the intercellular communications described above are mediated by different secreted or transmembrane mediators compiled in Table 1. As an example, the pathway downstream of CXCL-12 and its receptor CXC chemokine receptor type 4 ((CXCR-4) also known as fusin or CD184) is of great relevance for normal hematopoiesis, as CXCL-12–CXCR-4 axis is responsible for the retention of HSCs in the BM and for the maintenance of HSCs quiescence by various niche cells.

Table 1. Summary of the main soluble and transmembrane mediators of cell communication in BMN.

Factor	Soluble or secreted / transmembrane	Type of molecule	Cell producing it and its specific niche location	Effect and receptor cell
TGF-β (transforming growth factor β)	soluble	growth factor	nmSCs in CBMN and EBMN Megakaryocytes in CBMN-sinusoidal	Promotes HSCs quiescence.
SCF (stem cell factor)	soluble or transmembrane	cytokine	OBs in EMBN LepR+MSCs in CBMN-sinusoidal Nest+MSCs in CBMN-arteriolar	HSCs maintenance.
CXCL-12 / SDF-1 (CXC motif chemokine ligand 12 / stromal cell-derived factor 1)	soluble	chemokine protein	OBs in EMBN ECs LepR+MSCs in CBMN-sinusoidal Nest+MSCs in CBMN-arteriolar CAR cells	HSCs homing, retention, and repopulation. HSCs maintenance and self-renewal regulation. Maintenance of B-cell lymphopoiesis.
TPO (thrombopoietin)	soluble	cytokine	OBs in EMBN Megakaryocytes in CBMN-sinusoidal	Regulation of LT-HSCs quiescence. HSCs maintenance.

FGF-2 / bFGF (fibroblast growth factor 2 / basic fibroblast growth factor)	soluble	polypeptide	ECs	HSCs maintenance and self-renewal.
VEGF-A (vascular endothelial growth factor A)	soluble	dimeric glycoprotein	ECs	HSCs maintenance and self-renewal.
TSP-1 / THBS-1 (trombospondin-1)	soluble	adhesion glycoprotein	ECs	HSCs maintenance and self-renewal.
PF-4 / CXCL-4 (platelet factor 4 / chemokine C-X-C motif ligand 4)	soluble	cytokine	Megakaryocytes in CBMN-sinusoidal	HSCs quiescence.
ANG-1 (angiopoietin-1)	soluble	glycoprotein	OBs in EBMN ECs	HSCs quiescence and adhesion. HSCs maintenance and self-renewal.
OPN (osteopontin)	soluble	glycoprotein matrix component	OBs in EBMN	HSCs migration and retention. HSCs proliferation and differentiation.
G-CSF (Granulocyte-colony stimulating factor)	soluble	glycoprotein cytokine and hormone	OBs in EBMN and Osteocytes	Supports myelopoiesis.
ANXA-2 (annexin A2)	transmembrane	protein	OBs in EBMN ECs	HSCs homing and engraftment.
RNse angiogenin	soluble	ribonuclease (protein)	OBs and MSCs	HSCs quiescence.
IL-18	soluble	cytokine interleukin	OBs and MSCs	HSCs quiescence
Embigin	transmembrane	immunoglobulin (adhesion molecule)	OBs and MSCs	HSCs quiescence.
IL-7	soluble	cytokine	MSCs	Maintenance of B-cells lymphopoiesis.
Catecholamines: epinephrine, norepinephrine, dopamine	soluble	(organic compounds)	Blood stream or as neurotransmitter in nerve endings	HSCs transmigration.

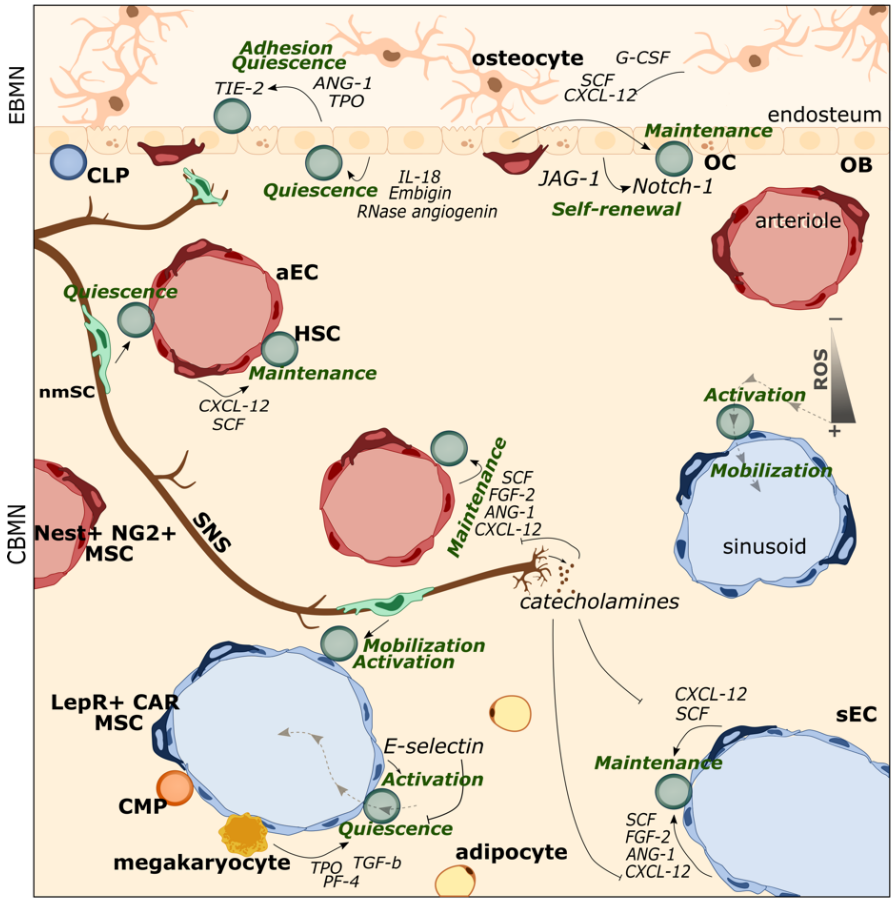

Figure 4. Scheme of healthy bone marrow niche (BMN). Representation of cell populations (bold text) and their locations in BMN; main cell-cell interactions by direct contact and soluble factors and their role in HSC homeostasis (green) are detailed. Abbreviations: EBMN, endosteal bone marrow niche; CBMN central bone marrow niche; ROS, reactive oxygen species; HSC, hematopoietic stem cell; CMP, common myeloid progenitor; CLP, common lymphoid progenitor; aEC, arteriolar endothelial cell; sEC, sinusoidal endothelial cell; LepR+ CAR MSCs, leptin receptor expressing cells and abundant reticular mesenchymal stem cells; Nest+ NG2+ MSCs, nestin and neural glial antigen expressing mesenchymal stem cells; SNS, sympathetic nerve fiber; nmSCs, non-myelinating Schwann cells; OBs, osteoblasts; OCs, osteoclasts; CXCL-12, CXC motif chemokine ligand 12; SCF, stem cell factor; ANG-1, angiopoietin 1; TIE-2, angiopoietin receptor; IL-18, interleukin 18; FGF-2, fibroblast growth factor 2; TGF-β, transforming growth factor beta; TPO, thrombopoietin; PF-4, platelet factor 4; JAG-1, Jagged-1; G-CSF, granulocyte-colony stimulating factor. Adapted from (Clara-Trujillo, Gallego Ferrer, and Gómez Ribelles 2020)**.**

1.2.3.6. Non cellular elements

Non cellular elements as oxygen levels are also niche factors that differentially affect HSCs among different niches. The hematopoietic compartment is relatively hypoxic. Oxygen levels in the periosteum region, where arterioles are enriched, is higher than in the perisinusoidal region located in the central BM (Morikawa and Takubo 2017; R. Kumar, Godavarthy, and Krause 2018). Hypoxia contributes to HSCs pluripotency maintenance by different mechanisms as the reduction of intracellular ROS. Cutting-edge imaging technics have allowed to confirm that HSCs maintain their hypoxic condition independently of their distance from vasculature, and that HSCs utilize the cellular hypoxia response system to maintain quiescence and glycolytic metabolic properties. This hypoxic profile has been linked to the presence of the transcription factor hypoxia inducible factor 1α (HIF-1α).

1.2.3.7. Extracellular matrix

The ECM produced by niche cells plays a role in BM niche formation (Radhakrishnan et al. 2020). Most abundant proteins in BM ECM are fibronectin (FN), collagens (COL) from I to XI, tenascin, osteopontin, thrombospondin or elastin. Also important are proteoglycans presenting glycosaminoglycan side chains as hyaluronic acid (HA), chondroitin sulfate (CS), heparan sulfate or heparin. These molecules have shown to provide more than just structural integrity. Their signalling trough cell-matrix interactions has demonstrated regulatory effect over niche-forming cells and HSCs. This signalling is mediated by transmembrane proteins as integrins, as well as by membrane bound immunoglobulins like intercellular adhesion molecule-1 (ICAM-1) or vascular adhesion molecule-1 (VCAM-1) (Klamer and Voermans 2014; R. Kumar, Godavarthy, and Krause 2018). Adhesion of HSCs to ECM molecules contributes to the BM niche and regulates HSCs maintenance.

Mechanical properties of BM are at great extent determined by ECM composition and have also shown to affect cell fate decision (Cantini et al. 2020).

Matrix density and biophysical properties, like specific presentation of adhesion ligands, contribute to HSCs niche modulation, there is still controversy about the mechanisms mediating this effect and the possibility of it being either under a direct or an indirect regulation. ECM density and components also modulate cell-cell direct communications in an indirect manner by means of conditioning secreted factors availability and presentation to cells (Klamer and Voermans 2014). Hence, the ECM acts as a surface for secreted cytokines and growth factors and cells to adhere to, enabling gradients to be established, and defines the complex 3D architecture of the BM, which has fundamental importance for the control of cell behaviour. Because of that, any attempt at physiological replication of the BM must incorporate this structure.

1.2.4. Hematological malignancies and their relationship with their microenvironment

Hematological malignancies are a collective term for neoplasic diseases of the hematopoietic and lymphoid tissues with clinical presentation as leukemia, lymphoma or myeloma (Lichtman 2008). Hematological malignancies are categorized depending on cell origin, maturation or tumor characteristics (Lichtman 2008). The World Health Organization (WHO) published a unified classification of neoplasic diseases of the hematopoietic and lymphoid tissues (Harris et al. 2000; Arber et al. 2016). In relation to the cell types primarily affected, two major classes can be found: myeloid neoplasms or lymphoid neoplasms. And then, rare histiocytic, dendritic or mast cell neoplasms. Each of these major groups is categorized in different subclasses, the most common of which are summarized in Figure 5.

Leukemias, lymphomas, and myelomas share some common features, but there are major differences among them. Leukemia (a term derived from the greek words “leukos” and “heima”) refers to an excess of leukocytes in the body and is originated within the BM. It can arise in either of two main groups (lymphocytes or myelocytes) and can be acute (a rapidly progressing form in which affected cells are very immature and unable to accomplish their func-

tion) or chronic (which progresses slowly from cells that are relatively differentiated but crudely functional). Lymphoma involves lymphocytes and is initiated in lymphoid tissues. Non-Hodgkin lymphoma is the more prevalent form, with the more indolent forms which progresses slowly with well differentiated cells and the more aggressive forms with less differentiated lymphocytes. Myeloma are plasma cells disorders characterized by clonal proliferation of malignant cells normally in the BM (Palumbo and Anderson 2011). In leukemia, the cancerous cells are discovered circulating in the blood and bone marrow, while in lymphoma cells tend to aggregate and form tumors in lymphatic tissues, and myeloma is mainly a tumor of the BM.

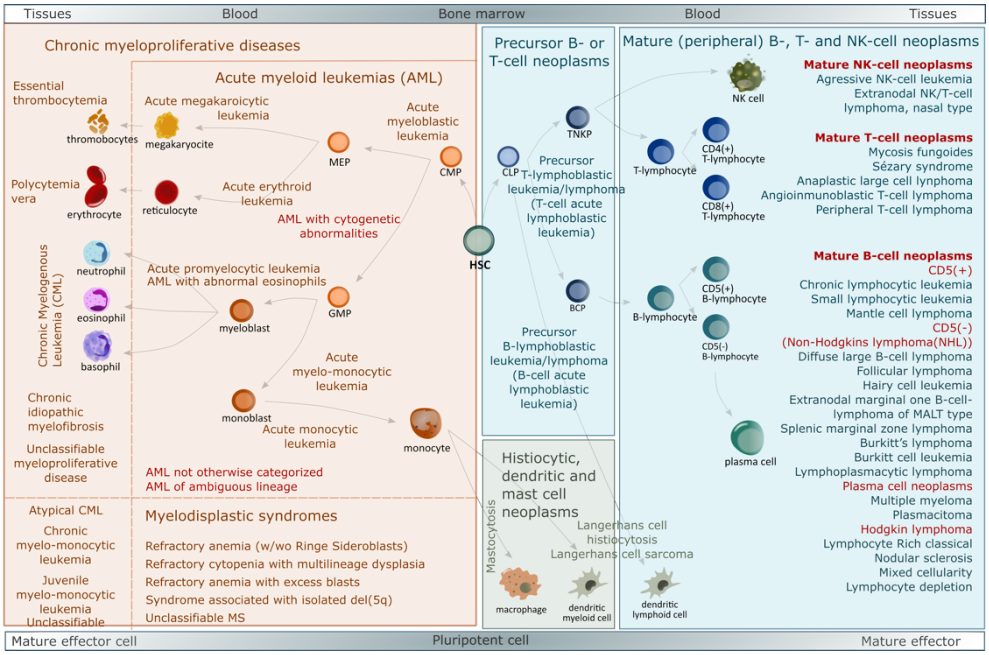

Figure 5. BM hematopoiesis together with the simplified WHO classification of neoplastic diseases of the hematopoietic and lymphoid tissues. Blue box contains lymphoid neoplasms, orange box myeloid neoplasms and green box rare histiocytic, dendritic or mast cell neoplasms. Abbreviations: del, deletion; HSC, hematopoietic stem cell; CMP, common myeloid progenitor; CLP, common lymphoid progenitor; MEP, megakaryocyte-erythrocyte progenitor; GMP, granulocyte-monocyte progenitor; TNKP, T-natural killer cell progenitor; BCP, B cell progenitor; NK, natural killer. Source: (Clara-Trujillo, Gallego Ferrer, and Gómez Ribelles 2020).

Thus, BM is the “home” of HSCs as well as of partial or terminal differentiated blood, immune and stromal cells from different origins. However, it is likewise the home of some malignant processes that can develop there. Multiple and intricate interactions arise to maintain HSCs physiology but also the pathophysiology of hematological malignancies. Hematological malignancies can alter de BMN and its normal interactions with HSCs to make it more affable for malignant progression. Although it is unclear if on hematological malignancies the main role of BMN is tumor initiation or progression, results obtained by different authors point out that these roles coexist since they are not mutually exclusive (Méndez-Ferrer et al. 2020). We will go back to this point below in more detail.

1.2.4.1. Competition between HSCs and tumor cells in the BMN

Different experimental mouse models have shown that malignant cells compete with HSCs for BMN occupancy during the progression of the disease, this competition disrupt normal interactions between HSCs and their BMN, hampering HSCs population and disturbing normal hematopoiesis. This also applies to solid tumors that metastasize to the BM. The dependence of malignant cells on canonical HSCs niche pathways, as the above mentioned CXCL-12-CXCR-4 axis, is one example. Final stages of this escalating competition can lead to the protection of transformed cells from chemotherapy and even to relapse of the disease. For instance, in models of acute lymphoblastic leukemia (ALL) residual leukemia cells persisted after chemotherapy by residing in specialized niche that was dependent on the production by leukemic cells of chemokine ligand 3 (CCL3) and TGF-β (Galán-Díez, Cuesta-Domínguez, and Kousteni 2018). However, studies have shown that upon disease progression, transformed cells become progressively independent of BMN control.

1.2.4.2. BMN as predisposition factor for tumor initiation

Several studies report that acquisition of mutations or functional alterations by BMN-forming cells predispose for malignancy development, meaning that

certain hematological malignancies can originate in the niche itself or that concomitant mutations of pre-malignant cells can be raised by BMN contributing to disease initiation. These so-called niche-driven transformations have been proposed to occur mainly in myeloid malignancies, whereas different studies reported genetic alterations of BMN-forming cells in mice can cause myelodisplasic syndrome (MDS) or myeloproliferative neoplasms (MPN), both considered pre-leukemic disorders with high risk of transformation to secondary leukemias. Osteolineage cells have shown to act in certain hematological malignancies as leukemia-initiating cells. First indication of the niche as a tumor initiating factor was provided by two studies reporting that genetic ablation of the tumor suppressor gene retinoblastoma (Rb) or retinoic acid receptor γ (Rar_{γ}) in mouse induced MPN-like syndrome (Walkley et al. 2007), despite, MPN development required the inactivation of either one of these genes in both, the hematopoietic cells and the BMN-forming cells. These discoveries presented for the first time the niche as a required component for the initiation of MPN. This observations among others suggest that genetic alterations in BMN-forming cells can initiate multistep pathways trough myeloid malignancies (Galán-Díez, Cuesta-Domínguez, and Kousteni 2018).

All these studies have the pro-inflammatory environment as shared factor. For example, development of MPN from Rar_{γ} mutations on niche and hematopoietic cells needs increased levels of tumor necrosis factor (TNF), a fundamental cytokine involved in systemic inflammation (Méndez-Ferrer et al. 2020). This fact is of great relevance as inflammation is a hallmark of aging, and myeloid malignancies are more prevalent among elderly people, implying that inflamed-like BMN might have implications as tumor initiating factor. In the BM of aged mice, the EBMN has been reported to be reduced, while CBMN and capillaries increase its presence, observation that concurs with the impairment of lymphopoiesis in favour of myelopoiesis that arises with aging. Consequently, some authors propose that ageing of the microenvironment might facilitate the growth of pre-malignant clones by overstimulating myeloid cells expansion, what can lead through the development of myeloid malignancies. That would mean that myeloid malignancies may develop over

many years as a continuous process involving the emergence of clonal somatic mutations in hematopoietic cells that in certain conditions can manage to clonal hematopoiesis, MPN, MDS or even secondary leukemias. It is still ambiguous why HSCs carrying these mutations persist in the BMN many years as small indolent mutant clones, since if the acquired mutations confer growth or survival advantage the mutant cells should become enriched. However, the clonal selection hypothesis must be understood in conjunction with the microenvironment, what means that probably mutations that provide no advantage under a healthy microenvironment may confer advantage in the atmosphere of a pathological microenvironment (Méndez-Ferrer et al. 2020; Galán-Díez, Cuesta-Domínguez, and Kousteni 2018).

1.2.4.3. BMN remodelling and BMN-forming cells reprogramming by malignant cells

Malignant cells alter the transcriptome, proteome and function of BMN-forming cells by means or secreted factors besides direct cell-to-cell contact. Exosomes, extracellular vesicles that contain constituents as DNA, RNA or proteins from cells that secret them are also important mediators in this crosstalk (Litwińska, Łuczkowska, and Machaliński 2019). In general terms the intricate network of cross talk between malignant and niche cells seems to reprogram cells and remodel the BMN towards angiogenesis and pro-inflammatory environments that ultimately lead to disease progression. MSCs, adipocytes, OBs, ECs and sympathetic neurons or their associated Schwann cells become affected. The result seems to be a landscape whereby alterations of the BMN contribute to malignancy progression over long periods of time synergistically with the accumulation of driver mutations in HSCs. These BMN-forming cells reprogramming has been described in both, myeloid and lymphoid malignancies.

1.2.4.4. Transformed BMN favours malignancy

Once transformed, BMN can favour malignancy though different mechanisms. The activation of survival pathways is one of these mechanisms that

is tightly related with pro-inflammatory pathways like nuclear factor κB (NFκB) pathway. This pathway is a common survival pathway in some lymphoid malignancies as chronic lymphoid leukemia (CLL), B cell acute lymphoid leukemia (B-ALL) or mantle-cell lymphoma (Hellmich et al. 2020).

Protection from excessive ROS is a different mechanism by which altered BMN protect malignant cells and promote survival and chemoresistance. Using *in vitro* co-culture models, it has been shown that BMN-forming altered cells provide CLL or B-ALL cells with cysteine. This amino acid is used by malignant cells for production of the tripeptide glutathione used for ROS detoxification. The ability of tumoral cells for ROS detoxification is key for their survival, as several chemotherapy effectiveness relies on ROS-induced DNA damage (Yao and Link 2017).

The adhesion molecule CD44 has shown important role in interaction of malignant cells with the BMN in myeloid malignancies as multiple myeloma, chronic myeloid leukemia (CML) or acute myeloid leukemia (AML). CD44 binding with its receptor E-selectin of the ECs mediates homing and engraftment of the malignant cells and enhanced drug resistance. Likewise, β1 integrins mediate adhesion to VCAM-1 or ICAM-1 molecules on stromal cells and induce CML cells adhesion to BMN. In AML, interaction between α4β1 integrin and VCAM-1 mediate chemoresistance towards activation of NFκB pathway in stromal cells. Consequently, several studies report how the blockade of these interactions may help in sensitization of malignant cells to conventional chemotherapy. In fact, the ultimate approaches for clinical treatment of hematological malignancies are combined therapies that not only attack malignant cells but also the altered BMN or more specifically the crosstalk between supporting and malignant cells (Méndez-Ferrer et al. 2020).

1.3. Multiple myeloma

Multiple myeloma (MM) is a malignancy that develops from an accumulation of terminally differentiated and antibody-producing monoclonal plasma cells

(PCs) in the BM. Represents 1% of all cancers and is the second most prevalent hematological malignancy worldwide, accounts 10% of all hematological malignancies (Pinto et al. 2020). Generally appears associated with the elderly, with a median onset of 60 years, although young patients have also been diagnosed (Pinto et al. 2020; Nass and Efferth 2018). In the last decades, better understanding of the pathobiology and heterogeneity of the disease has led to an improvement of the available treatments and thus translated into an increase of the median overall survival from 2-3 years to 8-10 years (S. K. Kumar et al. 2014). However MM remains still as an incurable disease, as most patients eventually relapse and even become refractory to existing therapies (Vijay Ramakrishnan and Souza 2016; Hu and Hu 2018).

MM is characterized by aberrant proliferation and BM infiltration of monoclonal PCs that overproduce monoclonal immunoglobulin that can be found in the blood and/or urine of patients. Accumulation of these inmunoglobulins will cause organ dysfunction, usually referred to as C-R-A-B (hypercalcemia, renal insufficiency, anemia and bone lesions) and at this stage patients will become symptomatic (Pinto et al. 2020). Thereby, MM is the final step of a multistage neoplasic transformation of PCs that is well recognized to evolve from a monoclonal gammopathy of undetermined clinical significance (MGUS) that progresses to smoldering myeloma (SMM), which finally will lead to symptomatic myeloma (Hu and Hu 2018) (Figure 6). The pre-malignant stage MGUS is present in over 3% of the population above of 50 years (Rajkumar 2020).

Pathogenesis of the disease is complicated as it is a biologically heterogeneous disease in which different elements contribute in a tangled way in disease initiation and progression. Changes in the BMN cellular and non-cellular components, genetic alterations as chromosome translocations, soluble mediators as cytokines and epigenetic changes are some of these factors.

All these mechanisms are complex by themselves, and moreover, interactions and crosstalk among them. The complicated regulation of MM pathophysiology leads ultimately to treatment failure and clinical relapse of the patients. Multi-drug resistance (MDR) is the process whereby the MM cells

become resistant to a wide variety of structurally and functionally unrelated anticancer drugs and their combinations. Initially, most patients respond effectively to initial induction therapy, however in time all patients relapse (Nass and Efferth 2018). All these complications have established the need for individualized treatments for patients with different underlying disease mechanisms.

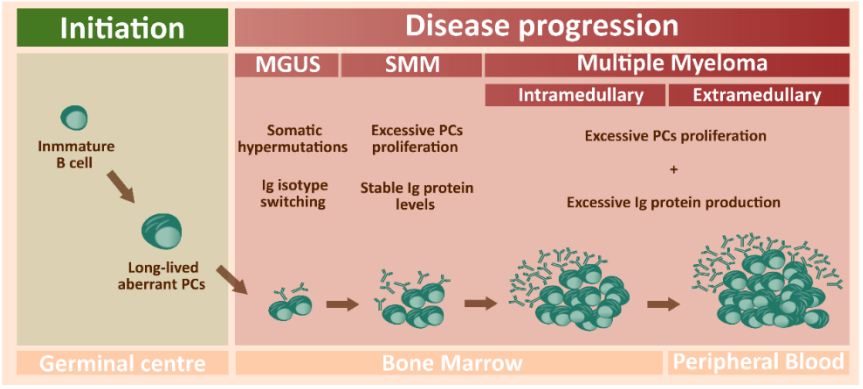

Figure 6. Multiple myeloma (MM) development and progression. The disease is the end stage of a multistep neoplastic transformation of PCs. MM initiates as a monoclonal gammopathy of undetermined significance (MGUS). The presence of abnormal amounts of PCs in the BM with slightly increased levels of immunoglobulins proteins but no clinical symptoms is defined as smoldering multiple myeloma (SMM). Nevertheless, these hyperproliferative PCs will endure additional secondary genetic mutations that aggravate this aberrant phenotype leading to the accumulation of high amounts of PCs in the BM and consequently to the secretion of excessive levels of immunoglobulins towards the blood stream. Ultimately, this will lead to MM. This disease may progress to extramedullary disease in more advanced stages.

1.3.1. Signaling pathways that sustain MM cells abnormal proliferation

The sum and interaction of genetic defects within the tumour and the interactions between MM cells and the BMN lead to the activation of signalling pathways that promote the expansion of the malignant clones and enhance their survival and drug resistance (DR). These signalling pathways include phosphatidyl-inositol-3-kinase (PI3K)/protein kinase B (PKB or Akt)/mammalian

target of rapamycin (mTOR) pathway, Ras/Raf/MEK/ extracellular signal regulated kinase (Erk) pathway, Janus kinase (JAK)/ signal transducer and activator of transcription (STAT) pathway, NFκB pathway and Wnt/β-catenin pathway (Donk, Lokhorst, and Bloem 2005).

1.3.1.1 The NFκB pathway

The NFκB is a family of transcription factors formed by 5 transcription factors: RelA/p65, RelB, c-Rel, p50, and p52. This family of proteins is characterized by the presence of a N-terminal Rel homology domain (RHD) that is essential for dimerization, nuclear translocation, and DNA binding. p50 and p52 are synthesized as larger inactive precursor proteins p105 and p100, respectively, and then undergo proteolytic processing in the C-terminal to yield the smaller active proteins. RelA, Rel B, and c-Rel contain a transcription activation domain, which is absent in p50 and p52, this implies that p50 and p52 can activate transcription only when they form dimers. In unstimulated cells, the NFκB proteins are retained in the cytoplasm by a family of proteins called inhibitory κB (IκB). This definition of the pathway allows its regulation without the need of protein synthesis, simply by the proteasome mediated degradation of IκBs proteins (Vrábel, Pour, and Sabina 2019). In unstimulated nucleated cells, NFκB is in its latent form bound to one of its IκBs. The activation of the pathway by external or internal stimulus can led to its activation by 2 different pathways (Figure 7, e):

- The canonical pathway can be induced by a large group of molecules, including inflammatory cytokines, pathogen-associated molecules, and antigen receptors. Typical stimulating ligands are tumour necrosis factor α (TNFα), lipopolysaccharides, or interleukin-1β (IL-1β); also, B-cell activating factor (BAFF) and a proliferation-inducing ligand (APRIL), which are two of the most important MM survival factors. This stimulation leads to recruitment of adaptors, to the cytoplasmic domain of the different receptors and activation of IκB kinase (IκK) complex. Canonical IκK complex consists of three subunits. Two catalytically active kinases IκKα and IκKβ, and regulatory subunit known as

NFκB essential modulator (NEMO) or IκKγ. Activated complex phosphorylates IκB proteins and allows its subsequent ubiquitination that marks IκB for degradation in the proteasome. This enables translocation of NFκB complex to the nucleus, where it can stimulate expression of its target genes. The canonical pathway activates NFκB dimers combining RelA, c-Rel, RelB and p50 (Vrábel, Pour, and Sabina 2019).

- The non-canonical, or alternative, pathway that can be induced only by a small set of cytokine stimuli, which includes CD40L, LTβ (lymphotoxin β), BAFF, RANKL (receptor activator of NFκB ligand) and TWEAK (TNF-related weak inducer of apoptosis). Mediates, predominantly, the activation of p52/RelB dimer. It is based on inducible processing of p100 precursor proteins that requires proteasomal processing, in contrast to the degradation of IκB proteins in the canonical pathway. The initial stimulation is followed by activation of the NFκB inducing kinase (NIK) that allows the activation of the IκK complex. Kinase part of IκK complex of non-canonical pathway is formed only by IκKα subunits that selectively phosphorylate and processes p52 precursor p100. Phosphorylation of p100 results in its degradation in proteasome. This process generates functional p52 protein, which is subsequently able to dimerize with RelB and translocate to the nucleus, where it regulates its target genes (Vrábel, Pour, and Sabina 2019).

In MM some different mechanisms led to sustained activation of this pathway. Stimuli such as paracrine secretion of BAFF or APRIL by BMN-forming cells or autocrine production of TNFα by MM cells. Also, up-regulation in the expression of receptors such as B-cell activating factor receptor (BAFFR) or tumour necrosis factor receptor (TNFR) on MM cell surfaces contribute to this over-activation by both, the canonical and non-canonical pathways. This activation enhances MM cells survival, promotes angiogenesis and metastasis, and hampers apoptotic signalling in MM cells. In addition to increased cytokines that activate NFκB activity, mutations, deletions, and gene rearrangements have been shown to occur in a plethora of genes involved in these pathways, (Nass and Efferth 2018; Vijay Ramakrishnan and Souza 2016; Hu

and Hu 2018; Donk, Lokhorst, and Bloem 2005). The NFκB pathway is a central and important signalling pathway that promotes MM cell viability and resistance to apoptosis, and it has been suggested that blocking both, the canonical and the non-canonical pathway, is important in order to induce durable responses in patients (Vijay Ramakrishnan and Souza 2016).

1.3.1.2. The PI3K/Akt/mTOR pathway

The PI3K/Akt/mTOR (Figure 7, b) is a pivotal pathway that gets initiated through the association of several cytokines (such as insulin growth factor 1 (IGF-1), IL-6, vascular endothelial growth factor (VEGF), IL-1β, SDF-1) with their cell surface receptors. Once activated, the cell surface receptors activate PI3K, and this activation results in the generation of phosphatidylinositol (3,4,5)-trisphosphate (PIP_3), a phospholipid that will bind Akt and induce its translocation to cell membrane, where Akt will become activated by phosphorylation mediated by inositide-dependent protein kinase 1 and 2 (PDK1 and PDK2). Akt (also known as PKB) is a serine-threonine kinase that plays a key role in multiple cellular processes such as glucose metabolism, apoptosis, cell proliferation, transcription, or cell migration. Once Akt gets activated, it promotes cell proliferation, anti-apoptosis, and metabolism signals leading to tumor growth and survival (Vijay Ramakrishnan and Kumar 2018; Nass and Efferth 2018; Hu and Hu 2018; Donk, Lokhorst, and Bloem 2005). One downstream target of Akt is mTOR, an atypical serine/threonine kinase that is present in two distinct multiprotein complexes: mTOR complex 1 and 2 (mTORC1 and mTORC2). The catalytic member of both these complexes is mTOR. mTORC1 and mTORC2 participate in complex feedbacks that regulate the levels of activated Akt. mTORC1 promotes protein synthesis, glycolysis and inhibits autophagy. In addition, activated mTORC1 causes feedback inhibition of the PI3K/Akt pathway. mTORC2 phosphorylates Akt and modulates survival and cell cycle progression signals through forkhead box protein O1 (FoxO1) phosphorylation and serum-and glucocorticoid-induced protein kinase (SGK) activation. Furthermore, it has been suggested that the

mTOR complexes cross inhibit each other complicating the pathway activation status (Vijay Ramakrishnan and Kumar 2018).

This pathway is constitutively activated in MM patients and cell lines and is necessary for its growth and for evasion of apoptosis induced by different drugs such as the glucocorticoid dexamethasone. MM cell lines and patient-derived primary MM cells present heterogeneous levels of activated Akt, but nearly 50 % MM patients express activated Akt. Different genetic abnormalities have been linked to altered expression of components of this pathway, but it should be stand out that, one of the most commonly reported in MM patients or MM cells lines cytogenetic abnormality is the t(4;14) translocation, that affects function of cyclin D (Brigle and Rogers 2017), and higher levels of activated Akt have been reported in presence of this genetic alteration (Vijay Ramakrishnan and Kumar 2018). And, moreover, mTOR, can be activated through mechanisms independent of Akt, including activation of the Ras/Raf/Mek/Erk pathway, energy levels in the cell, amino acids, and DNA damage.

1.3.1.3. The Ras/Raf/MEK/Erk pathway

The Ras/Raf/MEK/Erk signalling pathway is an important mediator for many essential cellular processes as survival, proliferation, angiogenesis or migration (Hu and Hu 2018). Ras protein subfamilies are a key group of proteins in cellular signal transduction functions, and nearly 30% of malignancies involve Ras proto-oncogene mutations (Hu and Hu 2018). In MM, Ras mutations may appear in 23-54% of newly diagnosed cases, however this percentage increases in relapsed or refractory cases, where it is reported to be between 45-81%. Ras mutations are frequently associated with more aggressive phenotypes, and are one of the recurrent differences between MGUS and MM, as Ras mutations are absent in patients with MGUS (Hu and Hu 2018). This pathway, also known as the Ras/MAPK or the MAPK/Erk signalling pathway is characterized by the mammalian MAPK based signal transduction networks. It consists of the Ras protein, the Raf kinase (Map3K) and the MAP2K kinases (MEK1 and MEK2) and pathway distal kinases Erk1 and Erk2; also,

different scaffolding and intermediate proteins participate. The pathway starts with binding of their specific ligands to different tyrosine-kinase receptors, as for example the binding of VEGF to the vascular endothelial growth factor receptor (VEGFR). This activation of the receptor leads to the recruitment of docking proteins such as growth factor receptor-bound protein 2 (Grb2) and son of sevenless homolog (Sos). The formation of this complex would promote the exchange of GDP by GTP in Ras, thus activating it. Then, activated Ras activate the protein kinase Raf that will phosphorylate and activate MEK (MEK1 or MEK2), this ultimately would lead to the activation of the MAPK Erk (Erk1 or Erk2) resulting in increased cell proliferation and survival and enhancing angiogenesis and cell migration.

In MM several alterations imply dysregulated signalling of this pathway. Ras activation has also crosstalk with different pathways of interest for MM progression such as the above mentioned NFκB or PI3K/Akt pathways. For all this, this pathway and its alterations are fundamental for MM initiation and progression, but also for relapse and resistance to existent therapies (Vijay Ramakrishnan and Souza 2016; Hu and Hu 2018; Donk, Lokhorst, and Bloem 2005).

1.3.1.4. The JAK/STAT pathway

The JAK/STAT pathway is a well-known signalling cascade that regulates cell proliferation, migration, differentiation, and apoptosis in MM. STAT proteins are transcription factors that in absence of specific receptor stimulation are localized in the cytoplasm. Specific receptor-ligand coupling implies recruitment to the receptor of JAK (JAK1 and JAK2) proteins that will phosphorylate the receptors and create docking sites for STAT proteins. Thus, meaning posterior STAT phosphorylation and dimerization that will promote its translocation to nucleus and activation of its different target genes. Specific ligand-receptor interactions generate active transcription complexes composed of distinct STAT proteins (Aaronson and Horvath 2002).

In MM, this pathway has been related with increased cell proliferation and decreased apoptosis, and the JAK/STAT pathway interacts with other signaling pathways that sustain MM (Hu and Hu 2018). IL-6 acts as a MM growth factor by stimulating IL-6 receptor (IL-6R) and triggers phosphorylation of STAT3 via JAK1. Moreover, STAT3 has been reported to be constitutively active in CD38+ cells from MM patients, as well as in 3D long-term cultures of MM cell-lines (Shain et al. 2009).

1.3.1.5. The Wnt/β-catenin pathway

The canonical Wnt signaling pathway relies on the stabilization of cytosolic β-catenin. In the absence of Wnt ligand, β-catenin is phosphorylated by glycogen synthase kinase 3 (GSK3) and casein kinase 1 (CK1) and targeted for ubiquitination and degradation by the proteasome. The binding of Wnt to its receptor (Frizzled) that forms a complex with low-density lipoprotein receptor-related protein 5/6 (LRP5/6) inhibits the activity of GSK3, resulting in the accumulation of β-catenin in the cytoplasm. If the concentration of β-catenin has reached certain level, it translocates to the nucleus, where it regulates the expression of canonical Wnt target genes affecting cellular proliferation, apoptosis, differentiation, and migration.

In MM, this pathway participates in the pathogenesis of the disease, as β-catenin is overexpressed in MM cells and Wnt responsiveness to myeloma plasma cells may be a significant factor in the progression of MM, moreover uncontrolled Wnt signalling has been reported to contribute to defects in apoptosis in MM cells (Hu and Hu 2018). Additionally, this pathway is employed by MM for transforming the BMN, as malignant cells can promote the development of osteolytic bone lesions by producing Wnt signalling inhibitors such as Dickkpf-1 (DKK-1) to directly suppress the osteoblast differentiation. Thus targeting this pathway has been of great interest not just to prevent disease progression, but also for impairment of myeloma bone disease (MBD) (Hu and Hu 2018).

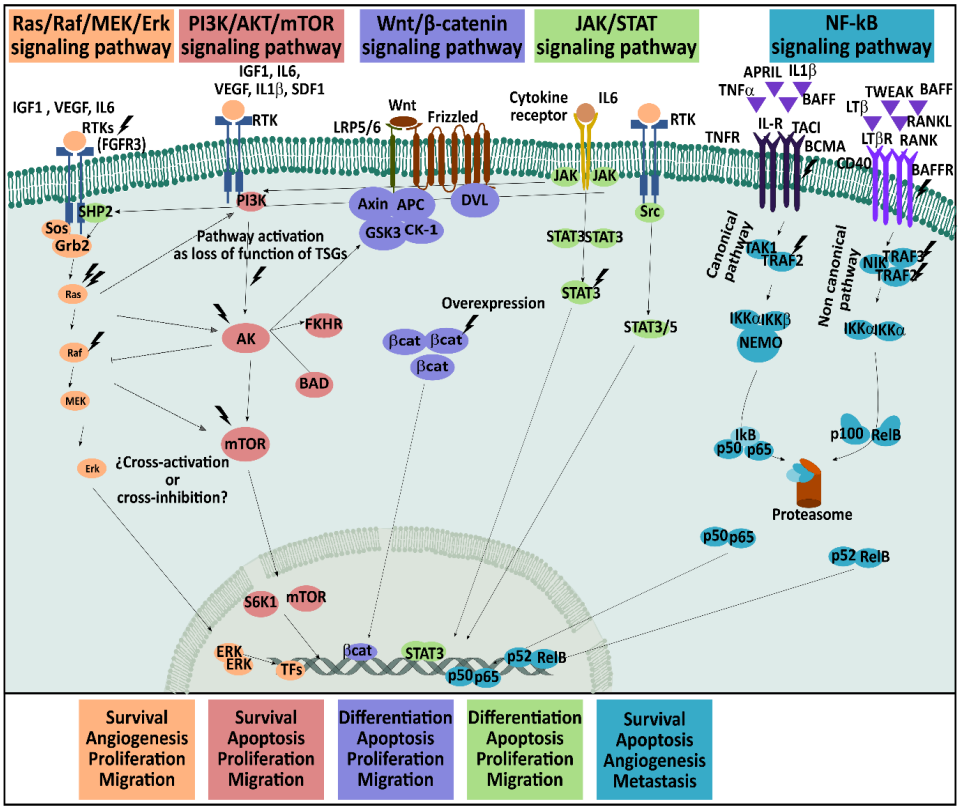

Figure 7. Molecular pathways altered in multiple myeloma. Hyperactivation of these pathways by different mechanism leads to aberrant cell proliferation, apoptosis regulation and drug resistance.

1.3.2. Multiple myeloma treatments

In past years, improvements in treatments and the use of autologous stem cell transplant (ASCT) have allowed an increase in the median overall survival. Treatment of MM usually is based on the combination of drugs which have different mechanisms of action. The main groups include corticosteroids, alkylating agents, anthracyclines, proteasome inhibitors (PIs), immunomodulatory drugs (IMIDs), histone deacetylase inhibitors (iHDACs), monoclonal antibodies (mAbs), nuclear export inhibitors and high-dose chemotherapy rescued by ASCT.

The use and optimization of combinations of these drugs has allowed the improvement in the overall patient survival (Pinto et al. 2020). Nowadays, the induction treatment for newly diagnosed patients usually includes triple combinations of bortezomib (PI), lenalidomide and dexamethasone (Pinto et al. 2020). However, the appearance of resistance to these agents has been observed and patients who become refractory to both IMIDs and PIs have significant worse outcomes, with relapse and disease progression being common even after a complete remission. New generation IMIDs and PIs were introduced for refractory patients, as well as mAbs used in combinatorial regimens with iHDACs (Chim et al. 2018).

1.3.2.1. Dexamethasone

Dexamethasone is a corticosteroid widely used in the treatment of MM. It is usually used in combination regimens. It is an apoptosis inductor. Dexamethasone is a glucocorticoid, and its effects occur through the bonding to the glucocorticoid receptor. Glucocorticorcoid (GC) binds the GC-receptor, which then translocates to the nucleus and interacts with either GC-response elements to induce gene transcription (transactivation) or directly interacts with transcription factors, such as NFκB or activating protein 1 (AP-1) to repress their activity (transrepression) (Kervoëlen et al. 2015).

1.3.2.2. Bortezomib

Bortezomib (Velcade, Millennium Pharmaceuticals, Inc., Cambridge, MA, and Johnson & Johnson Pharmaceutical Research & Development, L.L.C., Raritan, NJ) was the first proteasome inhibitor approved by the United States Food and Drug Administration (US FDA) for the treatment of newly diagnosed and relapsed MM patients. Its mechanism of action is based in preventing the degradation of pro-apoptotic proteins and promoting degradation of anti-apoptotic proteins, resulting in a programmed cell death of malignant cells. Additionally, by blocking the degradation of IκB, bortezomib suppresses the NFκB signaling pathway preventing the activation of numerous antiapoptotic genes involved in MM progression. Bortezomib also leads to the upregulation

of horbol-12-myristate-13-acetate-induced protein 1 (NOXA), a proapoptotic member of the B-cell lymphoma 2 (Bcl-2) protein family, which interacts with the antiapoptotic proteins of the same family, inducing the apoptosis of the MM cells. Bortezomib also inhibits OCs and stimulates OBs, thereby increasing bone formation.

1.3.3. Drug resistance in multiple myeloma

In most MM patients, the evolution of the disease is characterized by the development of DR. This phenomenon is nowadays the main clinical problem and is associated with an unfavorable prognosis. The main causes for DR are (Pinto et al. 2020):

I. Genetic alterations.

II. Epigenetic alterations.

III. Abnormal drug transport and/or metabolism, leading to a decrease in intracellular levels of drug.

IV. Dysregulation of apoptosis or other signaling pathways and activation of autophagy.

V. Persistence of cancer stem cells, which are insensitive to drugs and capable of self-initiating MM.

VI. Dysfunctional tumor microenvironment.

VII. Other mechanisms specific for immunotherapies with antibodies.

In general, cancer DR may result from intrinsic mechanisms by which malignant cells are resistant to treatment before the exposure to this treatment or acquired during treatment reflecting the selective pressure that the treatment implies for the cell. MM is a very heterogeneous disease and the reason why patients relapse and MM resistant clones persist after therapies are not fully understood, many different causes of DR are involved, as the ones listed

above. In this Thesis the focus is going to be pointed in the tumor microenvironment and its contribution to DR generation, as tissue engineering aims to include the microenvironment role in the *in vitro* models in order to better modeling of DR generation.

1.3.3.1. Tumor microenvironment

In hematological malignancies, as in MM, the BMN presents a transformed or dysregulated character that favors malignancy, as it has been previously discussed. The interaction between MM cells and the dysregulated BMN contributes to DR generation, and this acquired DR can be divided in 2 different categories: soluble factor-mediated drug resistance (SFM-DR) and cell adhesion mediated drug resistance (CAM-DR).

SFM-DR is referred to the DR mediated by all the cytokines and growth factors which are present in the BM milieu. They can be produced by MM cells themselves but also by different BM resident cells, such as HSCs, MSCs, OBs, OCs, ECs or blood or immune cells. The major soluble factors released are IL-6, IGF-1, VEGF, BAFF, FGF, SDF-1, and TNF. All of them are produced reciprocally by the cells above mentioned and support MM cells survival by different pathways activation, in particular the IL-6/JAK/STAT3 is a key target pathway. IL-6 overexpression is possibly involved in resistance to several chemotherapeutic drugs, including bortezomib (Catlett-Falcone et al. 1999). Another example, IGF-1 produced by the MM cells and present in the BM environment, promotes proliferation and DR through activation of the MAPK and PI3/Akt pathways (Spencer et al. 2014). Concerning SDF-1/CXCL-12, it is constitutively expressed and released by bone marrow stromal cells (BMSCs) and fibroblasts, while its receptor CXCR-4 is found in MM cells. The activation of the CXCL-12/CXCR-4 axis promotes trans-endothelial migration and BM homing and adhesion of MM cells. The CXCR-4 expression is correlated with bortezomib resistance in cell lines and the use of CXCR-4 inhibitors may enhance the sensitivity of MM cells by disrupting their adhesion to the BMSCs (Bianchi et al. 2012).

Also, extracellular vesicles (EVs) constitute an important mechanism of communication among different players of DR in the BMN. EVs have been associated with MM progression and DR. They can be produced by different niche cells, such as MSCs, and transport different molecules mediating intercellular communication, for example, oncogenic proteins, which offer a supporting role in tumor progression (Gargiulo, Paggetti, and Moussay 2019).

Several soluble mediators can influence the main MM proliferation pathways, moreover the ECM also presents a relevant role in SFM-DR as different molecules, especially proteoglycans or glycosaminoglycans such as HA can act as a reservoir, which directly can bind and concentrate soluble factors that will then be presented to cells in a more efficient manner.

However, from the point of view of this study the CAM-DR is of great relevance. CAM-DR is a mechanism whereby MM cells escape the cytotoxic effects of anti-cancer therapy via adhesive interactions with BM stromal cells and/or ECM components. Damiano et al. described for the first time this phenomenon as a reversible DR phenotype in fibronectin-adherent MM cells (Damiano et al. 1999). Some adhesion molecules involved are syndecan-1 (CD138) (Katz 2010), CD44 (Katz 2010; Vacca et al. 1995), VCAM-1 (Okada et al. 1999), Mucin-1 antigen (MUC- 1) (Morgan, Walker, and Davies 2012), Lymphocyte Function-Associated Antigen-1 (LFA-1), ICAM-1 (Vacca et al. 1995; Barker et al. 1992) and different proteins from the integrin family (α4β1, α5β1, αvβ3 and β7 integrins (Katz 2010; Damiano et al. 1999; Vacca et al. 1995)).

In the end, these interactions between MM cells and the BMN trigger the up regulation of many signaling pathways resulting in MM cell proliferation and survival. CAM-DR to common MM treatments such as doxorubicin, melphalan, vincristine or dexamethasone in MM cell lines and patients' primary MM cells has been described (Damiano et al. 1999; Chauhan et al. 1996; Hideshima et al. 2004) (Hatano-Noborio et al. 2009; Hideshima et al. 2001).

1.3.3.2. Extracellular matrix molecules with relevant roles in CAM-DR

Different biomolecules which conform the extracellular matrix ECM have been reported to take part in CAM-DR. Its study is of great relevance for this Thesis, as ECM molecules are natural polymers which can be included in 3D tissue engineering approaches for *in vitro* disease modeling.

Fibronectin (FN) is a dimeric glycoprotein which mediates a wide range of cellular interactions with the ECM and plays important roles in cell adhesion, migration, growth, and differentiation. It usually exists as a dimer composed of two nearly identical subunits of approximately 250 kDa linked covalently near their C- terminus by a pair of disulfide bonds (Pankov and Yamada 2002). FN is broadly studied in relation to MM pathogenesis (Hazlehurst et al. 2000; Damiano et al. 1999; Fei, Hang, and Hou 2013; Shain et al. 2009). The interaction between MM cells and FN is mediated by integrins (specially $\alpha 4\beta 1$ or VLA4 integrin) and plays a key role in CAM-DR to drugs such as dexamethasone. This adhesion regulates the levels of $p27^{kip1}$, which is a cyclin dependent kinase inhibitor, thus meaning that these adhesive signals can transduce into the anti-apoptotic and cell-cycle arrest signals. Adhesion of MM cell line RPMI8226 to FN increases $p27^{kip1}$ translocation to nucleus and inhibits cyclin A- and cyclin E-dependent kinase activity and as a result there is a cell-cycle arrest at G0-G1 phase (Fei, Hang, and Hou 2013).

Hyaluronic acid (HA) is a non-protein glycosaminoglycan which is also a major component of the mammalian BM ECM. It is a survival and proliferation factor for MM cells. Due to its high capacity to absorb water, the main effect of HA is mediated by IL-6, as HA retains and concentrates this cytokine close to its site of secretion favoring its autocrine activity. However, HA also participates in CAM-DR through direct interaction with MM cells mediated by the adhesion molecule CD44. HA-mediated proliferation of MM cells occurs through downregulation of $p27^{kip1}$ and a hyperphosphorylation of the retinoblastoma protein (Vincent et al. 2003). MM cells adhesion to HA has also been related with Wnt/β-catenin activation and resistance to lenalidomide and

with DR against DEX mediated by different signaling pathways, inducing STAT3 phosphorylation in IL6-dependent MM cell lines, whereas, in IL6-independent MM cell lines, resistance is due to the upregulation of Bcl-2 and the activation of the NFκB pathway (Bjorklund et al. 2014).

There exist several other biomolecules from the BM of the ECM whose role in MM progression and DR is not clearly stablished yet. Collagen I (COL 1) is one of the most abundant BM ECM proteins. Its role in cancer progression has been broadly reported, mainly in the context of solid tumors (such as breast cancer). Altered stromal collagens remodeling by different cells such as cancer-associated fibroblasts (CAFs) has been established as a key point driving tumorigenesis and affecting response to treatments (Nissen, Karsdal, and Willumsen 2019). In the BM ECM COL 1 interacts with different cellular types such as HSCs and MSCs, and because of that, it has been included in different *in vitro* models of the BMN (Lewis et al. 2017). In the context of MM, plasmatic cells interact with COL 1 by syndecan-1 (Ridley et al. 1993), although syndecan-1 is known to play a role in mediating MM cell interaction with the BMN and to promote Wnt/β-catenin signaling (Ren et al. 2018), the role of COL 1 in MM DR has not been directly studied.

Chondroitin sulphate (CS) is a sulfated glycosaminoglycan formed by repeating disaccharide units of glucuronic acid and N-acetyl galactosamine residues linked by β bonds. Depending on the residue that is sulfated in the N-acetyl galactosamine, there exist different types of CS. The more abundant in the BMN is chondroitin 6-sulfate, also called chondroitin sulfate C (Gandhi and Mancera 2008). It binds to proteins such as collagens and form proteoglycans. In cartilage CS is one of the main ECM molecules acting as a major structural component. However, its role is not only to present structural function, but also to intervene in the regulation of different cellular processes: CS presents anti-inflammatory and immunomodulatory effect. The effect of CS in MM cell lines survival to different drugs has not been reported when tested in conventional 2D cultures (Vincent et al. 2003), however it would be of great

interest to further evaluate the role of this biomolecule in more biomimetic *in vitro* conditions.

1.4. Modelling Multiple myeloma

Multiple myeloma develops almost exclusively in the BM, which highlights the relevance of the BMN in the development of this disease and in the process of DR. Indeed, while MM therapeutic approaches have significantly improved over the past 20 years, the disease remains incurable. This may be due to the high phenotypic and genetic heterogeneity of MM, but also to the inadequacy of two-dimensional conventional preclinical models in reproducing MM and its microenvironment. Because of that, in past decades tissue engineering approaches have attempted to reconstruct the MM microenvironment *in vitro* trying to include MM interactions with BM resident cells and BM ECM, and particularly, trying to reproduce *in vitro* the clinical problem of DR generation. These approaches have mainly based its 3D designs in hydrogel-based cultures, microfluidics devices, scaffolds or 3D culture of human MM tissue explants and of isolated MM cells in scaffolds in the microgravity-based rotary cell culture bioreactor system (Ferrarini et al. 2021).

1.4.1. Models based on hydrogels

In 2008, Kirshner and colleagues proposed a novel MM model termed the "rEnd-rBM" (Kirshner et al. 2008) (Figure 8, a). This model achieved the clonal expansion of MM cells and stands out for being pioneer in recreating *in vitro* the MM BM microenvironment. It consisted of mixture of different matrix components, COL 1 and FN to reconstruct the endosteum-marrow junction (rEnd), and then FN and Matrigel mixture to recreate the BM matrix (rBM), in which cells isolated from BM aspirates of MM patients were seeded. Cells spontaneously distributed throughout the different compartments, mimicking human BM architecture and BM-MM interactions, thus providing a powerful tool for understanding MM biology. Moreover, the impact of anti-MM drugs,

specifically bortezomib and melphalan, on distinct cellular compartments inside the 3D model was assessed. Interestingly, they demonstrated an enrichment of the non-proliferating cells from MM patients aspirate concentrate at the rEnd.

Later, in 2015 de la Puente and coworkers developed a 3D tissue engineered BM (termed as “3DTEBM”) (De la Puente et al. 2015) in which the hydrogel matrix was obtained by crosslinking the fibrinogen of BM aspirates from MM patients (Figure 8, b). Then autologous MM cells were cultured in these gels, the resulting matrix better recapitulates the BMN, as it contains higher number of cytokines, growth factors or other soluble mediators naturally found in the MM microenvironment. The authors demonstrated that the model reproduced the generation of hypoxia gradients, as it happens in BMN, and allowed *ex vivo* proliferation of primary MM cells for several weeks. They also tested DR generation in the 3DTEBM to various anti-myeloma drugs, such as carfilzomib and bortezomib.

Jakubikova et al. in 2016 also developed a 3D MM model (Jakubikova et al. 2016) based on a commercially available hydrogel (PuraMatrix) (Figure 8, c). The hydrogel harbored a co-culture of primary patient-derived MM cells and BM MSCs; and succeeded in maintaining MSCs phenotypic and functional properties together with osteogenic differentiation capacity. Moreover, they also used the system for the study of DR generation *in vitro*, and BM-driven CAM-DR to both novel (IMiDs, bortezomib, carfilzomib) and conventional agents (doxorubicin, dexamethasone and melphalan) achieving to reproduce certain aspects of DR generation *in vitro*.

In 2018 Braham and colleagues generated a novel *in vitro* 3D MM model using the commercially available Matrigel and different cell types of the BMN (MSC, EC and primary MM cells) (Braham et al. 2018) (Figure 8, d). The model was able to support long-term proliferation of MM cells (up to 28 days). They also used the 3D model to provide the first pre-clinical *in vitro* testing of immunotherapies on primary MM samples inside their tumor microenvironment; they showed that a novel class of engineered immune cells, TCRα/β

lymphocytes engineered to express tumor-specific Vγ9 VΔ2 T- cell receptors, were able to infiltrate the 3D construct and efficiently kill MM cells.

1.4.2. Models based on scaffolds

Few 3D models of MM have been developed based on the use of rigid and strong scaffolds. However, as MSC and the osteolinage cells that can differentiate from them arise as stromal cells in the BM with relevant role in MM progression and DR, some authors consider the importance of a substrate able to support MSC osteogenesis. Stiffness of the substrate has been demonstrated as relevant factor to direct the cell phenotype in differentiation processes. Thus, mimicking the stiffness of a particular tissue can guide cells towards this phenotype (Anderson et al. 2016). Because of that, strong 3D substrates, such as scaffolds, have been specially considered in MM models which include in the MSC and osteolineage cells in the equation.

For example, in 2014 Reagan et al. used a porous silk fibroin scaffold as 3D model for the co-culture of MM cells and MSCs (Reagan et al. 2014) (Figure 8, e). The system was able to reproduce *in vitro* the interactions between MM cells and bone and was then used for the study of effect of MM cells in osteogenesis, demonstrating the negative impact of MM on normal bone homeostasis. One main contribution of this model was the identification of a novel microRNA signature (miR-199a) associated with CAM-DR and the target microRNAs involved in the reactivation of osteogenesis in MSC altered by MM in MBD.

Calimeri and colleagues presented a 3D model based on a poly-ε-caprolactone polymeric scaffold designed for its implantation into a SCID mouse (Figure 8, f). They seeded the 3D scaffold internal surface with mouse or human BMSCs and this allowed the successful engraftment of human primary explanted MM cells in a 3D context based on its autologous BM milieu (Calimeri et al. 2011).

1.4.3. Models based on microfluidics and bioreactors

Also, a tissue engineering approach that must be mentioned is the use of microfluidics devices and bioreactors. Specially with the raise in past decades of the tumor-on-a-chip technology: microfluidic platforms which constitute simplified but efficient models of specific tumor traits, such as angiogenesis, hypoxia, and tumor–stroma interactions, thus representing promising tools for personalized medicine.

In 2014, Torisawa and coworkers published its *in vitro* model of the BM niche (Torisawa et al. 2014) (Figure 8, g). It consisted of an artificial bone inductive substrate that was implanted in mouse to be engineered *in vivo* and then assembled in a sophisticated microfluidic-on-a-chip device and cultured for 4 or 7 days and used for testing drug efficacies and toxicities. In this model, the objective was the generation of *in vitro* functional hematopoietic niches and its use as toxicity model. Although the model is not centered in MM disease, it is of great relevance for all hematological malignancies with BM homing.

In 2013 Ferrarini et al. proposed a dynamic 3D model based on the use of a rotary cell culture bioreactor system (RCCS™) for the *in vitro* culture of bone explants (Ferrarini et al. 2013) (Figure 8, h). The authors achieved the long-term maintenance of excised MM patient tissue explants in the system and demonstrated the viability of the MM cells and the presence of key components of the BMN. The system was also used for DR studies, assessing the impact of drugs not only on MM cells, but also on angiogenic vessels. They showed that bortezomib negatively impacted both the MM cells and the blood vessels. Notably, the effects of drugs measured in this system were more likely to those measured in patients.

BM is the perfect refuge for myeloma cells. It is the place where malignant cells survive, accumulate, and achieve drug resistance. However, it is also a complex and highly specialized microenvironment, for this reason, although the models reviewed here represent remarkable examples of translational research in cancer, it is worth mentioning the simplification they entail of reality and the path that still needs to be done. The variety of technical approaches

described (hydrogels, scaffolds, tumors-on-a-chip) demonstrate the versatility of tissue engineering and the wide possibilities that its fabrication tools offer. However, all these studies are based on static architectures in which the substrate has a predefined shape, mainly in the form of a scaffold or hydrogel, while the BM marrow native ECM could be better defined as a semi-solid media in which MM cells maintain its dynamic character but establish effective interactions with ECM and BMN cells.

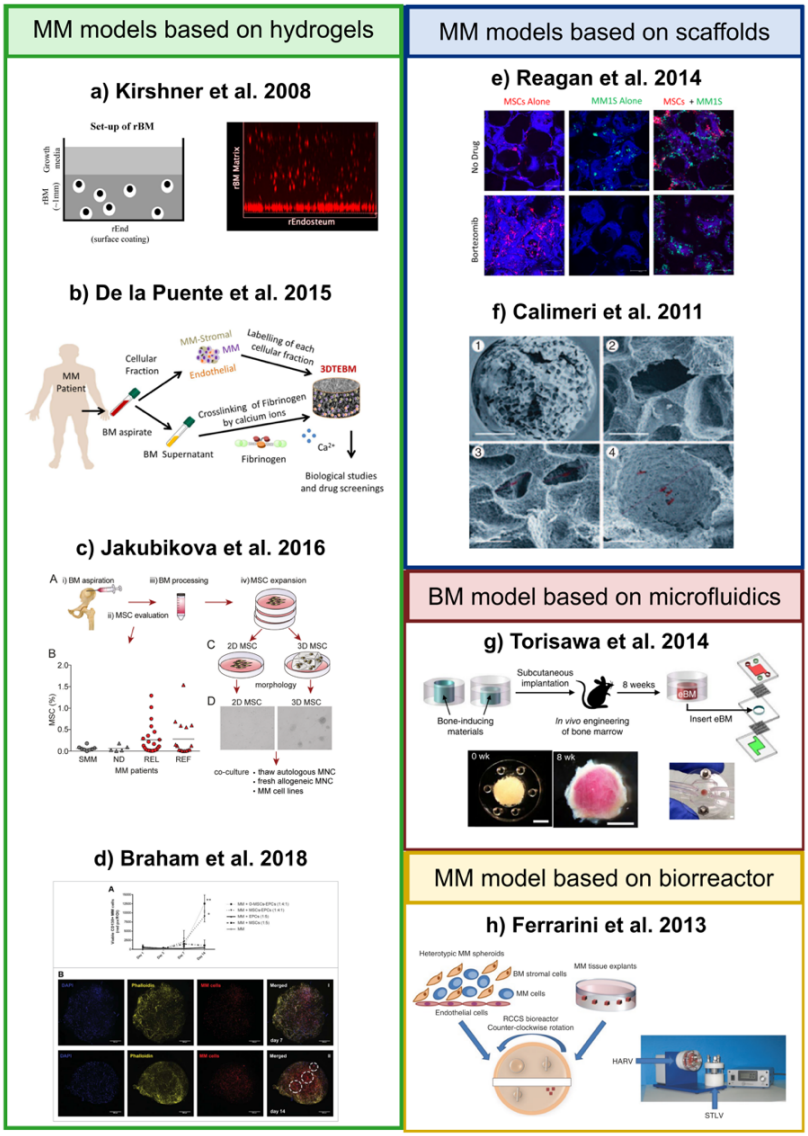

Figure 8. Different 3D models of MM. a) Schematic representation of the model from Kirshner et al. and BM aspirated particle grown in rBM for 21 days and stained with DAPI. Adapted from (Kirshner et al. 2008)**. b) Schematic representation of the model from de la Puente et al. Adapted from** (De la Puente et al. 2015)**. c) Schematic representation of the model from Jakubikova et al. Adapted from** (Jakubikova et al. 2016)**. d) Results from the model of Braham et al. Results of the co-culture of primary myeloma cells for 14 days; and confocal images showing one representative donor (red) cultured in 3D with MSCs and ECs for either 7 or 14 days, MSC-EPC networks are visualized using phalloidin (yellow). Adapted from** (Braham et al. 2018)**. e) Results from the model of Reagan et al. Confocal images of MM cell line growing in the scaffold alone or with MSCs under non-treated or bortezomib treated conditions. Adapted from** (Reagan et al. 2014)**. f) Results from the model of Calimeri et al. Electron microscopy images of the scaffold used in the model. Adapted from** (Calimeri et al. 2011)**. g) Schematic representation of the model from Torisawa et al. Images show the microfluidic device and the bone inductive material before and after mouse implantation. Adapted from** (Torisawa et al. 2014)**. h) Schematic representation of the model from Ferrarini et al. Image of the biorreactor used. Adapted from** (Ferrarini et al. 2013)

Chapter 2. Hypothesis and objectives

2.1. Hypothesis

In the previous chapter, the heterogeneity of MM disease and the relevance of the microenvironment in disease progression and DR generation has been discussed. Main MM 3D models available in literature have also been presented, highlighting the potential of tissue engineering to contribute to the development of better biomimetic models. This provides platforms in which DR processes can be studied with more clinically relevant conclusions, since the different models include different components of the BMN whose influence on DR has been previously demonstrated; whether BM resident cells, ECM components or both.

However, MM cells are non-adherent cells and, although great advances have been made, it is interesting that among the existing models, the development of *in vitro* models for the culture of suspension growing cells has not been exploited. It would be of great relevance to develop 3D models capable

of providing a biomimetic environment for MM cells while respecting its dynamic and non-adherent nature.

Microspheres offer extensive versatility as 3D substrates, as well as the possibility of assembling a microenvironment of semi-solid nature, formed by suspended microspheres and cells, whose particle density can be fine-tuned. In addition, microspheres can be functionalized with biologically relevant molecules from the BM ECM to provide an *in vitro* platform able to test the role of these biomolecules in DR generation under biomimetic conditions.

In previous studies, our group demonstrated the potential of using microspheres-based platforms for the culture of the MM cell line RPMI8226. As a proof of concept, we shown that this 3D environment could be a valuable tool to test antitumoral drugs efficiency (Marín-Payá et al. 2021).

The hypothesis of the present Doctoral Thesis is that to achieve a biomimetic MM model designed for the study of DR generation and based on tissue engineering approaches, there are certain aspects that must be considered:

I. A 3D environment is essential to effectively reproduce *in vitro* native interactions from the BMN.

II. The effect of guaranteeing MM cells motility must be addressed, as it could be of great relevance; not only because this would respect the suspension growing behavior of MM cells, but also because a more fluid model could increase the diffusion of growth factors and cytokines and reproduce to a greater extent the indirect communications between cells and ECM or between different cellular types.

III. A 3D model of semi-solid nature formed by suspended microspheres and non-encapsulated cells could effectively meet the requirements stated above.

IV. The incorporation of different BM ECM biomolecules on microspheres surface would increase biomimicry of the model, as well as turning the model into a tool to study the role of

different components of the ECM in DR generation. This model would render a simplified but biologically relevant representation, which will allow the cell-ECM interactions to be better understood.

2.2. Objectives

The main objective of this Doctoral Thesis is to develop, optimize and validate a 3D culture platform, termed as microgel, based on microspheres suspended in a liquid media and coexisting with MM non-adherent cells growing dynamically in suspension (Figure 9).

Microspheres will be made of different polymers, and the biomimetic character of the microgel platform rely on the inclusion of proteins and glycosaminoglycans from the BM ECM as active functionalization for the microspheres. The dynamic and 3D nature of the microgel and MM cells suspension will be maintained by keeping the platform in continuous stirring during cell culture.

Three different MM cell lines (RPMI8226, U226 and MM1.S) will be used to determine the optimal working parameters for the platform, validation of the microgel as 3D model for MM, and for testing DR generation in the presence of the different biomolecules of the ECM grafted on the microspheres.

The specific objectives of the Thesis are:

I. Synthesis of biostable polymeric microspheres based on acrylate and methacrylate copolymers with varying ranges of diameter distributions and different chemical compositions.

II. Functionalization of the microspheres with different ECM biomolecules from the BM. Characterization of the functionalizations.

III. Obtainment of alternative biomimetic microgels based on commercially available microspheres as an alternative to the

polyacrylates-based microgel system. Functionalization of the microspheres with ECM biomolecules and characterization.

IV. Optimization of microgel parameters for MM cell culture. Assessment of the influence of some aspects (microsphere size, stirring speed, microsphere functionalization) of the microgel on MM cell proliferation.

V. Utilization of the microgel 3D platform for the study of cell behavior and DR generation *in vitro* to two different drugs: dexamethasone and bortezomib.

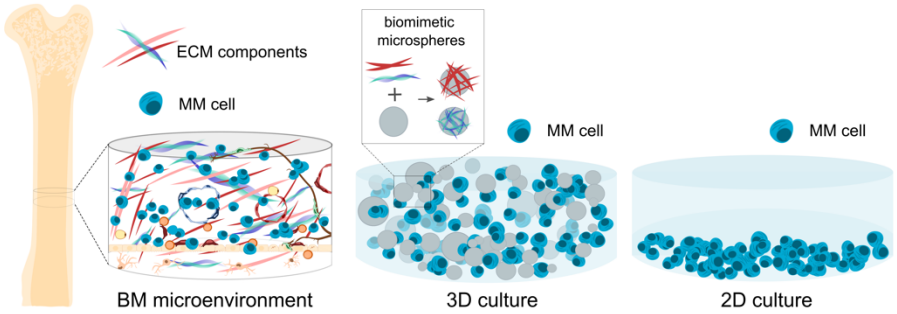

Figure 9. The microgel 3D cell culture platform. Scheme of the *in vivo* bone marrow microenvironment of MM cells and the developed cell culture system for the microgel conditions compared with the conventional 2D culture conditions with only myeloma cells.

SECTION II.

EXPERIMENTAL CHAPTERS

Chapter 3. Microspheres: synthesis, characterization and functionalization

3.1. Summary

In this Doctoral Thesis, various microspheres have been developed with different properties and functionalizations. In each case, microspheres were designed with appropriate physicochemical properties for the applications in which they were to be used. This chapter addresses the different microspheres produced in this Thesis, the rational criteria for its design, the protocols for their production and functionalization as well as the results related with their physicochemical characterization.

3.2. Introduction

3.2.1. Emulsion methods for microsphere production

Microspheres are polymeric particles, of organic or inorganic nature, with spherical morphology and free-flow capacity presenting a diameter ranging between 1 and 1000 μm. The history of microspheres or microparticles production begun in 1960s, however their application in biomedicine approaches has been significantly increased in recent decades after the expansion of their use as delivery agents or tissue engineering 3D substrates (Choi et al. 2017). Several different methods have been developed for polymeric microspheres production. Emulsion and solvent extraction, controlled phase separation, electrospraying or methods based on porous membranes are the most traditional approaches used for microsphere's obtaining from natural or synthetic polymers. Recently, the field has even extended possibilities, several novel approaches such as microfluidics-assisted, centrifugation-based, electrohydrodynamic-based, and template-based fabrication methods have been incorporated to provide flexibility in fabricating more complex engineered microspheres.

Emulsions are one of the most widely used methods for fabricating microspheres. Polymer or monomer is added to an immiscible phase with an emulsifier and stirred for several minutes to form the microspheres. Emulsion based methods are duly convenient operation processes requiring simple

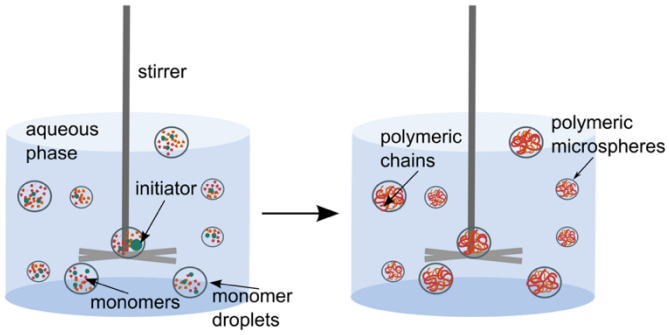

Figure 10. Emulsion polymerization method principles.

equipment and easily scalable. This has led to its broad application in different fields. However, this method also presents some disadvantages such as polydispersity, poor reproducibility, and lack of precision in constructing sophisticated morphologies. Several emulsion technics for microspheres production are based upon a mixture of monomers and polymerization initiator that are formed into spheres in a stabilizing non-miscible phase, these methods are called heterogeneous (or particle forming) polymerization processes (Figure 10) (R Arshady 1992). The most common of these are: suspension, emulsion, dispersion, and sedimentation polymerization (Piaopiao and Zihui 2019).

These differentiate on the size of the polymer particles produced. An arbitrary dividing line between emulsion and suspension is the droplet/particle size of 1 μm. Fluids containing droplets/particles smaller than about 1 μm are known as emulsions (latex or colloids), and those containing particles larger than about 1 μm as suspension. The upper limit of particle size for suspension systems is established about 1-2 mm. The term dispersion polymerization has been adopted because the technique replaced the process of polymer dispersion in the paint industry. Polymerization processes leading to the formation of macroscopic polymer precipitates are referred to as precipitation polymerization (Reza Arshady 1988).

For suspension polymerization, monomers; most commonly hydrophobic, are mixed with an initiator and dripped into a non-miscible phase, most commonly water, with surfactants or detergents acting as stabilizers. Surfactants are included to ensure formation of proper spherical particles. The solution is heated to induce activation of the initiator and thus initiate the radical polymerization reaction. After the polymerization, microspheres can be collected and washed from the unreacted monomers and stabilizers. The technique is simple and versatile, as most monomer mixtures can be used; even monomers that are partly soluble in water. With this technique, a wide range of microsphere sizes can be obtained, roughly ranging from ~10–1,000 μm (R Arshady 1992). High polydispersity is the main disadvantage of this method

(Saralidze, Koole, and Knetsch 2010). Micro-sieving of the microspheres is often required to obtain fractions with well-defined diameter range, although this leads to a reduction in yields.

3.2.2. Techniques for microsphere's functionalization

Cell-ECM interactions have been extensively incorporated in tissue engineering approaches in different ways. The presence of ECM biomolecules is not only limited to the use of natural polymers for microsphere's synthesis, biofunctionalizations can be applied to synthetic polymers to provide them with different functionalities. Purified ECM biomolecules, its fragments or synthetic peptides can be conjugated to, or coated on, polymer matrices that would exhibit stronger cellular effects compared to synthetic polymers alone.

Functionalization of synthetic substrates also offers the possibility of studying the role of isolated biomolecules or biomolecule's specific domains from the ECM in cell behaviors, such as DR development. Several different chemistries can be used for incorporating these biomolecules, depending on the nature of both, the substrate, and the biomolecule itself. The stabilization of biomolecules on different polymeric substrates should always consider preservation of both, the structure, and the functionality of the molecule of interest to preserve the cell culture performance of the immobilized biomolecule.

3.2.2.1. Physical adsorption

Numerous approaches to achieve adhesiveness and bioactivity of polymeric matrices are based on coating them with ECM macromolecules, such as FN, laminin, vitronectin, or collagens. Also, specific peptide sequences of these proteins known to act as integrin-binding epitopes, such as the RGD sequence have been extensively used. Conventional coating technics are based on physical adsorption of the macromolecules to the substrates, it's a non-site-specific method and implies a non-covalent immobilization. Molecules are immobilized via weak interactions between the them and the sur-

face (i.e., hydrogen bonds, electrostatic interactions, hydrophobic interactions, and van der Waals interactions) (Steen Redeker et al. 2013). Macromolecules, usually proteins, can be deposited into surfaces by immersion in solutions of the protein of interest or by different deposition technics such as spin-coating. The non-adsorbed protein is then removed in a washing step. The final amount, distribution and conformation of protein in the substrate depends on the nature of the protein and the polymeric material, but also on experimental parameters, e.g., protein concentration in the coating solution, time, pH temperature or ionic strength. This is the simplest way of surface modification to make biomimetic materials. Biomaterials can be coated with these proteins, which usually have promoted cell adhesion and proliferation (Briz et al. 2013). Although less stable, physical absorbed biomolecules could lead to higher amounts of the biomolecule of interest incorporated into material's surfaces. Moreover, avoid chemical cross-linking reactions could also preserve the native structure and sequence of these molecules and retain intact epitopes which are relevant for its interaction with different receptors in the cellular membrane. Some specific materials can even induce specific and functionally relevant conformation of these molecules when absorbed into them. As for example the material-driven assembly of FN into interconnected FN fibrils when adsorbed in poly(ethyl acrylate) surfaces, meaning that this material promotes the biomimetic assembly of FN in absence of cells (Salmerón-Sánchez et al. 2011).

3.2.2.2. Covalent grafting

Covalent immobilization of biomolecules on polymeric matrices offers a way to permanently fix them, these technics imply higher efficiency, specificity and stability than conventional coatings. It is a non-site-specific method which requires the presence of two mutually reactive chemical groups on the biomolecule and on the substrate surface. In addition, the reaction should ideally work under physiological conditions (i.e., aqueous buffers at neutral pH) to avoid alterations in biomolecules, such as protein denaturation, during the

coupling reaction (Steen Redeker et al. 2013). Most literature methods describing covalent coupling strategies exploit the reactivity of endogenous functional groups present in the molecule of interest. Amine, thiols and carboxylic acid groups are the most used in bioconjugation for non-specific covalent coupling.

The carbodiimide (EDC) chemistry is one of the most used approaches for covalent coupling of different biomolecules implying amines and carboxylic acid groups. The 1-ethyl-3-(3-dimethylaminopropyl) carbodiimide (EDC) is a water soluble carbodiimide which will react with the carboxyl groups on the substrate. The reaction between the carboxyl groups and EDC results in an active O-acylisourea intermediate which can be easily displaced by a nucleophilic attack from primary amino groups of the targeted biomolecule. However, there are a variety of undesirable O-acylisourea intermediates that can form and reduce reaction yield. Because of this, trapping agents are coupled with EDC to reduce side reactions. The trapping agent most frequently used for applications involving the immobilization of large molecules is N-hydroxysuccinimide (NHS) or sulfo-NHS. NHS rapidly reacts with the O-acylisourea intermediate creating reactive esters, drastically reducing the side reactions and improving reaction yield (Figure 11). The NHS ester will then react with the amine on biological agents by covalent attachment of an acyl group to the nucleophile with the release of the NHS leaving group.

This EDC/NHS reaction is termed as a zero-length crosslinking reaction because the crosslinkers catalyse the bonding but are not present in the resulting graft. Depending on the molecules and polymers involved and their side chains, the coupling can be performed in one-step reactions or may need a two-step process, requiring the introduction of a functional group before biomolecule coupling to provide the substrate with the necessary functional groups. For example, carboxyl groups containing polymers can react with molecules such as proteins in one-step processes by means of their amine terminal groups from the side chains of aminoacids such as lysine. However, biomolecules with carboxyl groups as side functional groups participating in the coupling with carboxyl groups containing polymers, such as hyaluronic

acid, may need a molecular bridge with amine terminal groups in both ends (S. Smith et al. 2020; Balcão and Vila 2015). This will allow the coupling of the HA by means of an EDC/NHS mediated amide bond. The result would not be a zero-length crosslinking, because the polymer and the biomolecule are tethered together with a spacer polymer. This approach would introduce a molecular spacer between the biomaterial and the biomolecule which could increase biomolecule motility and reduce steric hindrance, a situation that can result of special interest for increasing biomolecule functionality and the preservation of its native structure (Steen Redeker et al. 2013).

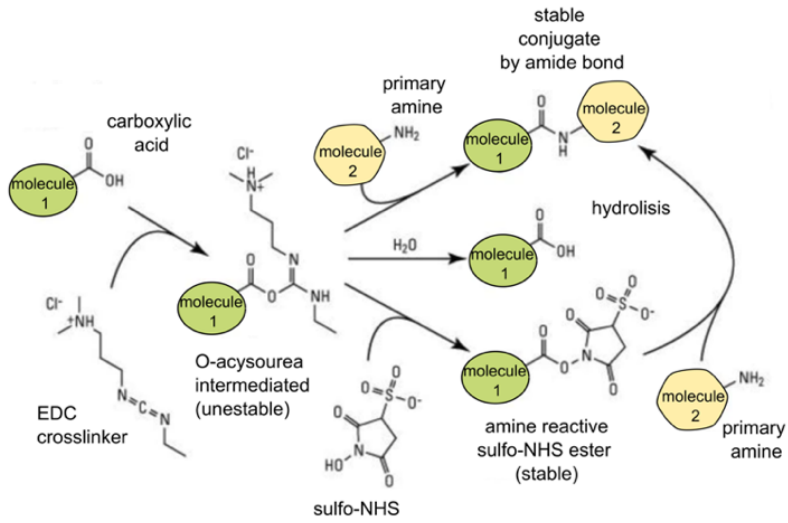

Figure 11. Reaction process for carboxyl-to-amine crosslinking using EDC and sulfo-NHS. Addition of NHS or Sulfo-NHS to EDC reactions increases efficiency and enables molecule (1) to be activated for storage and later use.

3.2.2.3. Layer- by-layer assembly

Layer-by-layer (LbL) assembly technique is based on the alternating exposure of a substrate (which can be of nearly any geometry) to positively and negatively charged polyelectrolytes (Figure 12, a). Some of the most classical methods for applying LbL coatings are dip coating, spraying, and spin coating (Figure 12, b). Each method has distinct advantages and disadvantages. Alternating dipping of the substrate into the solutions of polyelectrolytes is the

most widely used method for LbL deposition. This method is the most simple, robust, and versatile. However, it is also the most time consuming and leaves abundant residual polyelectrolyte from each deposition step (Campbell and Vikulina 2020). Depending on the nature of the polyelectrolytes, multilayers can be assembled from synthetic, from naturally occurring polymers, or from their mixture. Natural polyelectrolytes, such as components of the ECM have gained considerable attention as LbL building blocks, as they can generate multilayers functionalities which are useful for a variety of bioapplications (Al-Khoury et al. 2019). They also present high capacity for mimicking of the natural cellular microenvironment (Prokopovic, Duschl, and Volodkin 2015). In 1999, Elbert et al. (Elbert, Herbert, and Hubbell 1999) presented for the first time a protocol for coating biological proteinaceous surfaces with thin polymer layers of two different polyelectrolytes. Since that, the electrostatic assembly of multilayer structures through LbL has been broadly exploited by different authors. Structure and thickness of the resulting LbL depends on different processing conditions such as pH, temperature, solvent, ionic strength and the type and properties of each polyelectrolyte used (Richert, Arntz, et al. 2004). The effect of all these parameters has been studied to obtain multilayer films with tailor-made properties.

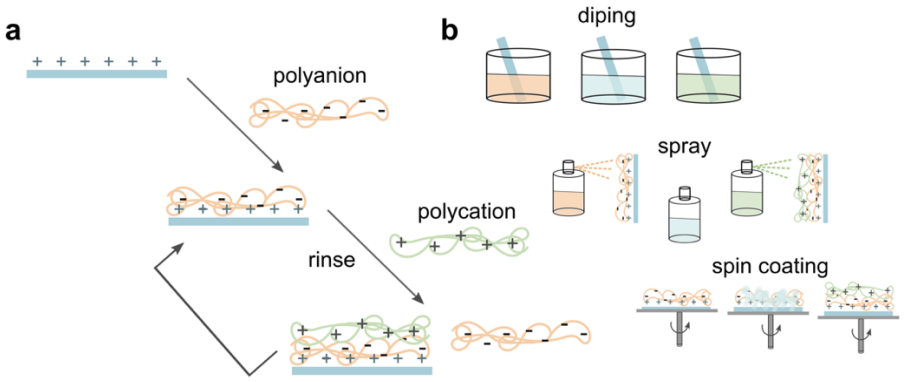

Figure 12. Layer-by-layer technic principle (a) and methodologies (b).

LbL technique involves different types of intermolecular interactions, such as electrostatic, charge-transfer, hydrophobic interactions, coordination chemistry interactions, and hydrogen and covalent bonding. Electrostatic interactions are the most studied (Criado-González, Mijangos, and Hernández 2021). During the electrostatic LbL assembly, different build-up mechanisms have been reported depending on the nature of the polyelectrolytes involved. Linear growth is the simplest one in which the thickness and mass of the film increase linearly with the number of deposited bilayers, and each polyelectrolyte layer interpenetrates only with the adjacent ones (Decher 1997). In contrast, in the exponential growth, there exists high chain mobility of the polyelectrolyte chains in the direction perpendicular to the film surface and in the plane of the film, leading to the diffusion of at least one of the polymer constituents. This phenomenon leads to a film architecture with the subsequent exponential thickness increase with the number of deposited bilayers (Porcel et al. 2006). It has also been reported that LbL made of polysaccharides renders the buildup of much thicker films, due to its high swelling capacity (Richert, Boulmedais, et al. 2004).

3.3. Materials and methods

3.3.1. Microsphere's production

3.3.1.1. Acrylates-based microspheres

Cross-linked copolymer microspheres were produced following a suspension polymerization protocol. The copolymer contained monomeric units of ethyl acrylate (EA), ethyl methacrylate (EMA) and acrylic acid (AA), what should be termed poly(EA-co-EMA-co-AA). In this Thesis, for simplicity they will be called hereafter acrylates microspheres. The co-polymerization reaction was performed in a sealed 500 mL volumetric flask under magnetic stirring immersed in a jacketed glass beaker connected to a thermostatic water bath. 4%w/v poly(vinyl alcohol) (PVA) (Sigma-Aldrich, USA) solution in deionized

water was used as emulsifier. Two different monomeric mixture formulations were prepared, with or without acrylic acid (Table 2).

Table 2. Microsphere's composition

Microsphere type	Initiator [g]	Monomer mixture [g]	Monomer mixture formulation		
			monomer	[g]	% w/v
0% AA	0.05	9.95	EA	5.47	55
			EMA	3.48	35
			EGDMA	0.99	10
			AA	0	0
10% AA	0.05	9.95	EA	4.97	50
			EMA	2.99	30
			EGDMA	0.99	10
			AA	0.99	10

Ethyl acrylate (EA), ethyl methacrylate (EMA), ethylene glycol dimethacrylate (EGDMA) and acrylic acid (AA). All monomers were purchased from Sigma-Aldrich, (USA).

100 mL of the dispersion phase were placed into the reactor at 30ºC and at a constant stirring rate of 800 rpm and let to stabilize for 30 minutes. Monomeric mixture (10 g) was prepared by mixing the non-water-soluble monomers, EA, EMA and ethyleneglycol dimethacrylate (EGDMA) as cross-linker and washed with 5% w/v sodium hydroxide (NaOH) (Sigma-Aldrich, USA) to remove the inhibitor. For the acrylic acid-containing microspheres, AA was added to the monomeric mixture after inhibitor removal. The initiator, benzoyl peroxide (BPO) (Fluka, Switzerland), was dissolved within the monomer phase at 0.5% w/w. This solution was then transferred into the dispersion medium and let to equilibrate for 10 minutes. Reactor temperature was kept at 65ºC for 6 hours for polymerization. Then, for post-polymerization, microspheres suspension was transferred into a glass beaker and diluted 1:1 with 10% w/v sodium chloride (NaCl) (Sigma-Aldrich, USA) solution prepared with distilled water. The dilution was kept 1 h at 90ºC.

To remove unreacted monomers, the physically adsorbed AA and PVA molecules, extensive cleanings were applied. In each cleaning microspheres were separated from the liquid phase by centrifugation 5 minutes at 5000 rpms. Microspheres were cleaned first with 5% w/v NaCl solution for 30 minutes, then 2 cleanings of 30 minutes with distilled water, one 30 minutes cleaning with ethanol (Sigma-Aldrich, USA) and finally 3 cleaning of 24 h under magnetic stirring in acetone (Sigma-Aldrich, USA). Finally, microspheres were rinsed twice with distilled water. Microspheres were then sieved with cell strainers of different mesh sizes (60 μm and 70 μm) to keep the fraction with the desired diameter distribution.

3.3.1.2. Cytodex 1 microspheres

As an alternative to acrylates-based microspheres, some work has been done in parallel on the development of microgels formed by commercially available microspheres. Cytodex 1 microspheres from Cytiva (USA) have been used. These microspheres have been designed as microcarriers for adherent cells. They are made of a cross-linked dextran matrix that is substituted with positively charged N,N-diethylaminoethyl (DEAE) groups to a degree that is optimal for cell growth. The charged groups are found throughout the entire matrix of the microcarrier. They present a monodisperse size distribution, with a mean diameter of 170 μm, and a minimum and maximum diameter of 140 and 200 μm, respectively. The density is 1.03 g/mL.

Microspheres are purchased as a lyophilized powder and were prepared for use following the manufacturer's instructions. Briefly, microspheres were hydrated in phosphate buffer saline (PBS) without calcium or magnesium (Gibco, USA) for 3 h at RT at 50 mL/g. Then a cleaning with PBS was performed. Finally, microspheres were sterilized in an autoclave at 115°C, 15 psi for 15 minutes. As Cytodex 1 are sterilized at the end of this process, all the functionalization procedures were carried out in a laminar flow hood under sterile conditions.

Microsphere's functionalization

3.3.2.1. Acrylates-based microspheres

Two proteins were adsorbed on the microspheres. Fibronectin (FN) from human plasma (Sigma-Aldrich, USA) as protein of interest in the study, and bovine serum albumin (BSA) (Sigma-Aldrich, USA) as anti-fouling control in some experiments. FN was adsorbed on 0% AA microspheres at 20 µg/ mL in miliQ water for 1 h at RT in an orbital shaker (Figure 13, a). For BSA coating, 10% AA microspheres were immersed in BSA solutions at 1 mg/mL in miliQ water, the coating was performed overnight at RT in an orbital shaker (Figure 13, b). After adsorption, samples were rinsed twice in PBS to eliminate the non-adsorbed protein.

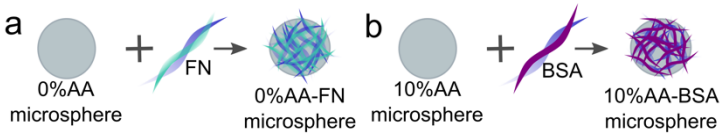

Figure 13. Scheme of the process for FN and BSA functionalization by physical adsorption.

Hyaluronic acid (HA) (Sigma-Aldrich, USA) molecular weight was reduced from 106 MDa to 320000 Da by means of acidic degradation (Poveda-Reyes et al. 2016). Briefly, 500 mg of high molecular weight HA were dissolved in 50 mL of hydrochloric acid (HCl) (Sigma-Aldrich, USA) at pH 0.5, and the solution was stirred for 24 h at 37ºC for HA degradation. Then, reaction was stopped by adjusting the pH to 7 with 1 M NaOH. The obtained solution was dialyzed (in a dialysis membrane of 3500 MWCO, (Sigma-Aldrich, USA)) against distilled water for 4 days and then lyophilized for 72 h. Resulting low molecular weight HA was used for microspheres functionalization using a two-step EDC (Sigma-Aldrich, USA)/sulfo-NHS (Sigma-Aldrich, USA) coupling (Figure 14, a). 10% AA microspheres were washed with activation buffer (0.1 M MES (Sigma-Aldrich, USA), 0.5 M NaCl, pH 6) and precipitated by centrifugation. 5 min at 7000 rpm, in following steps microspheres separation was always performed this way. Then EDC (2 mM) and sulfo-NHS (5 mM)

prepared in activation buffer were added to microspheres pellet in proportion 10 (EDC): 25 (sulfo-NHS): 1 (-COOH groups of the microspheres surface). Reaction components were mixed and keep in an orbital shaker 2 h at room temperature (RT). Two washes were performed with PBS pH 7.4. Activated -COOH groups were made to react with a molecular bridge, a di-amine terminated poly(ethylene glycol) (PEG-$_{di}NH_2$) (Sigma-Aldrich, USA) by incubation of the microspheres pellet in 2 mM PEG-$_{di}NH_2$ solution prepared in PBS, $PEG_{di}NH_2$ was added in proportion 10:1 to microspheres -COOH and kept in an orbital shaker overnight (ON) at RT. Two washes were performed with PBS pH 7.4. HA was dissolved at 5% w/v in PBS. 100 equivalents of EDC and 40 of sulfo-NHS were added to 1 equivalent of HA. The resulting solution was added to microspheres pellet in a proportion of 1 equivalent of HA to microspheres -COOH. Mixture was kept ON at RT in an orbital shaker. Finally, 2 cleanings in PBS were performed.

The COL 1 protein has also been grafted onto the 10%AA microspheres using one step EDC/sulfo-NHS chemical coupling (Figure 14, b). Activation of microsphere's -COOH groups was performed following the protocol described for the HA grafting. Then, microsphere's pellet was immersed in a COL 1 (Advanced BioMatrix, USA, 97% Type I atelocollagen) solution (1 mg/mL) and kept ON at RT in an orbital shaker. Finally, 2 cleanings in PBS were performed.

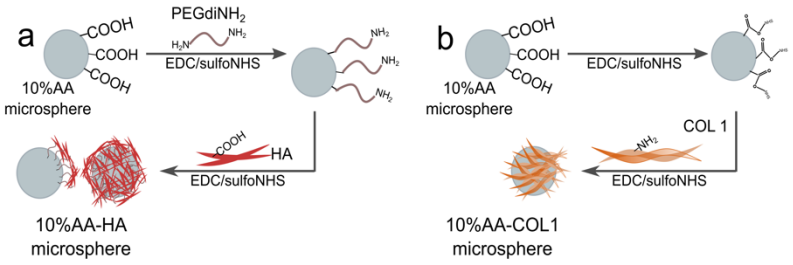

Figure 14. Scheme of the process for HA and COL 1 functionalization by covalent grafting using EDC/NHS coupling chemistry.

Finally, different peptides were incorporated on 10% AA microspheres also by means of EDC/sulfo-NHS chemistry. Peptides were produced by Dr. Annj

Zamuner from the Department of Industrial Engineering, University of Padova, Italy. Peptides where obtained by chemical synthesis as decribed elsewhere (Zamuner et al. 2017). The different peptides used are listed in Table 3 and all of them present motifs that are known ligands of β1 and β3 integrins or syndecan on MM cell's surface (Hozumi et al. 2016). These are adhesion molecules with reported roles in MM DR generation (Ren et al. 2018; Beauvais et al. 2016; Schmidmaier et al. 2006; Hosen 2020). These peptidic sequences are part of different proteinacinous ECM molecules, such as FN (Hozumi et al. 2016). The objective of using the peptides is to assess if biomateriales biofunctionalized with the synthetic peptides can serve as a FN-mimetic biomaterial.

Table 3. Peptides used for 10% AA microspheres grafting.

Name	Sequence	FN domain	Receptor
GRGD	Gly-Arg-Gly-Asp	III10	Integrin α4β1, αvβ3, αvδ, α5β1
IDAPS	Ile-Asp-Ala-Pro-Ser	III14	Integrin α4β1
PRARI	Pro-Arg-Ala-Arg-Ile	III14	Integrin α4β1, syndecan

Activation of microsphere's -COOH groups was performed following the protocol described for the HA grafting. Then, microsphere's pellet was immersed in the different peptides solutions prepared in PBS in a proportion of 10 equivalents of peptide to 1 -COOH groups of the microspheres surface and kept ON at RT in an orbital shaker. Finally, 2 cleanings in PBS were performed.

3.3.2.2. Cytodex 1 microspheres

Cytodex 1 microspheres present positively charged surface. Because of this a LBL approach was chosen for its functionalization with different BM ECM molecules. Two different LbL pairs (anion/cation) were tested. Chitosan (CHI) was chosen as cation in both pairs and the anions were the ECM molecules of interest: HA and CS (Sigma-Aldrich, USA). The technique is based on the electrostatic self-assembly in which alternating layers of CHI and HA or CS

are deposited one over the other, due to the electrostatic difference between the CHI and HA/CS layers. Polyelectrolytes (CHI, HA and CS) were dissolved in 0.15 M NaCl solution in distilled water at 1 mg/mL and pH was adjusted at 5-5.5 with acetic acid (Sigma-Aldrich, USA). 0.15 M NaCl at pH 5 in distilled water was used as rinsing buffer. All solutions were sterilized trough 0.22 μm filtration.

Cytodex 1 microspheres were immersed in 0.15 M NaCl at pH 5 as preconditioning step. LbL was performed by alternated immersion, in orbital agitation at 150 rpm, in CHI solution (positively charged at pH 5) for 15 minutes, and HA or CS solution (negatively charged at pH 5) for 20 minutes, with 3 cleanings of 5 minutes between them. By repeating those steps, layers were built up to 11 (Figure 15). During the process cell strainers were used to contain the microspheres and allow its change from one solution to another.

Once microspheres were functionalized, the LbL was cross-linked with glutaraldehyde (GA) (Sigma-Aldrich, USA) 2.5% v/v at RT for 1 h. Then, two washes of 5 minutes and one ON with milliQ water were performed. Then, a 0.1 M glycine (Sigma-Aldrich, USA) bath was performed for 1 h at 37ºC to avoid cytotoxicity. Finally, 3 washes with milliQ water of 5 minutes were performed. Functionalized microspheres were kept in PBS to avoid dehydration.

In regards of the experimental results, some modifications were applied to the initial protocol (protocol 1). The incubation in the first layer solution of the LbL (HA or CS) was kept ON, instead of 15 minutes. The GA crosslinking was substituted by EDC/NHS based crosslinking. Briefly, the functionalized microgel was incubated in a solution of 100 mM NHS and 260 mM EDC ON under stirring (150 rpm) at 4°C. Then, 3 washes of 1 h were carried out with 0.15 M

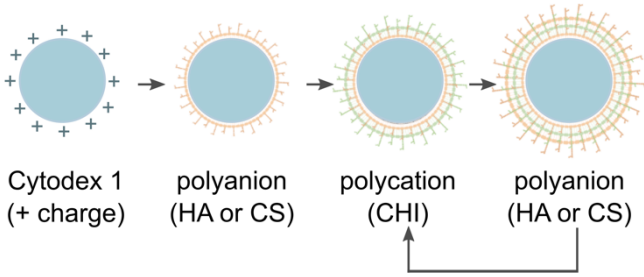

Figure 15. Scheme of the process for CS and HA functionalization of Cytodex 1 microspheres by layer-by-layer technic.

NaCl at pH 5.5. This new method was termed as protocol 2, while the original one will hereafter be named as protocol 1.

All the different types of microspheres obtained are summarized in Table 4.

Table 4. Different microspheres obtained and the acronym used for its designation.

Microsphere type	Obtaining protocol	Functionalization protocol			
		Acronym	ECM biomolecule	Functionalization protocol	Crosslinker
Acrylates, 0%AA	Suspension polymerization	0%AA CTRL	None (control)	-	-
		0%AA FN	FN	Coating	-
Acrylates, 10%AA	Suspension polymerization	10%AA CTRL	None (control)	-	-
		10%AA HA	HA	2 steps EDC/NHS coupling	-
		10%AA COL 1	COL 1	1 step EDC/NHS coupling	-
		10%AA PRARI	PRARI peptide	1 step EDC/NHS coupling	-

		10%AA IDAPS	IDAPS peptide	1 step EDC/NHS coupling	-
		10%AA GRGD	GRGD peptide	1 step EDC/NHS coupling	-
		10%AA BSA	BSA	Coating	
Cytodex 1	Commercial	Cyt CTRL	None (control)	-	-
		Cyt HA	HA	LbL protocol 1	-
		Cyt CS	CS	LbL protocol 1	-
		Cyt HA CHI	LbL control (CHI as outer layer)	LbL protocol 1	-
		Cyt CS CHI	LbL control (CHI as outer layer)	LbL protocol 1	-
		Cyt HA GA	HA	LbL protocol 1	GA
		Cyt CS GA	CS	LbL protocol 1	GA
		Cyt HA EDC	HA	LbL protocol 2	EDC/NHS
		Cyt CS EDC	CS	LbL protocol 2	EDC/NHS

3.3.3. Microsphere's characterizations

3.3.3.1. Acrylates-based microspheres

Surface morphology of the microspheres was observed under a field emission scanning electron microscope (FESEM) (Ultra 55, Zeiss Auriga Compact, Germany). Images were taken with an accelerating voltage of 1 kV. Microspheres were coated with platinum following a standard sputtering protocol for 90 s (JF1100, JEOL, Japan). Microsphere's diameter was as-

sessed from white field inverted microscope images. At least 350 microspheres of each type were measured using ImageJ software (National Institutes of Health, USA).

Thermogravimetric measurements (TGA) of dry and wet samples of 0% and 10%AA microspheres were performed using an SDT-Q600 system (TA Instruments, Great Britain). Dry samples were vacuum dried. Wet samples were immersed in liquid water and let to equilibrate for 48 h, after that samples were centrifuged in a falcon tube with a cell strainer (to retain the microspheres and drain unabsorbed water). TGA tests were carried out in alumina crucibles in which weight samples of between 5 and 10 mg were heated from 30°C to 800 °C at a heating rate of 10°C min^{-1}. TGA experiments were performed using a nitrogen atmosphere (flow 20 ml min^{-1}). The equilibrium water content (EWC) was calculated from experimental measurement of the wet samples as described in Equation (1):

Equation (1): Calculation of EWC wt% from TGA experiments

$$\text{EWC (wt.\%)} = \frac{m_{H_2O}}{m_{dry}} \times 100 = \frac{\text{initial wet weight 100 \% – dry weight \% at 100 ºC}}{\text{dry weight \% at 100 ºC}} \times 100$$

where the % of weight dry was the % percentage of weight remaining at 100ºC after water evaporation.

AA inclusion in microspheres and different functionalization presence was assessed by X-ray photoelectron spectroscopy (XPS) by means of a XPS Spectrometer AXIS Supra (Kratos Analytical, Japan) apparatus, which uses a monochromatic Al Kα X-ray source (1486.6 eV) covering an analyzing area of 700 x 300 μm (120 W power). Survey spectra were collected using a pass energy of 160 eV and a step size of 1 eV. High-resolution regions were collected using a pass energy of 20 eV and a step size of 0.1 eV. Data were processed using CasaXPS (Casa Software, United Kingdom) software.

For BSA adsorption testing, BSA conjugated with fluorescein-5-isothiocyanate (FITC) (Invitrogen, USA) was used following the described protocol for non-fluorescent BSA and samples were imaged under an epifluorescence

microscope Eclipse 80i (Nikon, Japan) in comparison with non-coated samples.

The micro bicinchoninic acid assay (BCA) Protein Assay Kit (Thermo Scientific, USA) was used to quantify the amount of FN and COL 1 adsorbed and grafted respectively, following the manufacturer's protocol. Coated and uncoated samples were analyzed on a Victor 3 microplate reader (Perkin Elmer, USA), reading at 550-570 nm.

To assess -COOH presence in microspheres surface, in order to compare -COOH content of 0% AA and 10% AA and to monitor the -COOH content after each step of the HA grafting process, indirect toluidine blue O (TBO) (Sigma-Aldrich, USA) assay was performed (Pérez-Álvarez et al. 2019). Carboxylic groups from microspheres react with TBO through the formation of ionic complexes. The different types of microspheres were immersed in a 0.5 mM TBO aqueous solution (pH 10) for 12 h at RT to allow complex formation. Then, microspheres were cleaned several times with a 0.1 mM NaOH solution to remove the excess of TBO. Finally, the TBO bonded to the membranes was desorbed by immersion of the substrates in a 50% acetic acid solution for 10 min. The absorbance at 633 nm was recorded by a UV–Vis spectrophotometer (Cary UV-Vis, Agilent Technologies, USA). The amount of the -COOHs was calculated by using a calibration curve of TBO/50% acetic acid solution measured in the same conditions and normalized to the dry mass of microspheres.

The thermal properties of the m10% AA microspheres were analyzed by differential scanning calorimetry (DSC) in a dry nitrogen atmosphere. The experiments were carried out in sealed aluminum pans with a DSC Pyris 1 (Perkin-Elmer, USA) in a temperature range from -60 °C to 200 °C with cooling and heating scans at a rate of 20 °C/min. The sample weight ranged between 4 and 10 mg. Two scans were performed to the same sample.

3.3.3.2. Cytodex 1 microspheres

Different characterizations applied to Cytodex 1 functionalized microspheres attempted to analyze effectiveness of the applied LbL protocols. For routinary image analysis of the microspheres, size distribution analysis and imaging after the different LbL protocols, inverted optical microscope (Nikon, Japan) white-field images were used and ImageJ software for image analysis.

Cryogenic field emission scanning electron microscope (cryoFESEM) (PP3010T, Quorum Technologies, UK) was used to determine the presence of the LbL functionalization on microsphere's surface. Images were taken with an accelerating voltage of 1 kV. Microspheres were coated with platinum following a standard sputtering protocol for 90 s (JF1100, JEOL, Japan). Images were taken with an accelerating voltage of 1 kV. Microspheres were frozen in slushy nitrogen freezing station, and transferred into the instrument with a vacuum transfer device. Then a standard sublimation protocol for 15 minutes was applied. As CHI is an autofluorescent polymer when crosslinked with GA (Q. Zhao et al. 2007; H. Zhao et al. 2013), laser scanning confocal microscopy (LSCM) was used to confirm the presence of LbL. An LSCM 780 (ZEISS, Germany) microscope was used. Microspheres were embedded in 2-hydroxyethyl-agarose (Sigma-Aldrich, USA) gels for imaging as individual microspheres in fixed position and without any stain.

Fourier transformed infrared spectroscopy (FTIR) was carried out to analyze if significant differences in the spectra can be attributed to different LbL or crosslinking protocols. Measurements were performed by an ALPHA FTIR spectrometer (Bruker, USA) in ATR mode from 4000 to 400 cm^{-1} at a wavenumber resolution of 4 cm^{-1}.

TGA of wet samples of Cyt CTRL, Cyt HA EDC and Cyt CS EDC were performed at the same conditions described in precious section for acrylates microspheres. The aim of the analysis was to determine the weight differences between samples that could be attributed to the LbL coatings. Samples were heated from 30°C to 800°C at a heating rate of 10°C min^{-1}. 3 independent replicates of each type of sample were analyzed. Data was analyzed and

graphed in Microsoft Excel 2021 (Microsoft Corporation, USA). First, the dry weight of the Cyt CTRL samples was determined, which was 100% of the dextran fraction. Subsequently, the dry weight of the samples Cyt CS EDC and Cyt HA EDC was determined, and it was compared with the average dry weight of the 3 replicates for Cyt CTRL samples. Thus, the weight fraction of each type of coating with respect to dextran weight fraction was obtained.

CS deposition in microsphere´s surface after LbL was assessed by Taylor's blue colorimetric method using Glycosaminoglycan Assay Blyscan (Biocolor, UK), which allows to quantify sulfated glycosaminoglycans and proteoglycans. Shortly, microspheres were soaked in 1 mL of Blyscan dye reagent containing 1,9- dimethyl methylene blue and incubated for 30 min under shacking at RT. After incubation, samples were washed with dH_2O and transferred to a new Eppendorf. 0.5 mL of dissociation reagent were added to favor CS dissociation from 1,9-di-methyl methylene. Microspheres were pelleted by centrifugation and supernatant absorbance was read at 652 nm (Victor3 microplate reader; Perkin Elmer, USA) transferring 100 µL of each sample to a 96-well plate. CS concentration was determined using a calibration curve (0–5 µg). All measurements were performed in triplicate.

3.3. Results and discussion

3.4.1. Synthesis and functionalization of acrylates microspheres

3.4.1.1. Synthesis and characterization of acrylates microspheres

In the present Doctoral Thesis, we have worked on the obtention and optimization of an emulsion technique protocol for the polymerization of microspheres with the desired composition and diameter range. A suspension polymerization protocol has been used for the obtention of acrylates-based biostable microspheres with two different polymeric compositions. The copol-

ymers consisted of EA, EMA and EGDMA and the two different types of microspheres differentiate in the presence (10%) or absence (0%) of AA. Microsphere composition has been designed to meet certain requirements:

I. Long term biostability.

II. Good performance in 3D culture.

III. Versatility for biomolecules coating or grafting.

IV. Stability in solvents frequently used for sterilization and molecular biology protocols, like ethanol or acetone.

Because of that mono-functional (EA, EMA) and difunctional (EGDMA) acrylate or methacrylate monomers were selected in the copolymer's composition. As microspheres composition was based on stable chemical crosslinking once its monomers were polymerized, the polymerization should be done in the final morphology desired for the copolymer. Because of that, among the wide variety of available methods for polymerization, suspension polymerization was chosen.

Poly (ethyl acrylate), PEA, has been shown to induce FN fibrillogenesis in the absence of cellular activity, which is the origin of this polymer's good performance in 3D cultures(Llopis-Hernández et al. 2013; Salmerón-Sánchez et al. 2011). Because of that it was chosen for microspheres production. However, EA gave rise to microspheres that were sticky and difficult to handle. Ethyl methacrylate was incorporated in the composition to improve their properties, increase the glass transition temperature (T_g), and make the microspheres easier to handle (Clara-Trujillo et al. 2019), the good biocompatibility of these monomers and their extended use in the biomedical field makes them good candidates for cell culture platforms generation. Ethyleneglycol dimethacrylate (EGDMA) is a di-functional vinyl monomer commonly used in free radical polymerizations as crosslinker, this monomer was incorporated to microspheres composition to achieve their cross-link and avoid its dissolution in solvents such as ethanol or acetone. Other fundamental aspect considered when defining microspheres chemical composition was their compatibility

with different molecular functionalizations. The presence of determined functional groups on microspheres surface was key for allowing posterior covalent grafting of several biomolecules with commonly used chemistries for biomaterials surface modification. Carboxyl groups (-COOH) presence on microsphere surface would accomplish this objective, as can be easily coupled with molecules with terminal amine groups by means of amide bonds mediated by the extensively used carbodiimide chemistry (Poveda-Reyes et al. 2016). Because of that acrylic acid (AA) was incorporated into microspheres composition.

A first protocol for the production of the microspheres used the monomers as received, without extracting the inhibitor they contain and adding an amount of initiator sufficient to neutralize it and then initiate radical polymerization. The developed protocol was based on the protocol from Tuncel et al. (Tuncel et al. 1996) which presents a method for the obtention of microspheres with similar composition and size distribution to the ones desired. The protocol from Tuncel et al. consisted in a conventional suspension polymerization procedure, the dispersion medium was prepared by dissolving 200 mg of PVA within 50 mL of distilled water. The desired amount of BPO was dissolved within the monomer phase. This solution was then transferred into the dispersion medium placed in a magnetically stirred (at a constant stirring rate of 600 rpm) glass polymerization reactor (100 mL), which was in a thermostatic water bath. The reactor temperature was kept at 65°C for 4 h. Then, the polymerization was completed at 90°C in 2 h.

However, when this initial protocol was tested for the monomeric composition described in Table 2, it didn't allow the obtention of microspheres. First, when polymerization was done following the original protocol from Tuncel et al., aggregation of monomer droplets in the emulsion took place in the post-polymerization step, and thus large amorphous particles were obtained instead of spherical microspheres (Figure 16, a). Macroscopically it was possible to appreciate that aggregation of the monomer microdroplets occurred at this step of the protocol. Different temperatures and stirring speed for this step were tested. However, all of them generated similar results in terms of

aggregation. Then polymerization time was increased from 4 to 6 hours before post-polymerization and spherical shapes in the resulting polymer aggregate started to appear, however individual microspheres seemed to aggregate in bigger formations (Figure 16, b). We hypothesized that during the polymerization step, microdroplets were effectively formed, however when the conditions of the emulsion were changed for post-polymerization, instabilities appear in the mixture resulting in microsphere aggregation. As an increase of polymerization time would led to a resulting protocol of more than 8 hours, this change was not assayed. It would have made difficult the experimental procedure, as emulsion polymerization cannot be left ON without monitoring. Instead, changes in post-polymerization step were introduced trying to avoid the monomer microdroplets formed in polymerization to aggregate before they complete their polymerization process.

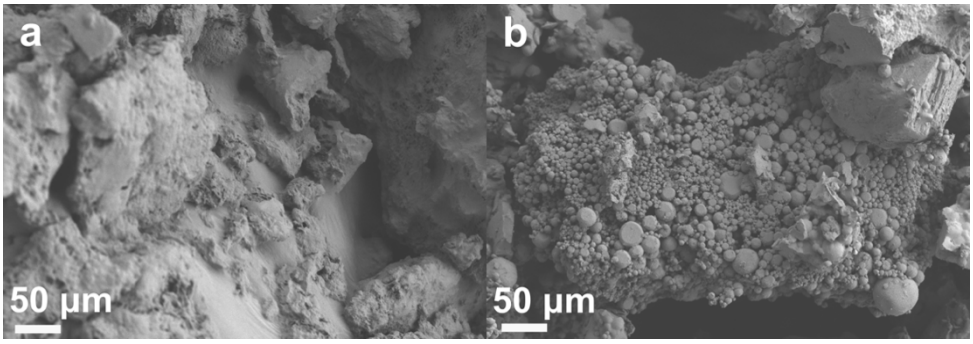

Figure 16. FESEM images of the polymer aggregates obtained with the initial suspension polymerization protocols tested. a) Results obtained with the original protocol from Tuncel at al. 4 h polymerization at 65º followed by 2 h post-polymerization at 90º. b) Results obtained with a protocol consisting of 6 h polymerization at 65º followed by 2 h post-polymerization at 90º

The recipient was changed for the post-polymerization step from the initial volumetric flask to a 500 mL glass beaker. A critical moment takes place when stirring is stopped for changing the reactor and few seconds are needed for stablishing a stable emulsion in the new reactor. To avoid aggregation risk in this critical step and reduce the probability of the droplets in phase of polymerization to collide, the emulsion content was diluted in 1:1 with 10% w/v NaCl

solution prepared with distilled water. NaCl was used to increase ionic strength in the continuous phase. The ionic strength is an experimental parameter which is known to affect stability of suspensions, it can increase charge and repulsion in the pre-formed polymeric microspheres and thus reduce coalescence in the post-polymerization step (Kiatkamjornwong and Phunchareon 1999). Then the dilution was kept 1 h at 90ºC for post-polymerization, higher post-polymerization times lead to evaporation of water and concentration of PVA in the continuous phase.

As a result of these changes, polymeric individual microspheres were finally obtained (Figure 17). To remove unreacted monomers and PVA molecules (Figure 17, c-f), extensive cleanings were applied. Cleanings with aqueous solvents removed PVA; PVA traces can be seen in pictures corresponding to ethanol (Figure 17, c and d) and acetone (Figure 17, e and f) cleaned samples but not in samples cleaned with distilled water. However, ethanol and acetone cleanings were included in cleaning procedure because in the water cleaned samples unreacted monomers weren't totally removed, as the characteristic monomer smell persisted. Another reason for including these cleanings was to test microspheres stability in these solvents. These cleanings should be performed after water-based cleanings, as they are not efficient for PVA solubilization and removal. Initially, microspheres partially dissolved after being immersed in ethanol or acetone for 1 hour (Figure 17, c-d and e-f respectively). This fact indicates that polymerization has not been completed and microspheres probably had unreacted monomer on its matrix. This was also confirmed by DSC (Figure 17, g), an exothermic peak corresponding to the polymerization of the remaining monomer in the matrix of the microspheres appeared as the sample reached higher temperatures in the first scan. In the

second scan of the same sample the exothermic peak disappears as polymerization has taken place in the instrument during the first scan.

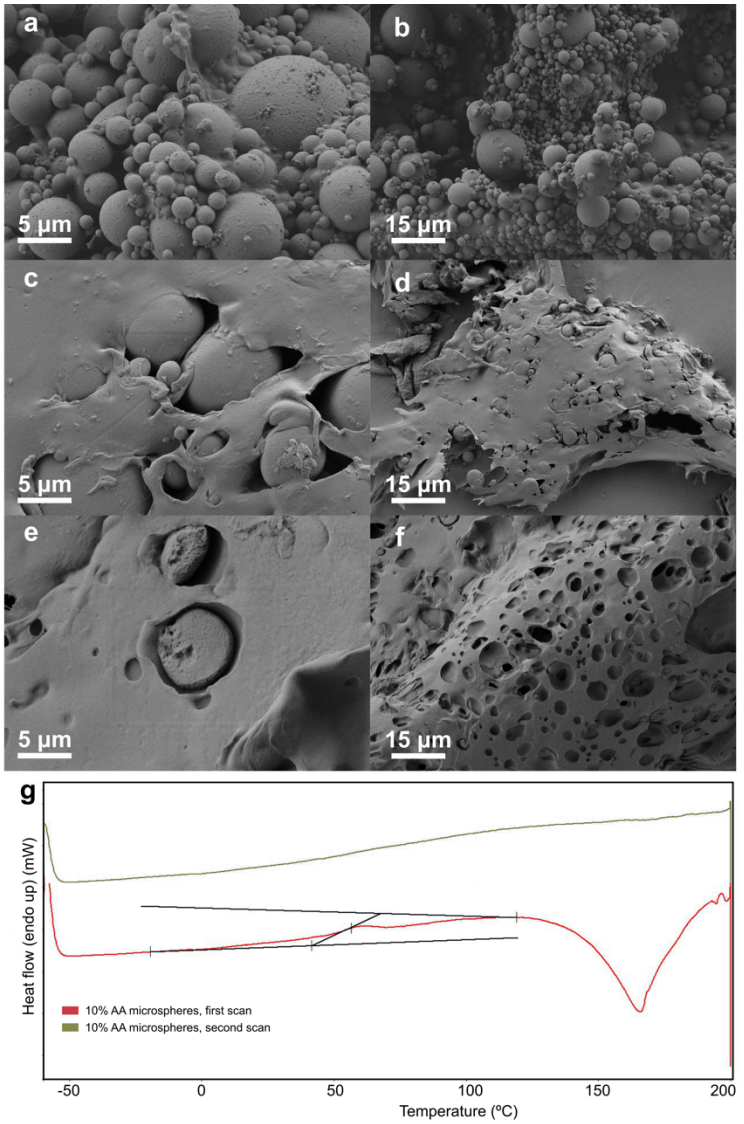

Figure 17. FESEM images of the microspheres obtained after the differential cleaning procedures. a-b) Microspheres after 3 cleanings in distilled water. c-d) Microspheres after 3 cleanings in ethanol. e-f) Microspheres after 3 cleanings in acetone.g) DSC heating thermograms of 10% AA microspheres. First scan (red line) shows the exothermic peak at around 160ºC, which disappears in the second scan (green line).

Given that, at this point, the protocol for microsphere obtention lasted 8 hours, increasing polymerization time for avoid the problem wouldn't have been a practical option. Instead, it was proposed to remove inhibitor from monomers prior to starting the polymerization process. Then the optimized protocol was tested with the monomer mixture previously subdued to NaOH inhibitor removal and polymeric microspheres where finally obtained (Figure 18) with the protocol extensively described in section 3.3.1.1.

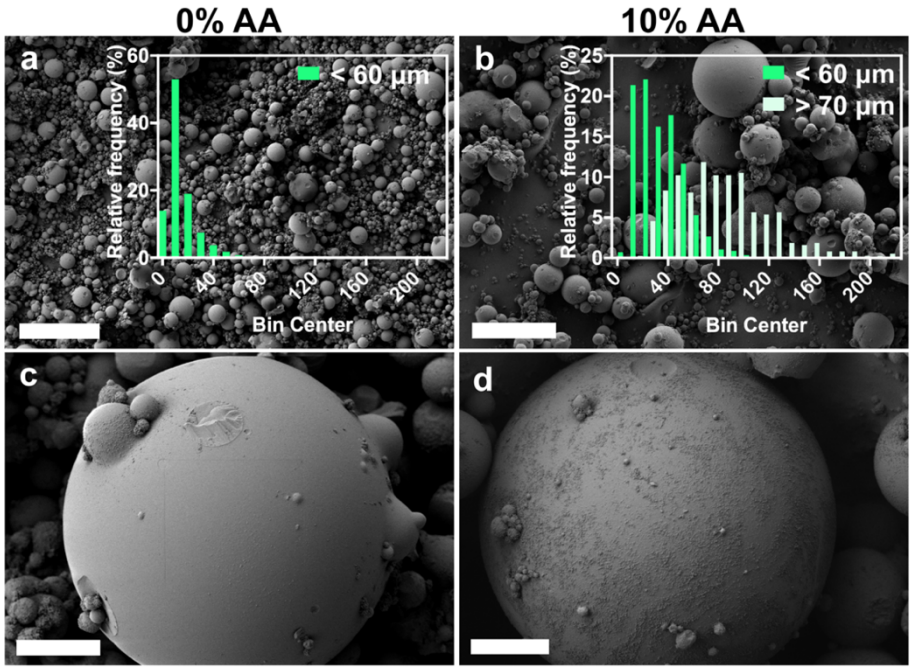

Figure 18. Acrylates-based biostable microspheres with different sizes and compositions. FESEM images of non-sieved 0% (a) and 10% (b) AA microspheres with the diameter distributions of the different size fractions separated after sieving (inserted histograms, bin size: 10 µm, at least 350 microspheres of each type were measured using ImageJ software, results are plotted in relative frequency (%)). Scale bar: 100 µm. c, d) Detail of microspheres topography. Scale bar: 10 µm.

FESEM images confirmed regular spherical morphology of the microspheres and showed that 10% AA microspheres present rougher topography (Figure 18 d) than 0% AA (Figure 18 c), with satellite nanospheres on its surface. Polymerization takes place in microdroplets of the organic phase containing

EA, EMA, EDGMA and the initiator, immersed in an agitated aqueous phase, and the AA is soluble both in the organic and in the aqueous phase. We hypothesize that, once polymerization has started inside the organic microdroplets, nanodroplets of AA migrate from the aqueous to the organic phase and polymerize preferentially on microspheres surface giving rise to this topography. A phenomenon that was reported by Wang et al (P. H. Wang and Pan 2002) for the distribution of acrylic acid monomers into the different phases of the emulsion.

For both compositions the emulsion polymerization protocol produced broad diameter distributions. As we intended to study the effect of microsphere size in cell proliferation, microspheres were sieved and separated in two different fractions: < 60 μm diameter and > 70 μm diameter (Figure 18 a and b). Plasmatic cells present an approximate diameter of 10 to 20 μm, because of that we sieved the microspheres as smaller than 60 μm and bigger of 70 μm, with the objective of obtaining a fraction of similar proportions to cellular size but with good yield and a second fraction significantly bigger than cellular sizes.

Descriptive statistics of the diameter distribution from the three different microspheres fractions obtained are shown in Table 5.

The phenomenon of AA preferentially polymerizing on microspheres surface from the aqueous phase and not from the monomeric phase of the microdroplets could also justify the larger diameters obtained for the 10% AA microspheres compared to those with 0% AA, despite that both were obtained with the same parameters in the synthesis protocol.

To assess AA incorporation in the 10% AA microspheres, the indirect colorimetric method of Toluidine Blue O (TBO), which stains the carboxyl groups, was used. As seen in Figure 19 a, 10% AA present statistically significant higher signal of TBO stain than 0% AA microspheres, confirming the presence of the AA on their surface.

A thermogravimetric analysis (TGA) of vacuum dried and wet samples was also performed (after equilibration in liquid water for 48 hours) of 0% and 10%

AA microspheres (Figure 19, b). The weight loss up to 100 ºC can determine the equilibrium water content (EWC) of the microspheres. Water sorption is 0.58 g of water per gram of polymer, i.e., EWC= 58 wt.% measured on a dry basis in the 10% AA sample due to the presence of the hydrophilic carboxylic groups of the monomeric units of AA, which act as sorption sites for water molecules (Tuncel et al. 1996). The equilibrium water sorption of 0%AA sample is much smaller, in the order of EWC= 8.3 wt.%, typical of hydrophobic poly-acrylates that do not contain hydrophilic groups. To further exploring AA incorporation on the 10% microspheres, X-ray photoelectron spectroscopy (XPS) analysis was carried out. Elemental composition was extracted from the survey spectra of two 0% AA and two 10% AA samples (Figure 19, c) and used for the calculation of the experimental O/C ratio that was plotted against the theoretical O/C ratio (of Table 6), calculated from the molecular formula and proportions of different monomers used (Figure 19, d). For both types of microspheres, experimental O/C ratios showed lower values than theoretical ones. The difference between 10% AA and 0% AA ratio, due to the higher proportion of O atoms in the acrylic acid monomer (Table 5), confirmed the AA incorporation into the surface of the 10% microspheres. Moreover, this difference is even greater in the experimental O/C ratios than in the theoretical ones, which may be attributed to the preferential polymerization of AA on microsphere's surface than in the bulk, reinforcing the hypothesis stated when studying microsphere's topography and diameter distributions. The scan spectra for C1s and O1s of both types of microspheres are shown in Figure 19, e. As expected, new peaks were not observed due to the incorporation of the AA, nevertheless the intensity of the (C=O)–O and the C-O peaks is increased in the 10% AA C1s scan compared to the C1s scan of the 0% AA microspheres. Similarly, the intensity of the (C=O)–O peak increased in the 10% AA O1s scan compared to the O1s scan of the 0% AA microspheres.

Thus, these characterizations confirmed AA incorporation into the 10% AA microspheres.

Table 5. Descriptive statistics from the diameter distributions of the different fractions obtained after sieving the 0% AA and the 10% AA microspheres.

Polymer composition	Sieved fraction	Mean diameter (μm) ± Standard deviation	Minimum diameter (μm)	Maximum diameter (μm)
0% AA	< 60μm	15 ± 11	2	66
10% AA	< 60μm	31 ± 19	4	102
10% AA	> 70μm	86 ± 19	22	220

Table 6. Molecular formula and theoretical O/C ratio of the different monomers used for the microsphere's synthesis.

Monomer*	Molecular Formula	Theoretical O/C Ratio
EA	$C_5O_2H_8$	0.4
EMA	$C_4O_2H_6$	0.5
EGDMA	$C_{10}O_4H_{14}$	0.4
AA	$C_3O_2H_4$	0.67

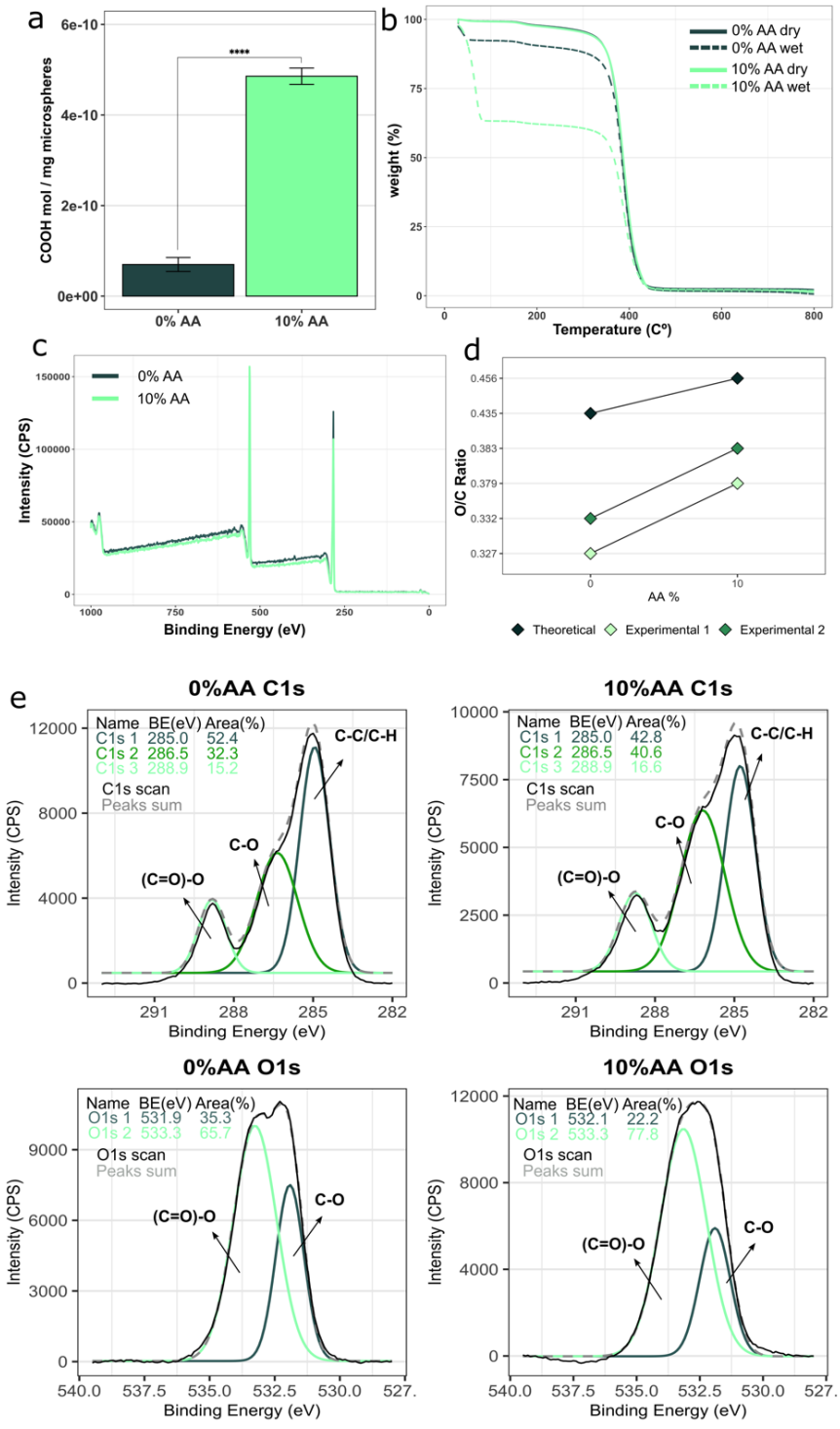
a
COOH mol / mg microspheres
6e-10
4e-10
2e-10
0e+00
****
0% AA
10% AA
b
weight (%)
100
75
50
25
0
0% AA dry
0% AA wet
10% AA dry
10% AA wet
0
200
400
600
800
Temperature (C°)
c
Intensity (CPS)
150000
100000
50000
0
0% AA
10% AA
1000
750
500
250
0
Binding Energy (eV)
d
O/C Ratio
0.456
0.435
0.383
0.379
0.332
0.327
0
10
AA %
Theoretical
Experimental 1
Experimental 2
e
0%AA C1s
Name BE(eV) Area(%)
C1s 1 285.0 52.4
C1s 2 286.5 32.3
C1s 3 288.9 15.2
C1s scan
Peaks sum
C-C/C-H
C-O
(C=O)-O
Intensity (CPS)
12000
8000
4000
0
291
288
285
282
Binding Energy (eV)
10%AA C1s
Name BE(eV) Area(%)
C1s 1 285.0 42.8
C1s 2 286.5 40.6
C1s 3 288.9 16.6
C1s scan
Peaks sum
C-C/C-H
C-O
(C=O)-O
Intensity (CPS)
10000
7500
5000
2500
0
291
288
285
282
Binding Energy (eV)
0%AA O1s
Name BE(eV) Area(%)
O1s 1 531.9 35.3
O1s 2 533.3 65.7
O1s scan
Peaks sum
(C=O)-O
C-O
Intensity (CPS)
9000
6000
3000
0
540.0
537.5
535.0
532.5
530.0
527.
Binding Energy (eV)
10%AA O1s
Name BE(eV) Area(%)
O1s 1 532.1 22.2
O1s 2 533.3 77.8
O1s scan
Peaks sum
(C=O)-O
C-O
Intensity (CPS)
12000
8000
4000
0
540.0
537.5
535.0
532.5
530.0
527.
Binding Energy (eV)

Figure 19. Characterization AA presence on 10% AA microspheres. a) TBO colorimetric determination of COOH groups (n=3, measured in duplicate). b) TGA of wet (dashed lines) and dry (solid lines) samples of 0% AA and 10% AA microspheres. c) XPS survey spectra of 0% AA and 10% AA microspheres. d) Theoretical and experimental O/C ratios calculated from elemental composition of 0% AA and 10% AA microspheres. For experimental ratios, n = 2 XPS survey spectra were analyzed. e) XPS scan spectra of C1s and O1s for 0% and 10% AA microspheres. P value legend: p ≤ 0.0001 (****).

3.4.1.2. Functionalization of acrylates microspheres

ECM has been established as a key player in MM disease development and DR acquisition (Di Marzo et al. 2016; Robak et al. 2018; Hou et al. 2019). The proteinaceous matrix of the ECM (mainly composed of fibronectin, laminin and collagens) is the main holder of the BM architecture. Adhesion of MM cells to FN is one of the most studied interactions that generates a DR phenotype in MM cells, it is mediated trough integrins $\alpha4\beta1$ and $\alpha4\beta5$ (Tancred et al. 2009). Glycosaminoglycans are incorporated to BM ECM by stromal cells. Hyaluronic acid is a major component of BM ECM and its adhesive interaction with MM cells, mainly mediated by CD44 and the receptor for hyaluronan-mediated motility (RHAMM) (Avigdor et al. 2004), has been related to MM BM homing and the generation of DR (Vincent et al. 2003; Katz 2010; Vacca et al. 1995). Moreover, the nature of glycosaminoglycans allow them to act as reservoirs of soluble factors from the milieu. We intended to study the effect of different ECM components presented on 3D microgels in the development of drug resistance in MM cell lines. We selected FN (Di Marzo et al. 2016; Damiano et al. 1999), and HA as ECM components of BM niche whose role on MM cell lines proliferation and drug resistance should be addressed in biomimetic models (Bjorklund et al. 2014). Furthermore, additional biomolecules were also optimized as biomimetic functionalization for these microspheres: COL 1 and different peptide fragments corresponding to FN and HA sequences with relevance in the interaction of these molecules with MM cells. Although these functionalizations have not been assayed in cell

culture in this Doctoral Thesis, they were developed and characterized to increase the range of available different microgels in the context of the project in which this Thesis is framed.

In the case of FN, covalent graft of FN by means of EDC/NHS chemistry is reported to increase probability of blocking key FN active sites, as it implies amino groups of FN which are randomly distributed throughout the molecule (Trujillo et al. 2020). Accordingly, FN was adsorbed on microspheres surface following a conventional coating protocol. 0% AA microspheres were used (Figure 20, a), as AA has been reported to decrease the efficiency of FN absorption on acrylic copolymers (Briz et al. 2013), a fact that was also confirmed by performing the FN coating in both types of microspheres (0% AA and 10% AA in equivalent conditions and quantifying the amount of FN adsorbed (Figure 20, b). To assess FN incorporation, bicinchoninic acid assay (microBCA) was used for quantification of the mass of adsorbed protein per mg of microspheres. As can be seen in Figure 20 b, 0% AA microsphere present increased FN absorption compared to 10% AA microspheres, moreover XPS scan spectra from N1s also confirmed this fact (Figure 20, c). Results confirmed presence of FN on 0% AA microspheres surface (Figure 20, b and c). Moreover, XPS analysis confirmed the presence of N in the surface of the coated microspheres (Figure 20, c), as the XPS N1s scan spectra of the 0% AA coated microspheres presented a significantly higher peak corresponding to N when compared to the non-coated 0% AA microspheres.

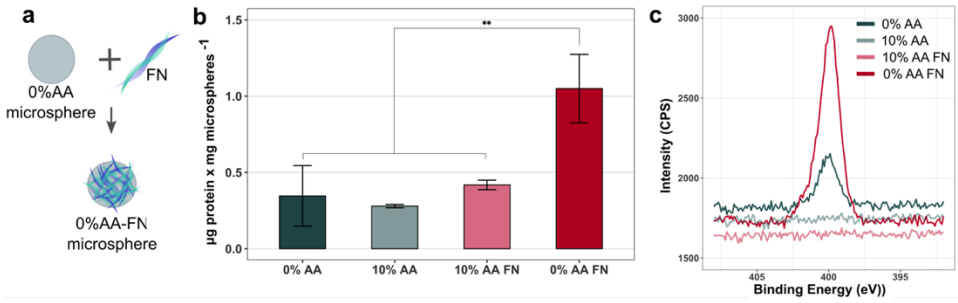

Figure 20. Characterization of microsphere functionalization with FN. a) Scheme of fibronectin (FN) coating on 0% AA and 10% AA microspheres. b) microBCA assay results

for FN coated and non-coated 0% AA and 10% AA microspheres (n=3, measured in duplicate, comparisons were made using one-way ANOVA with Tukey's test for post-hoc analysis). c) XPS scan spectra of N1s for FN coated and uncoated 0% AA and 10% AA microspheres.

HA was incorporated to microspheres trough covalent grafting and 10%AA microspheres were used, since this requires the presence of -COOH groups on their surface (Figure 21, a). Low molecular weight HA (~320,000 Da) was used for functionalization and TBO indirect method was performed to monitor the variation of -COOH groups on microsphere surface across the sequential steps of the grafting process (Figure 21, b). At the end of the process the 10% AA HA showed increased number of -COOH units per mg of microsphere, which confirmed the presence of HA. Although in low amount, due to the small proportion of N in HA molecule, XPS N1s scan spectra of 10% AA ungrafted and HA grafted microspheres showed the presence of N in the grafted microspheres (Figure 21, c).

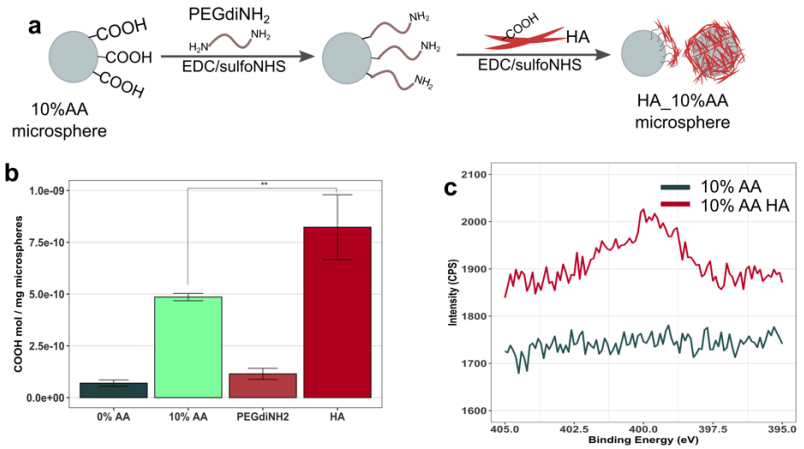

Figure 21. Characterization of microsphere functionalization with HA. a) Scheme of hyaluronic acid (HA) grafting process applied to 10%AA microspheres. b) Toluidine Blue O (TBO) colorimetric determination of COOH groups from 10%AA microspheres at the different stages of the HA grafting process (n=3, measured in duplicate, comparisons were made using one-way ANOVA with Tukey's test for post-hoc analysis). c) XPS scan spectra of N1s for HA-grafted and ungrafted 10% AA microspheres. P value legend: p ≤ 0.05 (*), p ≤ 0.01 (**), p ≤ 0.001 (***), p ≤ 0.0001 (****).

COL 1 was also incorporated in the microspheres by covalent coupling mediated by EDC/sulfo-NHS. 10% AA microspheres were used, since this requires the presence of -COOH groups on their surface (Figure 22, a). Due to the presence of terminal amine groups in the side chains of collagen amino-acids, the reaction can be done as one-step procedure without the need of introducing a molecular spacer. To assess COL 1 incorporation onto microspheres, microBCA assay was used for quantification of the mass of adsorbed protein per mg of microspheres. As can be seen in Figure 22 b, COL 1 coated microspheres presented significantly increased signal when compared with non-coated microspheres. Results confirmed the presence of COL 1 on 10% AA microspheres.

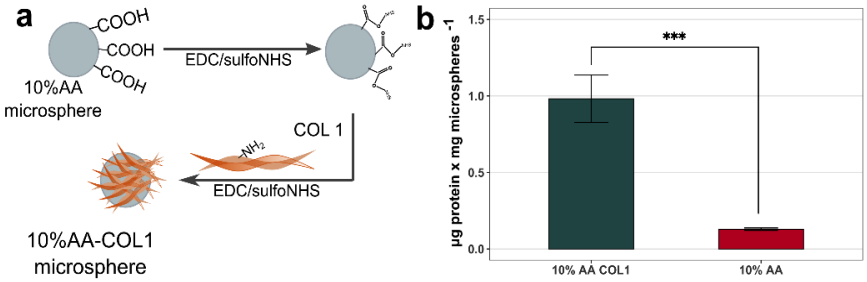

Figure 22. Characterization of microsphere functionalization with COL 1. a) Scheme of COL 1 coating on 10% microspheres. b) microBCA assay results for COL 1 coated and non-coated 10% AA microspheres (n=3, measured in duplicate, comparisons were made using Student's t-test). P value legend p ≤ 0.001 (***).

As antifouling control for certain cell culture experiments further described in Chapter 4, bovine serum albumin (BSA) was incorporated as functionalization for 10% AA microspheres. BSA has been used in research as a competing agent for the unspecific adhesion and generation of non-fouling surface. This molecule was incorporated on microspheres surface by physical adsorption (Figure 23, a). Its coating effectiveness and stability were confirmed by XPS and fluorescent labelling after 72 h of culture equivalent conditions. Figure 23 b shows coated (with FITC-BSA) and uncoated 10% AA microspheres, fluorescent signal from BSA can be seen homogeneously distributed on coated

microspheres surface. XPS scan spectra of S2p for BSA coated microspheres showed and increased peak due to the presence of N from the protein (Figure 23, c).

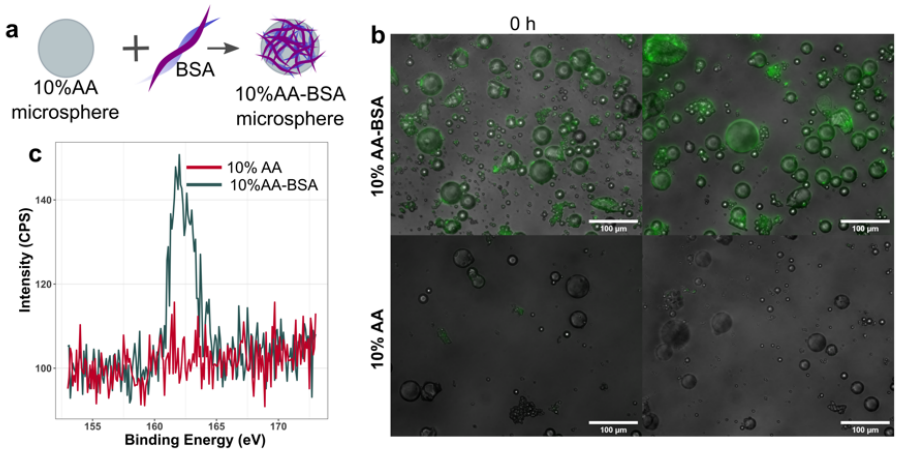

Figure 23. Characterization of 10% AA BSA coated microgel. a) Scheme of BSA coating process applied to 10%AA microspheres. b) Fluorescence images of BSA-FITC coated 10% AA microspheres at 0 h and 72 h of incubation in culture equivalent conditions. c) XPS scan spectra of S 2p for BSA-coated and uncoated 10% AA microspheres.

Finally, in collaboration with Dr. Annj Zamuner from the University of Padova, some peptidic sequences corresponding to different epitopes from FN sequence able to bind surface receptors on MM cell surface where chosen as peptides of interest. The 3 peptides chosen have been previosly used as bioinspired synthetic motifs to decorate 3D substrates (Hozumi et al. 2016), but never before used in the context of MM. Dr. Annj Zamuner provided the peptides that were grafted by covalent EDC/sulfo-NHS chemistry on 10%AA microspheres (Figure 24, a). XPS was used to confirm the presence of the peptides after the grafting process, as it allows to detect the S present in the peptidic sequences (due to the synthesis method used for peptide fragments production). As shown in Figure 24, b the 3 peptides were effectively incorporated onto microsphere's surface.

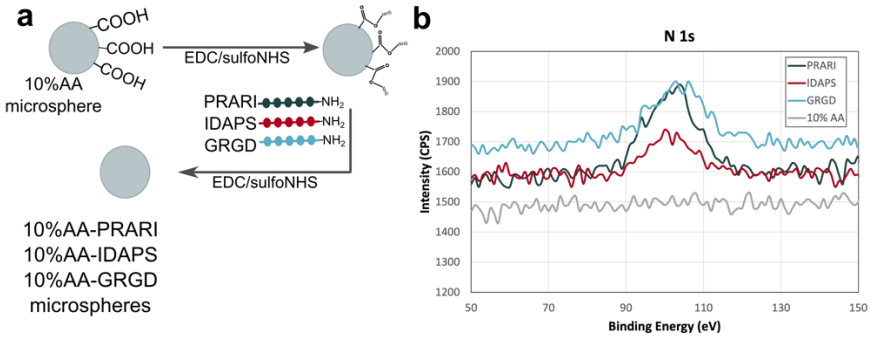

Figure 24. Characterization of peptide grafted microgels. a) Scheme of peptides covalent grafting process applied to 10%AA microspheres. b) XPS scan spectra of S 2p for PRARI, IDAPS, GRGD 10% AA and uncoated 10% AA microspheres.

In this section, it has been demonstrated that three different biomolecules which are natural constituents of the BM ECM or peptide fragments based on their sequence (FN, COL 1 and HA), as well as BSA, have been effectively incorporated onto microsphere's surface. Different functionalization strategies have been used depending on the nature of each biomolecule. And as a result, a set of different microgels which would allow to study how MM cell lines behave in the microgel system when it presents different size, chemical compositions or functionalizations have been generated.

3.4.2. Functionalization of Cytodex 1 microspheres

This chapter of the present Doctoral Thesis pursues the objective of generating a wide range of different microgels with different properties and functionalities that can be later used in cell culture approaches with different biomaterial requirements.

Cytodex 1 are commercially available microspheres designed as microcarriers. They are based on a cross-linked dextran matrix substituted with positively charged N,N-diethylaminoethyl (DEAE) groups to a degree that is optimal for cell growth. The charged groups are found throughout the entire matrix of the microcarrier. These microspheres have been designed with properties which enhance cell adhesion, as its major area of application is the

production of large numbers of adherent cells. This is because due to their high specific surface microsphere-based expansion systems allow the obtention of high yields of cells from small culture volumes.

However, in this work the Cytodex1 microspheres are not conceived as 3D platforms for the expansion of adherent cells. In this case it is intended to use them as alternative microspheres in the microgel system. The reasons for their choice as microspheres of interest are several. Firstly, dextran is a complex and branched polysaccharide which has high capacity to absorb water, this would give to the resulting microgel appropriate properties for cell culture and media diffusion. Secondly, they are commercially available microspheres, which implies ease to obtain them with good yield. This fact is important for cell culture experiments with different conditions and higher amounts of replicates needed. But the main reason for their choice has been the presence of positive charges in Cytodex 1 surfaces'. Although this characteristic has been designed to increase cell attachment, it would also be beneficial if a LbL functionalization of the microspheres is desired. The presence of a positively charged surface would allow the effective grafting of a polyanion as fist layer. Because of that, in this Thesis LbL was incorporated as a technique for biomolecule inclusion in the microspheres. The challenge with these microspheres lies in achieving an effective coating of them using LbL techniques. This will allow to neutralize their strong positive charge, that gives them an adherent character, while incorporating the biomolecules of interest to the surface of the microsphere.

Two different LbL pairs have been explored for the inclusion of the biomolecules of interest, CS and HA, on the Cytodex 1 microspheres. Chitosan (CHI) was chosen as polycation for both pairs. CHI is polycation obtained by deacetylation of chitin, which is extracted from crustacean shells (Schneider et al. 2007). CHI presents good stability in physiological conditions and biocompatibility (Silva et al. 2014). Moreover, CHI has been broadly used in literature in similar LbL protocols implying our biomolecules of interest: HA (Schneider et al. 2007; Salomäki and Kankare 2009; Rocha Neto et al. 2019) and CS (Sousa, Cleymand, and Mano 2016).

As described in section 3.3.2.2, two different LbL protocols were tested for Cytodex 1 functionalization. Initially (protocol 1), 15 minutes of immersion time in all the layers was applied and glutaraldehyde (GA) was used to carry out the crosslinking of the LbL by-layers. Functionalized microspheres with the LbL pair CS and CHI and finished in a CS layer (referred to as Cyt CS when not crosslinked and as Cyt CS GA when crosslinked with glutaraldehyde) were produced. In the same way, using the LbL pair of HA and CHI, the microspheres Cyt HA, without crosslinking, and Cyt HA GA, crosslinked with GA, were obtained. For each of the pairs, microspheres finished in the tenth layer (that is, with CHI as the outer layer) named Cyt CS CHI and Cyt HA CHI were also obtained as control for some experiments (FTIR). Crosslinking was incorporated to the protocol to improve LbL stability in aqueous and physiological environments (Ye et al. 2005; Q. Zhao et al. 2007; Grech, Mano, and Reis 2010). GA is one of the most used methods for crosslinking of biomaterials because it can react with functional groups present in the most used types of biomolecules in biofunctionalizations (proteins and carbohydrates). However, contradictory results have been published on the cytotoxicity of GA (Reddy, Reddy, and Jiang 2015). In this case, negative results in terms of cell viability were obtained when GA crosslinked microgels were tested in cell culture. In view of these results (further discussed in Chapter 4), a new protocol (protocol 2) was developed with two significant modifications. The immersion time in the first polyanion layer was increased (from 15 minutes to ON) with the objective of a better neutralization of the adherent character of the Cytodex 1 microspheres. The second modification that was incorporated into protocol 2 was a change in the crosslinking method. In protocol 2, EDC and NHS were used instead of GA. The microspheres obtained by this protocol were named Cyt CS EDC and Cyt HA EDC respectively. Finally, the control microspheres, to which no modification was applied, were called Cyt CTRL. All the acronyms used are detailed in Table 4. Because of the bad results of GA crosslinked microgels in cell culture, some of the LbL characterizations were only applied to EDC/NHS crosslinked microspheres, as the bad performance of Cyt GA samples was already known.

Brightfield microscopy images of the different functionalized microspheres can be seen in Figure 25. Cyt CTRL microspheres present a smooth surface (a and b). In the Cyt CS (c) and Cyt HA microspheres (d), functionalized by protocol 1 but without crosslinking, a change in the surface topography is observed. It becomes slightly rough compared to images (a) and (b). This change can be attributed to the presence of the bilayers, since the Cyt CTRL had been subjected to incubations in the same buffers (same pH and ionic strength conditions, but without the presence of polyelectrolytes) as the functionalized ones, thus the possibility of these changes being induced by pH or ionic strength was discarded. In Cyt CS GA (e) and Cyt HA GA (f) microspheres (crosslinked with GA) macroscopic changes become more pronounced, the topography increased its roughness, and a slight browning of the microspheres occurs. Surface browning was more evident in Cyt HA GA microspheres. Finally, when the crosslinking was performed with EDC/NHS (Cyt CS EDC (g) and Cyt HA EDC (h)) the same macroscopic changes were noticed, however Cyt CS EDC were the microspheres with the more noticeable browning on its surface with this protocol. The increase in surface roughness due to the LbL bilayers has been previously reported and studied by several authors (Ye et al. 2005; Kim et al. 1999). They reported that the presence of NaCl the LbL solutions and rinse steps, played an important role in the final topography of the bilayers. The use of high concentrations of NaCl, such as 0.15 M (the one used in the protocol described in section 3.3.2.2), favors the formation of a rougher surface. Also, the increase in roughness due to GA crosslink has been previously described by Grech et al. when working with CHI microspheres functionalized with the LbL pair CHI-HA and crosslinked with GA. They determined that the surface roughness doubled after crosslinking by atomic force microscopy measurements (Grech, Mano, and Reis 2010). An ionic strength of at least 0.15 M NaCl has been determined as key factor for built-up of CHI-HA bilayers (Richert, Boulmedais, et al. 2004), the presence of salts promotes the formation of thicker layers. The browning of the microspheres after glutaraldehyde crosslinking appear also

in the CHI microspheres crosslinked with GA developed by these authors (Grech, Mano, and Reis 2010).

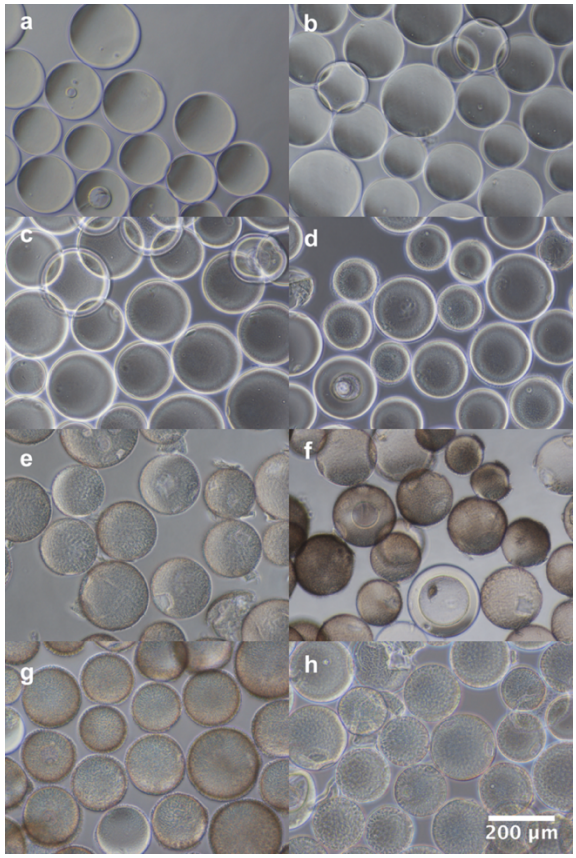

Figure 25. Brightfield images of LbL functionalized Cytodex 1 microspheres. a,b) Non functionalized microspheres subjected to the LbL protocol but without the presence of polyelectrolytes in the solutions (Cyt CTRL). c) Microspheres functionalized with the LbL pair CS CHI using protocol 1 and without crosslink (Cyt CS). d) Microspheres functionalized with the LbL pair HA CHI using protocol 1 and without crosslink (Cyt HA). e) Microspheres functionalized with the LbL pair CS CHI using protocol 1 and crosslinked with GA (Cyt CS GA). f) Microspheres functionalized with the LbL pair HA CHI using protocol 1 and crosslinked with GA (Cyt HA GA). g) Microspheres functionalized with the LbL pair CS CHI using protocol 2 and crosslinked with EDC/ NHS (Cyt CS EDC). h) Microspheres functionalized with the LbL pair HA CHI using protocol 2 and crosslinked with EDC/ NHS (Cyt HA EDC).

Morphology of the microspheres was analyzed in detail by cryoFESEM. This technique allowed the surface of the microspheres to be observed at higher magnifications but without the need of dehydration or fixation processes, since the hydrated samples are frozen inside the equipment and water is sublimated *in situ*. Figure 26 shows images corresponding to the cross section of the different microspheres (the microspheres were sectioned *in situ* in the equipment). As microspheres are introduced in the equipment fully hydrated, this type of microscopy provides information about bilayer size and polymer distribution in the microspheres closer to reality than microscopy techniques requiring fixatives. These images confirmed the presence of the LbL coatings in Cyt HA, Cyt CS, Cyt CS GA, Cyt CS EDC and Cyt HA EDC microspheres (Figure 26). They also confirmed a rather smooth surface in the Cyt CTRL microspheres compared to multilayered microspheres. The presence of an outer layer with properties different from the core of the microsphere is appreciated in all conditions, meaning that the Cytodex 1 present this structure. It is over this layer where the presence of the multilayered coatings of the LbL protocol can be seen in the different images. It is worth note that many holes on the surface of the Cyt CTRL microspheres remain uncovered. On the other hand, in the case of the functionalized microspheres, these holes appear covered. At the higher magnification pictures, the different Cyt CS microspheres (Cyt CS, Cyt CS GA and Cyt CS EDC) present different architecture of the bilayers among them. This can be attributed to the differences in the crosslinking. However, the most notorious differences in structure are noticed between the Cyt HA EDC microspheres and the CS functionalized microspheres. When comparing Cyt CS EDC and Cyt HA EDC microspheres, these differences can be attributed to different LbL pairs used on its functionalization, as the protocol is the same for both. Cyt HA EDC present an outer layer with formations like spikes while Cyt CS EDC outer layer is thicker and presents a morphology more like a spider's web. It should also be considered that, although the same protocol for sample preparation and imaging was followed in all samples, in the sublimation step of the sample preparation differ-

ent levels of ice sublimation were achieved. This can give rise to artificial differences between samples, because it causes the sample fraction remaining above the sublimation line to collapse. The cross-section of a Cyt CS GA microsphere can be seen in detail in Figure 27. For this sample, alignment of sublimation front and the surface of the microsphere was achieved, so that no collapse of the sample is observed because the ice level is not lower than that of the polymeric chains. This allows us to appreciate the size and distribution of the LbL layer without collapse. A height of 3,5 μm was measured for the LbL multilayers of this sample in the hydrated-like and frozen state allowed by cryoFESEM.

LSCM of coated (Cyt CS GA and Cyt HA GA) and uncoated microspheres (Cyt CTRL) was performed. Differences in the fluorescence of the control microspheres (Figure 28, a) and the coated microspheres were observed (Figure 28, b-c). These differences can be attributed to the autofluorescence of CHI, as it has been demonstrated that by cross-linking chitosan microspheres with various agents, such as GA or formaldehyde, chitosan exhibited autofluorescence without the need to conjugate a fluorochrome (Q. Zhao et al. 2007; H. Zhao et al. 2013). These results also confirmed the presence of chitosan from the LbL multilayers on Cyt HA GA and Cyt CS GA microspheres.

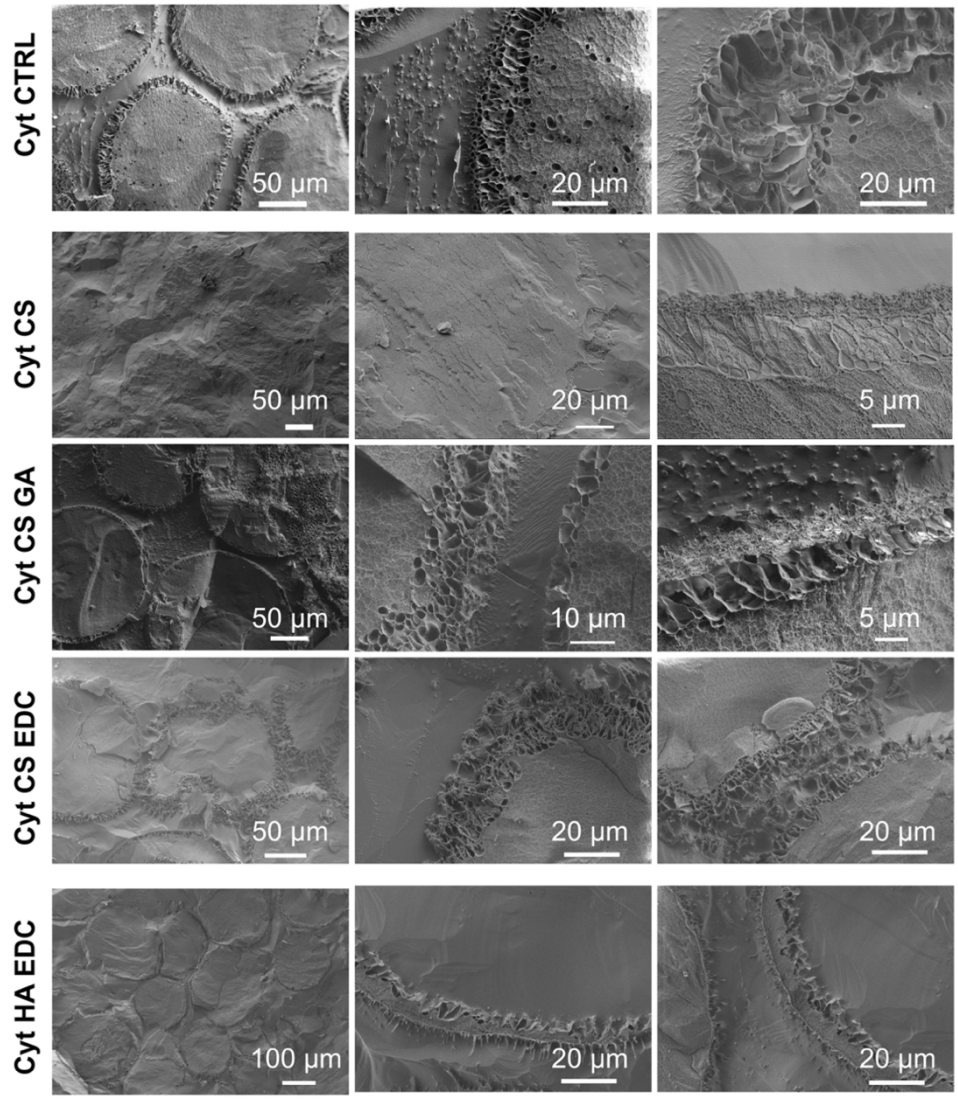

Figure 26. CryoFESEM images of the Cytodex 1 microspheres with the different LbL coatings developed. For each microsphere type, images at different magnifications are-shown. All images correspond to microsphere's cross-section. Samples were cross sectioned in situ before sublimation.

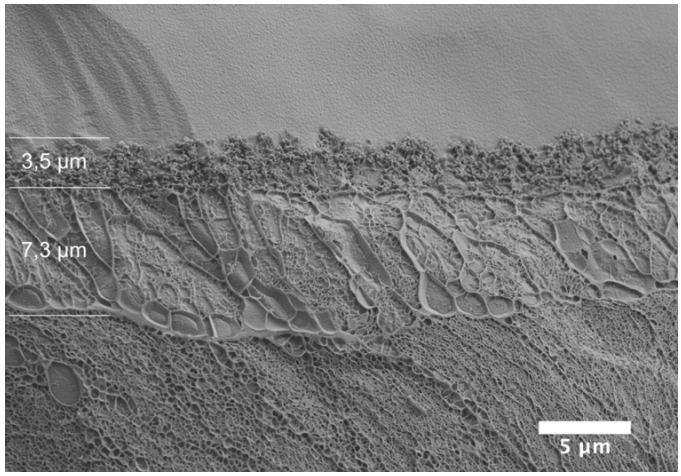

Figure 27. CryoFESEM image of a Cyt CS microsphere. Image corresponds to microsphere's cross-section. the sublimation line was at the same level as the polymeric chains allowing the sample to be observed without collapse. The external layer of Cytodex 1 microspheres can be appreciated (thickness 7,3 µm) and above this, the LbL bilayers (thickness 3,5 µm).

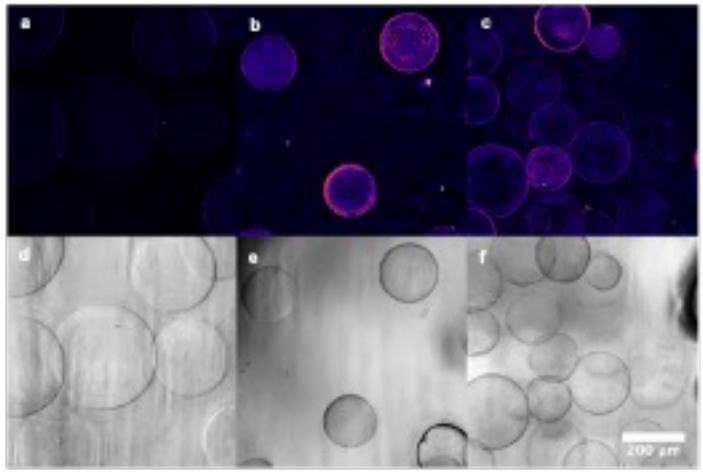

Figure 28. LSCM images of Cyt CTRL (a), Cyt CS GA (b) and Cyt HA GA (c). Brightfield images are also shown, Cyt CTRL (d), Cyt CS GA (e) and Cyt HA GA (f).

FTIR analysis of all the different samples generated by LbL protocol 1 and 2 and the control was performed. Different authors have reported this method for assessment of the bilayer's deposition in LbL protocols (Sousa, Cleymand, and Mano 2016; Alves, Picart, and Mano 2009; Boudou et al. 2009). However, in all these works the LbL was deposited on bidimensional

surfaces, the substrate on which de LbL coating were ensembled presented a different chemistry than the biomolecules used for the LbL and the number of bilayers was significantly higher than 5 (number of bilayers in the protocols developed here). Because of that the probability of detecting the bilayers or differences among them by this technique were reduced in this case. Moreover, the equipment used for spectra acquisition has been designed for bidimensional samples, and thus its performance is not guaranteed when working with microspheres powders.

In Figure 29 the spectra obtained for each sample can be seen. In general, all the spectra present the same trend and equivalents peaks. One differential peak that could be expected would be the one corresponding to the crosslinking of the sulfate and amine groups of CS and CHI respectively, about 1250 cm^{-1}. However, this peak is not evident in the samples that contain CS, since the presence of higher intensity peaks is also present in those wavenumbers corresponding to the microsphere matrix.

The only peak that seems to be differential between all the LbL functionalized samples and the Cyt CTRL is the one appearing between 2900 and 2980 cm^{-1}. At this wavenumber peaks corresponding to the C-H stretching are expected, antisymmetric CH_2 stretching vibration are typically observed at high frequency values (~2950 cm^{-1}), symmetrical CH_2 stretching may be displayed at lower frequency values (2850–2890 cm^{-1}) (Ozdemir, Çolak, and Güner 2007; Demirbilek and Dinç 2012), and therefore this peak should appear in all the samples. On the other hand, in crosslinked dextran systems this wavenumber has been reported to shift to lower fields and may occur almost ~80 cm^{-1} (except for GA), as reported by (Ozdemir, Çolak, and Güner 2007). Cytodex 1 microspheres are acquired from Cytiva, the information available about its chemical composition is that their matrix contains cross-linked dextran that is substituted with positively charged N,N-diethylaminoethyl (DEAE) groups. This chemistry could justify the reduction of the mentioned peak. Moreover, Demirbilek at al. also reported changes in this peak in a DEAE substituted dextran hydrogel (Demirbilek and Dinç 2012). Taking this into account, the presence of the mentioned peak in all the functionalized samples

indicates the presence of a differential layer from the cross-linked and DEAE substituted dextran matrix, this layer corresponds to the bilayers deposited by LbL protocols. Therefore, this technique allowed detecting that surface modification of the Cyt CTRL microspheres was achieved. However, it didn't t allow to assign differences between the different LbL pairs or the different crosslinking methods.

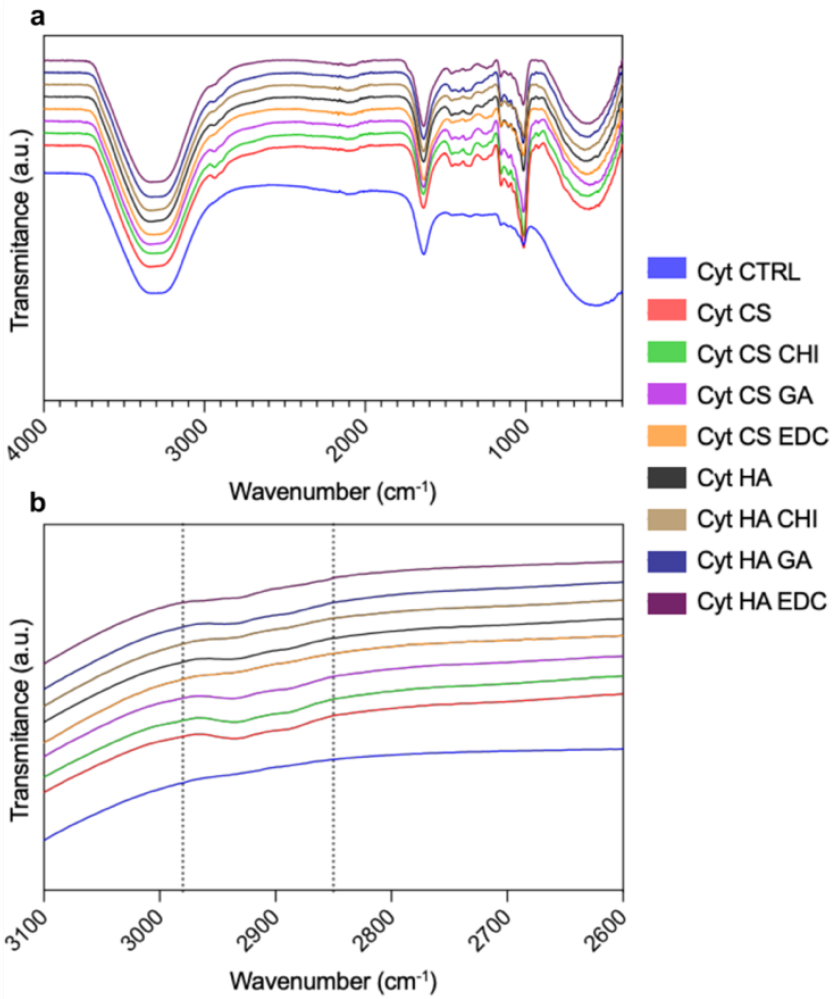

Figure 29. FTIR spectra of all the microspheres produced with the 2 LbL protocols developed. a) Complete FTIR spectra of all samples. b) Magnification of the area where peaks corresponding to the C-H stretching are expected.

TGA of the different samples was performed with the objective of studying the degradation of the microgels with increasing temperature. This allowed determining the mass fraction of LbL for each type of microspheres (Cyt CTRL, Cyt CS EDC and Cyt HA EDC).

Figure 30 a shows the total weight (W (mg)) of each microgel as a function of temperature. In the same graph but in dashed lines the derivative of mass with respect to temperature (dW/ dT) is displayed, this provides information about the rate at which the sample loses mass. The absolute minimum for the d(W)/d(T) of each sample concurs within the point of inflection in the total weight curve (W) for each sample analyzed. In TGA, a drop in sample mass occurs when the thermal energy provided to the sample exceeds the chemical energy of the bonds, thus separating the volatile groups and starting the degradation of the sample.

Taking the curve of total weight (W) as a function of temperature as a reference (Figure 30, a, continuous lines), the initial drop in samples weight occurs at 200ºC, where a plateau begins. This corresponds to the evaporation of the water absorbed in the microgel or among the microspheres. Therefore, the mass at 200ºC corresponds to the mass of the dry samples (W_{dry}) and was considered as 100% of the sample weight. A second drop takes place at 300ºC, where the samples remain approximately at 50% of the original W_{dry}. Between 300 and 700ºC, the degradation of the sample up to 20-30% of their W_{dry} is observed. The degradation is performed in nitrogen ambient, so the combustion of the sample is not possible, because of that, carbonized residue remains. The residual weight is about 10% of the W_{dry}. This behavior is representative of sugars, which are present in the analyzed samples (dextran, CS and HA).

Figure 30, b (continuous lines) shows the total weight of the different samples (starting from 200ºC) normalized to their W_{dry} (its weight at 200ºC). Its derivative ($d(w/w_{dry})/d(T)$) is also represented (dash lines). Differences between Cyt CTRL and Cyt CS EDC or Cyt HA GA samples can be seen. A displacement of the derivative peak is observed, which indicates differences in the

drop in weight. In addition, the final residual is greater for the functionalized samples and the three curves exhibit different trends of the fall.

Calculation of the mass fraction corresponding to the LbL multilayers was done based on the weight drop corresponding to the minimum value of the $d(W/W_{dry})/dT$, around 285ºC. This assumption was done because this peak corresponds to the degradation of the dextran from the core of the microspheres. Differences between samples in the weight loss at this point of the curve are proportional to the differences in the mass fraction of dextran, and thus to differences in the mass fraction corresponding to the LbL multilayers. Figure 30 c shows a detail of the of the $d(W/W_{dry})/dT$ for each sample, these curves have been adjusted to a normal Gaussian distribution (also shown in Figure 30, c). These normal Gaussian distributions have been used to obtain the areas under the $d(W/W_{dry})/dT$ peaks. This area represents, for each sample, the mass fraction degraded between 200 and 300 ºC, which has been attributed to the dextran matrix of the microspheres. Finally, by calculating the difference, the value of the mass fraction of the coating was obtained. These calculations have been performed with 3 replicates per sample and results are shown in Figure 30 d. Finally, these results confirmed that LbL multilayers are present in Cyt HA EDC and Cyt CS EDC samples. Results also confirmed that the coating layer is significantly thicker in CS than in the HA LbL pair. These data agree with cryoSEM images in Figure 26, where CS coatings appear thicker than HA ones. Also, in brightfield images for Cyt CS EDC the browning of the microspheres after LbL and crosslinking appears more evident than in the Cyt HA EDC samples.

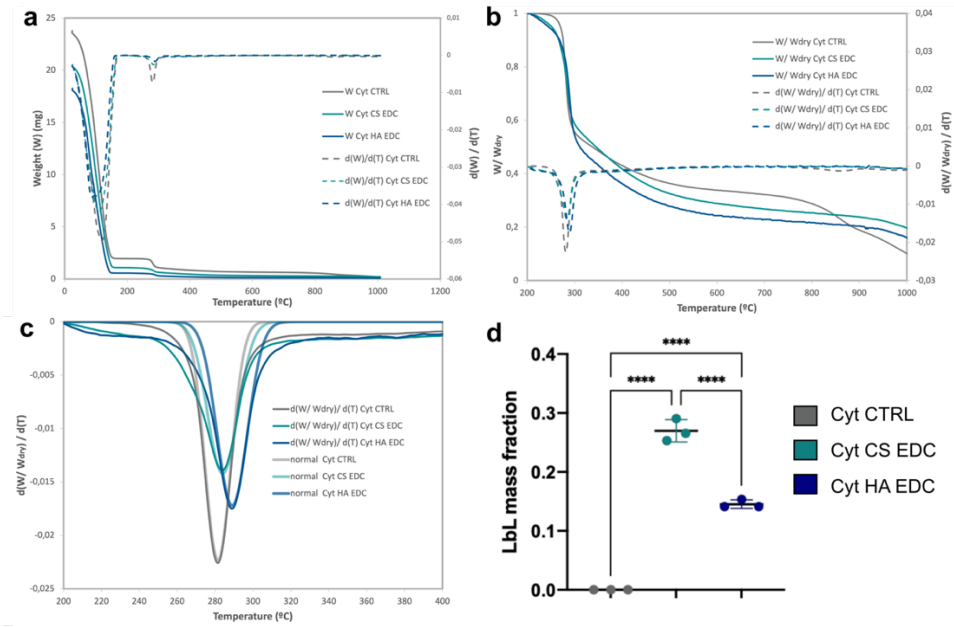

Figure 30. TGA analysis of Cyt CTRL, Cyt CS EDC and Cyt HA EDC samples. a) Continuous lines: total weight (W (mg)) of each microgel as a function of temperature; dash lines: derivative of mass with respect to temperature (dW/ dT). b) total weight (W, starting from 200ºC) normalized to their W_{dry} (its weight at 200ºC); dash lines: derivative of W normalized to W_{dry} ($d(w/w_{dry})/ d(T)$. c) Detail of $d(W/W_{dry})/dT$ for each sample corresponding to the minimum value of the $d(W/W_{dry})/dT$, around 285ºC. The original line appears in thin lines and the normal Gaussian distribution adjusted to each peak in wide lines. d) LbL mass fraction measured of each type of microspheres (n=3, comparisons were made using one-way ANOVA with Tukey's test for post-hoc analysis).

The use of methods that specifically detect functional groups present in the molecules of interest (CS or HA) would allow to quantify the mass of the LbL multilayers and corroborate TGA, cryoSEM, FTIR and LSCM results. However high similarity exists in the molecular structure of dextran with the one for the CHI and CS or HA (Figure 31), this fact makes difficult this approach for the quantification of the molecules of interest. However, there's one functional group only present in the CS molecule, as it is a sulfated glycosaminoglycan and is sulfated at position 6 (as CS B has been used in these experiments) (Figure 31).

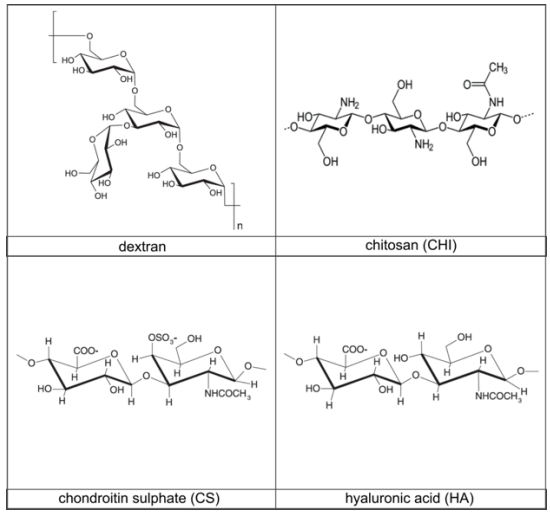

Figure 31. Molecular of structure of the different biomolecules present in Cytodex 1 and the different LbL pairs used for its functionalization.

This makes possible the use of Taylor's blue colorimetric method using Glycosaminoglycan Assay Blyscan (Biocolor, UK), which allows to quantify sulfated glycosaminoglycans and proteoglycans. As can be seen in Figure 32 a, no significant differences were found between Cyt CTRL and Cyt CS EDC samples when measuring the supernatant of the colorimetric assay. However, microspheres where imaged after removal of the 1,9- dimethyl methylene blue with the dissociation reagent, and it was noted that Cyt CTRL microspheres (Figure 32, b) recovered it original color, while Cyt CS EDC microspheres maintained the blue color (Figure 32, c). This means that the dissociation reagent was unable to recover the 1,9- dimethyl methylene blue complexed to the sulphated glycosaminoglycan (CS) in the microspheres. Probably, this can be attributed to the crosslinking of the LbL multilayer which allowed CS complexation with the 1,9- dimethyl methylene blue but avoids solubilization of the complexes by the dissociation reagent. The signal detected in the Cyt CTRL microspheres (Figure 32, a) can be attributed to 1,9-dimethyl methylene blue retained in the microsphere's matrix due to its hydrogel-like nature, because of that the signalling detected is equivalent in both

samples. This technique didn't allow the quantitation of the CS μg/ mg of microspheres (dry basis). However, macroscopic image analysis confirmed the presence of the sulphated glycosaminoglycan on Cyt CS EDC microspheres.

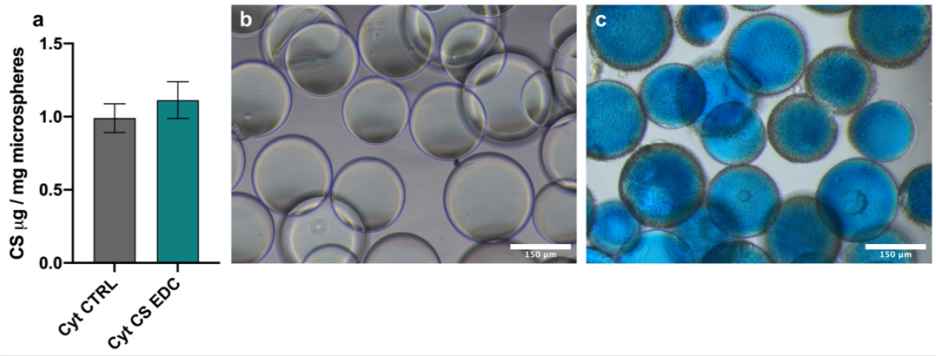

Figure 32. Determination of sulfated groups on LbL coated and uncoated Cytodex 1 microspheres. a) Quantitative Blyscan determination of Cyt CTRL and Cyt CS EDC microspheres. b) Images of the Cyt CTRL microspheres after Blyscan protocol. c) Images of Cyt CS EDC microspheres after Blyscan protocol.

In general, all the techniques applied (inverted microscopy, cryoFESEM, LSCM, FTIR, TGA and Blyscan colorimetric assay) allowed to confirm that both LbL pairs were effectively incorporated onto Cytodex 1 surface. The LbL pair formed by CHI-CS has generated thicker coatings than the CHI-HA pair, as demonstrated by cryoFESEM images (Figures 26 and 27) and TGA analysis confirmed increased LbL mass fraction for this samples in respect to ones from the pair CHI-HA (Figure 30).

As it was mentioned in Section 3.2.2, two different kinetics of LbL assembly exist: linear growth and exponential growth. Linear growth implies a coating that grows linearly with each layer deposited, therefore, the thickness increase in each deposition remains constant throughout the process. The exponential growth involves a multilayer whose thickness increases exponentially at each deposition step, with the thickness of each layer being greater than that of the previous one. Linear growth occurs only with strong polyelectrolytes, which generate highly ordered layers with large interaction forces

between them, since the charge of the added polyelectrolyte overcompensates the charge already deposited and allows the deposition of the next layer. Exponential growth will occur if at least one of the two polyelectrolytes used is capable of diffusing through the layers, that implies the existence of weaker electrostatic interactions between them, which makes easier the diffusion between layers and causes exponential growth (Campbell and Vikulina 2020). Therefore, it can be said that the exponential character of the film increases with decreasing polyanion–polycation interaction. Typically, all LbL pairs formed by biopolymers present exponential growth, due to their inherently low charge densities.

However, there comes a point during multilayers build-up in which the exponential switches to linear growth. The mechanism by which this transition occurs is still debated in the literature. An “island” model has been proposed, where, firstly, islands grow upon a substrate (their growth is exponential); at some point these islands will coalesce and form a uniform film across the substrate (Volodkin and Von Klitzing 2014). Nevertheless, other models have been proposed. Salomäki et al. proposed a model where the multilayer reaches a thickness at which the rate of diffusion is too low for exponential growth to continue (Salomäki, Vinokurov, and Kankare 2005). For example, HA-poly-L-lysine films have been shown to exhibit an exponential-to-linear transition point between twelve and eighteen bilayers (Porcel et al. 2006), and CHI-polyglycolic acid have been reported to transition around nine deposition cycles (Song et al. 2009). However, this number may vary with build-up conditions able to alter the diffusion of polyelectrolytes through the multilayer. Temperature, ionic strength, or pH are parameters to be considered.

For instance, an increase in ionic strength will result in the addition of counter ions which are able to diffuse throughout the pre-built film and reduce the extent of polyion pairing between polyelectrolytes (Campbell and Vikulina 2020). Multilayer’s stability (and thus growth behavior) is also highly dependent on the pH, as the charge of the polyelectrolyte at a certain pH is dependent upon its acid dissociation constant (pKa). Biopolymers are very sensitive

to changes in pH due to their already weak electrostatic properties. For example it has been described that, for films built at pH 5, HA is near-fully ionized, and the conformation in which it adsorbs is flatter than at pH 9 (Burke and Barrett 2003).

CS presents a lower pKa for its carboxylic groups than the pKa of HA carboxylic groups, moreover CS also presents another ionizable group (the sulfate group) which can contribute to polymer ionization. This means that in principle, CS is a stronger polyanion than HA and thus its exponential-to-linear transition should be easier, giving rise to flatter adsorption patterns and thus thinner multilayers and less LbL mass fraction than the pair HA-CHI.

However, Liu et al. analyzed the growth pattern of both LbL pairs (CHI-HA and CHI-CS) when assembled in flat or porous polycaprolactone films (Liu et al. 2017). Results obtained for the porous films are comparable to the ones obtained in this Doctoral Thesis, as Cytodex 1 microspheres present porous surface. They reported that both pairs presented and exponential growth, as the analysis made by fluorescence microscopy showed diffusion between layers. In general, they also reported increase LbL thickness in porous films, which could reinforce the hypothesis of exponential growth.

Moreover, they measured thickness of the multilayers after 6 layers and reported significant differences between CHI-CS (37 μm) and CHI-HA (19,3 μm) being CHI-CS the pair giving rise to thicker multilayers. Also, the water contact angle measurements showed increased variation between layers in the CHI-CS pair than in the CHI-HA pair. These results agree with the ones obtained in cryoFESEM and TGA analysis in the present Thesis.

Nevertheless, although the presence of the multilayers has been confirmed, it hasn't been possible to carry out an exhaustive quantification of the coatings, the uniformity of their layers, their thickness, or the surface charge of the microspheres after each layer or at the end of the process. In most of the literature related to the application of the LbL technique, different techniques are used to carry out these measurements. For example, water contact angle

measurements, quartz crystal microbalance (QCM), FTIR or atomic force microscopy (AFM). However, some of these techniques are not designed to be applied to microspheres or some others were not available. For the determination of the superficial charge and the size in particle suspensions, hydrodynamic size and charge measurements can be performed using zetasizer instruments. However, the Cytodex 1 microspheres present large diameters (approximately 150 μm) and is not possible to generate stable suspensions measurable by this technique.

A possible solution to this difficulty is to use flat surfaces of identical composition to that of the microspheres to reproduce the LbL protocol in a configuration that facilitates its exhaustive characterization. This approach has been considered. However, in this Doctoral Thesis, it was discarded because Cytodex 1 microspheres were used, since it is a commercial product, it is not possible to know exactly its composition and manufacturing process. And since the properties of the substrate on which it assembles influence the LbL process, it was difficult to generate two-dimensional replicates of the functionalization that has been carried out in 3D on Cytodex 1. Because of that, once the presence of the multilayers was confirmed, cell culture experiments (Chapter 4) were carried out, not only to analyze the cell response on the microgels, but also as an as an extra characterization of the LbL coatings.

3.5. Conclusions

Different types of microspheres have been obtained and characterized. These microspheres will be used to generate 3D MM environments based on the Microgel concept developed in the present Doctoral Thesis.

The microspheres that are the main object of study of this Doctoral Thesis are microspheres made of acrylates.

I. A suspension polymerization protocol able to produce microspheres that meet the desired properties has been developed and optimized.

II. Acrylates microspheres have been obtained with two different chemical compositions, with and without acrylic acid. Using different physical-chemical characterization techniques, the differences in the presence of AA have been demonstrated. These microspheres have also been obtained with different size distribution.

III. The functionalization of acrylates microspheres with different components of the ECM and using different techniques has been carried out. FN and BSA have been incorporated by physical adsorption. COL 1, HA and peptide sequences of interest have been covalently grafted using carbodiimide chemistry. All the functionalizations have been characterized and the effective incorporation of the different biomolecules has been demonstrated.

To increase the range of microspheres available to generate microgels and to have a control with different properties, the commercial Cytodex 1 microspheres have been modified for use in our 3D model of multiple myeloma.

IV. Cytodex 1 microspheres have been functionalized by means of LbL techniques. The pairs CHI/CS and CHI/HA have been used.

V. Different physicochemical techniques confirmed the presence of both LbL pairs on Cytodex 1 surface. Two different protocol (protocol 1 and 2) and crosslinking agents (GA or EDC/NHS) have been tested.

VI. Although precise quantitation of LbL multilayers has not been achieved, TGA analysis and cryoFESEM allowed to determine that the pair CHI/CS generated thicker multilayers than the CHI/HA.

Chapter 4.
The Microgel as 3D culture system for Multiple myeloma cell lines

4.1. Summary

The main objective of this Doctoral Thesis is to develop a 3D platform for MM cell culture based on microspheres. Various microspheres have been developed with different properties and functionalizations. This Chapter describes the experimental work performed to introduce the various microspheres developed in Chapter 3 into cell culture. After establishing the optimal conditions for the developed cell culture platform, initial drug resistance tests have been carried out in the 3D system.

4.2. Introduction

4.2.1. Microspheres as 3D systems for cell culture

In past decades, a novel technical approach has emerged among the main 3D platforms used in tissue engineering applications (Figure 33, a). Microspheres can be used in several applications of TERM, they can be used to provide biomimetic structures and biological functions in *in vitro* cell culture models, but also, they offer great possibilities as vehicles for controlled release or cell delivery *in vivo*. They present certain advantages in reference to more conventional 3D platforms. Such as the straightforward process for its large-scale fabrication or their high specific surface area. However, the main advantage of microspheres is their great versatility in terms of composition, size, structure, and functionalities. This arises from the existence of several methods for microsphere production (electrospray, emulsion polymerization, emulsion and solvent evaporation, porous membranes…) as well as from the wide range of polymeric materials (from natural or synthetic origin) available for its production.

In tissue engineering approaches, microspheres have been mainly used as building blocks for scaffold fabrication, drug delivery vehicles or cell carriers. In all these approaches, microspheres are conventionally used as “cell-on” systems; in which they provide support for cell adhesion, proliferation, and detachment via a number of methods (varying chemical materials, physical structures, and surface modifications); or as “cell-in” systems; used for cell encapsulation in which microspheres provide a protective environment for entrapped cells to ensure survival and proliferation. Both types of strategies have also been explored with regards to the role they play in affecting cellular fate and behavior as well as their application in cell delivery and microtissue engineering (He et al. 2020).

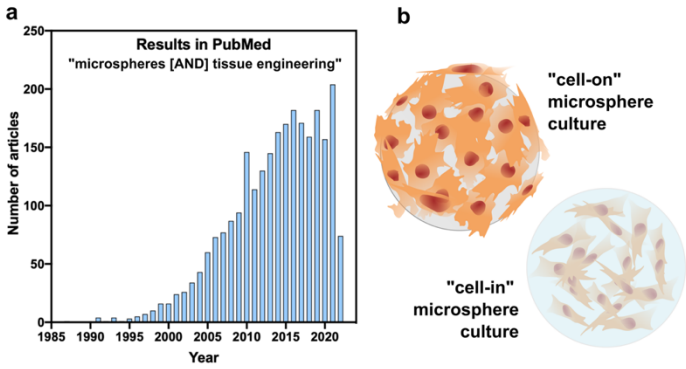

Figure 33. Microspheres and tissue engineering. a) Results for the search "(microsphere) AND (tissue engineering)" from 1985 to 2022 in the database PubMed. b) Schematic representation of the "cell-in" and "cell-on" approaches in microspheres-based cell culture tissue engineering approaches.

In the case of "cell-in" strategies, microspheres are usually hydrogel microparticles of spherical shape. Their properties make them suitable for numerous biomedical applications such as cell delivery and cell protection, drug delivery, scaffold building and microtissues generation. For example, a classical application is the encapsulation of therapeutic cells which permits the implantation of allogenic or xenogenic cells for the regulation of certain physiological processes damaged in the host tissues. This is the case of pancreatic islets encapsulation within alginate beads produced through a variety of methods, and crosslinked by immersion into an aqueous solution of divalent cations (Steele et al. 2014). In a different application, Rioja et al. cultured human endothelial cells and fibroblasts embedded in fibrin and collagen microbeads; they demonstrated that endothelial cell networks formed inside the microbead matrix and extended into the surrounding matrix, even forming anastomosis with vessels from adjacent microbeads (Rioja et al. 2016). This study demonstrates the improved capacity of vascularization of microsphere's based microtissues. Moreover, these microspheres can be used for the generation of granular hydrogels (Mealy et al. 2018), an agglomeration of hydrogel microspheres in the jammed state, where the term 'jammed' implies that an inside particle can only move if its neighboring particles also move (Daly et al. 2020).

The “cell-on” microspheres are considered as excellent cell expansion systems, they provide a high surface to volume ratio for the large-scale cultivation of anchorage dependent cells, such as MSCs, allowing to use less culture medium volumes and space than that required of conventional 2D culture systems. Therefore, they imply a step forward to the scale up in the cell expansion necessary for the obtaining of the cell numbers required for clinical applications. For example, Schop at al. efficiently expanded human BM-derived MSCs in a microcarrier-based spinner flask cultivation system (Schop et al. 2010). The microspheres used were Cytodex 1, the commercially available microspheres made of the natural polymer dextran which have been also used in this Doctoral Thesis with different objective. They were able to use lower serum concentrations and the phenotype and differentiation potential of the expanded MSCs remained unaltered. Several authors have explored this use of “cell-on” microspheres with commercially available microcarriers (Skardal et al. 2010) or with self-manufactured microspheres designed to fulfil highly specific properties and functionalities adapted to targeted applications (Clara-Trujillo et al. 2019; Lastra, Gómez Ribelles, and Cortizo 2020; D. Smith et al. 2019). “Cell-on” microspheres have also been exploited in bottom-up tissue engineering approaches, in which micrometer-scale cell-loaded microspheres are used as building blocks to build up millimeter-sized constructs with adaptive geometries. The resulting microtissues present advantages with respect to conventional scaffolds, such as more homogeneous cell distribution, better nutrient diffusion, easier vascularization and increased remodeling capacity. Functional microtissues with high activity can be assembled in a pre-shaped model *in vitro* (Zarkesh et al. 2020), or be directly injected *in vivo* for an accurate fit within the defect site (He et al. 2020). Microspheres can also be used in composites in which the particles are incorporated in a secondary material (such as a hydrogel) and confer specific functionalities to the resulting 3D construct (Carvalho et al. 2020).

These examples demonstrate the wide variety and possibilities that 3D culture approaches based on microspheres offer. All of them are designed for adherent cells, nevertheless, for the development of MM disease models it’s

interesting to expand the use of microspheres as 3D environment for the culture in suspension since MM cells are non-adherent cells. In spite of the great advances made both in the field of BM modeling *in vitro* and in that related to the use of microspheres as 3D substrates, the culture of suspension growing cells has not been exploited.

For this reason, we consider very interesting to work on optimizing protocols that allow the biomimetic microspheres developed in the previous chapter to be used for the generation 3D models of MM. These models aim to be a semi-solid culture medium for non-adherent cells. They are intended to be able to provide a dynamic 3D environment in which cells can perceive the presence of ECM biomolecules but without being confined by a material of defined shape.

4.2.2. Multiple myeloma cell lines as in vitro models.

MM is a disease of great genetic heterogeneity, this implies diverse clinical responses among patients and increases difficulties to understand the molecular bases of disease initiation and progression (Morgan, Walker, and Davies 2012). Historically, a major limitation in MM research is the availability of primary tumor cells. MM primary cells can survive several days, but they cannot be expanded *in vitro* for most patients. This is a significant limitation for undergoing meaningful biological studies about DR. Human MM cell lines appear as the available alternative (Vikova et al. 2019).

Human MM tumor cell lines constitute a keystone in MM research. They help to understand molecular processes that drive fundamental aspects of the disease. They have been used for the general understanding of MM biology, for the identification and validation of target genes or for the screening of anti-MM potential drugs. However, these cell lines do not reflect the heterogeneity of MM patients. The approach that most researchers have used to give increased significance to their results has been to perform the experiments with several cell lines (De la Puente et al. 2015; Sterling and Reagan 2018; Shi et al. 2017), however the number will always be restricted.

These facts are a further proof that the future for MM treatment lies in personalized medicine, which considers the genetic background of each patient. For that, improvements must be done in the cell culture conditions for patient's samples, as the conventional cell culture plates are not able to maintain primary cells viability. Tissue engineering can contribute to this issue by providing better biomimetic models adapted for myeloma cells that can support their proliferation *in vitro* (de la Puente and Azab 2016). The microgel concept introduced in this Doctoral Thesis has also been designed with the future aim of addressing this issue once it would have been validated with different MM cell lines to prove its suitability.

4.3. Materials and methods

4.3.1. Acrylates-based microsphere carboxyl group blockade

The 10% AA microspheres were subjected to carboxyl group activation, as described in Section 3.3.2.1. with EDC and sulfo-NHS. Then microspheres were incubated with ethanolamine 1 M at pH 9. Incubation was performed for 1 h at 4ºC in an orbital shaker. After that, microspheres were cleaned 3 times with distilled H_2O and 3 times with DPBS.

4.3.2. Microsphere sterilization

4.3.2.1. Acrylates-based microspheres

Microspheres were sanitized with 3 cleanings in 70% ethanol of 10 min each at RT in an orbital shaker. Then 3 washes in sterile DPBS were performed and one extra cleaning with culture media without supplements before seeding. Protein coated microspheres were first sanitized and then functionalized under sterile conditions. HA grafted microspheres were sanitized after functionalization.

4.3.2.2. Cytodex 1 microspheres

Cytodex 1 microspheres were sterilized previously to functionalization as described in Section 3.3.1.2. After sterilization, all subsequent procedures have been carried out in a laminar flow hood under sterile conditions.

4.3.3. Cell lines

The MM cell lines RPMI8226, U226-B1 and MM1.S were purchased from the American Type Culture Collection (ATCC, Rockville, MD). MM cell lines were cultured in RPMI1640 media (Thermo Fisher, USA) supplemented with 10% fetal bovine serum (FBS) (Thermo Fisher, USA), 2 mM L-glutamine (Thermo Fisher, USA), 100 μg mL^{-1} penicillin and 100 μg mL^{-1} streptomycin (Thermo Fisher, USA). All cells were cultured at 37°C and in 5% CO_2 in a Galaxy S incubator (Eppendorf New Brunswick, Germany).

4.3.4. Development of 3D microgel cultures

For microgel cultures, 100 000 cells were seeded in 500 μL of 7% v/v microsphere's suspension in complete cell culture media in non-treated p24 cell culture microplates. For suspension conventional cultures, each well was conformed 100 000 cells and 500 μL of media. Cell cultures were carried out under dynamic conditions in a PMS-1000i microplate shaker (GrantBio, United Kingdom). The stirring speed was 150 rpm unless otherwise is stated. For media renewal, each 24 h 50% volume of media culture was renewed, avoiding carrying cells or microspheres.

4.3.5. Cell proliferation

Cell proliferation was determined by colorimetric MTS assay following manufacturer's instructions (CellTiter 96® AQueous One Solution Cell Proliferation, Promega, USA). For each condition, the same microgel system (cell culture media in suspension conditions) without cells was used as blank. Before absorbance determination by using a Victor 3 microplate reader (Perkin Elmer, USA), cells and microgels were placed into 1.5 mL Eppendorf tubes

and centrifuged to remove suspension cells and microspheres. Supernatant was pipetted in a 96 well plate and read at 490 nm. After blank subtraction, absorbance data was converted to cell number by using a calibration curve for each cell line and the cell number at 72 h was obtained for each sample.

Results are presented % of MM proliferation from Day 0, considering the initial cell number as 100%. MM proliferation (% of Day 0) was calculated using Equation (2):

Equation (2): Calculation of MM proliferation (% of Day 0)

$$\text{MM proliferation (\% of Day 0)} = \frac{\text{cell number at 72 h}}{\text{cell number at Day 0}} \times 100$$

where cell number at 72 h was obtained from MTS results as described and 100 000 cells (the seeding density) was considered as the value of cell number at Day 0.

4.3.6. Ki67 expression

Immunofluorescence analysis of the proliferative state of MM cells was performed in suspension and microgel cultures. After 72 h of culture, the content of the cell culture wells was pre-fixed by adding 500 µL of 4% paraformaldehyde (Thermo Fisher, USA), 5 minutes at RT. Then 2 cleanings with PBS were performed and cells were fixed for 20 minutes at RT with 2% paraformaldehyde. Samples were permeabilized and blocked in 10% (v/v) FBS in DPBS/ 0.1% (v/v) Triton-X100 for 1 h at RT and incubated with primary polyclonal antibody against Ki67 (Abcam, 1:25) in blocking buffer (10% FBS in DPBS/0.1% Triton-X100 (Sigma Aldrich, USA)) ON at 4°C. The samples were then rinsed twice in DPBS/ 0.1% Triton X-100 and incubated with the secondary antibody (Alexa Fluor 555, Invitrogen, 1:500) and BODIPY FL phalloidin (Invitrogen, 1:500) prepared in blocking buffer at RT for 1 h. Finally, samples were washed twice in DPBS/ 0.1% Triton X-100 before mounting with Vectashield containing DAPI (Vector Laboratories) and observed under an epifluorescence microscope (Nikon Eclipse 80i) at 60×. Image analysis was carried out with Cell Profiller (Mcquin et al. 2018) and MATLAB (R2018b, MathWorks

Inc., Natick, MA, USA). Cell segmentation was performed with Cell Profiller. Briefly, DAPI images were thresholded (using an Otsu adaptative two-classes thresholding method) and used for nuclear segmentation. Then, with the obtained nuclear masks, the intensity of protein staining (sum of intensities of all pixels) and the region of interest area (total number of pixels) was quantified in the Ki67 images using an inhouse software tool developed in MATLAB. With these data, mean fluorescence intensity was obtained for each cell following Equation (3).

Equation (3): Calculation of Ki67 mean fluorescence intensity

$$\text{Mean fluorescence intensity / cell (a.u.)} = \frac{\text{sum of all pixels intensities}}{\text{total pixels}}$$

Data is expressed as mean fluorescence intensity per cell and at least 18 cells per condition, from 6 different pictures of 3 different samples, were analyzed for each condition.

4.3.7. Cell viability

4.3.7.1. Cell viability assessment in acrylates-based microgels

Live/ Dead assay (LIVE/DEAD™ Viability/Cytotoxicity Kit, for mammalian cells, Invitrogen, USA) was used, following manufacturer's instructions. Briefly, samples were transferred to an Eppendorf tube, washed twice in DPBS and then immersed in 2×10^{-3} M calcein-AM and 4×10^{-3} M ethidium homodimer-1 and incubated for 15 min at RT. For cells and microspheres precipitation centrifugations were performed at 125 G. Then, samples were washed twice with DPBS, extended in a cover glass, and imaged at 10× using an epifluorescence microscope (Nikon Eclipse 80i). MM cell line RPMI8226 cultured 24 h in standard culture conditions was used as negative control for the ethidium homodimer-1 staining. MM cell line RPMI8226 incubated 30 minutes in 30% DMSO (Sigma Aldrich, USA) at 37º C and 5% CO_2 was used as positive control for the ethidium homodimer-1 staining.

Six different fields of each sample were analyzed on ImageJ 1.51v (National Institutes of Health, USA) using the process tool Find Maxima.

The total number of cells was calculated using Equation (4) and the percentage of cell viability was calculated as determined in Equation (5).

Equation (4): Calculation of the total number of cells for Live/Dead staining

$$\text{N total} = \text{live cells} + \text{dead cells}$$

where live cells are the total number of cells quantified using the calcein channel and dead cells is the total number of cells quantified in the ethidium homodimer-1 stain.

Equation (5): Calculation of the Live Cells (%) for Live/Dead

$$\text{Live cells (\%)} = \frac{\text{live cells}}{\text{N total}} \times 100$$

4.3.7.2. Cell viability assessment in Cytodex 1-based microgels

Direct and indirect cytotoxicity of the Cytodex 1-based microgels was assessed. For direct assays, MM cell lines were cultured in the different microgels as described in section 4.3.3. for the desired cell culture times (72 h). For indirect assays, the different microgels were incubated in cell culture media RPMI1640 for 72 h at 37º C and 5% CO_2, the falcon tubes were kept under agitation. Then the cell culture media conditioned by the different microgels was supplemented (10% FBS, 2 mM L-glutamine, 100 µg mL^{-1} penicillin and 100 µg mL^{-1} streptomycin) and used for the culture of the cell line RPMI8226 (at a seeding density of 200 000 cells / mL). Samples were analyzed after 24 h of culture.

Then, hoechst-33342 (Thermo Fisher, USA) (blue) was used as supravital stain (for live and dead cells) and cell viability was determined by propidium iodide (IP (Thermo Fisher, USA), red) exclusion in both type of assays. Non-viable cells with compromised membrane permeability were identified by their positive red fluorescence in the nuclei. Samples were incubated 30 min in dark with at 1.5 µg/mL of IP and 1.5 µg/mL of hoechst-33342. MM cell line RPMI8226 incubated 30 minutes in 30% DMSO at 37º C and 5% CO_2 was used as positive control for the propidium iodide staining. Finally, samples were imaged using the INCELL 6000 Analyzer system (GE Healthcare, USA).

At least 6 fields per well were imaged with the 20x objective and analyzed on ImageJ 1.51v (National Institutes of Health, USA) using the process tool Find Maxima. The total number of cells per image corresponded to the total number of cells stained with hoechst-33342 and the percentage of cell viability was calculated as determined by Equation (6).

Equation (6): Calculation of the Live Cells (%) for IP exclusion analysis:

$$\text{Live cells } (\%) = \frac{\text{total cell number} - \text{number of IP positive cells}}{\text{total cell number}} \times 100$$

4.3.8. Drug resistance in microgel cultures

The different MM cell lines were cultured in the different microgel based systems detailed in Table 7 and in suspension for 72 h in presence of Dexamethasone 1μM (DEX, Fortecortin, Merck KGaA, Germany), Bortezomib 4 nM (BTZ, Velcade, STADA, Germany) or absence of drugs (non-treated). Cell proliferation, cell viability and Ki67 expression was evaluated as described before. For the cell proliferation data, the parameter MM proliferation (% of Day 0) was calculated as described above, and then for each sample this value was normalized by the mean MM proliferation (% of Day 0) of the non-treated samples cultured in the same condition (i.e. suspension). This means that a value of 1 implies no differences in cell proliferation in comparison with the non-treated condition.

Table 7. Drug resistance culture conditions

Legend	Microsphere's type	Functionalization
SUSP	-	-
0%AA-CTRL	0% acrylic acid 1-60 μm diameter	None
0%AA-FN	0% acrylic acid 1-60 μm diameter	FN
10%AA-CTRL	10% acrylic acid 1-60 μm diameter	None
10%AA-HA	10% acrylic acid 1-60 μm diameter	HA

4.3.9. RNA extraction and RT-PCR

Total RNA from the 3 MM cell lines cultured for 72 h in the 10% AA microgel and in suspension under non-treated condition was extracted using RNeasy Micro-kit (Qiagen, Germany) and its quantity and integrity was measured using Nanodrop ND-1000 (Thermo Fisher, USA). RNAs were reverse transcribed using Maxima First Strand cDNA synthesis kit with thermolabile dsDNAse (Thermofisher, USA).

4.3.10. qPCR gene expression analysis

Real-time qPCR was carried out using the Light Cycler 480 SYBR Green I Master Mix (Roche, Switzerland) and a Light Cycler 480 instrument from Roche. Amplifications were performed for 40 cycles. The reactions were run four times (independent biological experiments).

The primers used for amplification were designed based on sequences found in the GenBank database and summarized in Table 8. Primers were validated using dissociation curve/melt analysis. The cycle number at which fluorescence passed the threshold (Ct values) was used for gene expression quantification using the comparative ΔΔCT method. Sample values were normalized to the threshold value of housekeeping gene GAPDH and the suspension condition was used as control condition for each cell line and each gene. The data analysis was performed using the LC480 Conversion Software, 2014 version (Roche, Switzerland) and Microsoft Excel 2021 (Microsoft Corporation, USA).

Table 8. Primer sequences used for the qRT-PCR

Gene	Forward primer sequence (5'-3')	Reverse primer sequence (3'-5')	Annealing temperature (ºC)
GAPDH	GTCTCCTCTGACTTCAACAGCG	ACCACCCTGTTGCTGTAGCCAA	62.4
HIFA1	TATGAGCCAGAAGAACTTTTAGGC	CACCTCTTTTGGCAAGCATCCTG	63.3
AKT1	TGGACTACCTGCACTCGGAGAA	GTGCCGCAAAAGGTCTTCATGG	64
PI3K	GAAGCACCTGAATAGGCAAGTCG	GAGCATCCATGAAATCTGGTCGC	62.4

MTOR	AGCATCGGATGCTTAGGAGTGG	CAGCCAGTCATCTTTGGAGACC	62.7
STAT3	CTTTGAGACCGAGGTGTATCACC	GGTCAGCATGTTGTACCACAGG	62.2
CTNNB1	CACAAGCAGAGTGCTGAAGGTG	GATTCCTGAGAGTCCAAAGACAG	60
MEK1	GGTGTTCAAGGTCTCCCACAAG	GGTGTTCAAGGTCTCCCACAAG	63.4
MEK2	GTGGTCACCAAAGTCCAGCACA	CACGATGTACGGCGAGTTGCAT	63.8
NFKB1	GCAGCACTACTTCTTGACCACC	GCAGCACTACTTCTTGACCACC	62.4
ITGA4	GCATACAGGTGTCCAGCAGAGA	AGGACCAAGGTGGTAAGCAGCT	62.9
ITGB1	GGATTCTCCAGAAGGTGGTTTCG	TGCCACCAAGTTTCCCATCTCC	63.3

4.3.11. Statistical analysis and reproducibility

Cell culture experiments were performed in triplicates and repeated at least 2 independent times ($n \geq 6$). Results are presented as mean ± standard deviation (SD). For statistical analysis, the data were analyzed for normality using the Shapiro-Wilk normality test with an alpha of 0.05. When the normality test was passed, for comparisons of three or more groups, an ordinary one-way ANOVA test with a Tukey's post-hoc test ($p = 0.05$) was used to perform multiple comparisons between the column means. When the normality test was not passed, a non-parametric Kruskal-Wallis test with a post-hoc Dunn analysis ($p = 0.05$) was used to perform multiple comparisons between the column means. GraphPad Prism 9 software (Graphpad Software, USA) has been used for statistical analysis. Differences among groups are stated as $p \leq 0.05$ (*), $p \leq 0.01$ (**), $p \leq 0.001$ (***), $p \leq 0.0001$ (****). All graphs have been created with R the ggplot2 (Wickham 2008) package in R language, using R studio version 1.3.1093 (R Development Core Team, Vienna, Austria) or with GraphPad Prism 9 software.

4.4. Results and discussion

4.4.1. Assembling of the 3D culture platform using acrylates-based microgels

The objective of this Thesis is the development of 3D culture environments based on microspheres as a biomaterial. The main feature of these models is that they are designed to respect the non-adherent nature of MM cells. This feature is considered to be key, and is the main distinguishing trait of the models presented here compared to the models previously described in the literature and discussed in Section 1.4. (Kirshner et al. 2008; De la Puente et al. 2015; Raic et al. 2014; Jakubikova et al. 2016). Based on preliminary results (Marín-Payá et al. 2021), we believe that maintain the dynamic nature of these cells and respect their suspension growth pattern can yield more biomimetic models and lead to *in vitro* results with greater clinical relevance.

Working with this novel culture methodology is of great interest from the point of view of the relevance of the results obtained. However, it is a great experimental challenge since there are no previous guidelines in the literature to determine the methodology and parameters for the *in vitro* culture using this semi-solid condition. Therefore, the determination of the optimal culture conditions to generate a 3D platform based on microspheres is one of the first and main issues that has been studied in this project. Given that MM is a disease of great genetic heterogeneity and with great differences between patients in terms of drug response (Morgan, Walker, and Davies 2012), it is important to bear in mind that the work carried out with cell lines has limitations, as discussed in Section 4.2.2. With the aim of increasing the translational nature of the results, we have tried to carry out most of the experiments in this Doctoral Thesis using three different lines of MM that seek to partially represent this heterogeneity.

Acrylates-based microgels were the first ones to be used in cell culture and the platform assembly conditions were determined with them. These microgels were produced with two different diameter distributions (Table 5): < 60

μm and > 70 μm of diameter. To determine the effect of microsphere size on MM cell proliferation, < 60 μm and > 70 μm diameter sizes of the 10% AA microgel without functionalization were cultured with RPMI8226, U226 and MM1.S cell lines for 72 h. The microgel with microsphere sizes closest to cellular size (< 60 μm) had higher cell proliferation after 3 days of culture than those of > 70 μm diameter (Figure 34 a) for the 3 cell lines. The > 70 μm microgel achieved less proliferation than the suspension culture without microgel and did not distribute homogenously with the cells (Figure 34 d). Due to its higher weight, microspheres did not stay in suspension and fell to the bottom of the well, causing a cell distribution similar to the culture without a microgel (Figure 34 b), but with less space for cell growth due to the microspheres (Figure 34 d). The smallest diameter microgels (Figure 34 c) achieved a higher specific surface area, meaning increased cell contact with the 3D matrix provided by the microgel. Due to their lighter weight, stirring kept the cells and microspheres in suspension and generated a homogeneous 3D distribution (Figure 34 c). The < 60 μm diameter microspheres were thus used for subsequent experiments. Hence, it has been shown that the size of the microspheres that form the microgel is a factor that modulates proliferation of myeloma cells. Microspheres made of acrylates and with >70 μm diameter did not allow to establish true 3D environment and had a negative effect on cell proliferation.

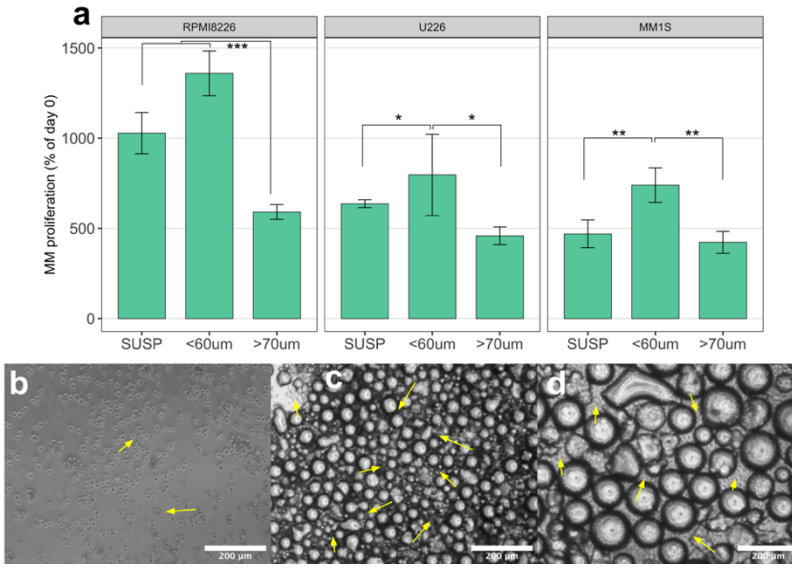

Figure 34. Effect of microsphere' size on MM proliferation. a) Growth of MM cell lines after 72h of culture in suspension or in 10% AA microgels with different diameters. b-d) Inverted microscope images at 72h of RPMI8226 cells cultured in suspension (b), microgel < 60 µm diameter (c) and > 70 µm diameter (d). Scale bar: 200 µm. Yellow arrows point to some MM cells. P value legend: p ≤ 0.001 (***). Comparisons were made using one-way ANOVA with Tukey's test for post-hoc analysis.

The dynamic physiology of the BM niche is not considered in conventional static cultures (Ferrarini et al. 2013; Zhang et al. 2014) or 3D cultures with predefined and static architectures (de la Puente and Azab 2016; Narayanan et al. 2014). This semi-solid platform creates a dynamic context, as cultures are carried out on agitated plates to keep microspheres suspended and generate a 3D environment. An initial experiment with the RPMI8226 MM cell line and 10% AA microgel (without functionalization) was conducted to assess the effect of agitation speeds on cell proliferation. Cells were cultured in suspension or in the 10% AA microgel at 0, 150, 200 and 300 rpm using an orbital plate shaker. Results are shown in Figure 35, a. After 72 h of culture, the microgel rated a higher cell proliferation than its suspension counterparts for all the agitation speeds tested. In the conventional suspension condition, the increase in the stirring speed had a negative effect on cell proliferation, a behavior that has been previously reported when culturing different cell lines

in agitated bioreactors or spinner flasks (Jing et al. 2013; Carswell and Papoutsakis 2000). However, in the case of the microgel condition the negative effect on cell proliferation due to the increase in the stirring speed was overcame. Interestingly, the presence of the microspheres protected cells of higher stirring speeds and allow normal cell proliferation rates. The mechanism behind this phenomenon has yet to be elucidated. Some literature reported that, circulating tumor cells (CTCs) extravasate to the blood stream in the metastasis process, hemodynamic shear stress can induce cell death, however some clusters of CTCs, known as circulating tumor microemboli, can retain their viability, in part due to the glycocalyx, the surrounding matrix components, and cell-cell adherence (Mitchell and King 2014). Maybe, the interaction of microspheres and cells can somehow mimic this behavior and reduce the shear stress of MM cells cultures in the system in comparison with suspension condition. Currently, a collaboration is being carried out with the group of Professor M.H. Doweidar, from the Applied Mechanics and Bioengineering group from the Aragón Institute of Engineering Research. This collaboration aims the computational modeling of the growth pattern of MM cells growing in the microgel, and of the distribution of cells and microspheres in the 3D space of the cell culture well at different stirring speeds. The development and validation of this model will allow us to understand the interactions, collisions and tensions to which a cell is subjected when it is cultivated in the microgel at the different stirring speeds, a fact that could help to understand the positive effect of the microgel that maintains cell proliferation at higher agitation speeds.

The experimental data (Figure 35, b) showed that, for the static culture, deposition of the microgel in the bottom of the well, takes place. Because of that, static culture was discarded, as it doesn't allow to keep the microspheres and the cells in suspension, maintaining the main characteristic pursued in this model. 150 rpm was chosen as the optimal speed for the subsequent culture experiments, as it was enough to maintain microgel suspension (Figure 35, b) and showed good cell proliferation for the suspension condition (Figure 35, a).

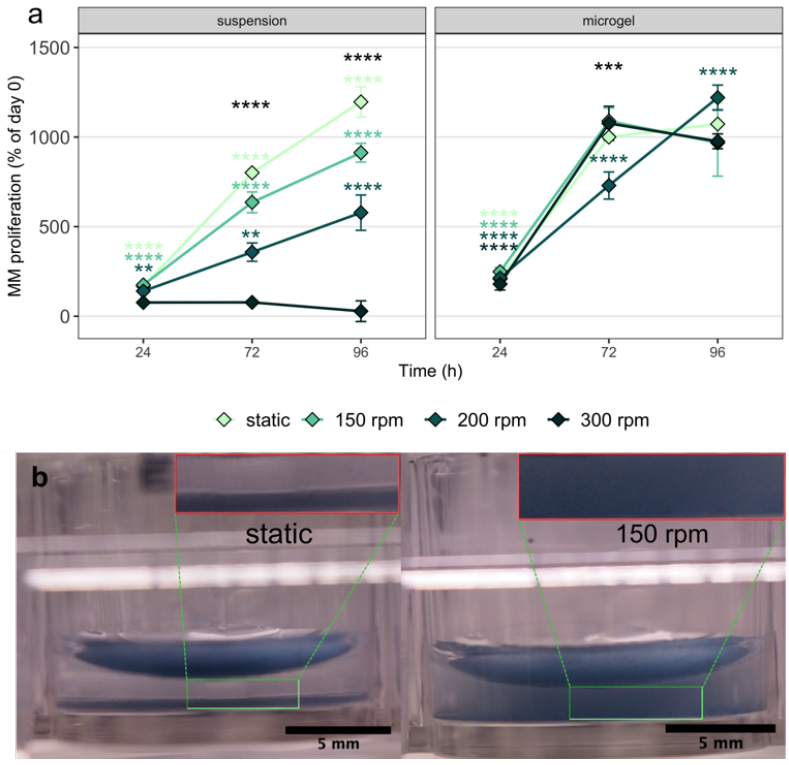

Figure 35. Effect of stirring speed on MM proliferation. a) Growth of the RPMI8226 cell line in suspension and microgel cultures at different agitation speeds (static and 150, 200 or 300 rpm). Comparisons between different time points for each speed and, at each time point between different speeds, were made using one-way ANOVA with Tukey's test for post-hoc analysis. P value legend: p ≤ 0.05 (*), p ≤ 0.01 (**), p ≤ 0.001 (***), p ≤ 0.0001 (****). Statistical differences shown in each stirring speed color refer to differences of this point with the different time points of the same speed. Statistical differences shown in black refer to differences between different stirring speeds at the same time point. b) Microgel distribution in cell culture wells at 24h of simulated culture (microspheres were stained in dark blue for visualization) under static and 150 rpm stirring. Scale bar: 5 mm.

4.4.2. Acrylates-based microgels allowed good cell proliferation of different MM cell lines

Once the optimal conditions were determined in terms of microsphere size (< 60 μm diameter) and stirring speed (150 rpm) for the culture of MM cell lines in the microgel, this experimental set up was used for studying the effect of

microspheres chemical composition and functionalization in different MM cell lines proliferation.

All the acrylates-based microgels listed in Table 4 were used for the culture of MM cell lines, at 72 h of culture, MM cell proliferation was determined. The microgels whose effect on cell proliferation and DR has been more extensively analyzed in this Thesis have been studied always with 3 different available MM cell lines. However, to simplify the experimental conditions some of the microgels developed have only been tested with one of the different MM cell lines. The different conditions studied are listed in Table 9.

Table 9. Different acrylates-based microgels used in cell culture and MM cell lines cultured in each microgel.

Microsphere type				MM cell lines cultured in each microgel
Polymer	Acronym	ECM biomolecule	Functionalization protocol	
Acrylates, 0%AA	0%AA CTRL	None (control)	-	RPMI8226, U226, MM1.S
	0%AA FN	FN	Coating	RPMI8226, U226, MM1.S
Acrylates, 10%AA	10%AA CTRL	None (control)	-	RPMI8226, U226, MM1.S
	10%AA HA	HA	2 steps EDC/NHS coupling	RPMI8226, U226, MM1.S
	10%AA COL 1	COL1	1 step EDC/NHS coupling	U226
	10%AA PRARI	PRARI peptide	1 step EDC/NHS coupling	RPMI8226
	10%AA IDAPS	IDAPS peptide	1 step EDC/NHS coupling	RPMI8226
	10%AA GRGD	GRGD peptide	1 step EDC/NHS coupling	RPMI8226
	10%AA BSA	BSA	Coating	RPMI8226

The microgels of 0% AA and 10% AA without functionalization, the 0% AA functionalized with FN and the 10% AA functionalized with HA were the ones more extensively analyzed to validate the 3D culture platform. The choice was made on the basis of having the unfunctionalized microgels as control of the 3D condition and the chemical composition of the microspheres and the FN and HA as biofunctionalizations whose role on MM DR generation has been previously studied (Hazlehurst et al. 2000; Damiano et al. 1999; Fei, Hang, and Hou 2013; Shain et al. 2009; Vincent et al. 2003; Bjorklund et al. 2014). These microgels were cultured with the 3 different MM cell lines. Results of cell proliferation after 72 h are shown in Figure 36.

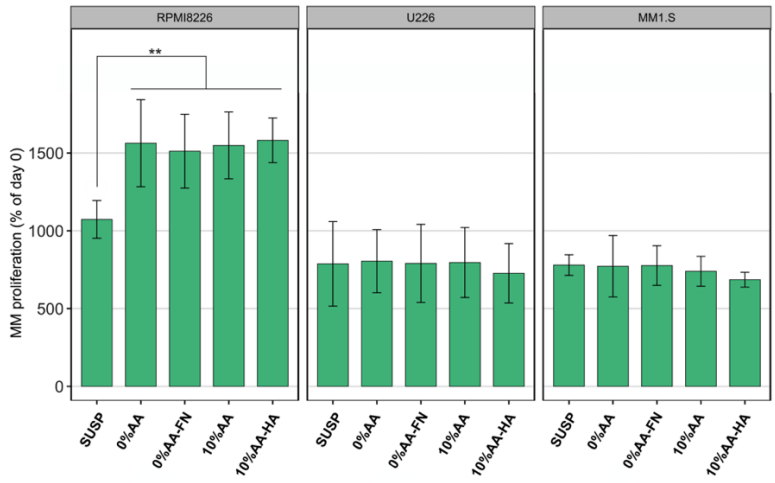

Figure 36. Growth of the cell lines RPMI8226, U226 and MM1.S after 72 h of culture in suspension or in microgels. Cultures were performed at 150 rpm. SUSP (suspension 2D culture), 0% AA (0% AA uncoated microgel), 0%AA FN (0% AA coated with fibronectin microgel), 10% AA (10% AA ungrafted microgel), 10%AA HA (10% AA grafted with hyaluronic acid microgel). P value legend: p ≤ 0.01 (**). For each cell line, comparisons between microgels were made using one-way ANOVA with Tukey's test for post-hoc analysis.

When cultured on all the different microgels the U226 and MM1.S cell lines showed proliferation rates similar to their suspension cultures, implying that the presence of the microgels does not have a negative effect on cell proliferation in these cell lines, regardless of the composition (0 or 10% AA) or

functionalization (FN, HA or none). In the case of the RPMI8226 cell line, all the microgels tested showed higher proliferation rates than those grown in suspension. We attribute this positive effect of the microgels on cell proliferation to the three-dimensionality achieved by the cell-sized microgel, regardless of its composition or functionalization. The cell and microsphere distribution in the different microgels after 72 h of culture is shown in Figure 37. Although the architecture and original distribution of the well was not strictly preserved (immunofluorescence was performed using a suspension protocol), the cells remained mostly in suspension and did not adhere to the microspheres. This applies to all microspheres except for the microgels coated with FN, in which most of the cells appear forming aggregates between them and the microspheres. These patterns can be seen in both the RPMI8226 and U226 cell lines (the behavior of MM1.S, was similar to that of the U226 line).

It was therefore established that the different microgels allow the growth of myeloma cell lines at least to the same extent as their conventional suspension culture and that most of the microgels respect the suspension growth of the MM cell lines. This result is in itself highly important, as previous research had reported that other commercially available 3D systems (poly lactic-co-glycolic acid (PLGA) microspheres, AlgiMatrix, and Matrigel) showed lower MM cell line proliferation rates than conventional 2D cultures after 72 h (3 days) of culture (De la Puente et al. 2015) (Figure 38, a).

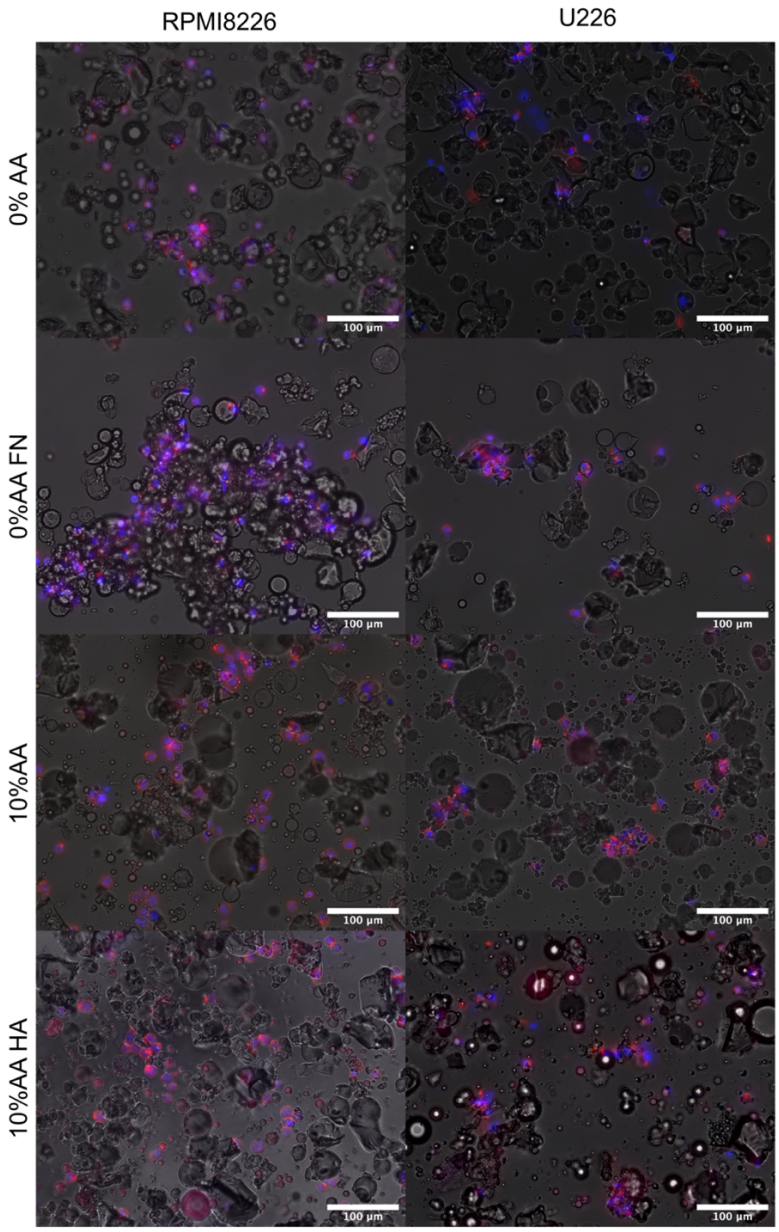

Figure 37. DNA (Hoechst33342-blue) and actin (phalloidin-red) staining of RPMI8226 and U226 cells after 72 h of culture under non-treated conditions in the different microgels. Scale bar: 100 µm.

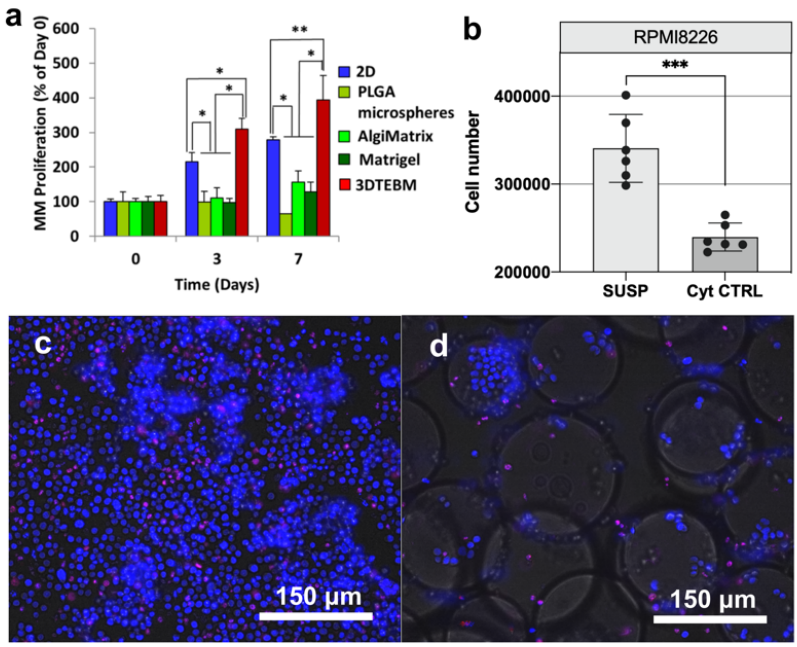

Figure 38. MM cell lines proliferation on different 3D systems. a) Results reproduced with permission from De la Puente et al. (De la Puente et al. 2015)**. Growth of MM1.S in multi-culture with MM-derived stromal cells and endothelial cells in classic 2D cultures, PLGA microspheres, AlgiMatrix, Matrigel, and inside 3DTEBM at days 3 and 7 compared to day 0, (*) p< 0.01, (**) p< 0.05. b) Growth of the cell line RPMI8226 after 72 h of culture in suspension or in Cytodex 1 microspheres. Cultures were performed at 150 rpm. P value legend: p ≤ 0.01 (**). c-d) Fluorescence images from propidium iodide exclusion assay (blue stains all cells (hoechst-33342), red stains dead cells (propidium iodide)) corresponding to RPMI8226 cells growing in suspension (c) or in Cytodex 1 microspheres (d).**

The positive effect of microgels compared to other commercial 3D systems on cell proliferation (Figure 38, a) was attributed to the fact that microgels can maintain the non-adherent and dynamic nature of MM cells. Analyzing the content of a cell culture well by microscopy without altering its native distribution is not possible, since it is a semi-solid culture. Therefore, to try to confirm that the ability to maintain myeloma cell growth in suspension while providing them with a 3D environment is the reason for the positive effect of the microgel, a second cell culture was carried out. In this case, a microgel made up of Cytodex 1 microspheres without any functionalization and the cell line RPMI8226 were used. These microspheres were used as a control because

they are microspheres that have been designed as microcarriers for adherent cells, therefore their surface has a high positive charge and stimulates cell adhesion. As can be seen in Figure 38 d, these microspheres induced MM cells attachment onto their surface, and, as expected, cell proliferation in this microgel was decreased in comparison with the conventional suspension condition (Figure 38, b), reinforcing the hypothesis previously raised. It must be pointed out that Cytodex 1 present higher diameter distribution (around 150 μm) and it has been demonstrated that the size of the microspheres can be a relevant factor that modulates cell proliferation. However, in the case of Cytodex 1, microspheres present a hydrogel like nature and, regardless of their size, their density is lower and thus there can be kept in suspension in the cell culture well and generate a real 3D environment, in contrast to what happened with the acrylate's microspheres of > 70 μm.

The rest of acrylates-based microgels developed (functionalized with collagen or with different synthetic peptides based on different cell surface receptors binding domains from MM cells) were also assayed for cell proliferation with one MM cell line.

As can be seen in Figure 39, a, the 10% AA microgel obtained also good cell proliferation results for the cell line RPMI8226 when functionalized with most of the different synthetic peptides. For the GRGD and PRARI sequences, proliferation was comparable to the results obtained in the SUSP condition. However, for the IDAPS sequence, proliferation resulted lower than the SUSP condition. GRGD and PRARI peptides are designed to interact with integrin $\alpha 4\beta 1$, $\alpha v3$, $\alpha v\delta$, $\alpha 5\beta 1$ and integrin $\alpha 4\beta 1$ and syndecan respectively; while IDAPS is designed to interact only with integrin $\alpha 4\beta 1$ on MM cells surface (Hozumi et al. 2016). The differences in the pattern of cell surface receptors activated by each ligand could be on the basis of these differences.

For the COL 1 grafted microgel, a cell culture with the cell line U226 was performed and samples were analyzed for viability and proliferation using a live/dead staining at days 0, 2, 4 and 6. Figure 39 b and d demonstrate that

the COL 1 grafted microgel presented good cell viability, moreover proliferation on this microgel was also higher than the one in conventional suspension culture (Figure 39, c).

All these data confirmed the importance of maintaining the suspension growth pattern of MM cell lines and demonstrated that the different acrylates-based microgels performed good in 3D culture in terms of MM cell lines viability and proliferation.

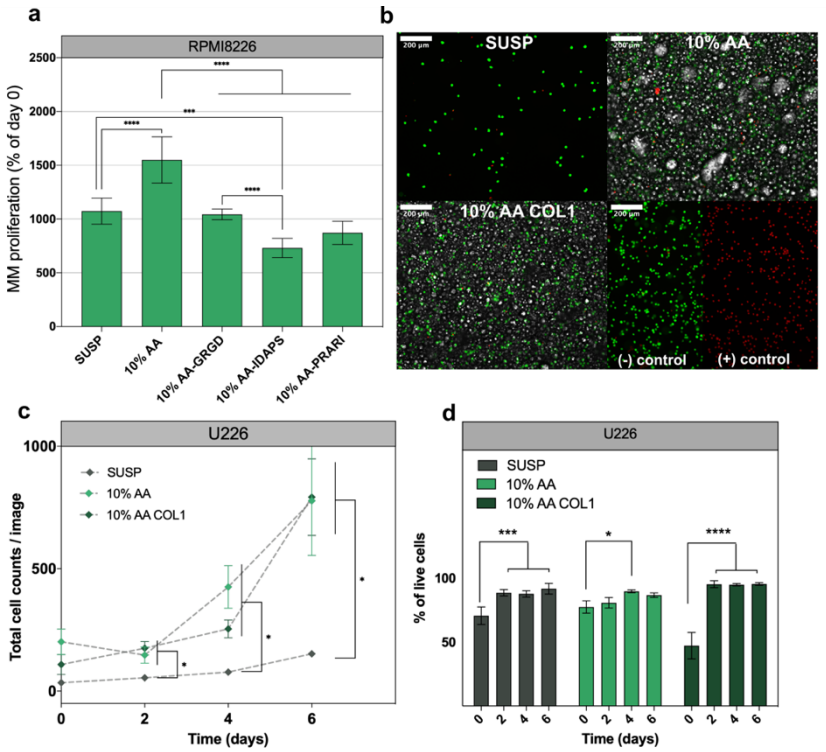

Figure 39. MM cell lines viability and proliferation on different microgels. a) Growth of the cell line RPMI8226 after 72 h of culture in suspension or in microgels. Cultures were performed at 150 rpm. SUSP (suspension 2D culture), 10% AA (10% AA ungrafted microgel), 10% AA GRGD (10% AA grafted with GRGD peptide microgel), 10% AA IDAPS (10% AA grafted with IDAPS peptide microgel), 10% AA PRARI (10% AA grafted with PRARI peptide microgel). P value legend: p ≤ 0.01 (**). Comparisons between microgels were made using one-way ANOVA with Tukey's test for post-hoc analysis. b-d) Results from live/dead staining of the U226 cell line growing in suspension (SUSP) or in 10% AA (10%

AA ungrafted microgel), 10% AA COL1 (10% AA grafted with collagen 1). b) Representative images of live/dead staining at day 6 (scale bar: 200 μm). c) Viability obtained from image analysis of 6 images per condition and time. For each condition, comparisons between time points were made using one-way ANOVA with Tukey's test for post-hoc analysis. d) Total cell counts per image. For each time point, comparisons between conditions were made using one-way ANOVA with Tukey's test for post-hoc analysis. P value legend: p ≤ 0.05 (*), p ≤ 0.01 (**), p ≤ 0.001 (***), p ≤ 0.0001 (****).

4.4.3. Drug resistance generation in acrylates-based microgels

Once the suitability of the microgel platform for the 3D culture of the different MM cell lines was proven, we further evaluated the ability of the different microgels to reproduce resistance to different MM drugs *in vitro*. Dexamethasone (DEX) and bortezomib (BTZ) are currently used for the clinical treatment of MM patients. DEX is a glucocorticoid that induces apoptosis in MM cells through up-regulation of pro-apoptotic genes, down-regulation of anti-apoptotic genes (Burwick and Sharma 2019), cleavage of poly (ADP-ribose) polymerase and caspase 3 (Chauhan et al. 1997) and activation of intrinsic apoptotic pathways (Chauhan et al. 2001). The proteasome inhibitor BTZ is a reversible inhibitor of the 26S proteasome complex. It produces apoptosis in MM cells by different mechanisms such as activation of caspase 8 and 9, upregulation of NOXA (Pinto et al. 2020), or suppression of the NF-κB pathway (Chen et al. 2011), which is a key regulator of growth and survival in MM cells.

To test the drug efficacy in our 3D model, the cell lines RPMI8226, U226 and MM1.S were grown in some of the developed microgels and in suspension without microgels for 72 h in three different conditions: non-treated, DEX 1 μM (Jakubikova et al. 2016; Ohwada et al. 2008) and BTZ 4 nM (Vidya Ramakrishnan and Mager 2018). In the experiments presented in this section cell proliferation was assessed after 72 h of culture and the data is represented for each microgel or suspension condition normalized by its non-treated equivalent.

4.4.3.1. Dexamethasone studies

For the RPMI8226 cell line when treated with DEX 1 μM, we found that the composition of their polymeric matrix determines the generation of resistance to DEX *in vitro*: the 10% AA microgels have mean proliferation rates which significantly differ from the suspension condition (Figure 40). This means that the presence of acrylic acid increases resistance to DEX *in vitro*. Although there is no significant statistical difference between 10% AA and 10% AA HA, the HA grafted microgels achieved the higher proliferation rate. This agrees with the reported role of HA as a survival factor against DEX-induced apoptosis in MM cell lines (Vincent et al. 2003; Ohwada et al. 2008). These authors demonstrated that HA could antagonize DEX induced apoptosis in MM cell lines. In IL-6 dependent MM cells lines HA protects, stabilizes, and concentrates IL-6 close to its site of secretion, thus favoring its autocrine activity and stimulating MM proliferation and survival. In contrast, in the IL-6 independent RPMI8226 cell line, HA survival effect was mediated through a IL-6 independent pathway, resulting in the upregulation of Bcl-2 anti-apoptotic protein expression and NF-κB activation (Vincent et al. 2003). Ohwada et al. in contrast, worked only with a fraction of the RPMI8226 cell line, the high-CD44 fraction. They demonstrated that HA binding to CD44 increases IκB phosphorylation, and as consequence its proteasomal degradation thus increasing NF-κB pathway activity. Taken together, these data suggest that HA antagonizes DEX-induced apoptosis of MM cells (IL-6 dependent or independent) by favoring their autocrine activity or by directly activating the NF-κB pathway.

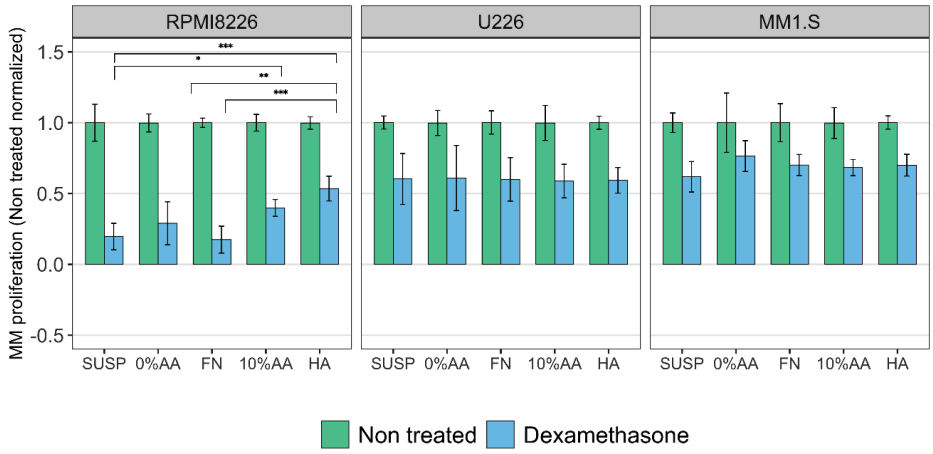

Figure 40. Proliferation rates of the cell lines RPMI8226, U226 and MM1.S at 72 h of culture growing in suspension or in microgels when treated with dexamethasone 1 μM (blue) or non-treated conditions (green). Data is expressed as % of MM proliferation with respect to day 0 and, for each condition, normalized by its non-treated counterpart. SUSP (suspension 2D culture), 0% AA (0% AA uncoated microgel), 0% AA FN (0% AA coated with fibronectin microgel), 10% AA (10% AA ungrafted microgel), 10% AA HA (10% AA grafted with hyaluronic acid microgel). P value legend: p ≤ 0.05 (*), p ≤ 0.01 (**), p ≤ 0.001 (***), p ≤ 0.0001 (****). For each cell line, comparisons were made independently for each drug. Comparisons between microgels were made using one-way ANOVA with Tukey's test for post-hoc analysis.

For cell lines U226 and MM1.S under DEX treatment, microgels did not increase proliferation rate compared to suspension, regardless of the composition or functionalization in either of the two cell lines. Interestingly, the 0% AA microgel coated with FN had the lowest proliferation the RPMI8226 cell line when treated with DEX. It has been reported that FN binding to malignant plasma cells can induce G0/G1 cell cycle arrest and confer drug resistance by means of this mechanism (Damiano et al. 1999; Shain et al. 2009; Hazlehurst et al. 2000). To assess whether the reduced proliferation in the cell lines cultured in FN-coated microgels was due to G0/G1 arrest, the expression of the Ki67 proliferation marker was quantified by immunofluorescence in RPMI8226 and U226 cell lines cultured in suspension and in the different microgels under non-treated and DEX-treated conditions (Figure 41, a).

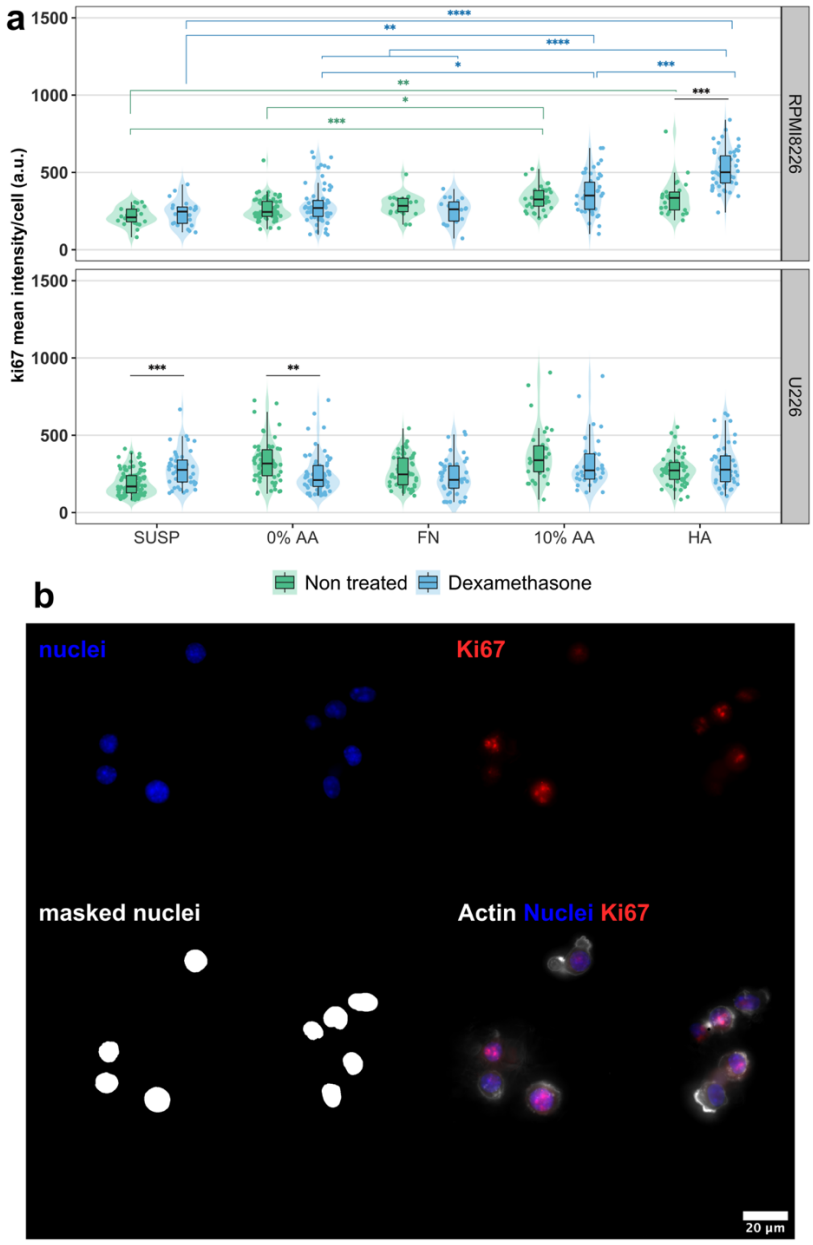

Figure 41. Ki67 analysis of RPMI8226 and U226. a) Ki67 expression of the cell lines RPMI8226 and U226 at 72 h of culture growing in suspension or in microgels when treated with dexamethasone 1 µM (blue) or in non-treated conditions (green). Data is expressed as mean fluorescence intensity x cell^{-1} (a.u). At least 18 cells per condition were analyzed from 6 different pictures of 3 different samples. SUSP (suspension 2D culture),

0% AA (0% AA uncoated microgel), 0% AA FN (0% AA coated with fibronectin microgel), 10% AA (10% AA ungrafted microgel), 10% AAHA (10% AA grafted with hyaluronic acid microgel). Statistical differences shown in black represent intra-condition differences. Statistical differences shown in green represent differences between the non-treated conditions. Statistical differences shown in blue represent differences between DEX treated samples. P value legend: p ≤ 0.05 (*), p ≤ 0.01 (**), p ≤ 0.001 (***), p ≤ 0.0001 (****). For each cell line, comparisons between microgel groups were made using a one-way ANOVA with Tukey's test for post-hoc analysis. b) Sample set of images used for the analysis (original immunofluorescence images and masks used for the analysis) corresponding to the cell line U226 cultured in the 10% AA HA and in non-treated condition.

Results showed that no significant differences in Ki67 expression were found for RPMI8226 or U226 between the 0% AA and the 0% AA FN microgels and G0/G1 cell cycle arrest induced by FN could not be confirmed. Figures 42, 43 and 44 show that MM cells distributed homogeneously in all microgels except those which are FN-coated. In these microgels the 3D distribution was not fully maintained, as the microsphere clusters were heavier. As a result, the FN conditions had a macroscopic distribution similar to that generated by the > 70 μm diameter microgels (Figure 34 d), which stayed at lower proliferation rates than the cell-sized microgels. These differences in the distribution of the microspheres and the formation of groups with cells and by themselves mean that the proliferation data cannot be properly compared with those of other systems. The results shown in Figure 41 for the FN-coated microgels can be attributed to this phenomenon. Again, these results show that the hypothesis defended in this Thesis of the importance of keeping myeloma cells growing in suspension is well founded. Since the only microgel condition unable to maintain this pattern consistently results in less cell proliferation. Demonstrating that keeping individual cells and microspheres in culture influences cell proliferation.

Ki67 expression was higher in the 10% AA HA microgel for the cell line RPMI8226 (Figure 41, a), a result which agrees with Figure 40 and with the hypothesis proven by Vincent et al. and Ohwada et al. (Vincent et al. 2003; Ohwada et al. 2008).

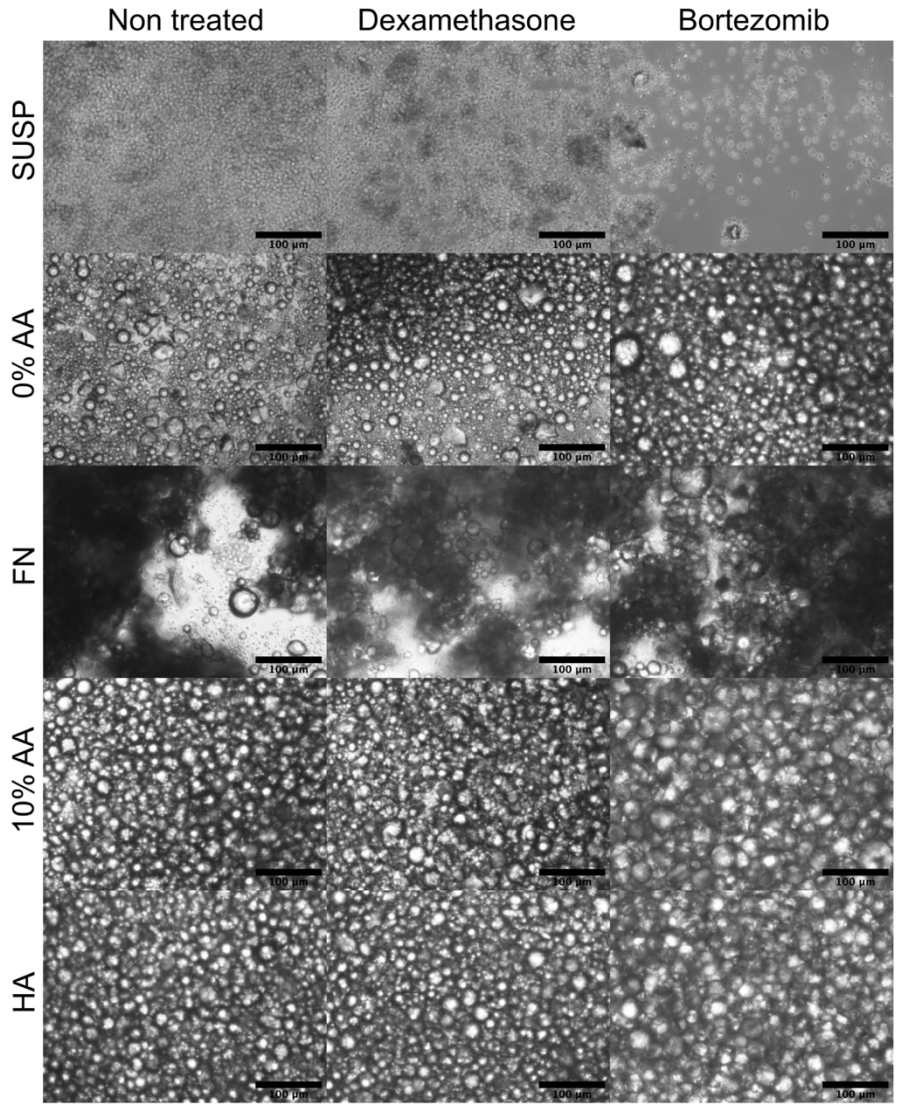

Figure 42. Inverted microscope images of the cell line RPMI8226 in the different micro-gels and in suspension, at 48 h of culture under non-treated, DEX 1 μM and BTZ 4 nM conditions. Scale bar: 100 μm.

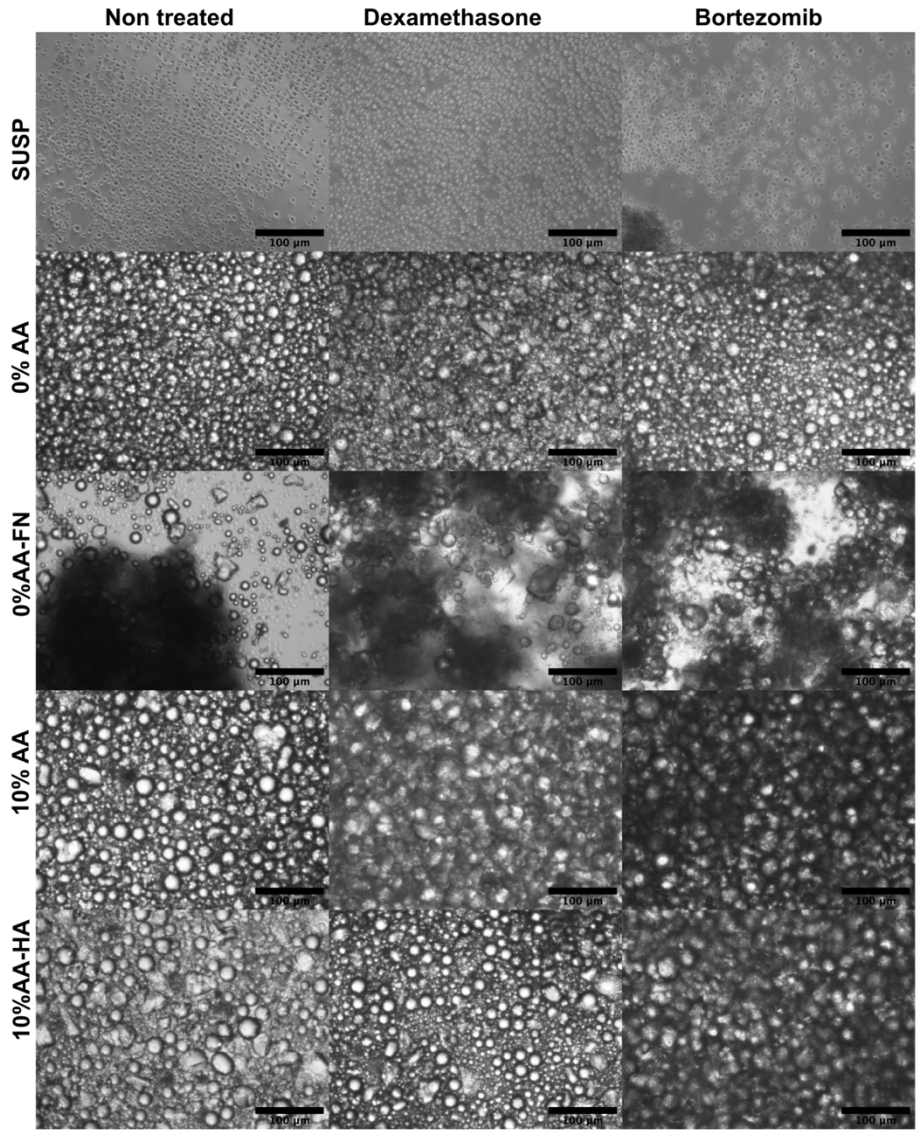

Figure 43. Inverted microscope images of the cell line U226 in the different microgels and in suspension, at 48 h of culture under non-treated, DEX 1 µM and BTZ 4 nM conditions. Scale bar: 100 µm.

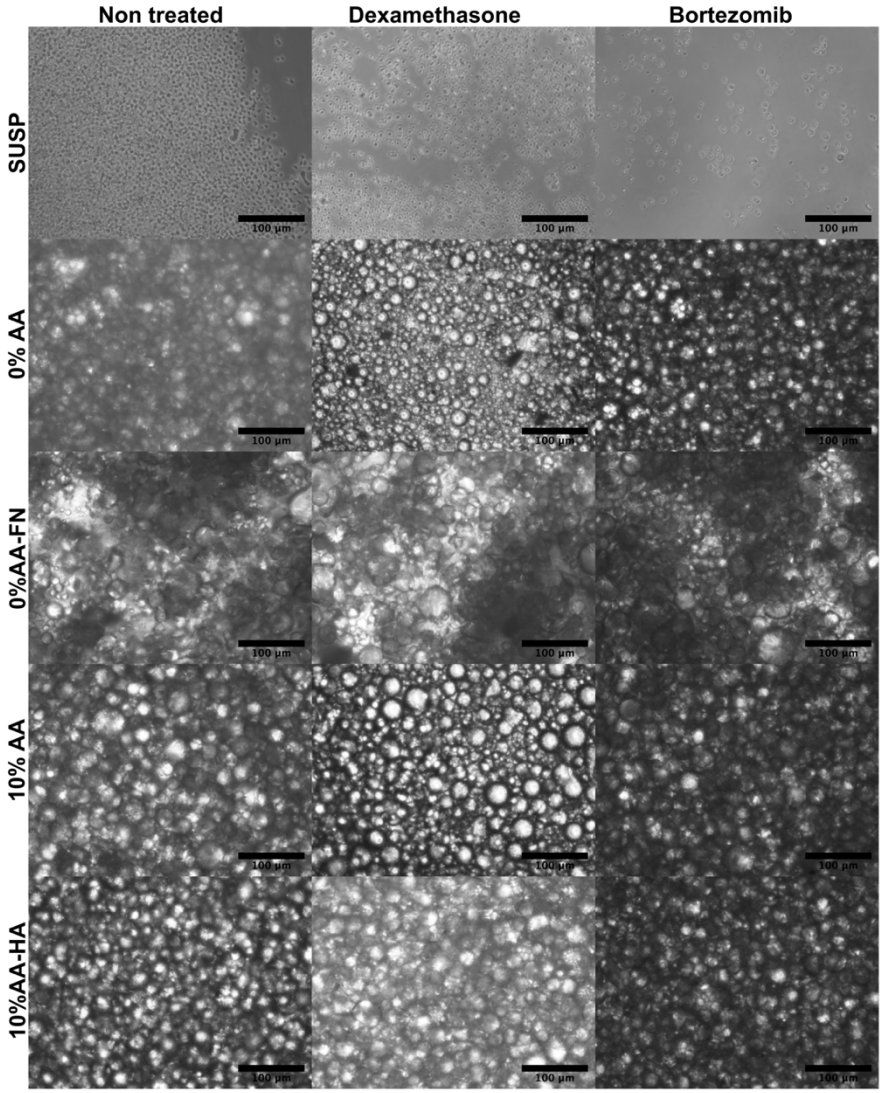

Figure 44. Inverted microscope images of the cell line MM1.S in the different microgels and in suspension, at 48 h of culture under non-treated, DEX 1 μM and BTZ 4 nM conditions. Scale bar: 100 μm.

An interesting point is to understand why, in the case of the RPMI8226 cell line, there is a different ability to generate resistance to DEX among the different microgels (Figure 40). It could be hypothesized that there is a 3D effect that goes further than the specific effect of the biomolecules we studied. However, this theory can be discarded, as the 3D effect could also be expected in the 0% AA microgel. The hypothesis that we put forward is that the AA present on the surface of the 10% AA microgels enhances their ability to bind and concentrate soluble factors from the medium (either from the FBS or paracrine factors produced by the plasmatic cells themselves, such as IL-6) and present them to the cells more efficiently than the conventional suspension culture, favoring their growth and resistance to drugs. This hypothesis is supported by the fact that the poly-acrylic acid has been reported to have protein-binding properties due to the presence of carboxyl (-COOH) groups, which make their surfaces hydrophilic and improve its adsorption properties (P. Y. Wang et al. 2015; Sharma et al. 2015). In our case, the effects due to AA on microsphere surfaces would be multiplied by the larger specific surface of the microspheres.

To further test this hypothesis, a 10% AA microgel was coated with bovine serum albumin (BSA), a protein used in research as a competing agent for the unspecific adhesion and generation of non-fouling surface (Punet et al. 2013). Cultures of the RPMI8226 cell line were grown in this microgel under non-treated and DEX treated conditions. The results (Figure 45) showed that the BSA antifouling coating did not significantly affect the proliferation rates of the 10% AA microgel in non-treated conditions or the generation of DEX resistance. This result demonstrates that the AA effect mechanism is not as simple as increasing adsorption properties of the microspheres and point out that future studies are needed to understand the mechanism underlying the positive effect of AA in terms of generating DR.

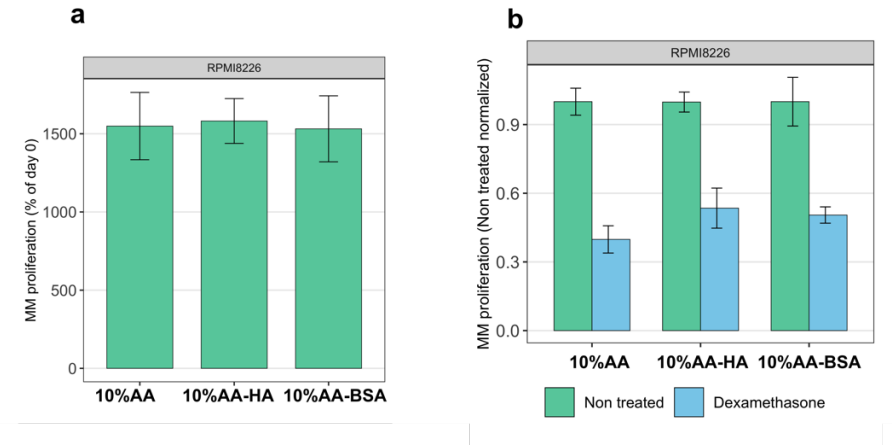

Figure 45. RPMI8226 growth on BSA coated microgel. a) Growth of the RPMI8226 cell line after 72 h of culture in 10% AA, 10% AA BSA or 10% AA HA microgels. b) Proliferation rates of the cell line RPMI8226 at 72 h of culture growing in 10% AA, 10% AA BSA or 10% AA HA microgels when treated with dexamethasone 1 μM (blue) or non-treated conditions (green). Data is expressed as % of MM proliferation in respect to day 0 for each condition normalized by its non-treated counterpart.

4.4.3.2. Bortezomib studies

In the case of the BTZ, the microgels yielded very interesting results in terms of drug resistance generation (Figure 46). Cell line RPMI8226 cultured in suspension had a proliferation rate of 0.04 when treated with BTZ 4 nM. However, when the same cell line was cultured in the different microgels and treated with BTZ 4 nM, the lowest proliferation rate was 0.72, achieved by the 0% AA FN microgel. The proliferation rates of 0% AA, 10% AA and 10% AA HA were 0.93, 0.90 and 0.93, respectively. This implies a remarkable increase in cell proliferation with respect to the suspension conditions and shows the ability of the proposed culture systems to generate drug resistance in *in vitro* cultures. Finally, for cell lines U226 and MM1.S, the proliferation rates in suspension when treated with BTZ 4 nM were even lower than 0 (-0.02 and -0.07, respectively) (negative values means cell number after 72 h has decreased to values lower than the 100 000 cells seeded at day 0). When these cells were cultured in the microgels, mean proliferation rates also increase significantly. As in the case of the RPMI8226 cell line, the 0% AA FN

microgel had the lowest proliferation rate followed by the 0% AA microgel. Finally, the 10% AA and 10% AA HA microgels had the highest proliferation rates with no significant differences. These data reinforce our previous results that pointed to the relevant role of AA in generating drug resistance in microgel systems. This is even more significant than the functionalization with biomolecules of the BM ECM such as fibronectin or hyaluronic acid, and it's a behavior consistent between the 3 MM cell lines tested.

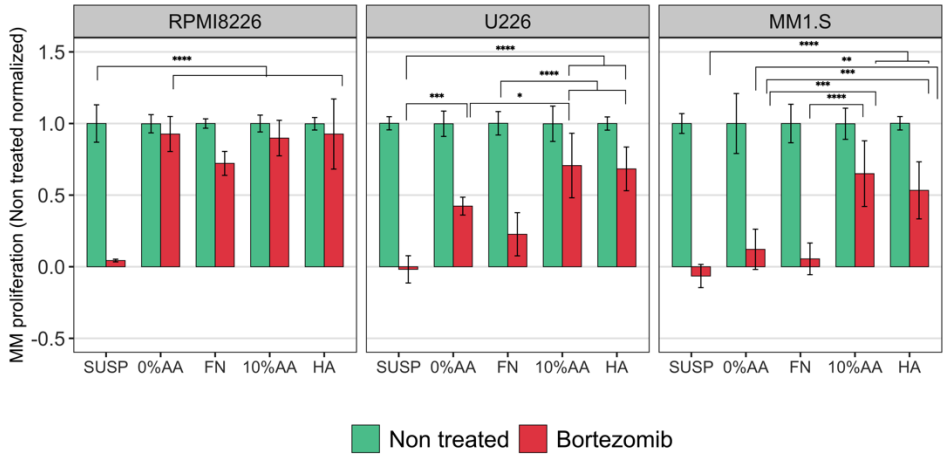

Figure 46. Proliferation rates of the cell lines RPMI8226, U226 and MM1.S at 72 h of culture growing in suspension or in microgels when treated with bortezomib 4 nM (red) or non-treated conditions (green). Data is expressed as % of MM proliferation with respect to day 0 and, for each condition, normalized by its non-treated counterpart. SUSP (suspension 2D culture), 0% AA (0% AA uncoated microgel), 0% AA FN (0% AA coated with fibronectin microgel), 10% AA (10% AA ungrafted microgel), 10% AA HA (10% AA grafted with hyaluronic acid microgel). P value legend: p ≤ 0.05 (*), p ≤ 0.01 (**), p ≤ 0.001 (***), p ≤ 0.0001 (****). For each cell line, comparisons between microgels were made using one-way ANOVA with Tukey's test for post-hoc analysis.

Results denote that the presence of AA itself could be a relevant factor for the *in vitro* mimicry of DR, something observed previously for the cell line RPMI8226 and the 1 μM DEX treatment. The 10% AA microgel maintained a cell viability of the BTZ treated samples equivalent to their non-treated counterparts, a result that was also confirmed by live/dead analysis (Figure 47, a-e). As in the case of the DEX-resistance in the RPMI8226 cell lines, it could

be hypothesized that there is a 3D effect that goes further than the specific effect of the biomolecules we studied. However, the 3D effect could also be expected in the 0% AA microgel. The increased ability to bind and concentrates soluble factors from the medium (either from the FBS or paracrine factors produced by the PCs themselves, such as IL-6) and present them to the cells, due to the acrylic acid presence was also considered. Previous results showed that the BSA antifouling coating did not significantly affect the generation of DEX resistance (Figure 45). However, a second experiment was carried out in this line. A 10% AA microgel with terminal -COOH groups blocked with ethanolamine was produced (Section 4.3.1.). This microgel, in which the functional groups conferring the high hydrophilic character have been modified, was used for the culture of the 3 MM cell lines under non-treated and BTZ-treated conditions (Figure 47, f). The 10% AA-blocked microgel did not lose the ability of the control microgel to generate resistance to BTZ. This result confirms that the AA effect mechanism is not as simple as increasing microsphere adsorption properties, as previously stated.

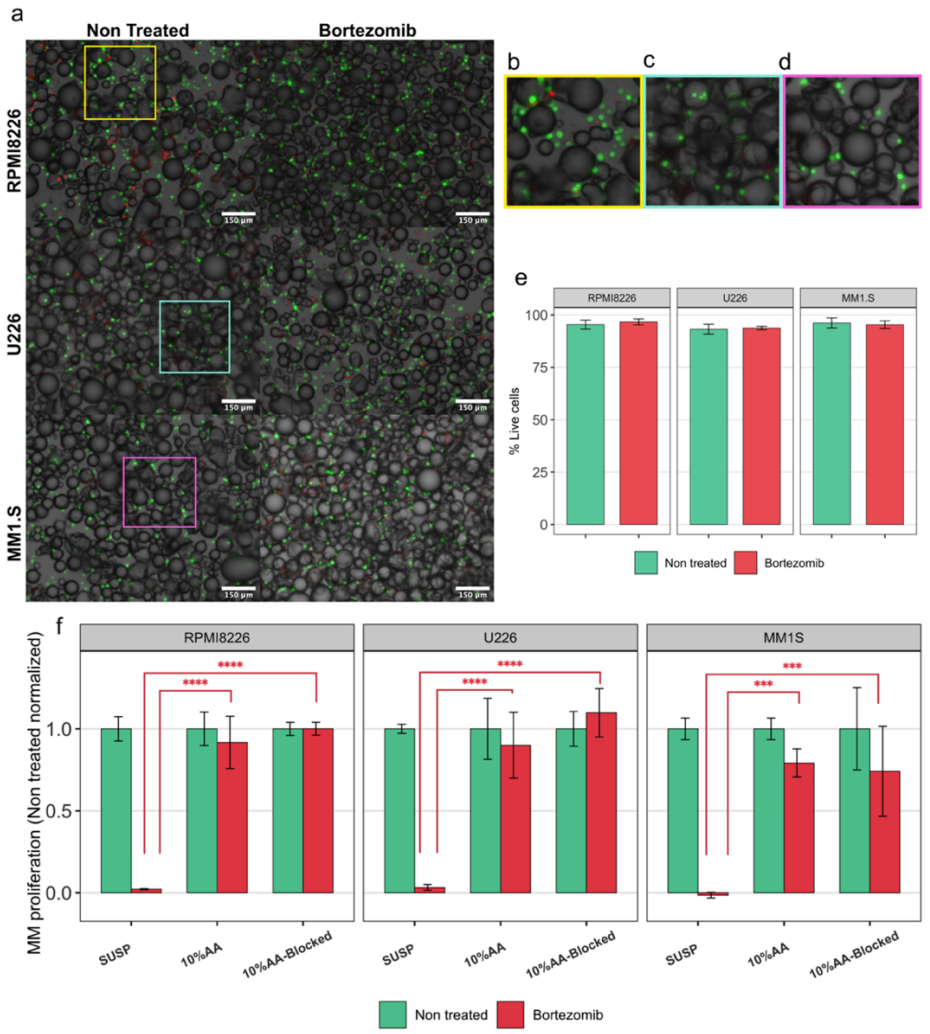

Figure 47. MM cells treated with BTZ show high viability. a) Images from the live/dead staining of the 3 MM cell lines after 72 h of culture in 10% AA microgels under non-treated or BTZ 4 nM conditions; green and red represent live and dead cells, respectively (scale bar: 150 µm). b,c,d) Magnified insets of the non-treated images of RPMI8226, U226 and MM1.S from panel a). e) Quantification of viability (mean ± SD, 6 fields from one sample were analyzed). f) Proliferation rates of the cell lines RPMI8226, U226 and MM1.S at 72 h of culture growing in suspension or in microgels when treated with bortezomib 4 nM (red) or non-treated conditions (green). Data is expressed as % of MM proliferation with respect to day 0 and, for each condition, normalized by its non-treated counterpart. SUSP (suspension 2D culture), 10% AA (10% AA ungrafted microgel), 10% AA-Blocked (10%

AA with -COOH blocked with ethanolamine). Statistical differences shown in red represent differences between BTZ treated samples. P value legend: p ≤ 0.001 (***), p ≤ 0.0001 (****). Comparisons between microgels were made using one-way ANOVA with Tukey's test for post-hoc analysis.

We also determined the effect of increasing bortezomib dosage in 10% AA microgel culture of the 3 different MM cell lines. In Figure 48, MM proliferation was analyzed for BTZ doses of 4, 6, 10 and 20 nM. The cell line RPMI8226 maintain good cell proliferation for all the BTZ doses tested when cultured in 10% AA microgels, however in the case of cell lines U226 and MM1.S, MM proliferation decreases when increasing BTZ dosage, as expected.

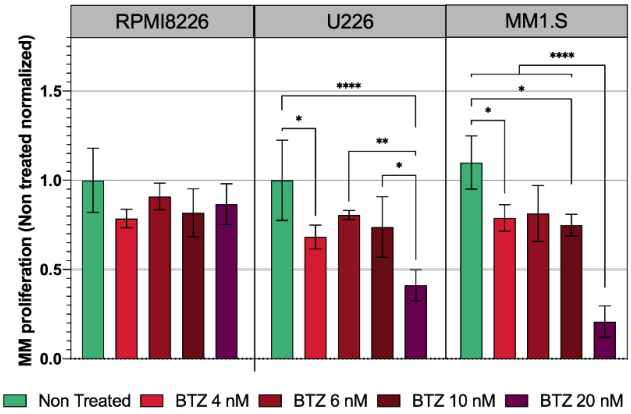

Figure 48. Proliferation rates of the cell lines RPMI8226, U226 and MM1.S at 72 h of culture growing in 10% AA microgels when treated with bortezomib 4, 6, 10 or 20 nM. Data is expressed as % of MM proliferation with respect to day 0 and, for each condition, normalized by its non-treated counterpart. P value legend: p ≤ 0.05 (*), p ≤ 0.01 (**), p ≤ 0.001 (***), p ≤ 0.0001 (****). For each cell line, comparisons were made independently for each drug. Comparisons between microgels were made using one-way ANOVA with Tukey's test for post-hoc analysis.

Future studies are needed to understand the mechanism underlying the strong effect of AA in terms of generating DR. Several discoveries reported in the literature lead us to the hypothesis that AA interaction with MM cells could condition the cellular phenotype related to the expression of integrins or other surface receptors, and thus alter cellular behavior, such as proliferation or DR. Modifying the expression of integrins in the cell could avoid the action of BTZ, as it has been reported that MM cell lines resistant to BTZ

present altered phenotype of cell surface adhesion molecules, such as integrin $\alpha 4\beta 1$ (Sevilla-Movilla et al. 2020).

Moreover, different hypothesis should also be considered. In general, the dynamics of the interaction between cells and materials can be classified as very complex, different properties of the materials can influence this process. Geometry, stiffness, topography, and surface charge must be taken into consideration. These parameters can alter cell proliferation, motility, attachment and differentiation and each cell type has its own unique characteristics including how cells react to differences in these parameters (Metwally and Stachewicz 2019).

Surface charge is an important parameter to be considered in this work. Charge of a surface originates mainly from the functional groups present on the surface. Burns et al. showed that AA surface charge originates from carboxyl groups, giving rise to a negatively charged surface which at physiological pH repel negatively charged proteins and slower their adsorption (Burns and Holmberg 1996). Although it has been impossible to proper measure superficial charge of the microspheres, the AA presence on microspheres surface, thoroughly demonstrated in Chapter 3, allows us to postulate that the microspheres containing AA will present a greater negative surface charge compared to those of the 0% AA microspheres. Surface charge plays a significant role in protein adsorption as proteins are amphoteric molecules carrying charges depending on surrounding pH (Kalasin and Santore 2009). Proteins are positively charged when their pH values are below their isoelectric point and negatively charged when pH is above their isoelectric point. Surface charge of materials determines the type of adsorbed proteins. Positively charged surfaces enhance adsorption of proteins with isoelectric point below 5.5, whereas negatively charged surfaces increase adsorption of proteins with isoelectric point above it (Gessner et al. 2003). Hence, cell-materials interactions are complex and need extended investigation regarding surface charge, topography, and chemical composition. The crucial molecular mech-

anism of controlling cellular behavior via surface properties is still poorly recognized in tissue engineering, especially in the case of cells growing in suspension.

In the literature, there is hardly any reference to how the properties of a material can modulate the behavior of non-adherent cells. However, in different contexts (mainly with adherent cells), some authors have described how material properties can alter the expression or activation of different surface receptors that modulate important signaling pathways for tumor cell proliferation and survival. Therefore, a possible hypothesis is that 10% AA microgel directly alters somehow MM cell lines phenotype contributing to cell proliferation and survival.

The glycocalyx is a surface layer that covers multiple cells (i.e., endothelial cells, smooth muscle cells, stem cells, and cancer cells, among others) and is mainly composed of proteoglycans and glycoproteins (Kang et al. 2018). The synthesis of glycocalyx components can be impaired during malignant transformation, in fact cancer cell-specific glycocalyx presents altered glycosylation and syndecan expression. Alterations in glycocalyx provide cancer cells with mechanisms that favor metastasis and contribute to DR generation. The underlying mechanisms are unclear, but they could be associated with glycocalyx's pivotal physiological role in growth factor storage and signaling, mechanotransduction, and as a protective barrier. The glycocalyx can control the spacing between receptors on cell surface and their different ligands. Multiple studies using leukocytes have shown that decreases in glycocalyx thickness directly correlate with increased cell adhesion (Hong et al. 2006; Kanyo et al. 2020; Kang et al. 2018; Mitchell and King 2014). For all this, another hypothesis that has to be postulated is that a possible effect induced by the microgel could be mediated by alterations in glycocalyx.

Finally, another interesting idea is the possibility that material physicochemical properties could condition epigenetic modifications leading to differences in gene expression on relevant survival and proliferation genes, and thus leading to DR generation.

The possibility of verifying each of these hypotheses has remained outside the scope of this Doctoral Thesis. However, all of them would imply that, for one reason or another, different proteins that participate in the main signaling pathways described in Section 1.3.1. would be overexpressed or activated. For this reason, it was decided to analyze the expression levels of different key molecules in each one of these signaling pathways by qPCR. The result obtained has been surprising. The expression of the genes detailed in Table 8, involved in the routes detailed in Figure 7, was analyzed. However, it has been observed that most of them show reduced expression at the mRNA level compared to suspension culture, except for MEK2 (Figure 49). This behavior was consistent between the 3 MM cell lines. MEK lies at the juncture within the Ras/Raf/MEK/Erk pathway, having a limited number of direct upstream activators and Erk1/2 as its only known targets, thereby making it an attractive target for cancer therapy. Because of that, several MEK inhibitors have been developed and investigated in preclinical and clinical tumor models. Results from these studies suggest that MEK inhibitors, whether alone or in combination with other anticancer therapies, may have a significant role to play in the future management of malignancy. Preclinical studies of MEK inhibitors in MM have demonstrated a capacity to induce MM apoptosis by overcoming the prosurvival effects of the BMN, however the therapeutic benefit of MEK inhibitors alone have only been assayed for solid tumors and are likely to be of limited benefit (Leow, Gerondakis, and Spencer 2013).

The experiment we developed compared the mRNA levels of these mRNA in suspension versus 10% AA cultures under non-treated conditions given that our hypothesis was that the microgel induces the changes in cell phenotype and then, this allows the cells to overcome BTZ effect. However, it is possible that the comparison should had been done between BTZ and non-treated conditions for cells cultured in the 10% AA microgels to better understand the cell response to the 10% AA microgel. Future experiments should be done to better understand the complete landscape, as the current results point out

that there exist some differences between suspension and 10% AA microgel condition.

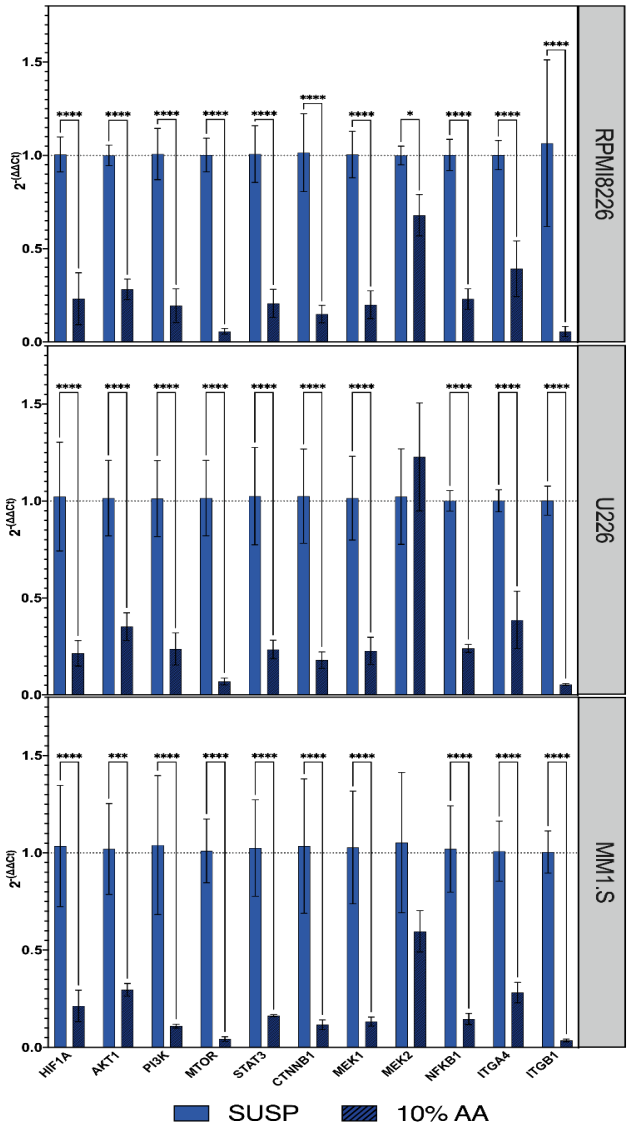

Figure 49. qPCR results for MM cell lines cultured on suspension or in 10% AA microgels. For each cell line, comparisons were made independently for each gene. Comparisons between microgels were made using Student's t-test. P value legend: p ≤ 0.05 (*), p ≤ 0.01 (**), p ≤ 0.001 (***), p ≤ 0.0001 (****).

4.4.4. Scale down of microgel-based culture conditions for future personalized medicine applications

As indicated above, this Doctoral Thesis is part of a project that aims to develop and optimize culture platforms based on microgels for the study of DR in MM. The project advances towards personalized medicine, since the ultimate goal is to use the supports developed for the cultivation of patient cells. Once the supports have been validated and optimized, they would allow predicting the specific response of a patient's cells to the different treatment regimens available. This would have a direct benefit on the patient, helping to reduce the risk of relapse that is today the main clinical problem.

However, to reach this stage, it is not only necessary to improve the characterization of microgels, their functionalization and their results and understanding in *in vitro* cultures with cell lines. But, it is also important to consider the production capacity of the biomaterials and the necessary quantities of microspheres to carry out a culture with sufficient replicates to reach statistical significance. This is an aspect that should be considered in the initial stages of the project since it can condition its progress when it reaches more advanced stages. Moreover, in future steps of the project the use of patient's cells will be introduced. Plasmatic cells will be purified from bone marrow aspirates and thus the available number of cells will also be a limiting factor.

In this case, the first *in vitro* trials, described in this Thesis, have made it possible to determine that the volume of microspheres necessary for a culture well (a biological replicate) as defined in these experiments is high compared to the production capacity of the microspheres. This could limit future experiments. For this reason, work has been carried out on a new culture system that allows obtaining equivalent results but with reduced quantities of microspheres. The orbital shaker system used in all cultures from previous sections (Figure 50, a) does not allow working with plates whose culture well has a diameter of less than 1.6 cm (corresponding to a 24-well plate). This is because the circumference described by the orbital shaker does not allow a true 3D environment to be generated if smaller wells are used. This implies that

the minimum necessary volume of culture is 500 μL, which implies large volume of microspheres for each culture.

Therefore, the possibility of using a rotator stirrer was considered (Figure 50, b). This allows culture to be carried out on Eppendorf tubes with permeable caps, which significantly reduce the minimum volume of culture required and therefore the number of microspheres and cells used per biological replicate. In addition, this system allows shaking with movements that are not limited to a flat circumference, but also vary in the vertical axis. This allows to generate 3D environments working with lower agitations.

Keeping the proportion of microspheres and cells in the culture, an experiment was carried out with the cell line RPMI8226. MM cell lines was culture in suspension and in the 10% AA microgel under non-treated and BTZ 4 nM treated conditions. The culture was performed using the conventional cell culture distribution and the new set-up, which consisted on 25 rpm and a total cell culture well of 200 μL instead of 500. As it can be seen in Figure 50 c, no significant differences were found between the new and the conventional set up of the culture well, opening the way for the scaling down of the platform.

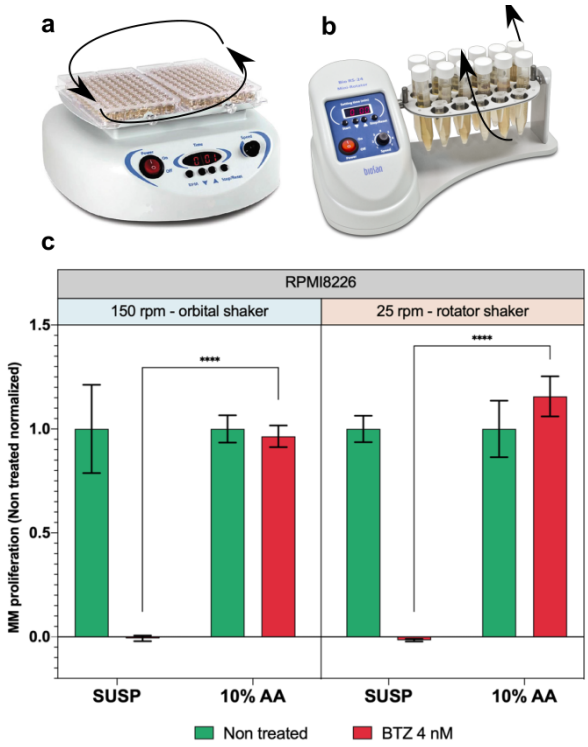

Figure 50. Trials for the scaling down of the cell culture platform. a) Orbital shaker used in the standard cell culture well (total cell culture volume: 500 μL) b) Rotator shaker used in the scaled cell culture well (total cell culture volume 200 μL. c) Proliferation or the MM cell line RPMI8226 cultured in the standard experimental set-up (150 rpm, orbital shaker) and in the scaled cell culture set-up (25 rpm, rotator shaker) when cultured in suspension and in the 10% AA microgel for non-treated and BTZ treated conditions. Data is expressed as % of MM proliferation with respect to day 0 and, for each condition, normalized by its non-treated counterpart. P value legend: p ≤ 0.05 (*), p ≤ 0.01 (**), p ≤ 0.001 (***), p ≤ 0.0001 (****).

4.4.5. Assembling of the 3D culture platform using Cytodex 1-based microgels

Finally, Cytodex 1-based microgels were also tested in cell culture using the RPMI8226 cell line. The developed systems were used with the experimental culture parameters defined with the acrylate microgels. Therefore, all cultures were used with the standard set-up, using 500 μL of total volume and at 150 rpm in orbital shaker.

In this case, the microgels were functionalized using LbL techniques with two different biomolecules of interest: chondroitin sulfate (CS) and hyaluronic acid (HA). However, the functionalization protocols and the characterizations necessary to evaluate them have not been fully optimized (Chapter 3). In some techniques, such as the use of the zetasizer to determine the surface charge, the measurement could not be carried out because the operation of the equipment is not designed to measure samples based on microspheres.

Therefore, it was decided to start cell cultures. Firstly, to evaluate the ability to generate 3D environments of MM and the specific effect of the biomolecules of interest used. And secondly, to assess whether the LbL protocols used had achieved effective coating of the microcarriers, and thus had reduced the forced adhesion of myeloma cells due to their positive charge that has been shown to have a negative effect on MM cell proliferation (Figure 38, b).

Cell viability and proliferation was assessed by live/dead assay (made by propidium iodide exclusion method) and image analysis, as these microspheres can be easily imaged *in situ* in the cell culture well. This technique was chosen because it allows to easily determine if the LbL protocols have transformed Cytodex 1 surface to allow MM cells to stay in suspension. Figure 51 shows the images corresponding to the cell line RPMI8226 growing on the different Cytodex 1-based microgels. For all of them direct and indirect characterizations of their cytotoxicity were performed. Then, images (Figure 51) were quantified using high-throughput technics (Figure 52).

In the images corresponding to the direct live/ dead, the Cyt CTRL microgel (conventional Cytodex 1 microspheres) has a negative effect in RPMI8226 viability (Figure 51 and 52). We had previously demonstrated that this is due to the surface properties of the microgel that force MM cell adhesion. Changing the surface of this microsphere with the LbL coatings (Cyt Cs and Cyt HA microgels) increases cell viability (Figure 51 and 52). However, we attributed this effect to the specific and positive effect over cell proliferation of the biomolecules of interest, CS and HA respectively (Vincent et al. 2001). Because

images in Figure 51 showed that the adherent character of Cytodex 1 microspheres is still inducing MM cell adhesion.

Morevover, we demonstrated that the first protocol used for crosslinking the LbL, based on the use of glutaraldehyde, resulted to be cytotoxic. In Figure 51 and 52 Cyt CS GA and Cyt HA GA present significantly lower viability than their non-crosslinked control (Cyt CS and Cyt HA respectively). It can be attributed to the presence of toxic residues that are retained in the microgel after crosslinking, given that indirect assays did not reveal increased cytotoxicity in microgels crosslinked by this method, in comparison with the non-crosslinked ones. For this reason, it was not considered worth trying to increase the washings of the crosslinking process and it was decided to implement a new method of crosslinking for LbL. Carbodiimide (EDC) chemistry was used as new crosslinking method. Cyt CS EDC and Cyt HA EDC showed higher cell viability than Cyt CS GA and Cyt HA GA respectively (Figure 51 and 52). However, although cell viability with this crosslinking method reached levels comparable to their non-croslinked counterparts (Figure 52), images in Figure 51 evidenced that cell numbers (cell proliferation) was lower than Cyt CS and Cyt HA.

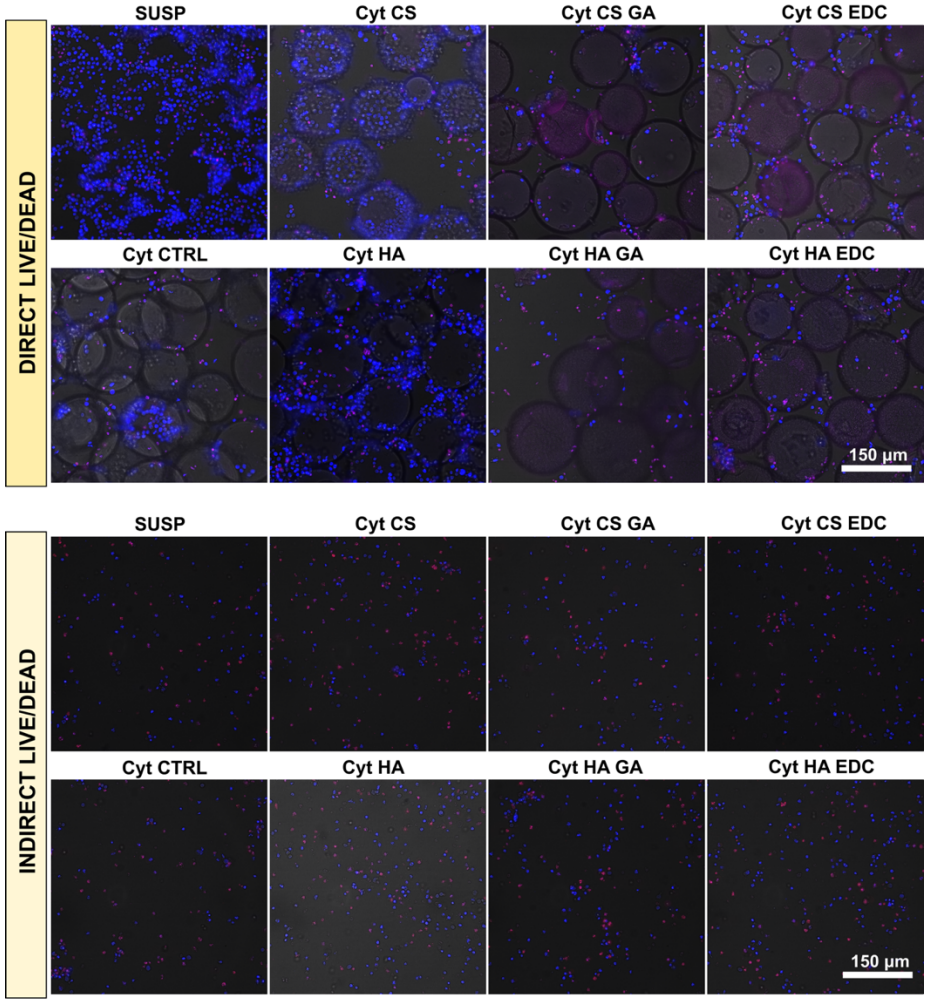

Figure 51. Representative images from the direct and indirect live/dead (propidium iodide exclusion assay) of the cell line RPMI8226 cultured in the different Cytodex 1-based microgels. Blue (hoechst-33342) stains all cells. Red (propidium iodide) stains all cells. Cyt CTRL (uncoated Cytodex 1 microspheres), Cyt CS (LbL coated microspheres with the pair CHI/CS), Cyt HA (LbL coated microspheres with the pair CHI/HA), Cyt CS GA (LbL coated microspheres with the pair CHI/CS and crosslinked with GA), Cyt HA GA (LbL coated microspheres with the pair CHI/HA and crosslinked with GA), Cyt CS EDC (LbL coated microspheres with the pair CHI/CS and crosslinked with EDC), Cyt HA EDC (LbL coated microspheres with the pair CHI/HA and crosslinked with EDC). Scale bar: 150 µm.

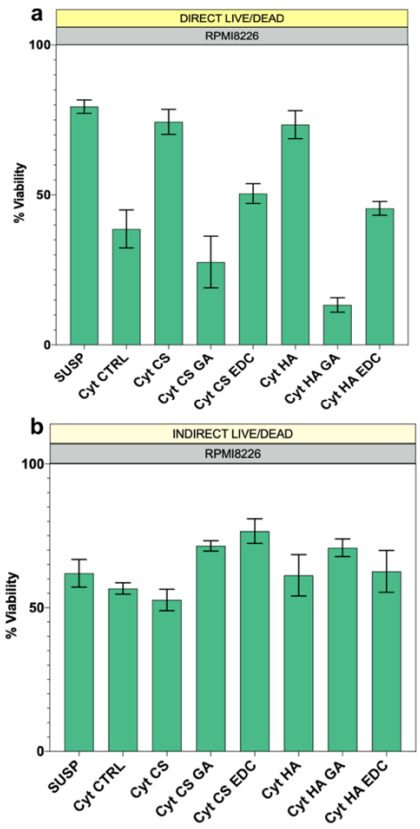

c

Tukey's multiple comparisons test	DIRECT Live/dead Statistical significance	INDIRECT Live/dead Statistical significance
Cyt CTRL vs. SUSP	****	ns
Cyt CS vs. SUSP	ns	ns
Cyt CS GA vs. SUSP	****	ns
Cyt CS EDC vs. SUSP	****	*
Cyt HA vs. SUSP	ns	ns
Cyt HA GA vs. SUSP	****	ns
Cyt HA EDC vs. SUSP	****	ns
Cyt CS vs. Cyt CTRL	****	ns
Cyt CS GA vs. Cyt CTRL	ns	*
Cyt CS EDC vs. Cyt CTRL	ns	**
Cyt HA vs. Cyt CTRL	****	ns
Cyt HA GA vs. Cyt CTRL	***	*
Cyt HA EDC vs. Cyt CTRL	ns	ns
Cyt CS GA vs. Cyt CS	****	**
Cyt CS EDC vs. Cyt CS	***	***
Cyt HA vs. Cyt CS	ns	ns
Cyt HA GA vs. Cyt CS	****	**
Cyt HA EDC vs. Cyt CS	****	ns
Cyt CS EDC vs. Cyt CS GA	***	ns
Cyt HA vs. Cyt CS GA	****	ns
Cyt HA GA vs. Cyt CS GA	*	ns
Cyt HA EDC vs. Cyt CS GA	**	ns
Cyt HA vs. Cyt CS EDC	***	*
Cyt HA GA vs. Cyt CS EDC	****	ns
Cyt HA EDC vs. Cyt CS EDC	ns	*
Cyt HA GA vs. Cyt HA	****	ns
Cyt HA EDC vs. Cyt HA	****	ns
Cyt HA EDC vs. Cyt HA GA	****	ns

Figure 52. Results of the image analysis of the direct (a) and indirect (b) live/dead (propidium iodide exclusion assay) of the cell line RPMI8226 cultured in the different Cytodex 1-based microgels. Cyt CTRL (uncoated Cytodex 1 microspheres), Cyt CS (LbL coated microspheres with the pair CHI/CS), Cyt HA (LbL coated microspheres with the pair CHI/HA), Cyt CS GA (LbL coated microspheres with the pair CHI/CS and crosslinked with GA), Cyt HA GA (LbL coated microspheres with the pair CHI/HA and crosslinked with GA), Cyt CS EDC (LbL coated microspheres with the pair CHI/CS and crosslinked with EDC), Cyt HA EDC (LbL coated microspheres with the pair CHI/HA and crosslinked with EDC). c) Statistical analysis corresponding to a and b. Comparisons between microgels were made using one-way ANOVA with Tukey's test for post-hoc analysis. P value legend: p ≤ 0.05 (*), p ≤ 0.01 (**), p ≤ 0.001 (***), p ≤ 0.0001 (****).

In view of the results obtained, it was decided that EDC is the best option for crosslinking the coatings by LbL. However, it is considered that it is still necessary to optimize these coatings to ensure that the microgels have the desired behavior. That is, they provide three-dimensionality and the presence

of biomolecules of interest (CS and HA), but their microcarrier character is effectively neutralized by LbL and does not force the adhesion of MM cells. For this reason, it is necessary to optimize the LbL protocols and to have techniques for measuring the surface charge that allow determining when a layer of LbL neutralizes the previous one and what is the final surface charge of the coated microspheres.

It is also important to consider that the size of these microspheres is significantly larger than that of the acrylates microspheres (size distribution centered on 150 μm versus sizes less than 60 μm in diameter). It is possible to consider that this facilitates the increased adhesion of MM cells to the Cytodex 1 microspheres, however it has been previously shown with acrylates microgels of sizes similar size to those of Cytodex 1 (sizes greater than 70 μm in diameter) that the bigger sizes, although they have a negative effect on cell proliferation, they do not induce or facilitate the adhesion of MM cells (Figure 34).

4.5. Conclusions

We have developed a novel cell culture system based on a semi-solid 3D media defined by microspheres and MM cells growing dynamically in suspension. The optimal cell culture conditions for the generation of semi-solid cell culture system have been determined in this chapter, and the effect of different parameters of the microgel over MM cell viability, proliferation and drug resistance generation have been studied.

The microspheres that are the main object of study of this Doctoral Thesis are microspheres made of acrylates, and after the experimental work done concerning these microgels, we can conclude that:

I. Microsphere size has a relevant role on modulating MM cell proliferation of the cell lines RPMI8226, U226 and MM1.S cultured in this 3D system. For the same composition, microgels composed of cell-sized microspheres

   < 60 μm diameter showed higher cell proliferation than microgels of > 70 μm diameter.

II. Agitation is needed for the generation of a real 3D environment with the microgel system. Increasing agitation speed has a negative effect on RPM8226 cell proliferation when grown in conventional suspension culture. However, microgels reduced this negative effect. The mechanism by which this phenomenon occurs must be studied in depth.

III. Optimal culture conditions for the microgel system were defined as 150 rpm of stirring speed using orbital shaker and cell-sized (< 60 μm diameter) microspheres.

IV. With the optimal culture conditions, the microgels with different compositions (0% AA, 10% AA) and functionalizations (none, HA, FN, COL 1, GRGD, IDAPS and PRARI) allow good cell proliferation of the cell lines RPMI8226, U226 and MM1.S under 3D culture conditions.

V. All the 3D systems developed respect the suspension growth pattern of the cell lines RPMI8226, U226 and MM1.S. The fibronectin coated microgels are the only ones in which the 3D model presents formation of cell-cell, microsphere-microsphere, and cell-microsphere aggregates.

VI. The MM cell line RPMI8226 cultured in the microgels with a polymeric matrix containing acrylic acid showed significantly higher resistance to dexamethasone than their conventional suspension cultures.

VII. The MM cell lines RPMI8226, U226 and MM1.S MM cultured in the different microgels showed significantly higher resistance to bortezomib than their conventional suspension cultures. Acrylic acid in the polymeric microsphere matrix showed a positive effect on the generation of resistance to BTZ *in vitro* and will require further studies.

VIII. The semi-solid system developed can be scaled to work with smaller volumes of microspheres and reduced cell numbers by using Eppendorf tubes and a rotator shaker. The results obtained with the cell line RPMI8226 in terms of resistance to bortezomib with the scaled set-up do not differ to those obtained with the conventional set-up thoroughly characterized in this Doctoral Thesis.

To increase the range of microgels characterized as MM 3D platform, initial cell cultures with the cell line RPMI8226 have been performed with the developed Cytodex 1-based microgels. We can conclude that:

IX. Cytodex 1 microspheres without modification used as 3D system have a negative effect on MM cell viability.

X. Layer-by-layer modification of Cytodex 1 microspheres with the pairs CHI/CS and CHI/HA increases MM cell viability. However, these systems do not respect the non-adherent character of MM cells. The LbL protocol should be improved to neutralize the high positive surface charge of the microcarriers.

XI. The crosslink of the LbL coated microgels with glutaraldehyde resulted in MM decreased cell viability compared to the non-crosslinked microgels.

XII. The crosslink of the LbL coated microgels with carbodiimide maintained the good MM cell viability of the non-crosslinked microgels.

SECTION III.

GENERAL CONCLUSIONS AND FUTURE PERSPECTIVES

Chapter 6. General conclusions

In this Doctoral Thesis, we aimed the development of 3D culture environments especially designed for the culture of multiple myeloma cells. These cells are characterized by their non-adherent nature and by growing in suspension. For this reason, the use of microspheres as biomaterial was explored. This approach is novel because it does not consider using microspheres as “cell-on” or “cell-in” supports for adherent cells. The microgel concept defined here is a semi-solid culture medium in which the microspheres coexist with the cells in suspension without forcing their adhesion. This seeks that the volume excluded by the microspheres in the culture well generates a 3D environment for the cells, bringing them closer and increasing the effect of the different interactions that may occur in the system compared to what they would perceive in a conventional 2D and suspension culture. These interactions can be either cell-cell, cell-microsphere, or cell-ECM. Since the microspheres were designed including components of the ECM. Therefore, the results generated in this Thesis can be summarized in two main lines: the

work aimed at generating and characterizing biomaterials based on microspheres that have the desired properties; and the work aimed at introducing these materials into the culture of myeloma cells and thus generating the desired 3D platform.

Taking this as starting point, we conclude that considerable progress has been made in the design and production of biomaterials that meet the described requirements. Acrylates-based microspheres have been obtained, we have optimized emulsion polymerization of protocols to generate microspheres with the desired size (from 1 to 60 μm diameter and with diameters bigger than 70 μm) and chemical composition (without acrylic acid and with 10 % acrylic acid). Once obtained, the presence of acrylic acid on its surface has been extensively characterized and proven, since this is important for its subsequent use. Next, work has been done to confer a biomimetic character to these microspheres. They have been functionalized with biomolecules that are natural constituents of the BM ECM. The effective incorporation of FN, HA, COL 1 and different peptides obtained by chemical synthesis on the surface of the microspheres has been demonstrated. HA, COL 1 and peptides (GRGD, IDAPS, PRARI) have been incorporated by covalent grafting, while FN was incorporated by adsorption.

In addition, trying to expand the possibilities of the 3D platform, the range of available microspheres has been expanded working on the adaptation to our needs of commercial microspheres such as Cytodex 1. These microspheres have been modified using LbL techniques to reduce their positive surface charge, which confers them strong adherent properties. In addition, LbL introduces relevant biomolecules of the BM ECM into their surface. For this purpose, the LbL pairs CHI/CS and CHI/HA have been used, with CS and HA being the biomolecules of interest. Two different methods of cross-linking for the LbL coatings have been tested, glutaraldehyde and carbodiimide. In this case, it has been difficult to carry out the desired characterization of the coatings. Since most of the techniques that usually offer relevant information on coatings generated by LbL do not allow them to be studied on configurations

with spherical morphology. However, some techniques such as TGA, cryoFESEM or FTIR have confirmed the presence of a surface coatings on Cytodex 1 microspheres.

Once a varied and well-characterized range of microspheres of interest became available, work has been done to introduce them for myeloma cell culture. The main challenges lay in establishing the optimal value of parameters such as agitation or the size of microspheres to carry out the cultures. Initially, experimental set-up was defined with the acrylates-based microspheres. Using a MM cell line (RPMI8226) the effect of microgel agitation speed has been determined, 150 rpm was defined as the optimum condition. Next, it was established that the size of the microgel modulates the proliferation of three different MM cell lines (RPMI8226, U226 and MM1.S), being the cell-sized microspheres the ones which support better cell proliferation and therefore those that were used in the later experiments. Using microspheres coated with FN, HA and uncoated with different chemical compositions (with or without acrylic acid in the polymeric matrix), it has been observed that all microgels provide similar proliferation to conventional cultures (as happened with the lines U226 and MM1.S) or even higher (RPMI8226 cell line gave this results). This is highly relevant, since *in vitro* 3D cultures on supports such as PLGA microspheres, AlgiMatrix or Matrigel, or even Cytodex 1 spheres tested under the same conditions, fail to maintain the proliferation of myeloma cell lines. This positive result of the microgel has been attributed to its ability to respect the characteristic suspension growth pattern of these cells, something that is particular to this 3D model of myeloma compared to all others available in the related literature.

Finally, once the potential of the platform developed in terms of cell proliferation has been demonstrated, initial drug resistance tests to anti-myeloma drugs were performed in the microgels. This is especially important, since the ultimate objective of the project that frames this Thesis is to use the systems developed to test drug resistance generation under biomimetic *in vitro* conditions that allow obtaining clinically relevant results.

Dexamethasone and bortezomib have been used as drugs that are currently first-line treatments for multiple myeloma. In the case of dexamethasone, it has been concluded that microgels containing acrylic acid induce resistance to dexamethasone *in vitro* in cultures of the RPMI8226 cell line. In the case of bortezomib, this same trend has been observed in cultures with lines RPMI8226, U226 and MM1.S. To try to better characterize the effect of acrylic acid, several hypotheses have been proposed and attempts have been made to confirm or refute them by using microgels with antifouling coatings (BSA) or by blocking the carboxyl groups of acrylic acid. However, it has only been possible to conclude that it is a complex effect that may be mediated by the ability of acrylic acid to adsorb different soluble factors, by its ability to interact and modify the expression or functionality of cell receptors or by its charge that it confers to the microspheres' surface. This is a very interesting result whose greater understanding in the future could help to better understand the mechanisms by which resistance to these drugs is generated.

The work carried out in terms of cultures with microgels based on Cytodex 1 microspheres modified by LbL should also be considered. In this case, it has been shown that reducing the surface charge of Cytodex 1 and introducing ECM biomolecules (CS and HA) on its surface improves the viability of RPMI8226 cells. Crosslinking with glutaraldehyde has also been shown to generate cytotoxic microgels. For this reason, the carbodiimide-based method has been chosen as the crosslinking method. In any case, the results obtained highlight the need to optimize LbL protocols, given that myeloma cells continue to adhere to the surface of the microcarriers.

After all the experimental evidence summarized in this Chapter, we can highlight the following general conclusions:

I. Acrylates-based microspheres have been obtained with the desired size (from 1 to 60 μm diameter and with diameters bigger than 70 μm) and chemical composition (without acrylic acid and with 10 % acrylic acid). The presence of acrylic acid on its surface has been extensively characterized and proven.

II. Acrylates-based microspheres have been functionalized with biomolecules that are natural constituents of the BM ECM. The effective incorporation of FN, HA, COL 1 and different peptides obtained by chemical synthesis on the surface of the microspheres has been demonstrated.

III. Cytodex 1 commercial microspheres have been modified using LbL techniques. CHI/HA and CHI/CS LbL pairs have been used to adapt Cytodex 1 properties to the microgel concept. Different crosslinking methods have been tested.

IV. The potential of the microgel platform as MM *in vitro* model has been demonstrated. All the acrylates-based microgels allow good cell proliferation of MM cell lines RPMI8226, U226 and MM1.S in 3D conditions.

V. Microsphere 's size and stirring speed of the microgels affect cell proliferation. The optimal conditions for the microgel have ben established as < 60 μm diameter and 150 rpm in an orbital shaker.

VI. The presence of acrylic acid on acrylates-based microsphere's surface increases *in vitro* drug resistance generation to the anti-myeloma drugs dexamethasone (in the cell line RPMI8226) and bortezomib (in the cell lines RPMI8226, U226 and MM1.S).

VII. The scale-down of the microgel platform developed with the acylates-based microspheres has been validated. Meaning that it has potential application in clinical practice as it can work with reduced numbers of microspheres and cells.

VIII. Conventional Cytodex 1 microspheres had a negative effect on RPMI8226 proliferation. LbL modification with CHI/CS and CHI/HA pairs improves RPMI8226 viability and proliferation. However, LbL protocols need to be improved to achieve the

characteristics pursued by the microgel, especially in terms of cell adhesion.

For all this, it is possible to conclude that we have developed a novel cell culture system based on a semi-solid 3D media defined by microspheres and MM cells growing dynamically in suspension. The microgel concept introduced here opens the way for novel 3D culture approaches specially designed for cells in suspension. It represents a novel and versatile tool that should be further explored for the 3D culture of hematological malignancies and generation of drug resistance, as it allows biomimetic *in vitro* platforms to be developed that maintain the dynamic and non-adherent properties of lymphoid and myeloid cells.

Chapter 7. Future perspectives

In this Thesis, the 3D platform generated with acrylates-based microgels has been generated and optimized. However, its use to obtain cell culture results that contribute to the clinical practice has yet to be explored. The possibility of adapting the platform to work with reduced amounts of microspheres and cells has been demonstrated. This opens the way for working with primary cells from multiple myeloma patients.

The scale-down of the system is crucial to advance to clinical application because primary myeloma cells cannot be expanded *in vitro*. Therefore, the next

natural step in this work is to check whether the system is capable of maintaining primary cells form MM patients *in vitro* for several days. This would be a result of great scientific relevance, since for the first time it would be possible to work *in vitro* with cells from patients for a period of more than few days. In addition, it would imply a great step towards personalized medicine, since the response of each patient's cells to different treatments could be studied, and even compared with the response that the patient is showing to those same treatments.

Finally, another aspect of this system that can be widely exploited is the role of each of the biomolecules incorporated into the microspheres in drug resistance. The system allows introducing a single biomolecule of interest or combining microspheres with several biomolecules in a single culture well, thus being able to study synergies between different biomolecules. Additional work could be also done in introducing new biomolecules in the system or new chemistries for grafting these biomolecules.

The research group is currently working on these lines in collaboration with the Hematology Department from "*Hospital Universitario y Politécnico La Fe*", in Valencia. A cryopreserved stock of BM aspirates from healthy donors and MM patients in now being conformed for exploring these future possibilities, progress is expected towards the validation of the microgel system as a platform and its use in the clinical practice.

On the other hand, Chapter 1 has extensively described the role of other cells in the BM microenvironment in the initiation, progression, and drug resistance generation of MM. Therefore, one factor that has been considered is the incorporation of other cell types into the model. Mesenchymal stem cells are of special interest in this regard. Currently, our group is working in the incorporation of MSCs into the platform by means of microspheres with properties adapted to their needs, such as adherent surfaces and larger diameters. The effect of introducing them at the bottom of the well is also being studied. This experimental approach would undoubtedly contribute to increase the biomimetic effect of the platform in the future.

The future possibilities of this 3D system based on microgels are limitless. The versatility offered by microspheres extends in several ways. The composition of its matrix, its physical or chemical properties can be varied, dynamic properties can be introduced (such as the capacity for controlled degradation or to respond to magnetic fields), the proportion of microspheres in the culture can be varied, different biomolecules can be introduced separately or combined... In conclusion, the microspheres are not only the key to this model, which makes it different from the rest, allowing the biomimetic culture of cells in suspension, but they also make it a versatile system and an optimal tool for designing custom experiments that will be able to respond in the future to very diverse scientific and clinical questions related to non-adherent growth cells.

Chapter 8. Contributions

The work realized along this Thesis has resulted in a large number of results. These results were diffused through several publications in scientific journals and national and international conferences listed following.

8.1. Publications in scientific journals

Publications as first author:

1. Biomimetic microspheres for 3D mesenchymal stem cell culture and characterization. **Sandra Clara-Trujillo**, Juan Carlos Marín-

Payá, Lourdes Cordón, Amparo Sempere, Gloria Gallego Ferrer, José Luis Gómez Ribelles. Colloids and Surfaces B: Biointerfaces. 2019. 177, 68-76, ISSN 0927-7765. https://doi.org/10.1016/j.colsurfb.2019.01.050.

2. *In Vitro* Modeling of Non-Solid Tumors: How Far Can Tissue Engineering Go? **Sandra Clara-Trujillo**, Gloria Gallego Ferrer, José Luis Gómez Ribelles. International Journal of Molecular Sciences. 2020. (16):5747. https://doi.org/10.3390/ijms21165747.

3. Novel microgel culture system as semi-solid three-dimensional *in vitro* model for the study of multiple myeloma proliferation and drug resistance. **Sandra Clara-Trujillo**, Laia Tolosa, Lourdes Cordón, Amparo Sempere, Gloria Gallego Ferrer, José Luis Gómez Ribelles. Biomaterials Advances. 2022. 212749, ISSN 2772-9508. https://doi.org/10.1016/j.bioadv.2022.212749.

Other contributions:

1. Biomimetic 3D Environment Based on Microgels as a Model for the Generation of Drug Resistance in Multiple Myeloma. Juan Carlos Marín-Payá, Blanca Díaz-Benito, Luis A. Martins, **Sandra Clara-Trujillo**, Lourdes Cordón, Senentxu Lanceros-Méndez, Gloria Gallego Ferrer, Amparo Sempere, José Luis Gómez Ribelles. Materials. 2021. 14, no. 23: 7121. https://doi.org/10.3390/ma14237121.

2. Effect of electrical stimulation on chondrogenic differentiation of mesenchymal stem cells cultured in hyaluronic acid – Gelatin injectable hydrogels. Juan Jairo Vaca-González, **Sandra Clara-Trujillo**, María Guillot-Ferriols, Joaquín Ródenas-Rochina, María J. Sanchis,

José Luis Gómez Ribelles, Diego Alexander Garzón-Alvarado, Gloria Gallego Ferrer. Bioelectrochemistry. 2020. Volume 134, 107536, ISSN 1567-5394. https://doi.org/10.1016/j.bioelechem.2020.107536.

8.2. International conferences

1. 3D Culture of multiple myeloma cells on protein functionalized microgel.

Conference: 45th Annual European Society for Artificial Organs Congress (ESAO)

City, Country / Year: Madrid, Spain / 2018

Format: Poster

Authors: Juan Carlos Marín-Payá, **Sandra Clara-Trujillo**, Lourdes Cordón, Amparo Sempere, Isidro Jarque, Gloria Gallego Ferrer, José Luis Gómez Ribelles.

2. A novel 3D cell culture microsphere-based platform.

Conference: European Society for Artificial Organs Congress (ESAO) Winter School 2019

City, Country / Year: Baden, Austria / 2019

Format: Poster

Authors: **Sandra Clara-Trujillo**, Juan Carlos Marín-Payá, Lourdes Cordón, Amparo Sempere, Gloria Gallego Ferrer, José Luis Gómez Ribelles.

1st Prize Young Researchers poster session

3. Stem cell chondrogenesis in electrically stimulated 3D injectable hydrogels.

Conference: 6th International Symposium Interface Biology of Implants (IBI 2019)

City, Country / Year: Rostock, Germany / 2019

Format: Poster

Authors: Juan Jairo Vaca-González, **Sandra Clara-Trujillo**, María Guillot-Ferriols, Joaquín Ródenas-Rochina, María J. Sanchis, José Luis Gómez Ribelles, Diego Alexander Garzón-Alvarado, Gloria Gallego Ferrer

4. Human hepatocytes encapsulated in injectable hydrogels for their use in liver cell therapy.

Conference: European Society of Gene and Cell Therapy (ESGCT) 2019 Annual Congress

City, Country / Year: Barcelona, Spain / 2019

Format: Poster

Authors: Julio Rodríguez-Fernández, Emma García-Legler, **Sandra Clara-Trujillo**, Estefanía Cabezas, María Teresa Donato, Gloria Gallego Ferrer, Laia Tolosa.

5. Electrical stimulation to mesenchymal stem cells cultured in hyaluronic acid gelatin hydrogel.

Conference: 8th Meeting of the International Federation for Artificial Organs (IFAO 2019). 57th Annual Meeting of the Japanese Society for Artificial Organs (JSAO 2019)

City, Country / Year: Osaka, Japan / 2019

Format: Poster

Authors: Juan Jairo Vaca-González, **Sandra Clara-Trujillo**, María Guillot-Ferriols, Joaquín Ródenas-Rochina, María J. Sanchis, José Luis Gómez Ribelles, Diego Alexander Garzón-Alvarado, Gloria Gallego Ferrer.

6. From 2D to 3D with biomimetic microgels.

Conference: EMBL-IBEC Winter Conference

City, Country / Year: Barcelona, Spain / 2020

Format: Poster

Authors: **Sandra Clara-Trujillo**, Juan Carlos Marín-Payá, Luis A. Martins, Annj Zammuner, Blanca Díaz-Benito, Lourdes Cordón, Amparo Sempere, Isidro Jarque, Gloria Gallego Ferrer, José Luis Gómez Ribelles

7. Microspheres as building-blocks for tunable *in vitro* cell culture microenvironments.

Conference: European Society for Artificial Organs Congress (ESAO) Winter School 2021

City, Country / Year: Jaca, Spain / 2021 (Online)

Format: Poster

Authors: **Sandra Clara-Trujillo**, Inmaculada García-Briega, Julià Pla-Salom, Gloria Gallego Ferrer, José Luis Gómez Ribelles

8. 3D Hydrogel microenvironments of gelatin and hyaluronic acid for liver tissue engineering.

Conference: 6th world congress of the Tissue Engineering and Regenerative Medicine International Society (TERMIS 2021)

City, Country / Year: Maastrich, The Netherlands / 2021 (Online)

Format: Oral communication

Authors: Gloria Gallego Ferrer, Julio Rodríguez-Fernández, Emma García-Legler, **Sandra Clara-Trujillo**, María Teresa Donato, Manuel Salmerón-Sánchez, Laia Tolosa.

9. Drug resistance induction in microgel-based Multiple Myeloma suspension cultures.

Conference: 6th world congress of the Tissue Engineering and Regenerative Medicine International Society (TERMIS 2021)

City, Country / Year: Maastrich, The Netherlands / 2021 (Online)

Format: Oral communication

Authors: **Sandra Clara-Trujillo,** José Luis Gómez Ribelles, Gloria Gallego Ferrer

8.3. National conferences

1. 3D Culture of Multiple Myeloma cells on protein functionalized microgels.

Conference: CIBER-BBN Annual Congress 2018

City, Country / Year: Valladolid, Spain / 2018

Format: Poster

Authors: Juan Carlos Marín-Payá, **Sandra Clara-Trujillo**, Lourdes Cordón, Amparo Sempere, Isidro Jarque, Gloria Gallego Ferrer, José Luis Gómez Ribelles.

2. Functionalized microgels for cell culture in 3D environment.

Conference: CIBER-BBN Annual Congress 2019

City, Country / Year: Tarragona, Spain / 2019

Format: Poster

Authors: **Sandra Clara Trujillo**, Juan Carlos Marín-Payá, Luis A. Martins, Blanca Díaz-Benito, Lourdes Cordón, Amparo Sempere, Isidro Jarque, Gloria Gallego Ferrer, José Luis Gómez Ribelles.

3. Hepatic cells encapsulated in injectable hydrogels of natural origin.

Conference: III Congreso Nacional de Investigadores jóvenes en Biomedicina

City, Country / Year: Valencia, Spain / 2019

Format: Poster
Authors: Julio Rodríguez-Fernández, Estefanía Cabezas, **Sandra Clara-Trujillo**, María Teresa Donato, Gloria Gallego Ferrer, Laia Tolosa.

4. BIOMICROGEL: modelling Multiple Myeloma with microspheres.
Conference: CIBER-BBN Annual Congress 2021
City, Country / Year: Online, Spain / 2021
Format: Poster
Authors: **Sandra Clara-Trujillo**, Inmaculada García-Briega, Joaquín Rodenas-Rochina, Gloria Gallego Ferrer, Amparo Sempere, José Luis Gómez Ribelles

5. Proliferation and drug resistance of Multiple myeloma cell lines cultured in a 3D biomimetic microgel.
Conference: IV Young Researchers Meeting CIBERONC_BBN
City, Country / Year: Barcelona, Spain / 2021
Format: Poster
Authors: **Sandra Clara-Trujillo**, Lourdes Cordón, Gloria Gallego Ferrer, Amparo Sempere, José Luis Gómez Ribelles

8.4. Education related publications

During this Doctoral Thesis it has been possible to participate in project "**Critical thinking as a step forward in VET education: VET students immersed in high technology teams"**. This project is a European project with partners from Spain, Portugal, Czech

Republic and Greece co-founded by the Erasmus+ Program of the European Commission.

The main objective is to provide VET centers and high technology centers and companies with tools that encourage and train the implementation of critical thinking skills in VET students. Different intellectual outputs have been generated as results of this project:

El pensamiento crítico como un paso adelante en la Formación Profesional. Estudiantes de Formación Profesional inmersos en centros de alta tecnología.

Conference: V Congreso Nacional de Innovación Educativa y Docencia en Red (IN-RED 2019)

City, Country / Year: Valencia, Spain / 2019

Format: Oral communication

ISBN/ ISSN: 978-84-9048-522-4 / 2603-5863

Authors: Concepción Solano Martínez, **Sandra Clara-Trujillo**, Maria Teresa Guillot-Ferriols, José Luis Gómez Estrada, José Luis Gómez Ribelles

Methodological guide for high tech centers to host VET student internships. José Luis Gómez Estrada, Concha Solano Martínez, Maria Guillot-Ferriols, Sandra Clara-Trujillo, Jivago Nunes, Senentxu Lanceros-Mendez, Pedro Martins, Panagiotis, Chatzipapas, Panagiotis Karampelas, Dimitrios Flygkos, Ioannis Kaliakatsos, konstantinos Petridis, Ivan Krakovski.

References

Aaronson, David S., and Curt M. Horvath. 2002. “A Road Map for Those Who Don ’ t Know JAK-STAT.” *Science* 296 (May): 1653–56. https://doi.org/DOI: 10.1126/science.1071545.

Abarrategi, Ander, Syed A. Mian, Diana Passaro, Kevin Rouault-Pierre, William Grey, and Dominique Bonnet. 2018. “Modeling the Human Bone Marrow Niche in Mice: From Host Bone Marrow Engraftment to Bioengineering Approaches.” *Journal of Experimental Medicine* 215 (3): 729–43. https://doi.org/10.1084/jem.20172139.

Al-Khoury, Hala, Eva Espinosa-Cano, María Rosa Aguilar, Julio San Román, Frank Syrowatka, Georg Schmidt, and Thomas Groth. 2019. “Anti-Inflammatory Surface Coatings Based on Polyelectrolyte Multilayers of Heparin and Polycationic Nanoparticles of Naproxen-Bearing Polymeric Drugs.” *Biomacromolecules* 20 (10): 4015–25. https://doi.org/10.1021/acs.biomac.9b01098.

Alves, Natália M., Catherine Picart, and João F. Mano. 2009. “Self Assembling and Crosslinking of Polyelectrolyte Multilayer Films of Chitosan and Alginate Studies by OCM and IR Spectroscopy.”

Macromolecular Bioscience 9 (8): 776–85. https://doi.org/10.1002/mabi.200800336.

Anderson, Hilary J, Jugal Kishore Sahoo, Rein V Ulijn, and Matthew J Dalby. 2016. “Mesenchymal Stem Cell Fate : Applying Biomaterials for Control of Stem Cell Behavior.” *Frontiers in Bioengineering and Biotechnology* 4 (May): 1–14. https://doi.org/10.3389/fbioe.2016.00038.

Arber, D. A., A. Orazi, R. Hasserijan, J. Thiele, M. J. Borowitz, M. M. Le Beau, C. D. Bloomfield, M. Cazzola, and J. W. Vardiman. 2016. “The 2016 Revision to the World Health Organization Classification of Myeloid Neoplasms and Acute Leukemia.” *Blood* 127 (20): 2391–2405. https://doi.org/10.1182/blood-2016-03-643544.The.

Arshady, R. 1992. “Leading Contribution Suspension , Emulsion , and Dispersion Polymerization : A Methodological Survey.” *Colloid and Polymer Science* 732. https://doi.org/https://doi.org/10.1007/BF00776142.

Arshady, Reza. 1988. “Preparation of Polymer Nano- and Microspheres by Vinyl Polymerization Techniques.” *Journal of Microencapsulation* 5 (2): 101–14. https://doi.org/10.3109/02652048809056474.

Avigdor, Abraham, Polina Goichberg, Shoham Shivtiel, Ayelet Dar, Amnon Peled, Sarit Samira, Orit Kollet, et al. 2004. “CD44 and Hyaluronic Acid Cooperate with SDF-1 in the Trafficking of Human CD34+ Stem/Progenitor Cells to Bone Marrow.” *Blood* 103 (8): 2981–89. https://doi.org/10.1182/blood-2003-10-3611.

Balcão, Victor M., and Marta M.D.C. Vila. 2015. “Structural and Functional Stabilization of Protein Entities: State-of-the-Art.” *Advanced Drug Delivery Reviews* 93: 25–41. https://doi.org/10.1016/j.addr.2014.10.005.

Barker, Helen F., Jennifer Ball, Marion Drew, Malcolm S. Hamilton, and Ian M. Franklin. 1992. “The Role of Adhesion Molecules in Multiple Myeloma.” *Leukemia and Lymphoma* 8 (3): 189–96.

https://doi.org/10.3109/10428199209054904.

Beauvais, Deanna Lee M., Oisun Jung, Yang Yang, Ralph D. Sanderson, and Alan C. Rapraeger. 2016. “Syndecan-1 (CD138) Suppresses Apoptosis in Multiple Myeloma by Activating IGF1 Receptor: Prevention by SynstatinIGF1R Inhibits Tumor Growth.” *Cancer Research* 76 (17): 4981–93. https://doi.org/10.1158/0008-5472.CAN-16-0232.

Bianchi, Giada, Shaji Kumar, Irene M. Ghobrial, and Aldo M. Roccaro. 2012. “Cell Trafficking in Multiple Myeloma.” *Open Journal of Hematology* 3 (4). https://doi.org/DOI: 10.13055/ojhmt_3_s1_04.120221.

Bjorklund, C. C., V. Baladandayuthapani, H. Y. Lin, R. J. Jones, I. Kuiatse, H. Wang, J. Yang, et al. 2014. “Evidence of a Role for CD44 and Cell Adhesion in Mediating Resistance to Lenalidomide in Multiple Myeloma: Therapeutic Implications.” *Leukemia* 28 (2): 373–83. https://doi.org/10.1038/leu.2013.174.

Boudou, Thomas, Thomas Crouzier, Rachel Auzély-Velty, Karine Glinel, and Catherine Picart. 2009. “Internal Composition versus the Mechanical Properties of Polyelectrolyte Multilayer Films: The Influence of Chemical Cross-Linking.” *Langmuir* 25 (24): 13809–19. https://doi.org/10.1021/la9018663.

Braham, Maaike V.J., Monique C. Minnema, Tineke Aarts, Zsolt Sebestyen, Trudy Straetemans, Anna Vyborova, Jurgen Kuball, F. Cumhur Öner, Catherine Robin, and Jacqueline Alblas. 2018. “Cellular Immunotherapy on Primary Multiple Myeloma Expanded in a 3D Bone Marrow Niche Model.” *OncoImmunology* 7 (6). https://doi.org/10.1080/2162402X.2018.1434465.

Brigle, Kevin, and Barbara Rogers. 2017. “Pathobiology and Diagnosis of Multiple Myeloma.” *Seminar in Oncology Nursing* 33 (3): 225–36. https://doi.org/10.1016/j.soncn.2017.05.012.

Briz, N., C. M. Antolinos-Turpin, J. Aliõ, N. Garagorri, J. L.Gõmez Ribelles, and J. A. Gõmez-Tejedor. 2013. “Fibronectin Fixation on Poly(Ethyl

Acrylate)-Based Copolymers." *Journal of Biomedical Materials Research - Part B Applied Biomaterials* 101 B (6): 991–97. https://doi.org/10.1002/jbm.b.32907.

Burke, Susan E., and Christopher J. Barrett. 2003. "PH-Responsive Properties of Multilayered Poly(L-Lysine)/Hyaluronic Acid Surfaces." *Biomacromolecules* 4 (6): 1773–83. https://doi.org/10.1021/bm034184w.

Burns, N. L., and K. Holmberg. 1996. "Surface Charge Characterization and Protein Adsorption at Biomaterials Surfaces." *Progress in Colloid and Polymer Science* 100: 271–75. https://doi.org/10.1007/bfb0115792.

Burwick, Nicholas, and Sanjai Sharma. 2019. "Glucocorticoids in Multiple Myeloma: Past, Present, and Future." *Annals of Hematology* 98 (1): 19–28. https://doi.org/10.1007/s00277-018-3465-8.

Calimeri, T., E. Battista, F. Conforti, P. Neri, M. T. Di Martino, M. Rossi, U. Foresta, et al. 2011. "A Unique Three-Dimensional SCID-Polymeric Scaffold (SCID-Synth-Hu) Model for in Vivo Expansion of Human Primary Multiple Myeloma Cells." *Leukemia* 25 (4): 707–11. https://doi.org/10.1038/leu.2010.300.

Campbell, Jack, and Anna S. Vikulina. 2020. "Layer-by-Layer Assemblies of Biopolymers: Build-up, Mechanical Stability and Molecular Dynamics." *Polymers* 12 (9): 1–30. https://doi.org/10.3390/polym12091949.

Cantini, Marco, Hannah Donnelly, Matthew J Dalby, and Manuel Salmeron-Sanchez. 2020. "The Plot Thickens: The Emerging Role of Matrix Viscosity in Cell Mechanotransduction." *Advanced Healthcare Materials* 9 (8). https://doi.org/10.1002/adhm.201901259.

Carswell, Kathleen S., and Eleftherios T. Papoutsakis. 2000. "Culture of Human T Cells in Stirred Bioreactors for Cellular Immunotherapy Applications: Shear, Proliferation, and the IL-2 Receptor." *Biotechnology and Bioengineering* 68 (3): 328–38. https://doi.org/10.1002/(SICI)1097-0290(20000505)68:3<328::AID-BIT11>3.0.CO;2-V.

Carvalho, Estela O., Clarisse Ribeiro, Daniela M. Correia, Gabriela Botelho, and Senentxu Lanceros-Mendez. 2020. “Biodegradable Hydrogels Loaded with Magnetically Responsive Microspheres as 2d and 3d Scaffolds.” *Nanomaterials* 10 (12): 1–12. https://doi.org/10.3390/nano10122421.

Catlett-Falcone, Robyn, Terry H. Landowski, Marc M. Oshiro, James Turkson, Alexander Levitzki, Rocco Savino, Gennaro Ciliberto, et al. 1999. “Constitutive Activation of Stat3 Signaling Confers Resistance to Apoptosis in Human U266 Myeloma Cells.” *Immunity* 10 (1): 105–15. https://doi.org/10.1016/S1074-7613(00)80011-4.

Chauhan, Dharminder, Teru Hideshima, Steven Rosen, John C. Reed, Surender Kharbanda, and Kenneth C. Anderson. 2001. “Apaf-1/Cytochrome c-Independent and Smac-Dependent Induction of Apoptosis in Multiple Myeloma (MM) Cells.” *The Journal of Biological Chemistry* 276 (27): 24453–56. https://doi.org/10.1074/jbc.C100074200.

Chauhan, Dharminder, Pramod Pandey, Atsushi Ogata, Gerrard Teoh, Steven Treon, Mitsuyoshi Urashima, Surender Kharbanda, and Kenneth C. Anderson. 1997. “Dexamethasone Induces Apoptosis of Multiple Myeloma Cells in a JNK/SAP Kinase Independent Mechanism.” *Oncogene* 15 (7): 837–43. https://doi.org/10.1038/sj.onc.1201253.

Chauhan, Dharminder, Hiroshi Uchiyama, Yasmin Akbarali, Mitsuyoshi Urashima, Ken Ichi Yamamoto, Towia A. Libermann, and Kenneth C. Anderson. 1996. “Multiple Myeloma Cell Adhesion-Induced Interleukin-6 Expression in Bone Marrow Stromal Cells Involves Activation of NF-KB.” *Blood* 87 (3): 1104–12. https://doi.org/10.1182/blood.v87.3.1104.bloodjournal8731104.

Chen, D., M. Frezza, S. Schmitt, J. Kanwar, and Q. P. Dou. 2011. “Bortezomib as the First Proteasome Inhibitor Anticancer Drug: Current Status and Future Perspectives.” *Current Cancer Drug Targets* 11 (3): 239–53. https://doi.org/10.2174/156800911794519752.

Chim, C. S., S. K. Kumar, R. Z. Orlowski, G. Cook, P. G. Richardson, M. A. Gertz, S. Giralt, M. V. Mateos, X. Leleu, and K. C. Anderson. 2018. “Management of Relapsed and Refractory Multiple Myeloma: Novel Agents, Antibodies, Immunotherapies and Beyond.” *Leukemia* 32 (2): 252–62. https://doi.org/10.1038/leu.2017.329.

Choi, Andrew, Kyoung Duck Seo, Do Wan Kim, Bum Chang Kim, and Dong Sung Kim. 2017. “Recent Advances in Engineering Microparticles and Their Nascent Utilization in Biomedical Delivery and Diagnostic Applications.” *Lab on a Chip* 17 (4): 591–613. https://doi.org/10.1039/c6lc01023g.

Clara-Trujillo, Sandra, Gloria Gallego Ferrer, and José Luis Gómez Ribelles. 2020. “In Vitro Modeling of Non-Solid Tumors: How Far Can Tissue Engineering Go?” *International Journal of Molecular Sciences* 21 (16): 1–31. https://doi.org/10.3390/ijms21165747.

Clara-Trujillo, Sandra, J.C. Juan Carlos Marín-Payá, Lourdes Cordón, Amparo Sempere, Gloria Gallego Ferrer, and José Luis Gómez Ribelles. 2019. “Biomimetic Microspheres for 3D Mesenchymal Stem Cell Culture and Characterization.” *Colloids and Surfaces B: Biointerfaces* 177 (October 2018): 68–76. https://doi.org/10.1016/j.colsurfb.2019.01.050.

Clarke, Bart. 2008. “Normal Bone Anatomy and Physiology.” *Clinical Journal of the American Society of Nephrology* 3 Suppl 3: 131–39. https://doi.org/10.2215/CJN.04151206.

Comazzetto, Stefano, Bo Shen, and Sean J. Morrison. 2021. “Niches That Regulate Stem Cells and Hematopoiesis in Adult Bone Marrow.” *Developmental Cell* 56 (13): 1848–60. https://doi.org/10.1016/j.devcel.2021.05.018.

Criado-González, Miryam, Carmen Mijangos, and Rebeca Hernández. 2021. “Polyelectrolyte Multilayer Films Based on Natural Polymers: From Fundamentals to Bio-Applications.” *Polymers* 13 (14): 1–30.

https://doi.org/10.3390/polym13142254.

Daly, Andrew C., Lindsay Riley, Tatiana Segura, and Jason A. Burdick. 2020. "Hydrogel Microparticles for Biomedical Applications." *Nature Reviews Materials* 5 (1): 20–43. https://doi.org/10.1038/s41578-019-0148-6.

Damiano, Jason S., Anne E. Cress, Lori A. Hazlehurst, Alexander A. Shtil, and William S. Dalton. 1999. "Cell Adhesion Mediated Drug Resistance (CAM-DR): Role of Integrins and Resistance to Apoptosis in Human Myeloma Cell Lines." *Blood* 176 (5): 139–48.

Decher, Gero. 1997. "Fuzzy Nanoassemblies: Toward Layered Polymeric Multicomposites." *Science* 277 (5330): 1232–37. https://doi.org/10.1126/science.277.5330.1232.

Demirbilek, Celile, and Cemile Özdemir Dinç. 2012. "Synthesis of Diethylaminoethyl Dextran Hydrogel and Its Heavy Metal Ion Adsorption Characteristics." *Carbohydrate Polymers* 90 (2): 1159–67. https://doi.org/10.1016/j.carbpol.2012.06.068.

Donk, NWCJ Van De, H M Lokhorst, and A C Bloem. 2005. "Growth Factors and Antiapoptotic Signaling Pathways in Multiple Myeloma." *Leukemia* 19: 2177–85. https://doi.org/10.1038/sj.leu.2403970.

Elbert, Donald L., Curtis B. Herbert, and Jeffrey A. Hubbell. 1999. "Thin Polymer Layers Formed by Polyelectrolyte Multilayer Techniques on Biological Surfaces." *Langmuir* 15 (16): 5355–62. https://doi.org/10.1021/la9815749.

Fei, Min, Qinglei Hang, and Sicong Hou. 2013. "Cell Adhesion to Fibronectin Down-Regulates the Expression of Spy1 and Contributes to Drug Resistance in Multiple Myeloma Cells." *International Journal of Hematology* 98: 446–55. https://doi.org/10.1007/s12185-013-1435-4.

Ferrarini, Marina, Magda Marcatti, Fabio Ciceri, and Elisabetta Ferrero. 2021. "3D Models of Surrogate Multiple Myeloma Bone Marrow Microenvironments: Insights on Disease Pathophysiology and Patient-

Specific Response to Drugs Response." In *Multiple Myeloma*, edited by Ota Fuchs, 126. IntechOpen. https://doi.org/10.5772/intechopen.87599.

Ferrarini, Marina, Nathalie Steimberg, Maurilio Ponzoni, Daniela Belloni, Angiola Berenzi, Stefania Girlanda, Federico Caligaris-Cappio, Giovanna Mazzoleni, and Elisabetta Ferrero. 2013. "Ex-Vivo Dynamic 3-D Culture of Human Tissues in the RCCS TM Bioreactor Allows the Study of Multiple Myeloma Biology and Response to Therapy." *PLoS ONE* 8 (8): 1–10. https://doi.org/10.1371/journal.pone.0071613.

Fujiwara, Shigeyoshi. 2018. "Humanized Mice: A Brief Overview on Their Diverse Applications in Biomedical Research." *Journal of Cellular Physiology* 233 (4): 2889–2901. https://doi.org/10.1002/jcp.26022.

Galán-Díez, Marta, Álvaro Cuesta-Domínguez, and Stavroula Kousteni. 2018. "The Bone Marrow Microenvironment in Health and Myeloid Malignancy." *Cold Spring Harbor Perspectives in Medicine* 8 (7). https://doi.org/10.1101/cshperspect.a031328.

Gandhi, Neha S., and Ricardo L. Mancera. 2008. "The Structure of Glycosaminoglycans and Their Interactions with Proteins." *Chemical Biology and Drug Design* 72 (6): 455–82. https://doi.org/10.1111/j.1747-0285.2008.00741.x.

Gargiulo, Ernesto, Jerome Paggetti, and Etienne Moussay. 2019. "Hematological Malignancy-Derived Small Extracellular Vesicles and Tumor Microenvironment: The Art of Turning Foes into Friends." *Cells* 8 (5). https://doi.org/doi:10.3390/cells8050511.

Gessner, Andrea, Antje Lieske, Bernd R. Paulke, and Rainer H. Müller. 2003. "Functional Groups on Polystyrene Model Nanoparticles: Influence on Protein Adsorption." *Journal of Biomedical Materials Research - Part A* 65 (3): 319–26. https://doi.org/10.1002/jbm.a.10371.

Gomes, Manuela E., Márcia T. Rodrigues, Rui M.A. Domingues, and Rui L. Reis. 2017. "Tissue Engineering and Regenerative Medicine: New Trends and Directions - A Year in Review." *Tissue Engineering - Part B:*

Reviews 23 (3): 211–24. https://doi.org/doi:10.1089/ten.TEB.2017.0081.

Grech, Jessica M.R., João F. Mano, and Rui L. Reis. 2010. "Processing and Characterization of Chitosan Microspheres to Be Used as Templates for Layer-by-Layer Assembly." *Journal of Materials Science: Materials in Medicine* 21 (6): 1855–65. https://doi.org/10.1007/s10856-010-4055-z.

Griffith, Linda G., and Melody A. Swartz. 2006. "Capturing Complex 3D Tissue Physiology in Vitro." *Nature Reviews Molecular Cell Biology* 7 (3): 211–24. https://doi.org/10.1038/nrm1858.

Grunsven, Leo A. Van. 2017. "3D in Vitro Models of Liver Fibrosis." *Advanced Drug Delivery Reviews* 121: 133–46. https://doi.org/10.1016/j.addr.2017.07.004.

Guillot-Ferriols, M., J. C. Rodríguez-Hernández, D. M. Correia, S. A.C. Carabineiro, S. Lanceros-Méndez, J. L. Gómez Ribelles, and G. Gallego Ferrer. 2020. "Poly(Vinylidene) Fluoride Membranes Coated by Heparin/Collagen Layer-by-Layer, Smart Biomimetic Approaches for Mesenchymal Stem Cell Culture." *Materials Science and Engineering C* 117 (May): 111281. https://doi.org/10.1016/j.msec.2020.111281.

Håkanson, Maria, Edna Cukierman, and Mirren Charnley. 2013. "Miniaturized Pre-Clinical Cancer Models as Research and Diagnostic Tools." *Advanced Drug Delivery Reviews* 69–70: 52–66. https://doi.org/10.1016/j.addr.2013.11.010.

Harris, N. L., E. S. Jaffe, J. Diebold, G. Flandrin, H. K. Muller-Hermelink, J. Vardiman, T. A. Lister, and C. D. Bloomfield. 2000. "The World Health Organization Classification of Neoplasms of the Hematopoietic and Lymphoid Tissues: Report of the Clinical Advisory Committee Meeting - Airlie House, Virginia, November, 1997." *Hematology Journal* Special Ar: 53–66. https://doi.org/10.1038/sj.thj.6200013.

Hatano-Noborio, K., J. Kikuchi, M. Takatoku, R. Shimizu, T. Wada, M. Ueda, M. Nobuyoshi, et al. 2009. "Bortezomib Overcomes Cell Adhesion-

Mediated Drug Resistance through Downregulation of VLA-4 Expression in Multiple Myeloma." *Oncogene* 28 (2): 231–42. https://doi.org/10.1038/onc.2008.385.

Hazlehurst, L. A., J. S. Damiano, I. Buyuksal, W. J. Pledger, and W. S. Dalton. 2000. "Adhesion to Fibronectin via B1 Integrins Regulates P27(Kip1) Levels and Contributes to Cell Adhesion Mediated Drug Resistance (CAM-DR)." *Oncogene* 19 (38): 4319–27. https://doi.org/10.1038/sj.onc.1203782.

He, Qiulin, Jingwei Zhang, Youguo Liao, and Enateri Verissarah Alakpa. 2020. "Current Advances in Microsphere Based Cell Culture and Tissue Engineering." *Biotechnology Advances* 39 (November 2019): 107459. https://doi.org/10.1016/j.biotechadv.2019.107459.

Hellmich, Charlotte, Jamie A. Moore, Kristian M. Bowles, and Stuart A. Rushworth. 2020. "Bone Marrow Senescence and the Microenvironment of Hematological Malignancies." *Frontiers in Oncology* 10 (February): 1–7. https://doi.org/10.3389/fonc.2020.00230.

Hideshima, Teru, P. Leif Bergsagel, W. Michael Kuehl, and Kenneth C. Anderson. 2004. "Advances in Biology of Multiple Myeloma: Clinical Applications." *Blood* 104 (3): 607–18. https://doi.org/10.1182/blood-2004-01-0037.

Hideshima, Teru, Paul Richardson, Dharminder Chauhan, Vito J. Palombella, Peter J. Elliott, Julian Adams, and Kenneth C. Anderson. 2001. "The Proteasome Inhibitor PS-341 Inhibits Growth, Induces Apoptosis, and Overcomes Drug Resistance in Human Multiple Myeloma Cells." *Cancer Research* 61 (7): 3071–76.

Hong, Soonjin, Ertan Ergezen, Ryszard Lec, and Kenneth A. Barbee. 2006. "Real-Time Analysis of Cell-Surface Adhesive Interactions Using Thickness Shear Mode Resonator." *Biomaterials* 27 (34): 5813–20. https://doi.org/10.1016/j.biomaterials.2006.07.031.

Hosen, Naoki. 2020. "Integrins in Multiple Myeloma." *Inflammation and*

Regeneration 40 (1): 20–23. https://doi.org/10.1186/s41232-020-00113-y.

Hou, Jianhao, Rongfang Wei, Jinjun Qian, Ronggen Wang, Zhimin Fan, Chunyan Gu, and Ye Yang. 2019. “The Impact of the Bone Marrow Microenvironment on Multiple Myeloma.” *Oncology Reports* 42 (4): 1272–82. https://doi.org/10.3892/or.2019.7261.

Hozumi, Kentaro, Kyotaro Nakamura, Haruna Hori, Mari Miyagi, Rika Nagao, Keiko Takasaki, Fumihiko Katagiri, Yamato Kikkawa, and Motoyoshi Nomizu. 2016. “Mixed Fibronectin-Derived Peptides Conjugated to a Chitosan Matrix Effectively Promotes Biological Activities through Integrins, A4b1, A5b1, Avb3, and Syndecan.” *BioResearch Open Access* 5 (1): 356–66. https://doi.org/10.1089/biores.2016.0037.

Hu, Jingping, and Wei-xin Hu. 2018. “Targeting Signaling Pathways in Multiple Myeloma : Pathogenesis and Implication for Treatments.” *Cancer Letters* 414: 214–21. https://doi.org/10.1016/j.canlet.2017.11.020.

Itkin, Tomer, Shiri Gur-cohen, Joel A Spencer, Amir Schajnovitz, K Saravana, M Ramasamy, Anjali P Kusumbe, et al. 2016. “Distinct Bone Marrow Blood Vessels Differentially Regulate Hematopoiesis.” *Nature* 532 (7599): 323–28. https://doi.org/10.1038/nature17624.Distinct.

Jakubikova, Jana, Danka Cholujova, Teru Hideshima, Paulina Gronesova, E Szalat, Paul G Richardson, Nikhil C Munshi, and David M Dorfman. 2016. “A Novel 3D Mesenchymal Stem Cell Model of the Multiple Myeloma Bone Marrow Niche : Biologic and Clinical Applications.” *Oncotarget* 7 (47). https://doi.org/https://doi.org/10.18632/oncotarget.12643.

Jing, Qiang, Haibo Cai, Zheng Du, Zhaoyang Ye, and Wen Song Tan. 2013. “Effects of Agitation Speed on the Ex Vivo Expansion of Cord Blood Hematopoietic Stem/Progenitor Cells in Stirred Suspension Culture.” *Artificial Cells, Nanomedicine and Biotechnology* 41 (2): 98–102.

https://doi.org/10.3109/10731199.2012.712043.

Kalasin, Surachate, and Maria M. Santore. 2009. “Non-Specific Adhesion on Biomaterial Surfaces Driven by Small Amounts of Protein Adsorption.” *Colloids and Surfaces B: Biointerfaces* 73 (2): 229–36. https://doi.org/10.1016/j.colsurfb.2009.05.028.

Kang, Hongyan, Qiuhong Wu, Anqiang Sun, Xiao Liu, Yubo Fan, and Xiaoyan Deng. 2018. “Cancer Cell Glycocalyx and Its Significance in Cancer Progression.” *International Journal of Molecular Sciences* 19 (9): 1–23. https://doi.org/10.3390/ijms19092484.

Kanyo, Nicolett, Kinga Dora Kovacs, Andras Saftics, Inna Szekacs, Beatrix Peter, Ana R. Santa-Maria, Fruzsina R. Walter, András Dér, Mária A. Deli, and Robert Horvath. 2020. “Glycocalyx Regulates the Strength and Kinetics of Cancer Cell Adhesion Revealed by Biophysical Models Based on High Resolution Label-Free Optical Data.” *Scientific Reports* 10 (1): 1–20. https://doi.org/10.1038/s41598-020-80033-6.

Katz, Ben-zion. 2010. “Adhesion Molecules — The Lifelines of Multiple Myeloma Cells.” *Seminars in Cancer Biology* 20 (3): 186–95. https://doi.org/10.1016/j.semcancer.2010.04.003.

Kelm, Jens M., Madhu Lal-Nag, Gurusingham Sitta Sittampalam, and Marc Ferrer. 2019. “Translational in Vitro Research: Integrating 3D Drug Discovery and Development Processes into the Drug Development Pipeline.” *Drug Discovery Today* 24 (1): 26–30. https://doi.org/10.1016/j.drudis.2018.07.007.

Kervoëlen, Charlotte, Emmanuelle Ménoret, Patricia Gomez-bougie, Catherine Godon, Séverine Marionneau-lambot, Philippe Moreau, Catherine Pellat-Deceunynck, and Martine Amiot. 2015. “Dexamethasone-Induced Cell Death Is Restricted to Specific Molecular Subgroups of Multiple Myeloma.” *Oncotarget* 6 (29). https://doi.org/DOI: 10.18632/oncotarget.4616.

Khetani, Salman R., and Sangeeta N. Bhatia. 2006. “Engineering Tissues for

in Vitro Applications." *Current Opinion in Biotechnology* 17 (5): 524–31. https://doi.org/10.1016/j.copbio.2006.08.009.

Kiatkamjornwong, Suda, and Pattama Phunchareon. 1999. "Influence of Reaction Parameters on Water Absorption of Neutralized Poly(Acrylic Acid-Co-Acrylamide) Synthesized by Inverse Suspension Polymerization." *Journal of Applied Polymer Science* 72 (10): 1349–66.

Kim, Dai Kyu, Sang Woo Han, Chang Hwan Kim, Jong Dal Hong, and Kwan Kim. 1999. "Morphology of Multilayers Assembled by Electrostatic Attraction of Oppositely Charged Model Polyelectrolytes." *Thin Solid Films* 350 (1): 153–60. https://doi.org/10.1016/S0040-6090(99)00351-X.

Kirshner, Julia, Kyle J. Thulien, Lorri D. Martin, Carina Debes Marun, Tony Reiman, Andrew R. Belch, and Linda M. Pilarski. 2008. "A Unique Three-Dimensional Model for Evaluating the Impact of Therapy on Multiple Myeloma." *Blood* 112 (7): 2935–45. https://doi.org/10.1182/blood-2008-02-142430.

Klamer, Sofieke, and Carlijn Voermans. 2014. "The Role of Novel and Known Extracellular Matrix and Adhesion Molecules in the Homeostatic and Regenerative Bone Marrow Microenvironment." *Cell Adhesion and Migration* 8 (6): 563–77. https://doi.org/10.4161/19336918.2014.968501.

Kumar, Rahul, P. Sonika Godavarthy, and Daniela S. Krause. 2018. "The Bone Marrow Microenvironment in Health and Disease at a Glance." *Journal of Cell Science* 131 (4). https://doi.org/10.1242/jcs.201707.

Kumar, Shaji K, Angela Dispenzieri, Martha Q. Lacy, Morie A. Gertz, Francis K. Buadi, Shivlal Pandey, Prashant Kapoor, et al. 2014. "Continued Improvement in Survival in Multiple Myeloma: Changes in Early Mortality and Outcomes in Older Patients." *Leukemia* 28 (5): 1122–28. https://doi.org/10.1038/leu.2013.313.Continued.

la Puente, Pilar de, and Abdel Kareem Azab. 2016. "3D Tissue-Engineered

Bone Marrow: What Does This Mean for the Treatment of Multiple Myeloma?" *Future Oncology* 12 (13): 1545–47. https://doi.org/10.2217/fon-2016-0057.

la Puente, Pilar De, Barbara Muz, Rebecca C. Gilson, Feda Azab, Micah Luderer, Justin King, Samuel Achilefu, Ravi Vij, and Abdel Kareem Azab. 2015. "3D Tissue-Engineered Bone Marrow as a Novel Model to Study Pathophysiology and Drug Resistance in Multiple Myeloma." *Biomaterials* 73 (December): 70–84. https://doi.org/10.1016/j.biomaterials.2015.09.017.

Langer, Robert, and Joseph P. Vacanti. 1993. "Tissue Engineering." *Science* 260 (5110): 920–26. https://doi.org/10.1126/science.8493529.

Lastra, María Laura, José Luis Gómez Ribelles, and Ana María Cortizo. 2020. "Design and Characterization of Microspheres for a 3D Mesenchymal Stem Cell Culture." *Colloids and Surfaces B: Biointerfaces* 196: 111322. https://doi.org/10.1016/j.colsurfb.2020.111322.

Leow, C. Chang Yew, S. Gerondakis, and A. Spencer. 2013. "MEK Inhibitors as a Chemotherapeutic Intervention in Multiple Myeloma." *Blood Cancer Journal* 3 (3). https://doi.org/10.1038/bcj.2013.1.

Lewis, Natasha S., Emily E.L. Lewis, Margaret Mullin, Helen Wheadon, Matthew J. Dalby, and Catherine C. Berry. 2017. "Magnetically Levitated Mesenchymal Stem Cell Spheroids Cultured with a Collagen Gel Maintain Phenotype and Quiescence." *Journal of Tissue Engineering* 8. https://doi.org/10.1177/2041731417704428.

Lichtman, Marshall A. 2008. "Battling the Hematological Malignancies: The 200 Years' War." *The Oncologist* 13 (2): 126–38. https://doi.org/10.1634/theoncologist.2007-0228.

Litwińska, Zofia, Karolina Łuczkowska, and Bogusław Machaliński. 2019. "Extracellular Vesicles in Hematological Malignancies." *Leukemia and Lymphoma* 60 (1): 29–36. https://doi.org/10.1080/10428194.2018.1459606.

Liu, Yanli, Jiazhu Xu, Yan Zhou, Zhaoyang Ye, and Wen Song Tan. 2017. "Layer-by-Layer Assembled Polyelectrolytes on Honeycomb-like Porous Poly(ε-Caprolactone) Films Modulate the Spatial Distribution of Mesenchymal Stem Cells." *Materials Science and Engineering C* 78: 579–88. https://doi.org/10.1016/j.msec.2017.04.140.

Llopis-Hernández, Virginia, Patricia Rico, David Moratal, George Altankov, and Manuel Salmerón-Sánchez. 2013. "Role of Material-Driven Fibronectin Fibrillogenesis in Protein Remodeling." *BioResearch Open Access* 2 (5): 364–73. https://doi.org/10.1089/biores.2013.0017.

Lord, B. I. 1990. "The Architecture of Bone Marrow Cell Populations." *The International Journal of Cell Cloning* 8 (5): 317–31. https://doi.org/10.1002/stem.5530080501.

Marín-Payá, Juan Carlos, Blanca Díaz-Benito, Luis Amaro Martins, Sandra Clara-Trujillo, Lourdes Cordón, Senentxu Lanceros-Méndez, Gallego, Gloria Ferrer, Amparo Sempere, and José Luis Gómez Ribelles. 2021. "Biomimetic 3d Environment Based on Microgels as a Model for the Generation of Drug Resistance in Multiple Myeloma." *Materials* 14 (23). https://doi.org/10.3390/ma14237121.

Marzo, Lucia Di, Vanessa Desantis, Antonio Giovanni Solimando, Tiziana Annese, Beatrice Nico, Ruggiero Fumarulo, Angelo Vacca, and Maria Antonia Frassanito. 2016. "Microenvironment Drug Emerging New Players Resistance in Multiple Myeloma :" *Oncotarget* 7 (37). https://doi.org/10.18632/oncotarget.10849.

Mcquin, Claire, Allen Goodman, Vasiliy Chernyshev, Lee Kamentsky, A Cimini, Kyle W Karhohs, Minh Doan, et al. 2018. "CellProfiler 3.0: Next-Generation Image Processing for Biology." *PLoS Biology*, 1–17. https://doi.org/10.1371/journal.pbio.2005970.

Mealy, Joshua E., Jennifer J. Chung, Heon Ho Jeong, David Issadore, Daeyeon Lee, Pavan Atluri, and Jason A. Burdick. 2018. "Injectable Granular Hydrogels with Multifunctional Properties for Biomedical

Applications." *Advanced Materials* 30 (20). https://doi.org/10.1002/adma.201705912.

Méndez-Ferrer, Simón, Dominique Bonnet, David P. Steensma, Robert P. Hasserjian, Irene M. Ghobrial, John G. Gribben, Michael Andreeff, and Daniela S. Krause. 2020. "Bone Marrow Niches in Haematological Malignancies." *Nature Reviews Cancer* 20: 285–90. https://doi.org/10.1038/s41568-020-0245-2.

Metwally, Sara, and Urszula Stachewicz. 2019. "Surface Potential and Charges Impact on Cell Responses on Biomaterials Interfaces for Medical Applications." *Materials Science and Engineering C* 104: 109883. https://doi.org/10.1016/j.msec.2019.109883.

Mitchell, Michael J., and Michael R. King. 2014. "Physical Biology in Cancer. 3. The Role of Cell Glycocalyx in Vascular Transport of Circulating Tumor Cells." *American Journal of Physiology - Cell Physiology* 306 (2). https://doi.org/10.1152/ajpcell.00285.2013.

Morgan, Gareth J., Brian A. Walker, and Faith E. Davies. 2012. "The Genetic Architecture of Multiple Myeloma." *Nature Reviews Cancer* 12 (5): 335–48. https://doi.org/10.1038/nrc3257.

Morikawa, Takayuki, and Keiyo Takubo. 2017. "Use of Imaging Techniques to Illuminate Dynamics of Hematopoietic Stem Cells and Their Niches." *Frontiers in Cell and Developmental Biology* 5. https://doi.org/10.3389/fcell.2017.00062.

Nakamura-Ishizu, Ayako, Hitoshi Takizawa, and Toshio Suda. 2014. "The Analysis, Roles and Regulation of Quiescence in Hematopoietic Stem Cells." *Development* 141 (24): 4656–66. https://doi.org/10.1242/dev.106575.

Narayanan, Narayanan k., Bin Duan, Jonathan T. Butcher, Amitabha Mazumder, and Bhagavathi A. Narayanan. 2014. "Characterization of Multiple Myeloma Clonal Cell Expansion and Stromal Wnt/β-Catenin Signaling in Hyaluronic Acid-Based 3D Hydrogel." *In Vivo* 28: 67–74.

Nass, Janine, and Thomas Efferth. 2018. “Drug Targets and Resistance Mechanisms in Multiple Myeloma.” *Cancer Drug Resistance* 1: 87–117. https://doi.org/10.20517/cdr.2018.04.

Nissen, Neel I., Morten Karsdal, and Nicholas Willumsen. 2019. “Collagens and Cancer Associated Fibroblasts in the Reactive Stroma and Its Relation to Cancer Biology.” *Journal of Experimental and Clinical Cancer Research* 38 (1): 1–12. https://doi.org/10.1186/s13046-019-1110-6.

Ohwada, Chikako, Chiaki Nakaseko, Masayuki Koizumi, Masahiro Takeuchi, and Shinichi Ozawa. 2008. “CD44 and Hyaluronan Engagement Promotes Dexamethasone Resistance in Human Myeloma Cells.” *European Journal of Hematology* 80: 245–50. https://doi.org/10.1111/j.1600-0609.2007.01014.x.

Okada, Tomoko, Robert G. Hawley, Masato Kodaka, and Hiroaki Okuno. 1999. “Significance of VLA-4-VCAM-1 Interaction and CD44 for Transendothelial Invasion in a Bone Marrow Metastatic Myeloma Model.” *Clinical and Experimental Metastasis* 17 (7): 623–29. https://doi.org/10.1023/A:1006715504719.

Olson, Oakley C., Yoon-A Kang, and Emmanuelle Passegué. 2020. “Normal Hematopoiesis Is a Balancing Act of Self-Renewal and Regeneration.” *Cold Spring Harbor Perspectives in Medicine*. https://doi.org/10.1101/cshperspect.a035519.

Ozdemir, Cemile, Nureddin Çolak, and Ali Güner. 2007. “Crystallization Behavior of Poly(ε-Caprolactone)/Layered Double Hydroxide Nanocomposites.” *Journal of Applied Polymer Science* 105 (5): 261177–87. https://doi.org/10.1002/app.

Palumbo, Antonio, and Kenneth Anderson. 2011. “Multiple Myeloma.” *New England Journal of Medicine*. Massachussetts Medical Society. https://doi.org/10.1056/NEJMra1011442.

Pankov, Roumen, and Kenneth M. Yamada. 2002. “Fibronectin at a Glance.”

Journal of Cell Science 115 (20): 3861–63. https://doi.org/10.1242/jcs.00059.

Pérez-Álvarez, Leyre, Leire Ruiz-Rubio, Isabel Moreno, and José Luis Vilas-Vilela. 2019. "Characterization and Optimization of the Alkaline Hydrolysis of Polyacrylonitrile Membranes." *Polymers* 11 (1843): 1–11. https://doi.org/10.3390/polym11111843.

Piaopiao, Wang, and Meng Zihui. 2019. "Progress in Polystyrene Microspheres." *IOP Conference Series: Materials Science and Engineering* 563. https://doi.org/10.1088/1757-899X/563/2/022001.

Pinto, Vanessa, Rui Bergantim, Hugo R Caires, Hugo Seca, Jose E. Guimaraes, and M. Helena Vasconcelos. 2020. "Multiple Myeloma : Available Therapies and Causes of Drug Resistance." *Cancers* 12 (407): 1–32. https://doi.org/10.3390/cancers12020407.

Porcel, Claudine, Philippe Lavalle, Vincent Ball, Gero Decher, Bernard Senger, Jean Claude Voegel, and Pierre Schaaf. 2006. "From Exponential to Linear Growth in Polyelectrolyte Multilayers." *Langmuir* 22 (9): 4376–83. https://doi.org/10.1021/la053218d.

Poveda-Reyes, Sara, Tatiana C. Gamboa-Martínez, Sara Manzano, Mohamed H Doweidar, José Luis Gómez Ribelles, Ignacio Ochoa, and Gloria Gallego Ferrer. 2015. "Engineering Interpenetrating Polymer Networks of Poly(2-Hydroxyethyl Acrylate) as Ex Vivo Platforms for Articular Cartilage Regeneration." *International Journal of Polymeric Materials and Polymeric Biomaterials* 64 (14): 745–54. https://doi.org/10.1080/00914037.2014.1002132.

Poveda-Reyes, Sara, Vladimira Moulisova, Esther Sanmartín-Masiá, Luis Quintanilla-Sierra, Manuel Salmerón-Sánchez, and Gloria Gallego Ferrer. 2016. "Gelatin—Hyaluronic Acid Hydrogels with Tuned Stiffness to Counterbalance Cellular Forces and Promote Cell Differentiation." *Macromolecular Bioscience* 16: 1311–24. https://doi.org/10.1002/mabi.201500469.

Pradhan, Shantanu, Iman Hassani, Jacob M. Clary, and Elizabeth A. Lipke. 2016. “Polymeric Biomaterials for In Vitro Cancer Tissue Engineering and Drug Testing Applications.” *Tissue Engineering Part B: Reviews* 22 (6): 470–84. https://doi.org/10.1089/ten.teb.2015.0567.

Prokopovic, Vladimir Z., Claus Duschl, and Dmitry Volodkin. 2015. “Hyaluronic Acid/Poly- l -Lysine Multilayers as Reservoirs for Storage and Release of Small Charged Molecules.” *Macromolecular Bioscience* 15 (10): 1357–63. https://doi.org/10.1002/mabi.201500093.

Punet, Xavier, Rodolphe Mauchauffé, Marina I. Giannotti, José C. Rodríguez-Cabello, Fausto Sanz, Elisabeth Engel, Miguel A. Mateos-Timoneda, and Josep A. Planell. 2013. “Enhanced Cell-Material Interactions through the Biofunctionalization of Polymeric Surfaces with Engineered Peptides.” *Biomacromolecules* 14 (8): 2690–2702. https://doi.org/10.1021/bm4005436.

Radhakrishnan, Janani, Sudha Varadaraj, Sanat Kumar Dash, Akriti Sharma, and Rama Shanker Verma. 2020. “Organotypic Cancer Tissue Models for Drug Screening: 3D Constructs, Bioprinting and Microfluidic Chips.” *Drug Discovery Today* 00 (00). https://doi.org/10.1016/j.drudis.2020.03.002.

Raic, Annamarija, Lisa Rödling, Hubert Kalbacher, and Cornelia Lee-Thedieck. 2014. “Biomimetic Macroporous PEG Hydrogels as 3D Scaffolds for the Multiplication of Human Hematopoietic Stem and Progenitor Cells.” *Biomaterials* 35 (3): 929–40. https://doi.org/10.1016/j.biomaterials.2013.10.038.

Rajkumar, S. Vincent. 2020. “Multiple Myeloma: 2020 Update on Diagnosis, Risk-Stratification and Management.” *American Journal of Hematology* 95 (5): 548–67. https://doi.org/10.1002/ajh.25791.

Ramakrishnan, Vidya, and Donald E. Mager. 2018. “Network-Based Analysis of Bortezomib Pharmacodynamic Heterogeneity in Multiple Myeloma Cells.” *The Journal of Pharmacology and Experimental Therapeutics*

365 (3): 734–51. https://doi.org/10.1124/jpet.118.247924.

Ramakrishnan, Vijay, and Shaji Kumar. 2018. “PI3K / AKT / MTOR Pathway in Multiple Myeloma : From Basic Biology to Clinical Promise.” *Leukemia & Lymphoma* 59: 2524–34. https://doi.org/10.1080/10428194.2017.1421760.

Ramakrishnan, Vijay, and Anita D Souza. 2016. “Signaling Pathways and Emerging Therapies in Multiple Myeloma.” *Current Hematologic Malignancy Reports* 11: 156–64. https://doi.org/10.1007/s11899-016-0315-4.

Reagan, Michaela R., Yuji Mishima, Siobhan V. Glavey, Yong Yu Zhang, Salomon Manier, Zhi Ning Lu, Masoumeh Memarzadeh, et al. 2014. “Investigating Osteogenic Differentiation in Multiple Myeloma Using a Novel 3D Bone Marrow Niche Model.” *Blood* 124 (22): 3250–59. https://doi.org/10.1182/blood-2014-02-558007.

Reddy, Narendra, Roopa Reddy, and Qiuran Jiang. 2015. “Crosslinking Biopolymers for Biomedical Applications.” *Trends in Biotechnology* 33 (6): 362–69. https://doi.org/10.1016/j.tibtech.2015.03.008.

Ren, Zemin, Harmen Van Andel, Wim De Lau, Robin B. Hartholt, Madelon M. Maurice, Hans Clevers, Marie José Kersten, Marcel Spaargaren, and Steven T. Pals. 2018. “Syndecan-1 Promotes Wnt/b-Catenin Signaling in Multiple Myeloma by Presenting Wnts and R-Spondins.” *Blood* 131 (9): 982–94. https://doi.org/10.1182/blood-2017-07-797050.

Richert, Ludovic, Youri Arntz, Pierre Schaaf, Jean Claude Voegel, and Catherine Picart. 2004. “Ph Dependent Growth of Poly(L-Lysine)/Poly(L-Glutamic) Acid Multilayer Films and Their Cell Adhesion Properties.” *Surface Science* 570 (1–2): 13–29. https://doi.org/10.1016/j.susc.2004.06.178.

Richert, Ludovic, Fouzia Boulmedais, Philippe Lavalle, Jérome Mutterer, Emmanuelle Ferreux, Gero Decher, Pierre Schaaf, Jean Claude Voegel, and Catherine Picart. 2004. “Improvement of Stability and Cell Adhesion

Properties of Polyelectrolyte Multilayer Films by Chemical Cross-Linking." *Biomacromolecules* 5 (2): 284–94. https://doi.org/10.1021/bm0342281.

Ridley, Ronnie C., Huiquing. Xiao, Hiroyuki. Hata, Jeff. Woodliff, Joshua. Epstein, and Ralph D. Sanderson. 1993. "Expression of Syndecan Regulates Human Myeloma Plasma Cell Adhesion to Type I Collagen." *Blood* 81 (3): 767–74. https://doi.org/10.1182/blood.v81.3.767.767.

Rioja, Ana Y., Ramkumar Tiruvannamalai Annamalai, Spencer Paris, Andrew J. Putnam, and Jan P. Stegemann. 2016. "Endothelial Sprouting and Network Formation in Collagen- and Fibrin-Based Modular Microbeads." *Acta Biomaterialia* 29: 33–41. https://doi.org/10.1016/j.actbio.2015.10.022.

Robak, Pawel, Izabela Drozdz, Janusz Szemraj, and Tadeusz Robak. 2018. "Drug Resistance in Multiple Myeloma." *Cancer Treatment Reviews* 70 (May): 199–208. https://doi.org/10.1016/j.ctrv.2018.09.001.

Rocha Neto, J. B.M., T. B. Taketa, R. A. Bataglioli, S. B. Pimentel, D. M. Santos, A. Fiamingo, C. A.R. Costa, S. P. Campana-Filho, H. F. Carvalho, and M. M. Beppu. 2019. "Tailored Chitosan/Hyaluronan Coatings for Tumor Cell Adhesion: Effects of Topography, Charge Density and Surface Composition." *Applied Surface Science* 486: 508–18. https://doi.org/10.1016/j.apsusc.2019.04.227.

Salmerón-Sánchez, Manuel, Patricia Rico, David Moratal, Ted T. Lee, Jean E. Schwarzbauer, and Andrés J. García. 2011. "Role of Material-Driven Fibronectin Fibrillogenesis in Cell Differentiation." *Biomaterials* 32 (8): 2099–2105. https://doi.org/10.1016/j.biomaterials.2010.11.057.

Salomäki, Mikko, and Jouko Kankare. 2009. "Influence of Synthetic Polyelectrolytes on the Growth and Properties of Hyaluronan-Chitosan Multilayers." *Biomacromolecules* 10 (2): 294–301. https://doi.org/10.1021/bm8010177.

Salomäki, Mikko, Igor A. Vinokurov, and Jouko Kankare. 2005. "Effect of

Temperature on the Buildup of Polyelectrolyte Multilayers." *Langmuir* 21 (24): 11232–40. https://doi.org/10.1021/la051600k.

Saralidze, Ketie, Leo H Koole, and Menno L W Knetsch. 2010. "Polymeric Microspheres for Medical Applications." *Materials* 3: 3537–64. https://doi.org/10.3390/ma3063537.

Schenke-Layland, Katja, and Robert M. Nerem. 2011. "In Vitro Human Tissue Models - Moving towards Personalized Regenerative Medicine." *Advanced Drug Delivery Reviews* 63 (4): 195–96. https://doi.org/10.1016/j.addr.2011.05.001.

Schmidmaier, R., K. Mörsdorf, P. Baumann, B. Emmerich, and G. Meinhardt. 2006. "Evidence for Cell Adhesion-Mediated Drug Resistance of Multiple Myeloma Cells in Vivo." *International Journal of Biological Markers* 21 (4): 218–22. https://doi.org/10.5301/JBM.2008.1098.

Schneider, Aurore, Ludovic Richert, Gregory Francius, Jean Claude Voegel, and Catherine Picart. 2007. "Elasticity, Biodegradability and Cell Adhesive Properties of Chitosan/Hyaluronan Multilayer Films." *Biomedical Materials* 2 (1): 545–51. https://doi.org/10.1088/1748-6041/2/1/S07.

Schop, D., R. Van Dijkhuizen-Radersma, E. Borgart, F. W. Janssen, H. Rozemuller, H. J. Prins, and J. D. De Bruijn. 2010. "Expansion of Human Mesenchymal Stromal Cells on Microcarriers: Growth and Metabolism." *Journal of Tissue Engineering and Regenerative Medicine* 4 (2): 131–40. https://doi.org/10.1002/term.224.

Sevilla-Movilla, Silvia, Nohemí Arellano-Sánchez, Mónica Martínez-Moreno, Consuelo Gajate, Anna Sánchez-Vencells, Luis V. Valcárcel, Xabier Agirre, et al. 2020. "Upregulated Expression and Function of the A4β1 Integrin in Multiple Myeloma Cells Resistant to Bortezomib." *Journal of Pathology* 252 (1): 29–40. https://doi.org/10.1002/path.5480.

Shain, Kenneth H., Danielle N. Yarde, Mark B. Meads, Mei Huang, Richard Jove, Lori A. Hazlehurst, and William S. Dalton. 2009. "B1 Integrin

Adhesion Enhances IL-6-Mediated STAT3 Signaling in Myeloma Cells: Implications for Microenvironment Influence on Tumor Survival and Proliferation." *Cancer Research* 69 (3): 1009–15. https://doi.org/10.1158/0008-5472.CAN-08-2419.

Sharma, Vaibhav, Keith A. Blackwood, David Haddow, Lilian Hook, Chris Mason, Julian F. Dye, and Elena García-Gareta. 2015. "Method for Estimating Protein Binding Capacity of Polymeric Systems." *Biochimie Open* 1: 40–50. https://doi.org/10.1016/j.biopen.2015.10.001.

Shi, Wei, Dan Yan, Chongqiang Zhao, Miaomiao Xiao, Yina Wang, Haiyan Ma, Tianshu Liu, et al. 2017. "Inhibition of IL-6/STAT3 Signaling in Human Cancer Cells Using Evista." *Biochemical and Biophysical Research Communications* 491 (1): 159–65. https://doi.org/10.1016/j.bbrc.2017.07.067.

Silva, Joana M., Ana Rita C. Duarte, Sofia G. Caridade, Catherine Picart, Rui L. Reis, and João F. Mano. 2014. "Tailored Freestanding Multilayered Membranes Based on Chitosan and Alginate." *Biomacromolecules* 15 (10): 3817–26. https://doi.org/10.1021/bm501156v.

Skardal, Aleksander, Shameema F. Sarker, Aurélie Crabbé, Cheryl A. Nickerson, and Glenn D. Prestwich. 2010. "The Generation of 3-D Tissue Models Based on Hyaluronan Hydrogel-Coated Microcarriers within a Rotating Wall Vessel Bioreactor." *Biomaterials* 31 (32): 8426–35. https://doi.org/10.1016/j.biomaterials.2010.07.047.

Smith, Daniel, Chase Herman, Sidharth Razdan, Muhammad Raisul Abedin, William Van Stoecker, and Sutapa Barua. 2019. "Microparticles for Suspension Culture of Mammalian Cells." *ACS Applied Bio Materials* 2 (7): 2791–2801. https://doi.org/10.1021/acsabm.9b00215.

Smith, Soshana, Katarina Goodge, Michael Delaney, Ariel Struzyk, Nicole Tansey, and Margaret Frey. 2020. "A Comprehensive Review of the Covalent Immobilization of Biomolecules onto Electrospun Nanofibers." *Nanomaterials* 10 (11): 1–39. https://doi.org/10.3390/nano10112142.

Song, Zhijiang, Jingbo Yin, Kun Luo, Yanzhen Zheng, Yan Yang, Qiong Li, Shifeng Yan, and Xuesi Chen. 2009. “Layer-by-Layer Buildup of Poly(L-Glutamic Acid)/Chitosan Film for Biologically Active Coating.” *Macromolecular Bioscience* 9 (3): 268–78. https://doi.org/10.1002/mabi.200800164.

Sousa, M. P., F. Cleymand, and J. F. Mano. 2016. “Elastic Chitosan/Chondroitin Sulfate Multilayer Membranes.” *Biomedical Materials (Bristol)* 11 (3). https://doi.org/10.1088/1748-6041/11/3/035008.

Spencer, Andrew, Sung Soo Yoon, Simon J. Harrison, Shannon R. Morris, Deborah A. Smith, Richard A. Brigandi, Jennifer Gauvin, Rakesh Kumar, Joanna B. Opalinska, and Christine Chen. 2014. “The Novel AKT Inhibitor Afuresertib Shows Favorable Safety, Pharmacokinetics, and Clinical Activity in Multiple Myeloma.” *Blood* 124 (14): 2190–95. https://doi.org/10.1182/blood-2014-03-559963.

Steele, J. A.M., J. P. Hallé, D. Poncelet, and R. J. Neufeld. 2014. “Therapeutic Cell Encapsulation Techniques and Applications in Diabetes.” *Advanced Drug Delivery Reviews* 67–68: 74–83. https://doi.org/10.1016/j.addr.2013.09.015.

Steen Redeker, Erik, Duy Tien Ta, David Cortens, Brecht Billen, Wanda Guedens, and Peter Adriaensens. 2013. “Protein Engineering for Directed Immobilization.” *Bioconjugate Chemistry* 24 (11): 1761–77. https://doi.org/10.1021/bc4002823.

Sterling, Julie A, and Michaela R Reagan. 2018. “Soluble and Cell – Cell-Mediated Drivers of Proteasome Inhibitor Resistance in Multiple Myeloma.” *Frontiers in Endocrinology* 9 (May): 1–7. https://doi.org/10.3389/fendo.2018.00218.

Tancred, Tara M., Andrew R. Belch, Tony Reiman, Linda M. Pilarski, and Julia Kirshner. 2009. “Altered Expression of Fibronectin and Collagens I and IV in Multiple Myeloma and Monoclonal Gammopathy of

Undetermined Significance." *Journal of Histochemistry and Cytochemistry* 57 (3): 239–47. https://doi.org/10.1369/jhc.2008.952200.

Torisawa, Yu Suke, Catherine S. Spina, Tadanori Mammoto, Akiko Mammoto, James C. Weaver, Tracy Tat, James J. Collins, and Donald E. Ingber. 2014. "Bone Marrow-on-a-Chip Replicates Hematopoietic Niche Physiology in Vitro." *Nature Methods* 11 (6): 663–69. https://doi.org/10.1038/nmeth.2938.

Travlos, Gregory S. 2006. "Normal Structure, Function, and Histology of the Bone Marrow." *Toxicologic Pathology* 34 (5): 548–65. https://doi.org/10.1080/01926230600939856.

Trujillo, Sara, Sebastián L. Vega, Kwang Hoon Song, Ana San Félix, Matthew J. Dalby, Jason A. Burdick, and Manuel Salmerón-Sánchez. 2020. "Engineered Full-Length Fibronectin–Hyaluronic Acid Hydrogels for Stem Cell Engineering." *Advanced Healthcare Materials* 9 (21): 1–12. https://doi.org/10.1002/adhm.202000989.

Tsukamoto, Yoshinari, Takami Akagi, and Mitsuru Akashi. 2020. "Vascularized Cardiac Tissue Construction with Orientation by Layer-by-Layer Method and 3D Printer." *Scientific Reports* 10:5484: 1–11. https://doi.org/10.1038/s41598-020-59371-y.

Tuncel, Ali, Kutay Ecevit, Kemal Kesenci, and Erhan Piskin. 1996. "Nonswellable and Swellable Ethylene Glycol Dimethacrylate-Acrylic Acid Copolymer Microspheres." *Journal of Polymer Science: Part A: Polymer Chemistry* 34: 45–55.

Vacca, Angelo, Michela Di Loreto, Domenico Ribatti, Rita Di Stefano, Gennaro Gadaleta-Caldarola, Giuseppe Iodice, Daniela Caloro, and Franco Dammacco. 1995. "Bone Marrow of Patients with Active Multiple Myeloma: Angiogenesis and Plasma Cell Adhesion Molecules LFA-1, VLA-4, LAM-1, and CD44." *American Journal of Hematology* 50 (1): 9–14. https://doi.org/10.1002/ajh.2830500103.

Vikova, Veronika, Michel Jourdan, Nicolas Robert, Guilhem Requirand,

Stéphanie Boireau, Angélique Bruyer, Laure Vincent, et al. 2019. “Comprehensive Characterization of the Mutational Landscape in Multiple Myeloma Cell Lines Reveals Potential Drivers and Pathways Associated with Tumor Progression and Drug Resistance.” *Theranostics* 9 (2): 540–53. https://doi.org/10.7150/thno.28374.

Vincent, Thierry, Michel Jourdan, Man Sun Sy, Bernard Klein, and Nadir Mechti. 2001. “Hyaluronic Acid Induces Survival and Proliferation of Human Myeloma Cells through an Interleukin-6-Mediated Pathway Involving the Phosphorylation of Retinoblastoma Protein.” *Journal of Biological Chemistry* 276 (18): 14728–36. https://doi.org/10.1074/jbc.M003965200.

Vincent, Thierry, Laurence Molina, Lucile Espert, and Nadir Mechti. 2003. “Hyaluronan, a Major Non-Protein Glycosaminoglycan Component of the Extracellular Matrix in Human Bone Marrow, Mediates Dexamethasone Resistance in Multiple Myeloma.” *British Journal of Haematology* 121 (2): 259–69. https://doi.org/10.1046/j.1365-2141.2003.04282.x.

Volodkin, Dmitry, and Regine Von Klitzing. 2014. “Competing Mechanisms in Polyelectrolyte Multilayer Formation and Swelling: Polycation-Polyanion Pairing vs. Polyelectrolyte-Ion Pairing.” *Current Opinion in Colloid and Interface Science* 19 (1): 25–31. https://doi.org/10.1016/j.cocis.2014.01.001.

Vrábel, Dávid, Ludek Pour, and Š Sabina. 2019. “The Impact of NF- κ B Signaling on Pathogenesis and Current Treatment Strategies in Multiple Myeloma.” *Blood Reviews* 34: 56–66. https://doi.org/10.1016/j.blre.2018.11.003.

Walkley, C. R., J. M. Shea, N. A. Sims, L. E. Purton, and S. H. Orkin. 2007. “PRb Extrinsically Regulates Hematopoietic Stem Cells via Myeloid Cell -Bone Marrow Microenvironment Interactions.” *Cell* 129 (6): 1081–95. https://doi.org/doi:10.1016/j.cell.2007.03.055.

Wang, P. H., and C. Y. Pan. 2002. “Preparation of Styrene/Acrylic Acid Copolymer Microspheres: Polymerization Mechanism and Carboxyl Group Distribution.” *Colloid and Polymer Science* 280 (2): 152–59. https://doi.org/10.1007/s003960100588.

Wang, Peng Yuan, Lauren R. Clements, Helmut Thissend, Wei Bor Tsaia, and Nicolas H. Voelckere. 2015. “Screening Rat Mesenchymal Stem Cell Attachment and Differentiation on Surface Chemistries Using Plasma Polymer Gradients.” *Acta Biomaterialia* 11 (1): 58–67. https://doi.org/10.1016/j.actbio.2014.09.027.

Wang, Zhan, Sang Jin Lee, Heng-jie Cheng, James J Yoo, and Anthony Atala. 2018. “3D Bioprinted Functional and Contractile Cardiac Tissue Constructs.” *Acta Biomaterialia* 70: 48–56. https://doi.org/10.1016/j.actbio.2018.02.007.

Wickham, Hadley. 2008. *Elegant Graphics for Data Analysis: Ggplot2*. *Applied Spatial Data Analysis with R*. Springer.

Wobma, Holly, and Gordana Vunjak-Novakovic. 2016. “Tissue Engineering and Regenerative Medicine 2015: A Year in Review.” *Tissue Engineering - Part B: Reviews*. Mary Ann Liebert Inc. https://doi.org/10.1089/ten.teb.2015.0535.

Yao, Juo Chin, and Daniel C. Link. 2017. “The Malignant Hematopoietic Stem Cell Niche.” *Stem Cells*. https://doi.org/10.1002/stem.2487.

Ye, Shiqu, Chaoyang Wang, Xinxing Liu, and Zhen Tong. 2005. “Multilayer Nanocapsules of Polysaccharide Chitosan and Alginate through Layer-by-Layer Assembly Directly on PS Nanoparticles for Release.” *Journal of Biomaterials Science, Polymer Edition* 16 (7): 909–23. https://doi.org/10.1163/1568562054255691.

Zamuner, Annj, Paola Brun, Michele Scorzeto, Giuseppe Sica, Ignazio Castagliuolo, and Monica Dettin. 2017. “Smart Biomaterials: Surfaces Functionalized with Proteolytically Stable Osteoblast-Adhesive Peptides.” *Bioactive Materials* 2 (3): 121–30.

https://doi.org/10.1016/j.bioactmat.2017.05.004.

Zarkesh, Ibrahim, Majid Halvaei, Mohammad Hossein Ghanian, Fatemeh Bagheri, Forough Azam Sayahpour, Mahmoud Azami, Javad Mohammadi, Hossein Baharvand, and Mohamadreza Baghaban Eslaminejad. 2020. “Scalable and Cost-Effective Generation of Osteogenic Micro-Tissues through the Incorporation of Inorganic Microparticles within Mesenchymal Stem Cell Spheroids.” *Biofabrication* 12 (1). https://doi.org/10.1088/1758-5090/ab51ae.

Zhang, Wenting, Woo Y. Lee, David S. Siegel, Peter Tolias, and Jenny Zilberberg. 2014. “Patient-Specific 3D Microfluidic Tissue Model for Multiple Myeloma.” *Tissue Engineering - Part C: Methods* 20 (8): 663–70. https://doi.org/10.1089/ten.tec.2013.0490.

Zhao, Hong, Jian Hong Xu, Peng Fei Dong, and Guang Sheng Luo. 2013. “A Novel Microfluidic Approach for Monodispersed Chitosan Microspheres with Enhanced Autofluorescence.” *Chemical Engineering Journal* 215–216: 784–90. https://doi.org/10.1016/j.cej.2012.10.063.

Zhao, Qinghe, Baosan Han, Zhaohai Wang, Changyou Gao, Chenghong Peng, and Jiacong Shen. 2007. “Hollow Chitosan-Alginate Multilayer Microcapsules as Drug Delivery Vehicle: Doxorubicin Loading and in Vitro and in Vivo Studies.” *Nanomedicine: Nanotechnology, Biology, and Medicine* 3 (1): 63–74. https://doi.org/10.1016/j.nano.2006.11.007.